Ingeniaritza Goi Eskola Teknikoa
Escuela Técnica Superior de Ingeniería
Bilbao

eman ta zabal zazu
Euskal Herriko Unibertsitatea
Universidad del País Vasco

EUSKAL HERRIKO UNIBERTSITATEA / UNIVERSIDAD DEL PAÍS VASCO
BILBOKO INGENIARITZA GOI ESKOLA TEKNIKOA
ESCUELA TÉCNICA SUPERIOR DE INGENIERÍA DE BILBAO

INNOVATIVE REACTION SYSTEMS FOR ACETAL (1,1 DIETHOXY BUTANE) PRODUCTION FROM RENEWABLE SOURCES

A dissertation
Submitted to the University of the Basque Country
In partial fulfillment of the requirements
For the degree of

Ph.D. in Chemical Engineering
by

Mr. Ion Agirre Arisketa

Thesis Advisor: **Prof. Pedro Luis Arias Ergueta**

Bilbao 2010

ISBN: 978-84-694-5814-3

Nire gurasoei eta familia osoari eskeiniriko laguntza guztiagatik.

ESKERRAK

Tesi hau burutu ahal izateko laguntza eman didaten guztiei nire eskerrik beroenak eman nahiko nizkieke. Batez ere tesi honen zuzendaria, ***Pedro Luis Arias Ergueta*** *doktorea aipatu nahiko nuke, hasiera hasieratik uneoro erakutsi didan laguntzagatik eta oso baliotsuak izan zaizkidan bere gomendio zientifikoengatik ere. Ezin ahaztu "****SuPrEn****" ikerkuntza taldea osatzen duten doktore, laborategiko teknikari eta tesia burutzen ari diren nire kideak ere, denen artean tesi honen gauzatzea erraztu didatelako. Bestalde, Bilboko "****Ingeniaritza Kimikoa eta Ingurumenaren Ingeniaritza Saila****" ere ez dut aipatu gabe utzi nahi.*

*"****Energy research Centre of the Netherlands****"eko (ECN-ko) "****Membrane Technology Group****" eta "****Process Intensification Group****" taldeak ere ez nituzke ahaztu nahi, tesi honen zati garrantzitsu bat bertan burutu baita. Nire eskerrik beroenak eman nahi dizkiot* ***Henk M. van Veen****-i nire Herbeheretako estantzia erosoagoa egiteaz gain, membranen inguruan erakutsi eta lagundu didan guztiarengatik.*

Azkenik Euskal Herriko Unibertsitatea, Eusko Jaurlaritza eta espainiar estatuko Zientzia eta Teknologia Ministerioa aipatu nahi nituzke, erakunde hauek izan baitira Holandako ECN zentroarekin batera lan honen atal esperimentala burutzeko diru-laguntza eman dutenak.

ESKERRIK ASKO!

MUCHAS GRACIAS! THANK YOU VERY MUCH! DANK JE WEL!

Table of contents

Table of contents

List of tables

List of figures

Abstract

The production of oxygenated compounds as petrol additives like ETBE has increased a lot. Nowadays, the use of biofuels in conventional car engines has become one of the technological goals towards a sustainable development and oxygenated compounds like acetals seem to be good candidates to enhance the cetane number of biodiesels as well as their oxidation stability and reduce nitrogen oxides emissions.

In the present doctoral thesis the acetalization reaction between butanal and ethanol was considered. The main reaction implies the production of the corresponding acetal (1,1 diethoxy butane) and water in the presence of acidic ion exchange resins. The great advantage of the selected diesel additive (1,1 diethoxy butane) is its completely renewable origin as the aldehyde can be obtained from its corresponding alcohol via partial oxidation or via dehydrogenation. Moreover, the mentioned acetal fulfils most of the diesel specifications. Other smaller acetals reported in the literature like 1,1 diethoxy ethane do not fulfill some diesel specifications like the flash point.

According to the literature, this kind of reactions shows high thermodynamic limitations leading to low conversions in conventional reaction systems. However, due to the lack of data in the literature about the studied reaction, a **kinetic study** was performed in a batch stirred reactor. Different parameters like temperature, catalyst type and loading or initial compositions were studied in order to observe the reaction behavior and define an appropriate reaction mechanism. The achieved conversions were around 40-50% at temperatures generating acceptable kinetic rates. In order to overcome these thermodynamic limitations two different innovative reaction systems were studied as possible alternatives: the use of a reactive distillation systems and dehydration membranes.

Reactive distillation experiments were carried out in a semi pilot plant. Katapak SP-11 modules with Amberlyst 47 ion exchange resin were used as catalytic structured packing. The effect of different parameters was studied: effect of the reaction section height, effect of the reflux ratio, different feeding configurations. All these experiments allowed finding the best column configuration for optimum performance. Once the experimental work was finished, a steady state reactive distillation model based on conventional MESH equations was developed in order to gain further insights and to predict results without carrying out additional experiments. The model was validated

with experimental data and afterwards several column configurations were tested in order to find the most appropriate one. It was demonstrated that the equilibrium conversions can be overcome from 40% to 50% using an appropriate column configuration and process conditions.

As a second alternative, the use of **dehydration membranes or membrane reactors** was studied. Experimental work in a lab-scale batch reactor was carried out using HybSi® membranes. Permeance data were obtained performing ethanol, butanal, 1,1 diethoxy butane and water mixture separation experiments (without reaction) at different temperatures. Moreover, reaction separation experiments were carried out in the same batch reactor proving that equilibrium conversions can be easily overcome from 40% to 70%. It was also tested that Amberlyst catalyst particles do not damage the membrane surface. From all the gathered data in the batch experiments two different models were developed. On one hand, a discontinuous batch pervaporation-reactor was simulated and a comparison between experimental and predicted data showed good agreement. On the other hand, a continuous membrane reactor model was developed for an initial pilot/bench scale/industrial reactor design.

Finally, conceptual **process engineering work and cost estimations** were calculated. Based on the experimental results and the modeling work, different processes using reactive distillation, dehydration membranes were synthesized at industrial scale. Moreover, a base case using a conventional tubular reactor was also considered in order to compare it with the non-conventional systems.

As a main conclusion, it can be stated that the case in which dehydration membranes were used is the best option not only from the process engineering point of view but also due to lower economic costs.

Laburpena

Gaur egun ETBE-a bezalako konposatu oxigenatuen ekoizpena nabarmen hazi da gasolinen gehigarri moduan erabiltzeko. Garapen iraunkorraren bila, bioerregaien erabilpena ibilgailu arrunten motorretan erronka teknologiko bihurtu da eta halaber, azetalak bezalako konposatu oxigenatuek biodieselaren zetano indizea hobetu dezakete. Zetano indizeaz gain, biodieselaren oxidazio egonkortasuna hobetzen dute nitrogeno oxidoen igorpena gutxitzearekin batera.

Tesi doktorego honetan etanola eta butanalaren arteko azetalizazio erreakzioa aztertu da. Erreakzio hau elkartrukaketa ionikoa burutzen duten erretxina azidoen presentzian eraman da aurrera eta 1,1 dietoxi butanoa (azetala) eta ura dira sortutako produktuak. Azetal honen abantailarik handiena bere jatorri berriztagarria da; alkohola azukreetan aberatsak diren landareen hartziduratik lortu baitaiteke eta aldehidoa berriz dagokion alkoholaren deshidrogenaziotik edota bere oxidazio partzialetik. Honez gain, 1,1 dietoxi butanoak dieselaren espezifikazio gehienak betetzen ditu. 1,1 dietoxi etanoa bezalako azetal txikiagoek ez dituzte zenbait espezifikazio behar bezala betetzen, "flash point"a kasu.

Erreakzio mota hauek muga termodinamikoak erakutsi ohi dituzte bukaerako konbertsio baxuak lortuz ohiko erreaktoreak erabiliz gero. Hala ere, azterturiko erreakzioaren inguruko datu eza dela eta, bere **zinetika** aztertu da erreaktore ez-jarrai batean. Tenperatura, katalizatzaile mota, katalizatzaile karga eta irabiaketa abiadura bezalako parametroak aztertu dira eta modu honetan erreakzioaren zinetika eta mekanismo global egoki bat definitu ahal izan da. Honela, %40-50eko konbertsioak lortu dira zinetikoki onargarria den tenperatura tarte batean. Muga termodinamiko hauek gainditu nahian bi erreakzio sistema berritzaile aztertu dira, distilazio erreaktiboaren erabilera batetik eta deshidratazio mintzen edota mintz erreaktoreen erabilera bestetik.

Distilazio erreaktiboaren zati esperimentala instalazio erdi-pilotu batean burutu da Amberlyst 47a duen Katapak SP-11 zutabe betegarri egituratu katalitikoak erabiliz.moduan. Sekzio katalitikoaren altuera, elikadura konfigurazio eta errefluxua bezalako parametro ezberdinen aldaketen ondorioak aztertu dira. Esperimentu guzti hauek distilazio zutabe konfigurazio egokiena aurkitzeko balio izan dute. Bestalde, oreka etapetan oinarrituriko eredu matematiko bat garatu da prozesua hobeto ulertu ahal

izateko eta konfigurazio zehatzago bat aurkitu ahal izateko inongo esperimenturik egin gabe. Eredu matematikoa datu esperimentalekin balioztatua izan da. Orokorrean, distilazio erreaktiboa erabiliz oreka konbertsioak %40tik %50era igo daitekeela frogatu ahal izan da.

Deshidratazio mintzen edo mintz erreaktoreen erabilera izan da azterturiko bigarren aukera. Kasu honetan zati esperimentala HybSi® motako mintzak dituen erreaktore ez jarrai (edo erdi jarrai) batean burutu da. Permeazio datuak erreakziorik gabeko etanol/butanal/azetal/ur nahasteen deshidratazio esperimentuetatik atera ahal izan dira. Honez gain, erreakzioa eta bereizketa erreaktore berean burutu ahal izan dira, konbertsioak %40tik %70era igo daitezkeela frogatuz. Era berean, Amberlyst katalizatzaile partikulen talkek mintzaren gainazala hondatzen ez dutela ere ikusi da. Datu esperimental guzti hauetatik bi eredu matematiko mota garatu dira. Alde batetik, eredu ez-jarrai bat laborategiko esperimentuak iragarri ahal izateko (ereduak iragarritako datuak datu esperimentalekin guztiz bat datozela frogatu da) eta beste aldetik eredu jarrai bat. Bigarren eredu hau azetalen ekoizpen prozesu jarrai baten diseinurako erabili da.

Azkenekoz, **prozesuen ingeniaritza lana eta kostu estimazioak** burutu dira. Azken fase honetan, esperimentuetatik eta ereduetatik ateratako datuak erabiliz, distilazio erreaktiboan eta deshidratazio mintzetan oinarritutako prozesu ezberdinak garatu dira industri eskalan. Kasu base bat ere garatu da (erreaktore tubular batean oinarritua) prozesu ezberdinak aldaratu ahal izateko.

Tesi honen ondorio nagusienetako bat, ohiko distilazioarekin batera deshidratazio mintzen erabilerak ekartzen dituen onurak dira, bai ingeniaritza ikuspuntutik eta baita ekonomikoki ere. Prozesu eraginkorrago bat garatzean energia eta lehengaien erabilera optimoago bat egiten da.

Resumen

La producción de compuestos oxigenados como el ETBE para su uso como aditivos de combustibles se ha visto incrementada notablemente durante los últimos años. Hoy en día, el uso de los biocombustibles en motores convencionales de vehículos se ha convertido en uno de los retos tecnológicos para lograr un mayor desarrollo sostenible en el campo de la automoción. Compuestos oxigenados como los acetales prometen ser buenos candidatos para su utilización como aditivos en biocombustibles diesel al mejorar su índice de cetano, al mismo tiempo que mejoran su estabilidad a la oxidación y disminuyen las emisiones de óxidos de nitrógeno.

En la presente tesis doctoral se ha estudiado la reacción de acetalización entre el etanol y el butanal utilizando como catalizadores ácidos resinas de intercambio iónico. Como productos de esta reacción se obtiene el correspondiente acetal (1,1 dietoxi butano) y agua. La gran ventaja de este acetal es que tiene un origen potencial totalmente renovable, ya que el alcohol se puede obtener por vía fermentativa mientras que el aldehído se puede obtener bien a partir de la deshidrogenación de su correspondiente alcohol, o bien por la oxigenación parcial de éste último. Además, el 1,1 dietoxi butano cumple la mayoría de las especificaciones del diesel a diferencia de otros acetales de menor tamaño como el 1,1 dietoxi etano ya que éstos no cumplen la especificación del "flash point".

Este tipo de reacciones presentan grandes límites termodinámicos obteniéndose bajas conversiones en sistemas de reacción convencionales. En primer lugar, debido a la falta de información sobre esta reacción se ha efectuado un **estudio cinético** en un reactor discontinuo a escala de laboratorio estudiando la influencia de diferentes parámetros como la temperatura, tipos de catalizador, carga de catalizador o la composición de la mezcla inicial. De esta manera se ha podido determinar la cinética de la reacción y se ha elucidado el mecanismo de reacción global más adecuado. Las conversiones alcanzadas rondan el 40-50% a temperaturas en las que la cinética es aceptable. Para poder vencer estos límites termodinámicos y para alcanzar mayores conversiones se han estudiado dos tipos de sistemas reaccionantes no convencionales: la destilación reactiva y los reactores de membranas de deshidratación.

Los ensayos de **destilación reactiva** se han efectuado en una planta semi-piloto utilizando relleno estructurado del tipo Katapak SP-11 con Amberlyst 47 como

catalizador. Se han estudiado diferentes parámetros como la altura de la sección de reacción, el efecto de la relación de reflujo o diferentes configuraciones de alimentación para poder así establecer la configuración y condiciones óptimas. Una vez realizados los experimentos se ha desarrollado un modelo para simular el funcionamiento de la planta piloto basado en etapas de equilibrio; de esta manera el modelo ha permitido comprender de una manera más exhaustiva el comportamiento del sistema con un esfuerzo experimental razonable. El modelo ha sido validado con los datos experimentales y después se ha trabajado con él en la optimización del proceso. De esta manera, se ha demostrado que las conversiones se pueden aumentar desde un 40% a un 50% usando una configuración adecuada.

Como segunda alternativa, se ha estudiado el uso de **membranas de deshidratación o reactores de membranas**. En este caso los experimentos se han realizado en un reactor discontinuo incluyendo membranas HybSi®. En primer lugar, se han efectuado experimentos de deshidratación (sin reacción) de la mezcla cuaternaria que constituyen los compuestos que toman parte en la reacción; estos experimentos han servido para obtener las permeabilidades de cada uno de ellos. A continuación se han realizado ensayos en el que en un mismo reactor se dan tanto la reacción como la separación. De esta manera se ha demostrado que las conversiones pueden aumentar de un 40% a un 70%. De modo paralelo, se ha demostrado que los impactos de las partículas del catalizador Amberlyst no deterioran la superficie de la membrana. A partir de estos datos experimentales se han desarrollado dos tipos de modelos. Por una parte se han simulado los experimentos realizados obteniendo una buena concordancia entre datos experimentales y simulados y por otra parte se ha desarrollado el diseño de un modelo para un proceso continuo más apropiado para la producción de acetales a escala industrial.

Finalmente se ha realizado un trabajo de **ingeniería de procesos conceptual y un estudio para estimar los costes económicos asociados** basado en los resultados experimentales y los derivados de la modelización, utilizando sistemas de destilación reactiva o membranas de deshidratación para poder establecer la opción más adecuada. También se ha considerado un caso base (utilizando reactores tubulares convencionales) para poderlo comparar con los mencionados anteriormente.

Así, se ha concluido en que la opción que combina membranas de deshidratación con destilación convencional es la opción más prometedora de todas las analizadas, no sólo desde el punto de vista de la eficiencia del proceso sino también desde el punto de vista económico.

Chapter I

Introduction and state of the art

1 Introduction and state of the art

1.1 World energy outlook: Current situation

In the beginning of the 20th Century, coal was the origin of the most industrial organic compounds; products like tar were obtained by coal pyrolysis besides a gas rich in ethylene and propylene.

Nowadays, oil is the source of the vast majority of fuels used for transport and heating; moreover it is the main raw material for the hydrocarbons used in petrochemical industry. However, oil is a fossil fuel and some experts predict that the reserves will exhaust approximately in 20–30 years. However, the use of other raw materials have already been started to explore due to the economical fluctuations (see Figure 1.1) and the geopolitical instability in the producer countries (see Figure 1.2). Coal, vegetal or mineral oils and biomass are the most important alternatives.

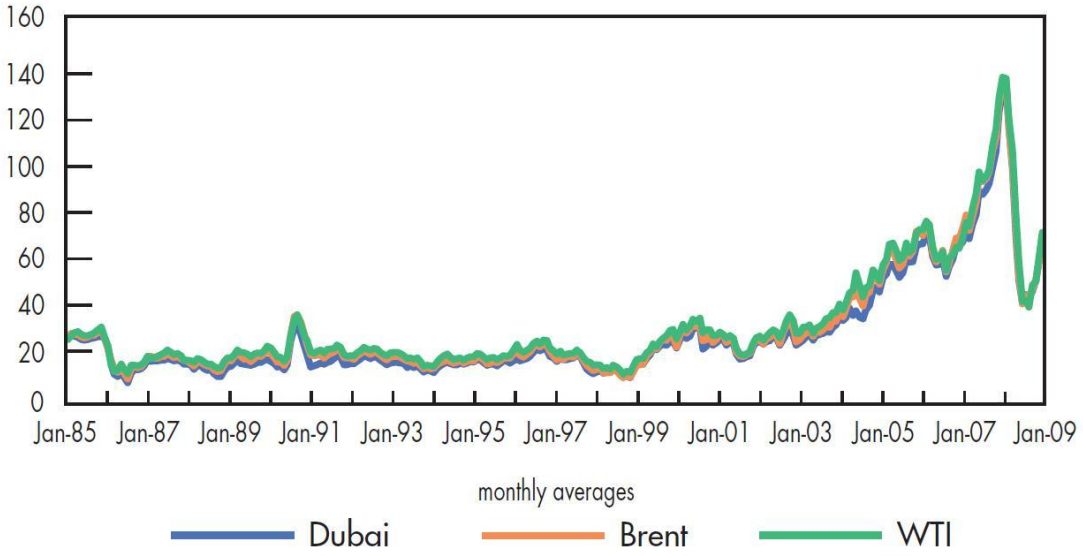

Figure 1.1 Variation of the Crude Oil Spot Prices in US Dollars/barrel (1)

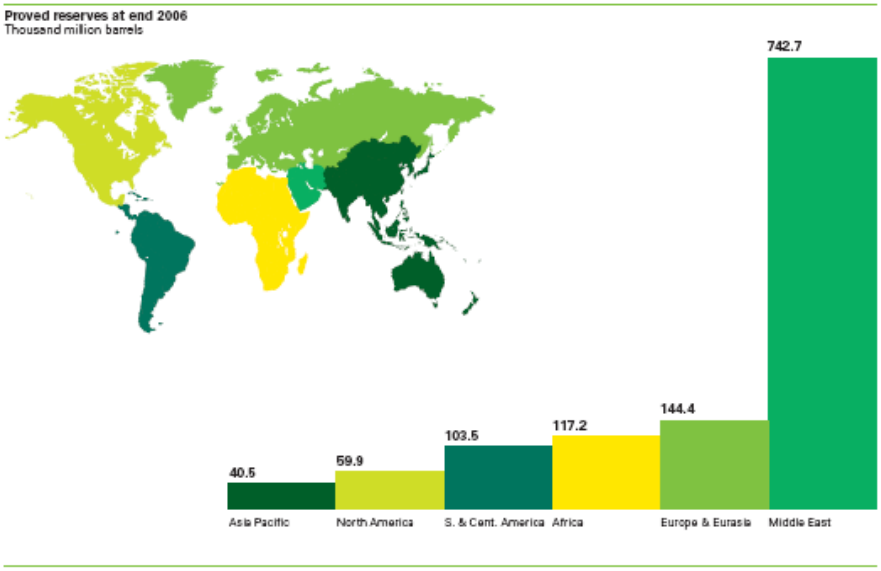

Figure 1.2 Proved oil reserves at the end of 2006 (2)

Despite all these data, it seems that the demand of fossil fuels will increase according to "World Energy Outlook"(3) elaborated by the International Energy Agency (IEA). However, as it can be observed in Figure 1.3 the use of renewable sources will also increase.

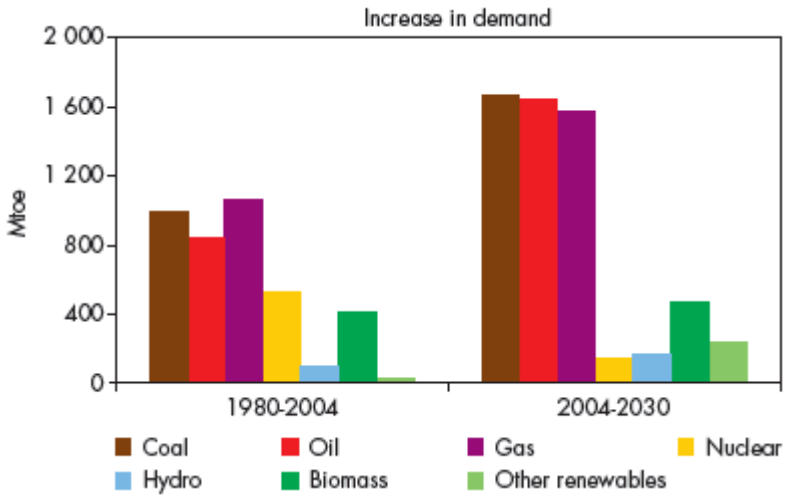

Figure 1.3 Demand of different energy sources (3).

Apart from all these data, there are evidences that the climate of the planet is changing due to the global warming. The temperature of the earth is increasing, and the ice of the poles is beginning to melt; all these changes are attributed to the Greenhouse Effect.

There are several Greenhouse Effect gases (water vapor, carbon dioxide, methane, and nitrous oxide) but it is the CO_2 concentration which is rising in the largest proportion as it can be seen in Figure 1.4.

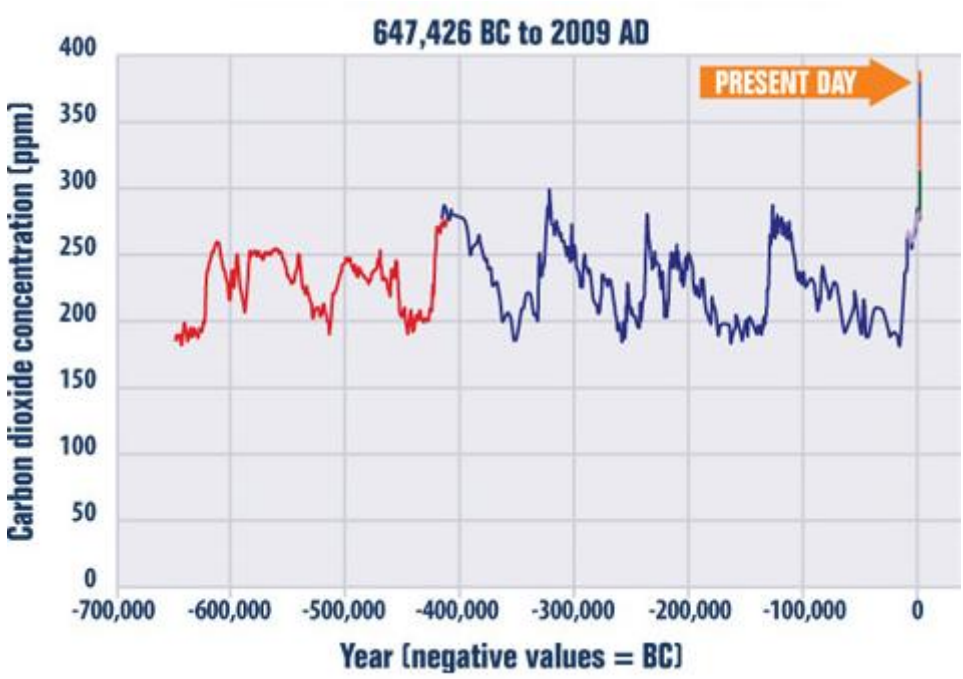

Figure 1.4 CO_2 concentration evolution in the last 400000 years (4).

Besides, it can be seen that the 82 % of the anthropogenic CO_2 emissions are due to fossil fuel combustion so it is clear that alternative energy sources are needed. One possible alternative is the use of biofuels.

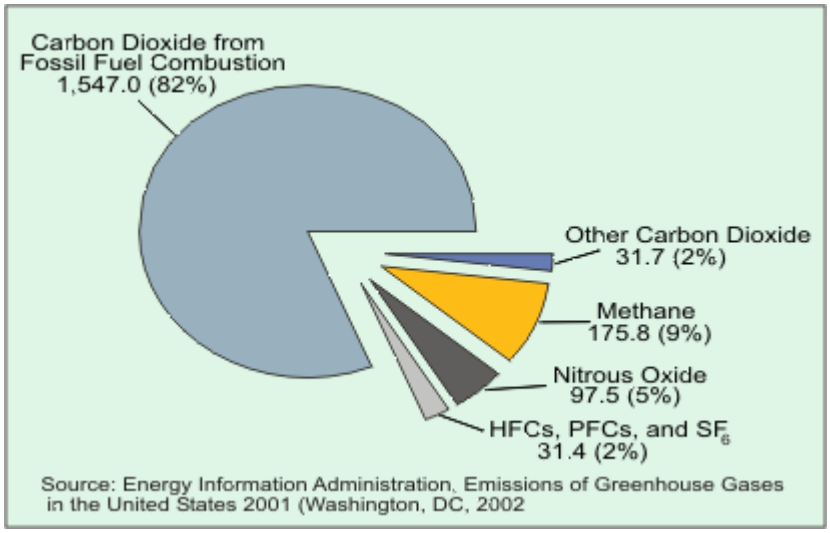

Figure 1.5 U.S. Anthropogenic Greenhouse Gas Emissions.

1.2 Use of biofuels

In the last years, research on alternative fuels for automotive motor engines is rising due to an increase in both the price of petroleum and the environmental concerns.

A biofuel can be broadly defined as a solid, liquid, or gas fuel derived from recently dead biological material, most commonly plants. This distinguishes it from fossil fuels, which are derived from long dead biological material.

Plants use photosynthesis to grow and produce biomass. During the day, plants catch CO_2 and emit O_2 and during the night this process is reversed. The net balance is that plants catch more CO_2 than the quantity they emit, using the accumulated carbon dioxide to grow them up. For this reason it is said that the net balance of CO_2 emissions for biofuels is neutral, since the emitted carbon dioxide by cars was previously caught from the atmosphere by the plants.

On the other hand, it is said that biofuels are a renewable energy source since the plants could be replaced so they would be an endless source of energy. Depending on the type of the plants and on the followed strategy, two different types of liquid fuels can be obtained for transportation: bioalcohols and biodiesels.

1.2.1 Bioalcohol

Bioalcohols, most commonly ethanol and less commonly propanol and butanol, are manufactured from the fermentation of plants that are rich in sugar or starch, such us sugar cane, sugar beet, corn or maize.

Their chemical properties allow them to substitute or to be blended with fossil petrols (conventional 95-octane fuel). Depending on whether the percentage of biofuel is 5%, 10% or 85%, these blends are called E5, E10, E85, respectively and they have higher octane number since ethanol increases octane number of the blend. While the first two bioethanol blends do not require any modification of car engines, E85 can be used only in flexi fuel car engines. These engines can safely run on any combination of bioethanol and petrol, up to 100% bioethanol. They dynamically sense exhaust oxygen content, and adjust through the engine's computer systems, the spark and the fuel injection accordingly.

One important parameter for measuring the fuel energy efficiency is what is known as the "*Fossil Energy Ratio"*, which compares the energy that can be extracted from the fuel and the energy consumed in its manufacturing and distribution. It defined as the quotient between the energy contained in the fuel and the energy actually consumed in producing and distributing it.

$$Fossil\ Energy\ Ratio = \frac{Energy\ contained\ in\ the\ fuel}{Energy\ consumed\ prod.and\ distrib.the\ fuel} \qquad (1.1)$$

"*Fossil Energy Ratio"* of petrol and E5 and E85 are shown in Table 1.1.

Table 1.1 "Fossil Energy Ratio" for petrol, E5 and E 85. (5)

Fuel	***Fossil Energy Ratio***
Petrol	0.90
E5	0.91
E85	1.29

In the introduction of the section 1.2 it is explained that the balance of the emitted CO_2 is neutral due to the renewable origin of bioethanol. Furthermore, when this fuel is burned in a car engine, it gives off less sulphur compounds and heavy metals (see Figure 1.6) contributing to a reduction of the acid rain.

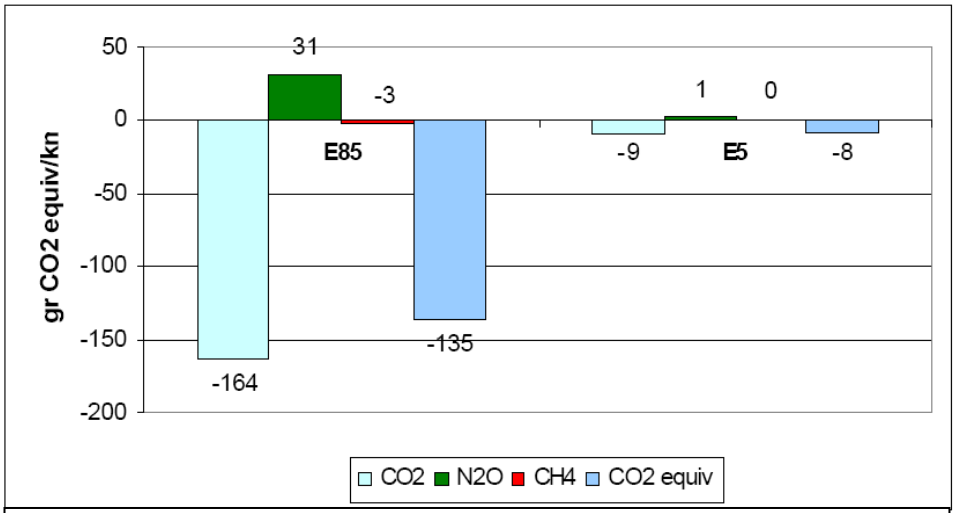

E85: 135 g CO_2 equivalent per driven km (67%)
E5: 8g CO_2 equivalent per driven km (4%)

Figure 1.6 Avoided emissions using bioethanol as automotive fuel (5).

Nowadays the main bioethanol producer is Brazil where the 40 % of this fuel al around the world is produced from sugar cane; whereas the highest bioethanol demand comes from the U.S.A.

1.2.2 Biodiesel

Biodiesel is a renewable biofuel made up of methyl or ethyl esters of long chain fatty acids; if methyl ester is used, it is named as FAME (Fatty acid methyl ester). It is obtained from the chemical reaction between methanol (or ethanol) with vegetable oils (rapeseed, sunflower, soybean, palm). This reaction is called "Transesterification reaction". (see Figure 1.7)

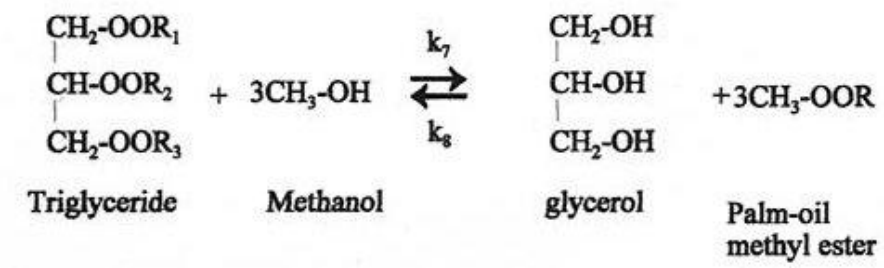

Figure 1.7 Transesterification reaction.

Biodiesel does not contain sulphur and, with respect to the diesel obtained from petroleum, it diminishes greenhouse gas emissions due to its partial renewable origin. Figure 1.8 shows relative CO_2, particulate matter (PM) and NO_x emissions for different fuel types.

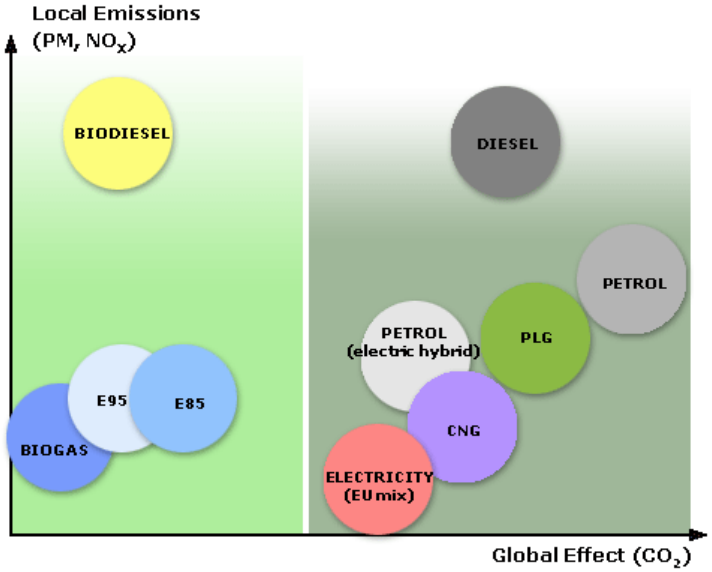

Figure 1.8 Relative CO_2 emissions (horizontal axis), and emissions of particles (PM) and NOx (vertical axis) of different fuels used in transport.

The main advantages of biodiesel use are the next ones:

- It is derived from a much cleaner fuel source and is renewable.
- It reduces the dependency on oil.
- It can be used in all diesel-engine vehicles and no motor modifications, adjustments or special regulations are required in the vehicle engine.
- It can be easily produced and stored.
- It generates between 40-80% less greenhouse gas emissions than with fossil fuels. (6)
- It increases the lubricity of the engine and the ignition point, therefore reducing the danger of explosions by gas emanation.

As well as with bioethanol, different blends exist for biodiesel and in this case they are indicated by "B" or "BD" ant then the biodiesel percentage. "B10", for example, contains 10% of biodiesel and 90% of diesel coming from oil. Sometimes after the percentage number there is another indication like "A1" or "A2". A1 indicates that the used biodiesel was obtained from raw vegetable oils whereas "A2" indicates that the biodiesel was obtained form used vegetable oils.

As in the case of bioethanol, the Fossil Energy Ratio of biodiesels is higher than the conventional diesel one as it can be seen in Table 1.2.

Table 1.2 Fossil Energy Ratio for diesel and different blends of biodiesel. (5)

Fuel	***Fossil Energy Ratio***
Diesel	0.97
BD5A1	1.00
BD10A1	1.04
BD100A1	3.86
BD5A2	1.01
BD10A2	1.06
BD100A2	21.86

The main disadvantages of diesel or biodiesel fuels are the NO_x compounds and particles emissions which are really harmful from the environmental point of view. After several tests, it seems that NO_x emissions are correlated with the unsaturation of fatty esters (7). For this reason legislation is becoming stricter in order to limit this impact. One possibility to overcome this problem is the use of suitable additives.

1.3 The use of additives in diesel & biodiesel fuels.

As it is explained in section 1.2.2, biodiesel is an alternative fuel obtained from vegetable oils or animal fats and it has several technical advantages over petro-diesel such as the reduction of exhaust emissions, improved lubricity and biodegradability, higher flash point and reduced toxicity. There are some other properties like cetane number, gross heat of combustion and viscosity that are very similar in biodiesels and in conventional diesels. In terms of oxidation stability, nitrogen oxides emissions, energy content and cold weather operability the biodiesels are inferior to conventional diesels (8).

There are different alternatives in order to enhance the properties of biodiesels like the use of petrodiesel blends, feedstock modification and the employment of additives (8). However, it must be taken into account that the developed additives for conventional diesels are generally ineffective when they are used with biodiesels (8).

1.3.1 Different types of additives

A vast variety of fuel additives are added to diesel fuels to improve the engine efficiency and to reduce harmful emissions. An important group of diesel additives are metal-based ones that have been used as combustion catalysts for hydrocarbon fuels. These metals are manganese, iron, copper, barium, cerium, calcium and platinum which present catalytic activity in combustion process (9;10). The presence of this type of additive reduces diesel engine pollutant emissions and fuel consumption. The metallic function can react with water to produce hydroxyl radicals, enhancing soot oxidation, or can react directly with the carbon atoms in the soot lowering the emissions (9). However, non-metallic, renewable ashless diesel combustion enhancer additives would be the best option, avoiding the emission of metallic compounds.

Nowadays ethers like MTBE and ETBE are the most well known oxygenated additives for gasoline. ETBE is synthesized by mixing ethanol and isobutylene and it offers better characteristics than the ethanol being less volatile and more miscible with the gasoline.

Ethanol-diesel blend fuel has been studied because ethanol contains 34.3 % of oxygen (11) so it can reduce the emission of particulate matter (PM) in the diesel engine (12). Ethanol is an appropriate additive for petrol engines due to its high octane number but

its low cetane number and its high heat of vaporization resists self-ignition in diesel engines (11). Besides that, ethanol – diesel blends are rather instable even at low temperatures (13). An alternative to ethanol as oxygenated bio-additives for diesel fuel could be different dieters like acetals (1,1 diethoxy ethane and others).

1.3.2 Acetals as diesel fuel additives

Acetals can be obtained following several ways:

- Reacting methyl 9,10-dihydroxystearate and long chain aldehydes obtaining the corresponding cyclic acetal (14).
- Reacting glyoxylic acid with aliphatic alcohols using cationic exchange resins as catalysts (15).
- From allylic ethers using as catalysts cobalt compounds (16).
- Reacting aldehydes and ketones with trimethyl/triethyl orthoformate at room temperature in the presence of copper(II) tetrafluoroborate as catalyst (17).
- Reacting ethanol and acetaldehyde in the presence of an acid catalyst. The aldehyde can be obtained from its corresponding alcohol via partial oxidation or via dehydrogenation so the origin of the acetal can be totally bio/renewable. The main reaction implies the production of 1,1 diethoxy ethane and water (18-23).

1,1 diethoxy ethane (known as "acetal") has been used as a solvent, as an intermediate in chemical synthesis for the protection of the carbonyl group in ketones and aldehydes, in the fragrance industry as well as in alcoholic drinks like brandy or in several liquors (18). However, it seems that it offers good properties to be used as diesel additive.

Apart from these uses, 1,1 diethoxy ethane is completely miscible in diesel fuel and its viscosity and auto-ignition temperature seems to be quite promising. Acetals with longer alkyl branches show higher viscosity on a molecular weight basis compared to branched alkanes (14). The main characteristics of this compound are shown in Table 1.3.

Table 1.3 Main properties of 1,1 diethoxy ethane (18)

Molecular formula	$C_6H_{14}O_2$
Density (g/mL at 25 ºC)	0.831
Boiling point (ºC)	103
Melting point (ºC)	-100
Relative density (diesel fuel)	≈ 1
Solubility in water (g/100 mL)	5.0
Vapor pressure (kPa at 20 ºC)	2.7
Relative vapor density (air = 1)	4.1
Flash point (ºC)	-21
Auto-ignition temperature (ºC)	230
Explosive limits (vol % in air)	1.6-10.4

Acetals are produced via homogeneous catalytic processes using as catalyst strong mineral acids such as H_2SO_4, HF, HCl or p-toluensuphonic acid (13;20;24). Kaufhold et al. explain in a patent (20) an industrial process for acetal production. In this process, apart from a homogeneous strong acid catalyst, an entrainer (hexane, pentane) is used having a boiling point of from 25 ºC to 75 ºC. This entrainer must be water insoluble (<3% soluble in water), thus the water is continuously removed from the reacting phase shifting the reversible reaction to the desired direction. However, these processes entail corrosion problems, are uneconomical and they are not environmentally friendly. The use of a heterogeneous catalytic process would overcome all these problems so, nowadays, several solid acid catalysts are being tested.

1.3.3 Solid catalysts for acetal production

One of the first heterogeneous catalytic process for acetal production was described by Andrade et al. (23) in 1986. In this patent an acetal production process from saturated or unsaturated aldehydes and alcohols using strongly acidic ion exchange resins or zeolites is explained. The reaction takes place in the liquid phase and after removal of the catalyst the conversion mixture is extracted by means of water and by means of water insoluble organic solvents. This process is valid for certain alcohols and aldehydes:

- An aldehyde of the formula:

  $$R_1\text{-CHO}$$

  Where R_1 is a straight chain alkyl group having 1 to 3 carbon atoms or alkenyl group with 2 or 3 carbon atoms is reacted with an alcohol of the formula:

  $$R_2\text{–OH}$$

In which R_2 is an alkyl group of 1 or 2 carbon atoms.

The method of this invention serves particularly well for the preparation of acetals of the formula:

$$R_1\text{-}CH\text{-}(OR_2)_2$$

In terms of catalyst requirement it is recommended to use at least 1.0 g of ion exchange resin and 0.5 g of zeolites per mol of aldehyde used.

In order to find some new active, selective and stable solid acid catalysts for acetal production, Capeletti et al. (18) reported the performance of several solid acid catalysts of various types, from commercial, natural and laboratory sources shown in Table 1.4.

Table 1.4 Properties of the catalysts (18)

Catalyst	**Surface area** ($m^2\ g^{-1}$)	**Pore vol.** ($mL\ g^{-1}$)	**Acidity** ($meq\ g^{-1}$)
A15. Polystyrene-polydivinylbenzene sulphonic resin, Rohm & Haas	45	0.360	4.7
Acid-treated montmorillonite, Aldrich	345	0.564	0.273
Mordenite, Norton	436	0.210	0.649
Acid treated montmorillonite, natural	235	0.262	0.640
Zeolite FCC cat., Fresh BR1160, Engelhard, UCS: 24.72 Å	342	0.259	0.540
Zeolite FCC catalyst, Isoplus 1000, Engelhard, UCS: 24.40 Å	336	n.a.	0.474
Amorphous FCC catalyst, HA-HPV, Ketjen 25 % Al_2O_3	454	0.688	0.382
Amorphous FCC catalyst, LA-LPV, Ketjen 12 % Al_2O_3	559	0.642	0.350
Equilibrium zeolitic FCC catalyst, BR1160, Engelhard, UCS: 24.31 Å	175	0.213	0.065
Equilibrium zeolitic FCC catalyst, Octavision, FCC S.A., UCS: 24.24 Å	151	0.120	0.160

After characterizing all these catalysts and determining their acidity, their catalytic performances were evaluated by means of experiments reacting ethanol and acetaldehyde. As a conclusion, Capeletti et al. proved that A15 ion exchange resin show better performance than other catalysts reaching equilibrium values much faster than with the others. They also observed that water, a reaction product, seems to have an inhibitory effect on the reaction rate (15;18)

In a review made by Sharma (25) it is explained how ion-exchange resins, particularly the macroporous variety, are suitable catalysts for oligomerization of olefins, cross-

dimerization of olefins, acetalization and ketalization reactions…offering high selectivity rates. Resin catalysts can be used in batch or semi-batch reactors as well as in continuous fixed, expanded or fluidized bed reactors. The heterogenized acidity can exceed the value of 100 % H_2SO_4. In Table 1.5 Hammett acidity function (H_0) for various acids used as catalysts is shown.

Table 1.5 Values of Hammett acidity function (H_0) (25).

Acid	**H_0**
p-Toluenesulfonic acid	+0.55
Montmorillonite	
Natural	1.5 to -3.0
Cation exchanged	-5.6 to -8.0
Amberlyst 15	-2.2
Sulfuric acid (40 %)	-2.4
Sulfuric acid (100 %)	-12.3
Nafion	-11 to -13
NY Zeolites	-13.6 to -12.7
$H_3PW_{12}O_4$ and $Cs_{2.5}H_{0.5}PW_{12}O_{40}$ (HPA)	-13.16
Lanthanum and cerium exchanged	
HY zeolites	<-14.5
Fluorosulfonic acid	-15.07
Sulfated zirconia	-16
H_3SO_3F-SbF_5	-20

However, acetalization reactions offer really low equilibrium conversions (around 50 % depending on the operating conditions) if they are carried out in a conventional batch reactor (18;19;21;22;25). In order to enhance the performance of the acetalization reaction, innovative reaction systems are required. According to the literature reactive distillation processes as well as reactors integrating dehydration membranes seem to be the most promising systems (21;22;25-33).

1.4 Innovative reaction systems for acetalization reactions

As it is explained in section 1.3.3 low equilibrium conversions are obtained for acetalization reactions using conventional batch reactors so innovative reaction systems like reactive distillation or reactors integrating dehydration membranes are required in order to achieve high conversions. In these both systems the reaction products, or at least one of the products, are being removed from the reaction shifting the reaction in the forward direction according to Le Chatelier's law.

1.4.1 Reactive distillation

Reactive distillation (RD) has become an interesting alternative to some conventional processes, especially for those that present high thermodynamic limitations like the acetalization reaction as well as etherification and esterification reactions. RD combines chemical reaction and thermal separation in the same unit. Thus, the reaction products are being removed from the reaction mixture and thermodynamic limitations can be overcome achieving high conversions.

Sharma and Chopade (21;22) and Dhale et al. (34) used RD columns for acetalization reactions achieving high conversions. Also Calvar et al. (26) and Klöker et al. (35) showed the benefits of using reactive distillation systems in similar reactions like esterification of acetic acid with ethanol and in the synthesis of ethyl acetate.

RD presents several advantages:

- Capital savings associated to the integration of reaction and separation in just one unit.
- Achievement of high conversions. Benefit associated to lower recycle costs.
- Improved selectivity. Removing the products from the reaction volume, side reactions can be limited.
- Significantly smaller catalyst requirement for the same degree of conversion.
- Heat integration benefits. In case of exothermic reactions, the reaction heat helps reducing the reboiler duty.

However, RD has some difficulties and constraints:

- Volatility constraints. The compounds must have suitable volatilities in order to keep high reactant concentrations and low product concentrations in the reaction mixture.

- Residence time. If the required residence time is too long the column dimensions must be really large.

Normally, the catalytic section is placed in the middle of the column having two different feed streams, one just above of the catalytic section and the second one just below the catalytic section. A scheme of a typical RD column is shown in Figure 1.9.

The most volatile reactant is introduced through the lower feed point while the less volatile reactant is introduced through the top feed point. However, the column can have a single feed stream feeding a mixture of the reactants. This feeding configuration must be studied in order to observe different system performances and choose the best option.

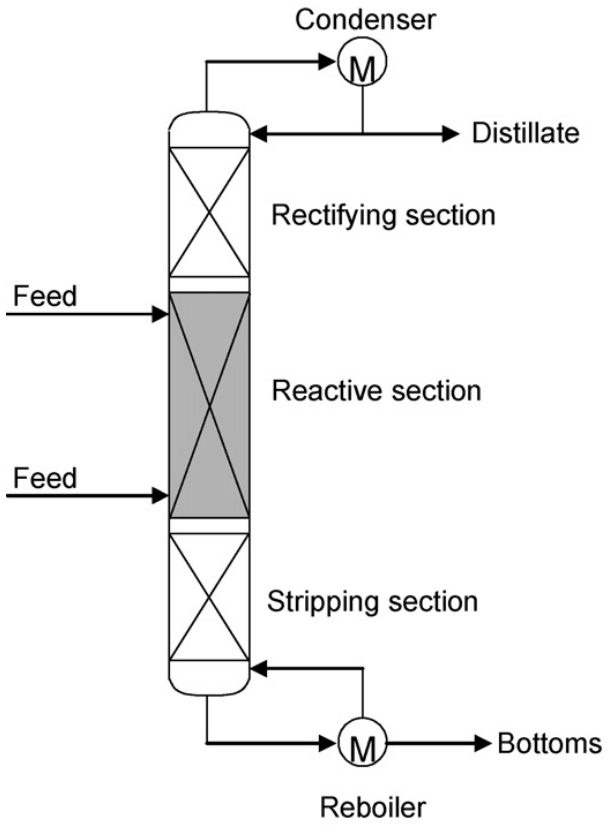

Figure 1.9 A schematic diagram of a typical reactive distillation configuration.

1.4.1.1 Reactive section

As it is explained in section 1.3.3, Capeletti et al. (18) and Sharma (25) concluded that the best catalysts for acetalization reactions were ion-exchange resins. According to the literature, it seems that these resins are the most suitable ones to be used in the acetals production throughout reactive distillation (21;22;25;26;34) being Amberlyst 15 the most tested commercial resin for this purpose. Also Indion 130 has been tested by

several researchers (15;21;22) but Mahajani (15) concluded that the performance of both macroporous resins was almost equivalent as they have similar properties (see Table 1.6).

Table 1.6 Physical properties of Amberlyst 15 and Indion 130 (15).

Properties	**A15**	**Indion 130**
Size (mm)	0.5	0.55
Internal surface area (m^2/g)	55	
Weight capacity (meq. W/g)	4.7	4.8
Crosslinking density (% DVB)	20-25	
Porosity (%)	36	
Temperature stability K	393	403

After choosing the catalyst, another important issue is the way of placement of the resin. Usually the particle size is in the range of 0.5-3 mm so, a simple catalytic bed would offer unacceptable pressure drops. Taylor & Krishna (36) summarizes in a review the most common configurations for the reactive section of a reactive distillation process.

- Porous spheres filled with catalyst. (see Figure 1.10(a))
- Cylindrical shaped envelopes with catalyst inside them. (see Figure 1.10(b))
- Wire gauze envelopes with various shapes: spheres, tablets, doughnuts, etc (see Figure 1.10(c))
- Horizontally disposed wire-mesh "gutters", filled with catalyst. (see Figure 1.11 (a)).
- Horizontally disposed wire-mesh tubes containing the catalyst. (see Figure 1.11(b))
- Catalyst particles enclosed in cloth wrapped in the form of bales. (see Figure 1.12)
- Structured packing. Catalyst particles sandwiched between corrugated sheets of wire gauze (Katapak S). (see Figure 1.13)
- Structured packing Katapak SP. Similar to Katapak S but its modular design allows varying the catalyst amount (different number of modules) and the separation efficiency. (see Figure 1.14)
- Another option is to make Raschig rings catalytically active (see Figure 1.15 (a)). The catalyst rings can be prepared by block polymerization in the annular space. Also, another option is to coat structured packing with zeolite catalysts. (see Figure 1.15 (b)).

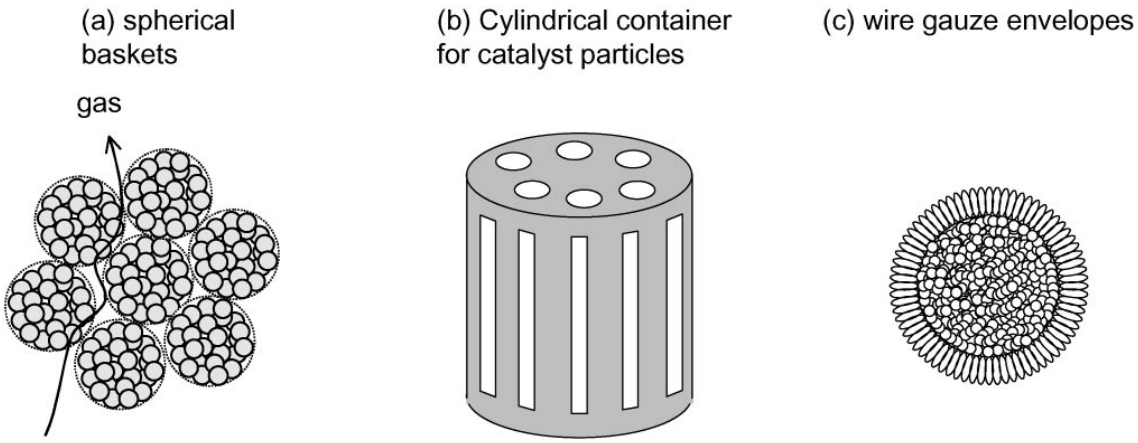

Figure 1.10 Various "tea-bag" configurations. Catalyst particles need to be enveloped in wire gauze packings and place inside RD columns.

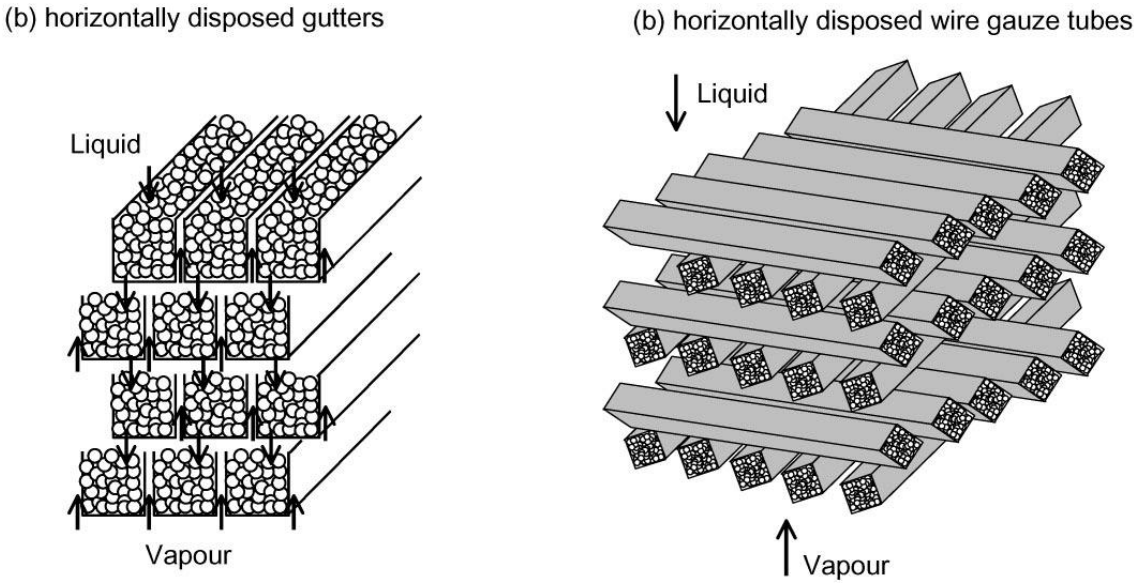

Figure 1.11 Horizontally disposed (a) wire gauze gutters and (b) wire gauze tubes containing catalyst.

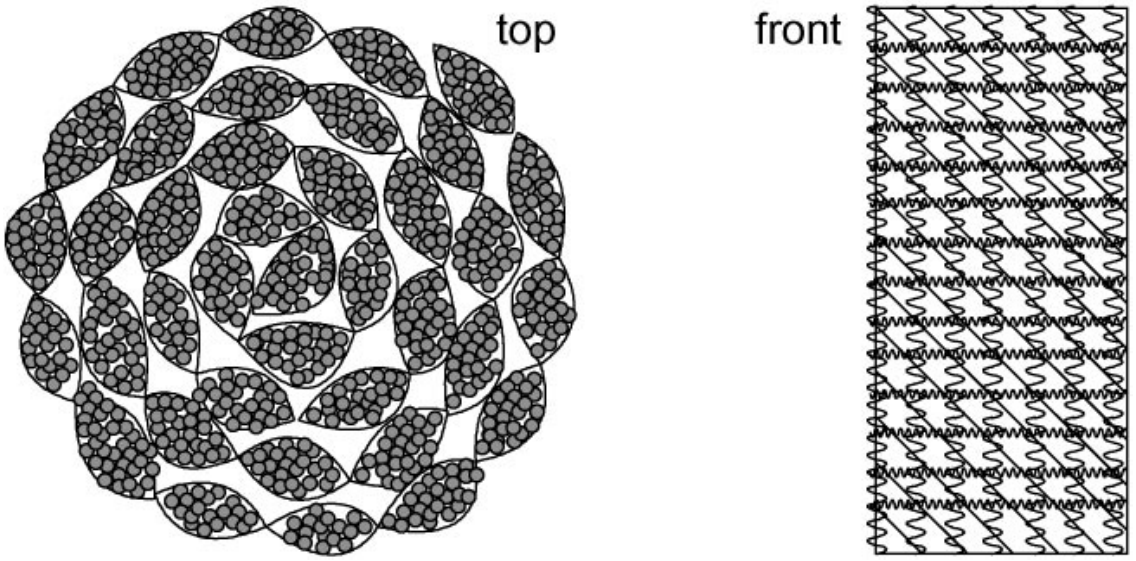

Figure 1.12 Catalyst bales.

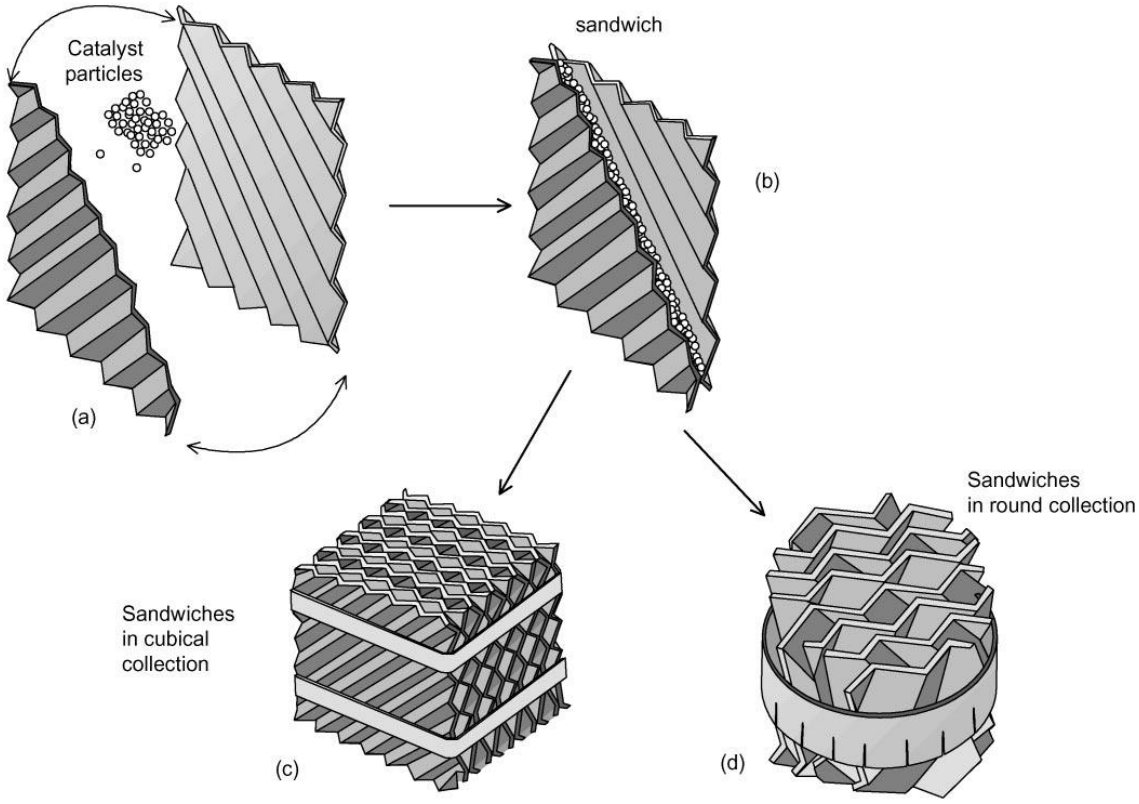

Figure 1.13 Structured catalyst-sandwiches (Katapak S). (a) Catalyst sandwiched between two corrugated wire gauze sheets. (b) The wire gauze sheets are joined together and sewn on all four sides. (c) The sandwich elements arranged into a cubical collection. (d) The sandwich elements arranged in a round collection.

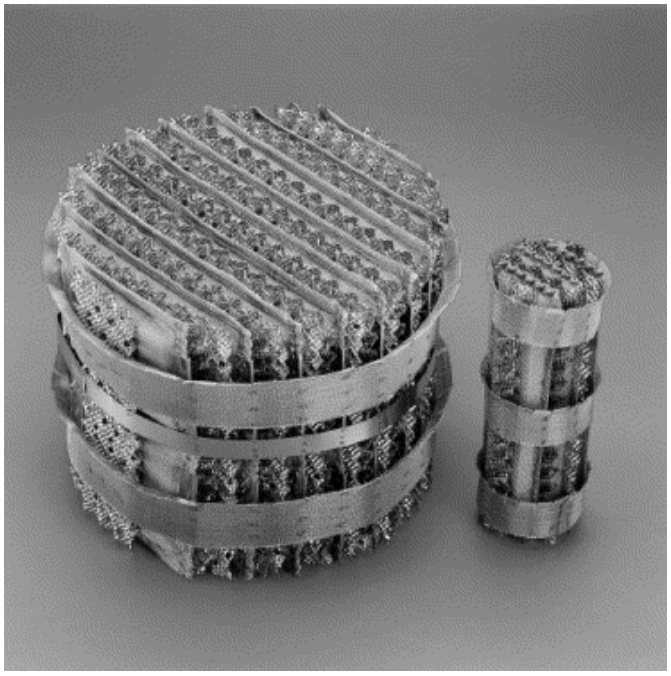

Figure 1.14 Structured packing Katapak SP.

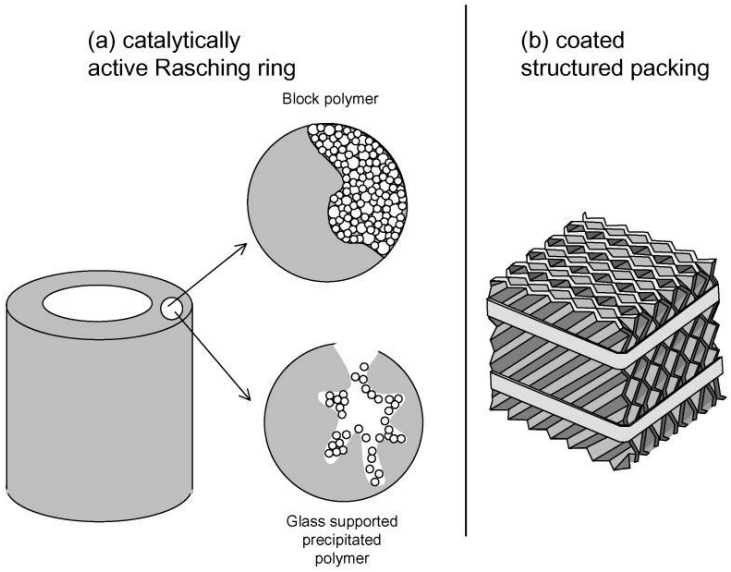

Figure 1.15 (a) Catalytically active Raschig ring. (b) Structured packings coated with catalyst.

The use of structured packing seems to be one of the most suitable options due to its low pressure drop and its high throughput (35). However, when compared to conventional non-reactive structured packings, the specific surface area is moderate. This type of packing presents a really good radial distribution of the liquid phase. Besides, when the catalyst is spent and the columns must be shut down, the packing can be easily removed and replaced by another module.

1.4.1.2 Design considerations

Reactive distillation systems are rather more complex than conventional chemical reactors or simple distillation columns. The introduction of an in-situ reaction and separation system leads to complex interactions between vapor-liquid equilibrium, vapor-liquid mass transfer, intra-catalyst diffusion and chemical kinetics.

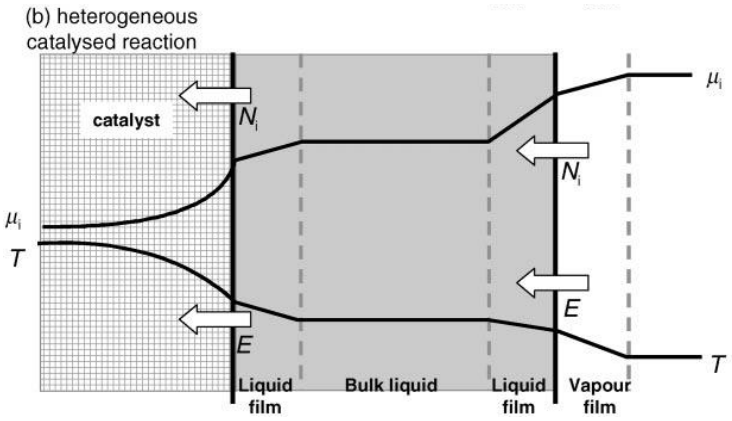

Where:

E is energy flux, $W \cdot m^{-2}$

N_i is molar flux of species *i*, $mol \cdot m^{-2} \cdot s^{-1}$

T is temperature, K

μ_I is chemical potential, $J \cdot mol^{-1}$

Figure 1.16 Transport process in a heterogeneously catalyzed reactive distillation process.

Because of this complexity, the benefits of a reactive distillation process could disappear if proper feed stage, reflux, amount of catalyst, boilup rate, etc are not chosen.

There are some practical aspects that must be taken into account in order to obtain satisfactory results:

1. *Installation and removal of the catalyst.* In case of catalyst deactivation, the regeneration usually takes place out of the column so the RD column must be correctly designed in order to change the catalyst from the reacting section in an easy way.
2. *Efficient contacting of liquid phase and catalytic particles.*
    - Liquid maldistribution can generate more severe effects in RD processes than in conventional distillation processes, so, good liquid distribution is essential as well as the avoidance of channeling effects.
    - Good radial dispersion of liquid through the catalyst bed avoids the appearance of hot spots. A good packing choice is essential in this case. Structured packings like Katapak S or Katapak SP contribute to avoid this effect, guaranteeing good radial liquid dispersion.
3. *Good vapor-liquid contact in the reactive zone.* If the reaction rate is fast and the reaction is equilibrium-limited then the required size of the reactive zone is

strongly influenced by the effectiveness of the vapor-liquid contact. Vapor-liquid contact becomes less important for slower reactions.

4. *Low pressure drop.* In order to avoid intra-particle diffusion limitations small particle size is used (0.5 – 1.0 mm) but they must be carefully placed in order to avoid high pressure drops as well as flooding problems. The use of structured packings helps for this purpose.
5. *Enough liquid hold-up in the reactive section.* Liquid hold-up, mean residence time, and liquid residence time distribution in the reactive section are all important in determining the conversion and selectivity of RD.

1.4.2 Membrane reactors

While reactive distillation systems are based on reaction and thermal based separation, membrane reactor technology is based on reaction and a barrier based separation. In principle, membrane based processes require much less energy supply reducing considerably the operating costs. However, it must be taken into account that in membrane technology processes, the capital costs could be much higher so a study of the life cycle of the membrane is required in order to evaluate all the economic aspects.

Membranes have gained an important place in chemical technology and are used in a broad range of applications. The key property on which this technology is based is the ability of a membrane to control the permeation rate of chemical species through it. In separation applications, the goal is to favor one component of a mixture to permeate the membrane, while hindering permeation of the other components. (See Figure 1.17)

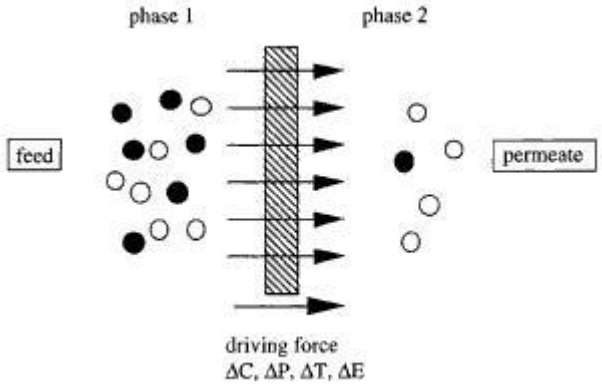

Figure 1.17 Schematic representation of a two-phase system separated by a membrane (37).

There are four different types of membrane separation processes that could be used: Nanofiltration, pervaporation, vapor permeation and gas separation. The differences between these four processes are found in the phase, type of compound to be separated and in the thermodynamic conditions of the feed mixture.

- Nanofiltration, is used when low molecular weight solutes such as inorganic salts or small organic molecules (such as glucose and sucrose) have to be separated from a solvent. The Nanofiltration membranes can be considered as being intermediate between open porous types of membrane (microfiltration/ultrafiltration) and dense nonporous membrane (pervaporation/gas separation).
- Pervaporation: a liquid mixture (feed) contacts one side of a membrane while permeate is removed as a vapor from the other. The process driving force is the low vapor pressure on the permeate side of the membrane generated by evacuation, cooling and condensing the permeate vapor.
- Vapor permeation: is comparable to pervaporation, however, in this case, the liquid feed to be separated is pre-evaporated and a saturated or near saturated vapor phase gets directly in contact with the membrane surface.
- Gas separation: the feed mixture is in the gas phase, the partial vapor pressures of all components in the feed mixture are far below saturation. The gradient in partial vapor pressure is usually maintained by an increase of total feed side pressure. The permeate is not condensed and it is removed as a gas.

For acetalization reactions dehydration membranes would be suitable in order to separate water from the reaction mixture and thus, shift the reaction to the forward direction.

$$Alcohol + Aldehyde \leftrightarrow Acetal + Water$$

As the reaction takes place in liquid phase, the water separation process can be studied using a pervaporation process or a vapor permeation process. However, in the literature, most of the articles show pervaporation as the most suitable process for water removal for similar reactions like esterification, ketalization or etherification (38). No references for acetalization reactions were found. A simple scheme of the process is shown in Figure 1.18. As the feed is in the liquid phase pervaporation is preferred above vapor permeation.

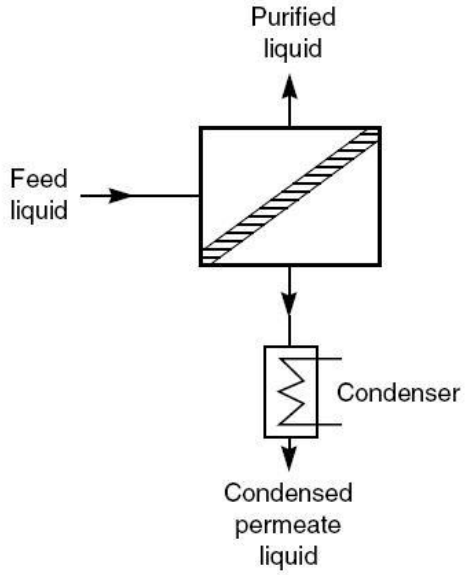

Figure 1.18 Schematic diagram of the basic pervaporation process. (38)

One of the first processes using a dehydration membrane was the water removal from ethanol-water mixtures. Water and alcohols form azeotropes but by means of pervaporation, all the problems of azeotropic distillation are avoided achieving high separation yields at low costs.

In the recent years several dehydration membranes were developed in order to apply them in etherification and esterification processes. In principle two big classifications can be made, the first one depends on the membrane material (ceramic or polymeric) and the second one depends on the reaction taking place in the membrane or not.

1.4.2.1 Catalytic or non-catalytic dehydration membranes

In pervaporation systems, the reaction and the separation can be carried out following different configurations:

1. Passive membrane in recycle loop: it is the most common option (see Figure 1.19(b)). The reaction takes place in a conventional reactor and then the desired or undesired product is separated in a membrane module.
2. Passive membrane in reactor: the reaction and separation are carried out in the same unit using non-catalytic membranes and keeping catalyst particles as slurry in the reaction media.
3. Active membrane in reactor: when the reaction and separation takes place in the same unit using catalytically active membranes (Figure 1.19(a)).

With regards to the level of complexity, the first configuration is the simplest one and the last one is the most complex one showing some limitations. On the one hand there is one degree of freedom less than using non-catalytic or inert membranes since the catalyst amount – membrane area ratio uses to be fixed. On the other hand, if the catalyst is deactivated the whole membrane must be replaced and vice versa, if the selective separation layer is damaged for a certain reason it must be replaced including the catalyst. These aspects could represent really big inconveniences at industrial scale. Moreover, due to this complexity, the time to market of catalytically active membranes will be longer than the non-catalytic membrane ones. In terms of the second configuration, passive membranes in reactor, the main issues are to have impact resistant membranes in case of slurry reactors and the design constraints that the presence of catalyst particles implies in case of multi-tube membranes.

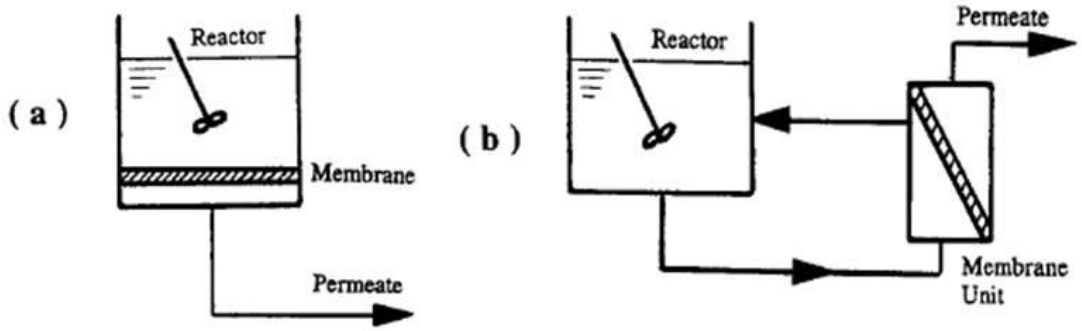

Figure 1.19 (a) An idealized batch membrane reactor. (b) Its equivalent integrating a membrane unit with a batch reactor (28).

Esterification reactions are the main class of reactions that have been studied in pervaporation membrane reactors (PVMR) (29). In a catalytic membrane, the selective permeation and the catalytic functions is recommended to be in two different layers (see Figure 1.20) to achieve a good separation yield and a good catalytic performance. In order to achieve high separation selectivities the diffusion of the reactants and the desired product inside the material should be low, whereas from the catalytic point of view, high diffusion of the reactants and products is required. Thus, the selective permeation layer and the catalytic layer can and have to be optimized independently (39;40)

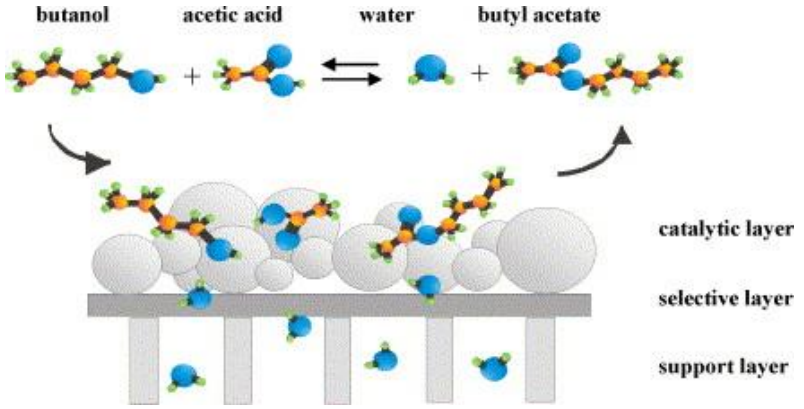

Figure 1.20 Schematic representation of the esterification reaction between acetic acid and butanol in a composite catalytic membrane reactor (39).

In 1993 Bagnell et al. (41) studying the esterification of acetic acid with methanol and n-butanol, concluded that catalytically active membranes show higher permselectivities for water at the same or higher flux, compared to when no reaction was taking place within the membrane phase.

In 1996, Zhu et al. (27) modeled a continuous PV membrane reactor for the esterification of acetic acid and ethanol achieving also higher reaction conversions than the ones predicted by thermodynamics. In this case, they also modeled the reaction and separation processes in the same unit.

In 2005 Peters et al. (39) developed a zeolite-coated pervaporation membrane depositing zeolite H-USY layers on a silica membrane by dip-coating using TEOS and Ludox AS-40 as binder material. This membrane was tested in the esterification reaction between acetic acid and butanol. The catalytic activity of the membrane was comparable to the activity of the bulk zeolite catalyst. However, the performance of the system could be improved using a more active catalyst.

On the other hand, other authors have studied pervaporation processes apart from the reaction unit achieving also high efficiencies. Domingues et al. (30) studied the esterification of benzyl alcohol with acetic acid achieving 96 % separation efficiency in water and a reaction conversion of 99 %. Benedict et al. (31) studied the esterification of lactic and succinic acids with ethanol using a pervaporation unit. Removing water from the reaction mixture, they obtained reaction conversions very close to 1. High water fluxes through the membrane were obtained maintaining high recirculation rates and low permeate pressures. Sanz and Gmehling (32;33) studied the esterification of

acetic acid with isopropanol removing the water formed using a pervaporation membrane. Also in this case, conversions above 90 % were achieved.

As it can be observed, both types of configurations offer good reaction conversions (above 90 % in all the cases) and shift of the equilibrium. However, if the reaction and separation could be coupled the process would be more integrated and efficient since in one unique unit two different processes would happen: reaction and separation.

1.4.2.2 Membrane types

Another important classification concerns the membrane material. In principle there are two important membrane material groups, ceramic and polymeric ones.

Broadly speaking, polymeric membranes may have the desired selectivity but they often lack the ability to withstand reaction conditions (temperature, concentrations, pH…). Polyvinyl alcohol is currently the most used and commercially available polymeric membrane material, but permeances are generally lower than for ceramic membranes (42;43). On the other hand, micro porous inorganic membranes are able to resist harder operating conditions but their separation selectivity used to be lower (43). Sommer & Melin (44) show a great application potential of inorganic membranes in many molecular separations. Moreover, they tested the great thermal and mechanical resistance that these kind of membranes offer. The only disadvantages that they found were the limited hydrothermal stability of silica and the low acid resistance of alumina rich zeolites.

According to the literature, in esterification processes where the pervaporation unit is not integrated in the reaction unit, most of the articles mention commercial polymeric dehydration membranes (30-33)

On the other hand, in those processes where the reaction and the separation take place in the same unit polymeric, ceramic and polymeric/ceramic membranes are mentioned in the literature. In 1993 Bagnell (41) used Nafion tubes as supports for both the reaction catalyst and the pervaporation membrane increasing the yield in the esterification of acetic acid with methanol and n-butanol. In 1996 Zhu et al. (27) used a polymeric/ceramic composite membrane. In this case, the membrane was not commercially available and it was prepared by dip-coating method. Polyetherimide was dissolved in dichloroethane to form a 3 wt% polymer solution. A ceramic support tube was then dipped in the polymeric solution and after 1 hour the tube was withdrawn from the solution.

In more recent articles, zeolite membranes were used as catalytic dehydration membranes. In 2002, for example, Bernal et al. (43) used H-ZSM-5 membranes for ethanol esterification and in 2005 Peters et al. (39) developed another zeolite dehydration membrane prepared depositing H-USY layers on silica membranes by dip-coating using TEOS and Ludox AS-40 as binder material.

In 2002, Moon-Sung Kang et al. (45) developed water-swollen cation-exchange membranes prepared using poly(vinyl alcohol) (PVA) / poly(styrene sulfonic acid-co-maleic acid) (PSSA-MA). Ion-exchange membranes (IEMs) have been widely used in various separation and chemical processes, such as diffusion dialysis, electrodialysis, fuel cells, etc. Nowadays the use of IEMs is increasing being the water soluble polymer based membranes suitable for pervaporation of water-alcohol mixtures (46). In 2007 Peters et al. (40) developed Amberlyst-coated pervaporation membranes by dip-coating technique in order to use them in the esterification of acetic acid and butanol.

1.4.2.3 HybSi® membranes

In the present research project HybSi® inorganic/organic hybrid membranes were used. This membrane type was developed in cooperation between the Department of Science and Technology of University of Twente, the University of Amsterdam and the "Membrane Technology Group" of "Energy research Centre of the Netherlands" (ECN). Currently this membrane development is in a pre-commercial phase.

As it is mentioned above, both inorganic and organic (polymeric) membranes show some disadvantages and HybSi® team has been working over the years to overcome common disadvantages and offer membranes for a wider application window. This has been achieved by enhancing the stability towards

- Hydrothermal attack.
- The presence of acids.
- The presence of aggressive organic solvents.

All of this results in a membrane system that is applicable in a wide range of solvents and is stable in the presence of water and acid at relatively high temperatures.
HybSi® is an organic-inorganic hybrid silica-based amorphous material. The hybrid nature of this material lies in the fact that each silicon atom is not only connected to oxygen atoms as in pure silica, but also to an organic fragment. The special feature of HybSi® is that the organic fragments are acting as integral bridging fragments of the structure, and not just as end standing groups as in the methylated silica. The result is a true hybrid silica pore network in which organic and inorganic fragments cooperate. It is

prepared by a sol-gel process from so-called bis-silyl precursors, such as BTESE ($(EtO)_3Si–CH_2CH_2–Si(OEt)_3$) and BTESM ($(EtO)_3Si–CH_2–Si(OEt)_3$) (47).

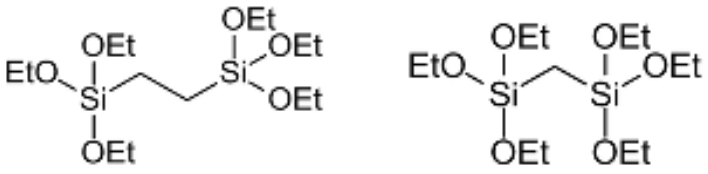

Figure 1.21 BTESE & BTESM molecular structure

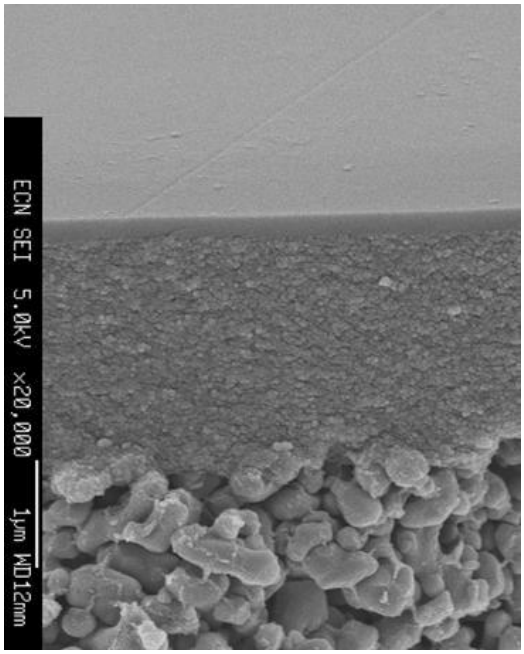

Figure 1.22 Cross-sectional SEM micrograph of the layered structure of a hybrid membrane, showing the supporting layers and the ~150 nm thick selective hybrid silica top layer.(47)

In order to test the durability of HybSi® membranes pervaporation of a 95 wt% n-butanol – 5 wt% water mixture at 150 ºC tests were performed by Castricum et al. (42;48) since inorganic and methylated silica membranes were tested at the same conditions. They could check that initial water fluxes of about 10 kg m^{-2} h^{-1} can be obtained. They observed that after a stabilization period typical for inorganic membranes, the flux changes only 4% per month (see Figure 1.23-A). The half of the flux was reached after about 500 days and the water content in the permeate remained at 98 wt%, even after 1.5 years of continuous testing. Inorganic silica and methylated silica deteriorated within weeks at 95 ºC and 115 ºC respectively (see Figure 1.23-B).

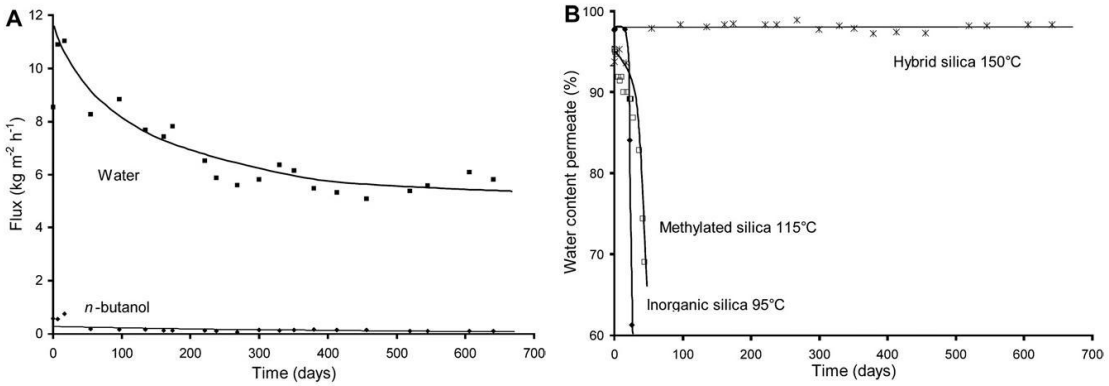

Figure 1.23 Long-term separation performance. A: water flux and n-butanol flux with HybSi® membranes. B: water content in the permeate during pervaporation of 5 wt% of water in n-butanol. (42;48)

Apart from the durability, HybSi® membranes show a great chemical resistance to the acid containing liquid mixtures. Long term pervaporation measurements were performed in the presence of HNO_3 and acetic acid (49). Figure 1.24 shows the separation performance between n-butanol and water at 95 ºC at various concentrations of HNO_3. It can be seen that the acid stability is high even at acid concentrations equivalent to a pH of about 2. Only at higher acid concentrations a decrease in the flux and selectivity is observed.

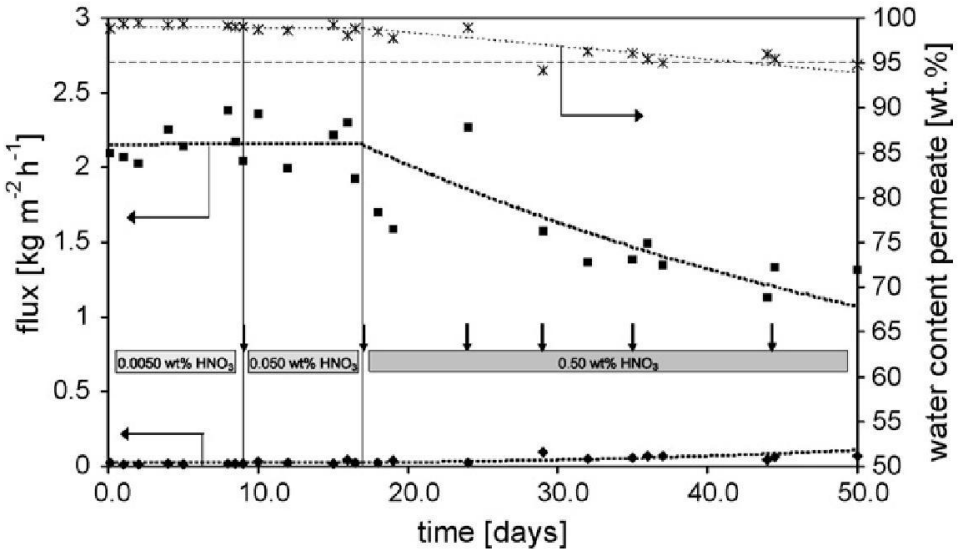

Figure 1.24 Long-term separation performance between n-butanol and water at 95 ºC in the presence of HNO_3. (49)

In terms of acetic acid, the membrane shows quite a similar behavior. In this case EtOH/H_2O (95:5 wt%) test were performed containing 0, 0.15 and 1.5 wt% of acetic acid. Figure 1.25 shows that the presence of acetic acid does not have a significant

influence on the long-term performance. Thus the acid stability of HybSi® membranes is much higher than the stability of Zeolite A membranes (50).

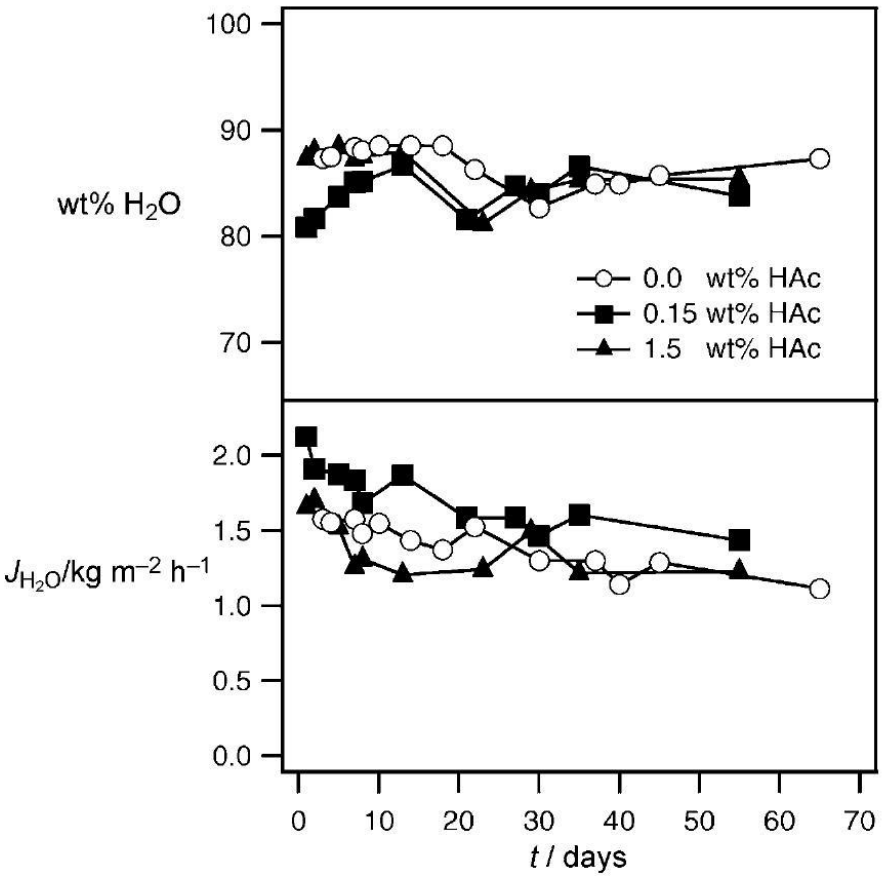

Figure 1.25 Dehydration performance of BTESM-based membranes for EtOH/H_2O mixtures containing acetic acid at 70 ºC. The water content permeate (wt% H_2O) and water flux (J_{H2O}) are shown (50).

Apart from the durability and chemical resistance HybSi® membranes present high water selectivity and a high water flux compared to other available membranes. The separation factors are around 220 and water fluxes are around 0.8-1.5 $kg \cdot m^{-2} \cdot h^{-1}$ (50). A summary of other available membranes and their characteristics is shown in Table 1.7, Table 1.8 and Table 1.9. This information was elaborated from (51) taking only part of the data corresponding to the separation of ethanol-water mixtures. It can be observed that for fluxes around 0.8-1.5 $kg \cdot m^{-2} \cdot h^{-1}$ most of the membranes are not as selective as HybSi® membranes.

Table 1.7 Dehydration of ethanol using different polymer type based membranes (51).

Polymer	Binary mix	Mass ratio	Membrane support	Separation Layer	Cross-linker/modification	Separation factor	Flux (kgm−2 h−1)	T (ºC)
Poly Vinil Alcohol	EtOH/H2O	(95:5)	PVA, PAAM	PVA, PAAM	-	45–4100	0.1–0.06	75
	EtOH/H2O	(95:5)	PESF	PVA, PAAM	-	Lower than PVA,PAAM	up to 3.8	75
	EtOH/H2O	(95:5)	PAA, PVA	PAA, PVA	-	50	0.26	50
Chitosan	EtOH/H2O	(95:5)	Chitosan/PAA	Chitosan/PAA	–	up to 19000	≈0.001	Various
	EtOH/H2O	(95:5)	PESF	Chitosan	80 min H_2SO_4 cross-linked	≈350	≈0.65	80
Alginate	EtOH/H2O	(95.4:4.6)	Na-Alg/PVP (3:1)	Na-Alg/PVP (3:1)	Phosphoric acid	364	0.09	30
	EtOH/H2O	(90:10)	Alginate based	Alginate based	Ionically cross-linked, Ca2+	300	0.230	50
Polysulfone	EtOH/H2O	(90:10)	Sodium sulfonate PSF	Sodium sulfonate PSF	Chlorosulfonic acid	≈1300	≈0.88	45
Polyimide	EtOH/H2O	(90:10)	BAPP	BAPP	–	22	0.27	25
	EtOH/H2O	(88.9:11.1)	PMDA-ODA	PMDA-ODA	Thermal treatment	346	0.014	45
	EtOH/H2O	(88.9:11.1)	PMDA-ODA	PMDA-ODA	Thermal treatment	445	0.043	75
	EtOH/H2O	(88.9:11.1)	PMDA-MDA	PMDA-MDA	Thermal treatment	47	0.023	45
	EtOH/H2O	(88.9:11.1)	PMDA-MDA	PMDA-MDA	Thermal treatment	19	0.130	75
	EtOH/H2O	(88.9:11.1)	BTDA-PDA	BTDA-PDA	Thermal treatment	1386	0.003	45
	EtOH/H2O	(88.9:11.1)	BTDA-PDA	BTDA-PDA	Thermal treatment	1594	0.005	75
	EtOH/H2O	(88.9:11.1)	BTDA-ODA	BTDA-ODA	Thermal treatment	395	0.011	75
	EtOH/H2O	(88.9:11.1)	BTDA-ODA	BTDA-ODA	Thermal treatment	562	0.022	45
	EtOH/H2O	(88.9:11.1)	BTDA-MDA	BTDA-MDA	Thermal treatment	237	0.015	75
	EtOH/H2O	(88.9:11.1)	BTDA-MDA	BTDA-MDA	Thermal treatment	478	0.035	45
	EtOH/H2O	(90:10)	BHTDA-BATB	BHTDA-BATB	–	27	0.282	35
	EtOH/H2O	(90:10)	BHTDA-BADTB	BHTDA-BADTB	–	15	0.325	35
	EtOH/H2O	(90:10)	BHTDA-DBAPB	BHTDA-DBAPB	–	141	0.255	35
	EtOH/H2O	(95:5)	PI-2080 aromatic polyimide	PI-2080 aromatic polyimide	–	900	1.0	60
Polyamide	EtOH/H2O	(90:10)	Nylon-4	Nylon-4	–	≈4.5	≈0.35	25
	EtOH/H2O	(90:10)	Nylon-4	Nylon-4/PVAc	PVA grafted, NaOH hydrolysis	≈13	≈0.40	25
	EtOH/H2O	(90:10)	Nylon-4	Nylon-4/PVA	PVA grafted	13.5	0.42	25
	EtOH/H2O	(90:10)	PASA	PASA	–	1984	0.007–0.034	20
Polyelectrolyte	EtOH/H2O	(95:5)	PAN hydrolysed with NaOH	PEI/PAA	Layer-by-layer deposition	604	0.314	70
	EtOH/H2O	(95:5)	PESF	PEI/PAA	Layer-by-layer deposition	1207	0.140	40

Table 1.8 Dehydration of ethanol using different inorganic membranes (51).

Type	Binary mix	Mass ratio	Membrane support	Separation Layer	Separation factor	Flux (kgm−2 h−1)	T (ºC)
	EtOH/H2O	(96.4:3.6)	ECN silica membrane	ECN silica membrane	350	≈1.6	70
	EtOH/H2O	(95.5:4.5)	ECN silica membrane	ECN silica membrane	208	≈1.3	71
	EtOH/H2O	(90:10)	α-alumina	PVA	≈38	≈1.05	70
	EtOH/H2O	(89.0:11.0)	Pervatech amorphous silica	Pervatech amorphous silica	160	2.00	70
Ceramics	EtOH/H2O	(89.7:10.3)	ECN silica membrane	ECN silica membrane	60	2.33	70
	EtOH/H2O	(89.9:10.1)	Mitsui (T-type zeolite)	Mitsui (T-type zeolite)	1000	0.91	70
	EtOH/H2O	(89.7:10.3)	Mitsui (A-type zeolite)	Mitsui (A-type zeolite)	18	1.12	70
	EtOH/H2O	(91:9)	α-alumina	Silica	50	0.35	70
	EtOH/H2O	(98:2)	α-alumina	Silica	160	0.15	70
	EtOH/H2O	(95:5)	Mullite, Al_2O_3, cristobalite	NaA Zeolite	> 5000	2.35	95
Zeolite	EtOH/H2O	(95:5)	α-alumina	Al_2O_3:SiO_2:Na_2O:H_2O 1:2:2:120, zeolite NaA	16	1.10	75
	EtOH/H2O	(95:5)	UV-irradiated TiO2 coated metal	Zeolite A	Up to 54000	0.86	45

Table 1.9 Dehydration of ethanol using different mixed matrix membranes (51).

Binary mix	Mass ratio	Membrane support	Separation Layer	Cross-linker/modification	Separation factor	Flux (kgm−2 h−1)	T (ºC)
EtOH/H2O	(95:5)	PVA/clay	PVA/clay	–	58	0.057	Not given
EtOH/H2O	(95:5)	PVA/clay	PVA/clay	–	112	0.039	Not given
EtOH/H2O	(96.5:3.5)	q-Chitosan	q-Chitosan	HCl catalyst to homogenise	726	≈1.3×10−6	40
EtOH/H2O	(96.5:3.5)	q-Chitosan/10mol% TEOS	q-Chitosan/10mol% TEOS	HCl catalyst to homogenise	3098	≈1.1×10−6	40
EtOH/H2O	(96.5:3.5)	q-Chitosan/10mol% TEOS	q-Chitosan/10mol% TEOS	HCl catalyst to homogenise	>35	,500 7×10−7	40
EtOH/H2O	(96.5:3.5)	q-Chitosan/10mol% TEOS	q-Chitosan/10mol% TEOS	HCl catalyst to homogenise	35	480 8×10−7	40
EtOH/H2O	(96.5:3.5)	q-Chitosan/10mol% TEOS	q-Chitosan/10mol% TEOS	HCl catalyst to homogenise	30	≈1.8×10−6	40
EtOH/H2O	(90:10)	PVA with 5 wt% APTEOS	PVA with 5 wt% APTEOS	HCl catalyst to homogenise	1580	0.0265	30

Chapter II

Objectives and Approach of the Doctoral Thesis

2 Objectives and Approach of the Doctoral Thesis

This research has two different main objectives:

1. The development of innovative and advanced reaction systems in order to achieve higher conversions than the achievable ones using conventional reaction systems when reversible reactions are involved.
2. The application and validation of these innovative approaches to reactions related to biofuels and biofuel additives optimal production.

The links between these two main objectives deal with some thermodynamic limitations that biofuel and biofuel additives production processes present. The use of innovative reaction systems could be beneficial in order to overcome them.

2.1 Development of innovative and advanced reaction systems

The use of reaction systems where the reaction and the separation of the products (or one of the products) take place in the same unit can be highly positive for catalytic reversible reactions. Removing the products (or one of the products) from the reaction unit as soon as they/it are/is produced implies the achievement of higher conversions and selectivities and therefore, a great economical saving. Reactive distillation processes and membrane reactors are two promising alternatives for this kind of reacting systems. Different partial goals have been established for each system in order to achieve the main objective:

- A continuous update of the new relevant published information, once the state-of-the-art revision is included in the previous chapter.
- Design, set up and start up of two experimental facilities at semi-pilot scale in order to be able to use them for the intended research program.
- The development of the corresponding experimental studies in order to optimize their operation and to test their adequacy for catalytic reversible reactions related to biorefinery processes.
- The conceptual and technical comparison of both reaction systems.

For the experimental tests of these non conventional reactor configurations a suitable reaction must be chosen. In the present research, an acetal formation reaction has been chosen. This kind of reactions is highly limited from the thermodynamics point of view.

2.2 Development of acetal (1,1 diethoxy butane) production processes

As it is mentioned in the "Introduction" part, acetals can be obtained following several procedures. In this project the reaction between an alcohol (ethanol) and an aldehyde (butanal) in the presence of an acid catalyst was chosen due to its possible renewable origin and because of the high potential application of innovative reactors like reactive distillation and membrane reactors for this type of reactions. The global reaction implies the production of the corresponding acetal (1,1 diethoxy butane) and water (see Figure 2.1), so in this case, dehydration membranes would be the most suitable ones for the membrane reactor.

The alcohol can be obtained from the fermentation of plants that are rich in sugar or starch, such us sugar cane, sugar beet, corn or maize. On the other hand, the aldehyde can be obtained from its corresponding alcohol via partial oxidation or via dehydrogenation. In this way, all the raw materials used can be obtained from renewable resources as a contribution towards a more sustainable development.

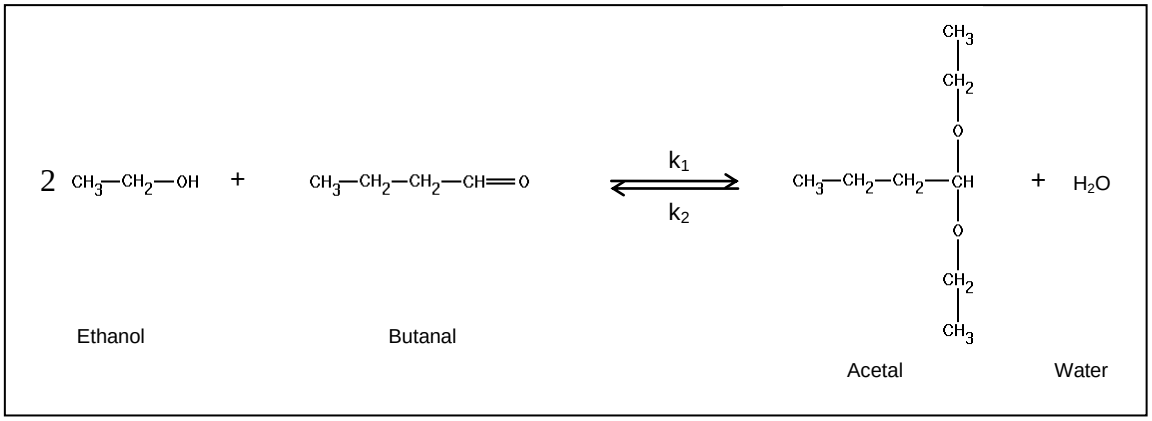

Figure 2.1 The global acetalization reaction.

Smaller acetal molecules like 1,1 diethoxy ethane show good properties to be used as a diesel additive as it is described previously. Bigger acetal molecules like 1,1 diethoxy butane seems to be even better potential diesel additives as they fulfill better diesel specifications.

In order to achieve the main objective, different tasks have been defined in order to fulfill the partial objectives that have been also fixed for each one:

- A thermodynamic study.
  - A theoretical study of the chemical and physical equilibria involved in order to obtain equilibrium constants at different temperatures as well as vapor-liquid-liquid equilibria data for ethanol, butanal, 1,1 diethoxy butane and water mixtures.
  - The estimation of the reaction enthalpy required for energy balances calculations.

- A kinetic study of 1,1 diethoxy butane production varying different parameters as temperature (to calculate experimental kinetic constants, reaction enthalpy…), degree of mixing, feed concentration and catalyst load. In this study, different catalysts will be tested and the most suitable one will be chosen for the reactive distillation experimental work as well as for the dehydration membrane reactor.

  From the thermodynamic and kinetic information gathered in the kinetic study, maximum conversions achievable using conventional reactor systems will be estimated.

- The design and modeling of the reaction systems (reactive distillation, a pervaporation system using a dehydration membrane). For this purpose different tasks are required:

  - Reactive distillation system tests varying different parameters like pressure drop, feed flow, feed temperature, reflux ratio etc, in order to get the best operating conditions.

  - Pervaporation system tests using dehydration membrane modules. In this case, parameters like temperature, driving force, etc, will be studied.

  Conversions to 1,1 diethoxy butane clearly above the ones previously estimated for conventional systems are the main target of these experiments and simulation studies.

- The last task will be to consider the most significant technical and economic aspects of both reaction systems in order to establish which one is the best approach to be used depending on the feed specifications and other boundary restrictions (energy prices, membrane cost and stability, etc). These final

analyses will be crucial in order to fix the objectives and procedures of further research on this area of work.

The *material balances* will allow determining the process which offers the best product yield i.e., the process that optimizes the fed raw materials use.

The *energy balances* will help to establish the most efficient process from the energetic point of view, i.e., the process achieving the lowest energy requirements/product unit ratio.

In terms of the *final process economy* it will be difficult to state if 1,1 diethoxy butane will be a possible economic biodiesel additive (€/J ratio), at least in the near future. Butanal is not still a commodity for this kind of industries and therefore its price is rather high for this purposes.

Chapter III

Kinetics of 1,1 diethoxy butane production from ethanol and butanal

3 Kinetics of 1,1 diethoxy butane production from ethanol and butanal

The main objective of this set of experiments is to fully characterize the kinetics of the reaction under study in order to use it in non-conventional chemical reactors as reactive distillation columns or membrane reactors. For this purpose a kinetic study was carried out in a laboratory batch reactor observing the behavior of the reaction. The influence of the temperature, feed concentration, type of catalyst, catalyst loading and speed of agitation was studied.

3.1 Experimental procedure

3.1.1 Materials

3.1.1.1 Reactants

The reagents were ethanol (99.5 % w/w for synthesis) from Panreac and butanal (99 % w/w) from Merck.

3.1.1.2 Catalysts

As catalysts, several Amberlyst sulphonic ion exchange resins were used such as A15Wet, A35Wet, A47 and A70 kindly provided by Rohm & Haas, USA. (52)

- Amberlyst 15Wet: is a strongly acidic, macroreticular polymeric resin based on cross-linked styrene divinylbenzene copolymers. It presents a continuous open pore structure and excellent physical, thermal and chemical stability.
- Amberlyst 35Wet: is also a macroreticular, strongly acidic, cationic, polymeric catalyst with an open continuous pore structure. This catalyst possesses a novel acid functionality which gives it higher thermal stability than standard polymeric catalysts. Its polymeric structure is resistant to oxidants and breakdown caused by mechanical and osmotic shocks.
- Amberlyst 47: is also a macroreticular, acid polymeric catalyst specifically produced for use in pressure drop sensitive reactors like tubular reactors or in structured packings for reactive distillation columns. This catalyst is extremely resistant to breakdown by osmotic, mechanical and thermal shocks.

- Amberlyst 70: is a new macroporous acid polymer catalyst designed for use in high-temperature heterogeneous catalysis, in fact, this resin is the one able to achieve the highest temperatures among the four catalysts tested (190 ºC).

The general properties of these four catalysts are shown in Table 3.2

3.1.2 Apparatus and procedure

The experiments were carried out in a 1 L glass jacketed stirred reactor (see Figure 3.1). The reaction temperature was controlled by an external thermostat (Lauda RE 304). This thermostat contains an external thermocouple to be introduced inside the reacting mixture and allows the reaction temperature control with an accuracy of ± 0.02 K. The reactor also contains a condenser in order to reflux all the vapors keeping the same reaction volume and avoiding emissions by evaporation.

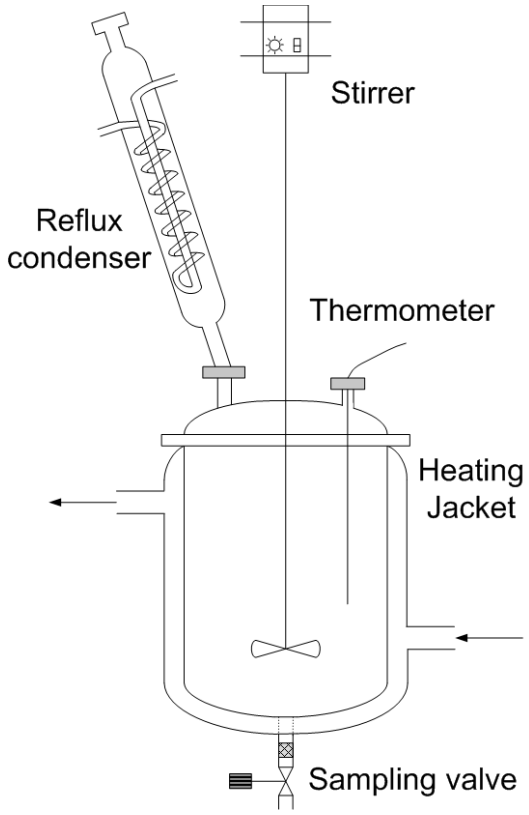

Figure 3.1 Schematic diagram of the stirred batch reaction system.

The reactants were charged into the reactor (total initial volume 0.5 L) and after stabilizing the system to the desired temperature, the catalyst was added; this time was considered as the starting time of the reaction. At certain specific time intervals different samples were withdrawn (≈ 3 mL) in order to analyze them by GC. A bit of glass wool

was placed in the output sampling valve in order to keep the catalyst amount constant in the reactor.

Before adding the catalyst sample, it was previously dried at room temperature due to its high moisture content. Thus, the catalyst had only the equilibrium humidity with the air and therefore the weighing was constant.

3.1.3 Analysis

Both reactants (ethanol and butanal) and reaction products (1,1 diethoxy butane and water) were analyzed by gas chromatography (Agilent 6890N) using a flame ionization detector (FID) and a thermal conductivity detector (TCD). A Meta Wax 30 m x 0.53 mm x 1.2 μm (Teknokroma, Barcelona) capillary column was used with helium as a carrier gas. In Table 3.1 more details of the method are shown.

Table 3.1 GC method conditions.

GC: Agilent 6890 N
Sample Injection
Diluted 1/3 (in vol.) with Dimethyl sulfoxide
Using an autosampler (Agilent 7683)
Injection temperature: 200 ºC
Injection mode: Split
Split ratio: 4:1
Carrier gas pressure: 2.79 psig
Carrier gas: He (99.999 %)
Column: Meta Wax 30 m x 0.53 mm x 1.2 μm capillary column
Temperature ramps:
Initial temperature: 50 ºC along 2 min
Rate: 7 ºC/min until 140 ºC
100 ºC/min until 220 ºC
Detectors: FID & TCD
Detector temperatures
FID: 250 ºC
TCD: 250 ºC

Table 3.2 Characteristics of the catalysts. (52)

	Amberlyst 15Wet	**Amberlyst 47**	**Amberlyst 35Wet**	**Amberlyst 70**
Physical form	Opaque beads	Opaque spherical beads	Opaque beads	Dark brown, spherical beads
Ionic form as shipped	Hydrogen	HSO_3	Hydrogen (98 % min.)	Hydrogen (98 % min.)
Concentration of active sites (eq/L)	≥ 1.7	≥ 1.65	≥ 1.9	≥ 0.9
Moisture holding capacity (H+ form)	52 to 57 %	50 to 57 %	51 to 57 %	53 to 59 %
Shipping weight (g/L)	770	770	800	770
Particle size				
Uniformity coefficient	≤ 1.70	-	≤ 1.70	≤ 1.50
Harmonic mean size (mm)	0.600 to 0.850	-	0.700 to 0.950	0.5
Fine contents	<0.355 mm : 1.0% max	<0.600 mm : 1.0% max	<0.425 mm : 1.0% max	<0.425 mm : 0.5% max
Coarse beads	>1.180 mm : 5.0% max	>1.180 mm : 15.0% max	>1.180 mm : 9.0% max	-
Nitrogen BET				
Surface area (m2/g)	53	50	50	36
Average pore diameter (Å)	300	240	300	220
Total pore volume (mL/g)	0.4	-	0.35	-
Maximun operating temperature (ºC)	120	120	150	190

3.2 Results and discussion

This section contains all the information from all the experiments that were carried out with the lab-scale batch reactor. The reaction mechanism for acetalization of ethanol with butanal as well as the influence of the temperature, type of catalyst, catalyst loading, feed concentration and stirring speed will be discussed.

3.2.1 Initial experiments

Before carrying out different experiments in the described reactor, some previous experiments were performed in an Erlenmeyer flask using H_2SO_4 as homogeneous catalyst. The aim of these experiments was to determine and identify the different products that could appear apart from 1,1 diethoxy butane and water due to side reactions. The presence of the sulphuric acid gives a really acid character to the medium forcing possible side reactions.

As a result of these experiments, using a GC/MS, the following compounds were identified:

- 1,1 diethoxy butane
- Water
- Trans -1- ethoxy-1-butene
- Cis -1- ethoxy-1-butene
- Butanoic acid, ethyl ester
- Other residual non-identified compounds

After having finished these experiments, they were repeated but using A15Wet, A35Wet, A47 and A70 as catalysts. In these cases, the selectivity increased obtaining only the desired compounds (1,1 diethoxy butane and water). The concentrations of ethyl ester butanoic acid, trans (cis)-1ethoxy-1-butene and the other residual compounds were completely negligible.

3.2.2 Reaction mechanism

According to Sharma & Chopade (21;53), the reaction mechanism for acetalization of ethanol or ethylene glycol with formaldehyde involves two reversible steps: the first one where one alcohol molecule reacts with one aldehyde molecule leading to the formation of the corresponding hemiacetal and the second one, where another alcohol molecule reacts with the OH of the hemiacetal to form the acetal and water. In the present case, the reactions are:

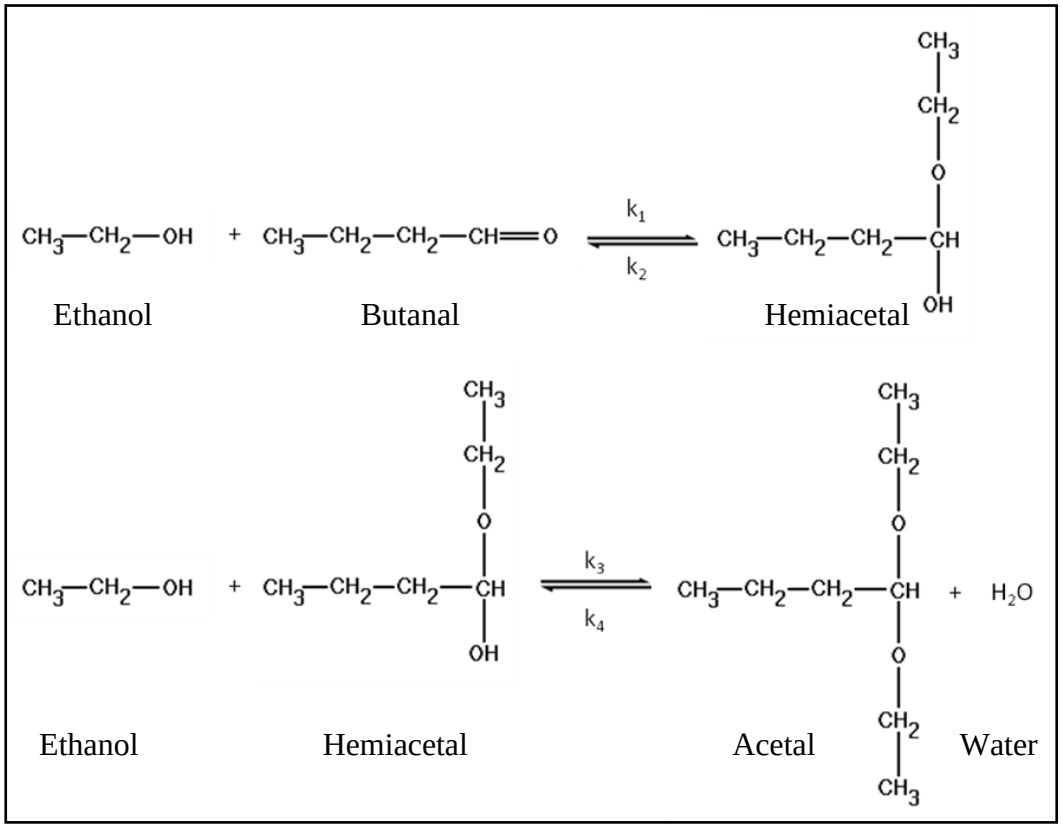

Figure 3.2 Acetalization reaction mechanism using ethanol and butanal as reactants.

The first of these two steps, which does not require a catalyst, is much faster than the second one (21;53). There are also some evidences that indicate a similar behavior when ethanol and butanal are used as reactants. Just after mixing these compounds at room temperature the mixture temperature increases notably taking place as a non-catalyzed exothermic reaction. However, some difficulties were found when analyzing these samples since the hemiacetal peak did not appear in the different chromatograms. There are some possible hypotheses to explain this issue: one of them is that the hemiacetal peak is overlapped with another peak, but the most probable explanation is that this fact could be related to the exothermicity of a non-catalyzed reaction. When the sample is injected into the GC (which is at 200 ºC) the reverse reaction occurs due to a high decrease of the equilibrium constant with temperature disappearing most of the hemiacetal and thus, limiting its detection. In order to prove this hypothesis, HPLC/MS analyses of ethanol-butanal mixtures at room temperature were performed. These measurements confirmed, indeed, the presence of the hemiacetal in the samples. (54)

As the hemiacetal formation and decomposition reactions rates are so high at the operating temperatures, the hemiacetal (HA) can be considered to be at equilibrium with ethanol and butanal.

$$[HA] = K_1[BHO][EtOH] \tag{3.1}$$

The formation rate of acetal (AC) could be written as

$$\frac{d[Ac]}{dt} = wk_3[HA][EtOH] - wk_4[AC][W] \tag{3.2}$$

Where w = (g cat)/(reacting volume)
Substituting [HA] from Eq. (3.1),

$$\frac{d[Ac]}{dt} = wk[BHO][EtOH]^2 - wk_4[AC][W] \tag{3.3}$$

Where $k = k_3K_1$. At *t=0*, the initial conditions are:

$$\begin{aligned} &[BHO] = [BHO]_0 \\ &[EtOH] = [EtOH]_0 \\ &[AC] = [AC]_0 = 0 \\ &[W] = [W]_0 \end{aligned} \tag{3.4}$$

As it is explained in section 3.2.1 there are no side reactions when operating with Amberlyst resins as catalyst, so, the concentration of other compounds can be calculated by mass balances:

$$[BHO] = [BHO]_0 - ([AC]-[AC]_0) \tag{3.5}$$
$$[EtOH] = [EtOH]_0 - 2([AC]-[AC]_0) \tag{3.6}$$
$$[W] = [W]_0 + ([AC]-[AC]_0) \tag{3.7}$$

The equilibrium constant can be expressed as:

$$K_2 = \frac{[AC][W]}{[BHO][EtOH]^2} = \frac{k}{k_4} \tag{3.8}$$

As it can be seen, the forward reaction is 2nd order with respect to ethanol and 1st order with respect to butanal. The reverse reaction is also 1st order with respect to acetal and water. This order of reaction will be confirmed in section 3.2.7.

3.2.3 Mass transfer resistance

In order to avoid mass transfer resistance a wide range of stirring speeds (from 500 rpm to 1200 rpm) was tested. There was not observed any effect of the agitation on the reaction rate (see Figure 3.3) proving the absence of any external mass transfer resistance at the lowest stirring speed (500 rpm), so all further experiments were carried out at 500 rpm.

These experiments were performed at 333 K, the highest temperature at which the experiments were performed in the experimental study, since the effect of the temperature is much higher over the reaction rate (exponential) than over the mass transfer coefficient (approximately linear); so, if there was any external mass resistance, it would be observed much more clearly at the highest temperature.

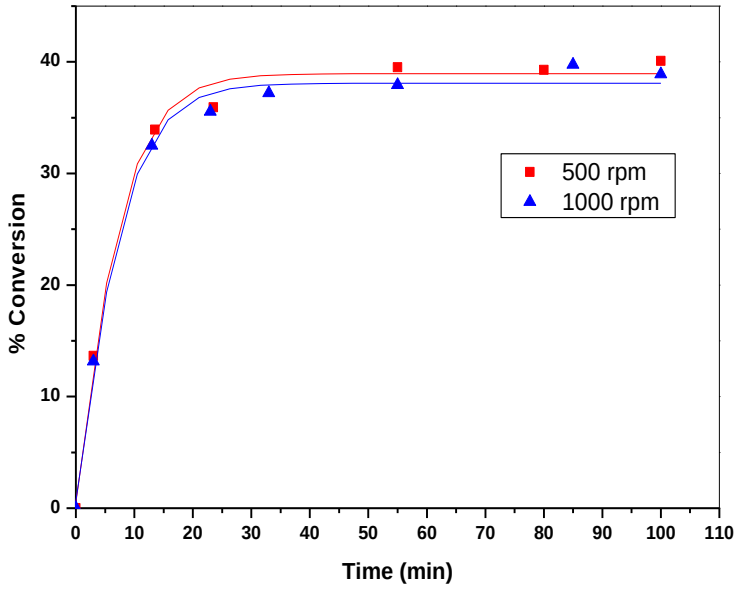

Figure 3.3 Effect of the stirring speed. EtOH:BHO mol ratio 2:1, 333 K, catalyst loading of 1.0 % w/w A47. Solid lines indicate just trends.

3.2.4 Effect of type of catalyst

As it is explained in section 3.1.1 four different resins were tested. All the experiments were carried out under identical conditions (313 K, 500 rpm, 1.0 % w/w of catalyst loading and stoichiometric feed mole ratio -2:1 EtOH:BHO-). As in all the experiments, each test was carried out at least three times in order to get accurate enough results. The tests were repeated at least three times in order to estimate accurate enough parameter values within a predeterminated tolerance range for a confidence interval of 95% according to the t-student distribution.

The evolution of the conversion along the reaction time is shown in Figure 3.4 for every single catalyst. As it can be seen, in all the cases the reaction performs in a similar way, being very similar the reaction rates.

In order to discriminate among the catalysts the *turnover number* was calculated for each one. This number is a parameter used to quantify the activity of catalyst active sites and it is also called *turnover frequency*. It indicates the number of molecules that reacts per active site per time unit at the experimental conditions. In Table 3.3 turnover frequencies and the obtained kinetic parameters are showed for each catalyst.

$$T_N = \frac{r_A\left(molecules \cdot g\ cat^{-1} \cdot \min^{-1}\right)}{N_S\left(H^+ \cdot g\, cat^{-1}\right)} \tag{3.9}$$

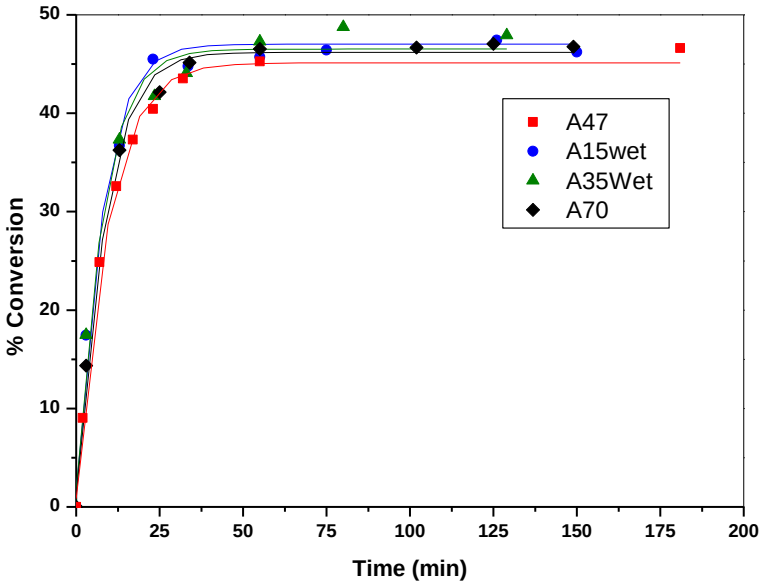

Figure 3.4 Comparison of the kinetic behavior of the different catalysts tested. Conditions: 313 K, EtOH:BHO of 2:1, 500 rpm, catalyst loading of 1.0 % w/w. Solid lines indicate just trends.

Table 3.3 Kinetic parameters and turnover frequencies for each catalyst.

Catalyst	wk (mol/L)$^{-2}$min^{-1}	wk_4 (mol/L)$^{-1}$min^{-1}	T_N (min^{-1})
A15Wet	889.0 ± 58.4	7.8 ± 1.1	11.44
A35Wet	823.2 ± 46.7	7.2 ± 0.6	9.88
A70	744.6 ± 109.8	7.4 ± 1.0	17.64
A47	629.9 ± 21.5	7.2 ± 0.8	8.30

As it can be observed, the activity of the acid sites of A15Wet, A47 and A35Wet are quite similar but the acid sites of A70 seems to be more active than the other ones. On the other hand, the concentration of acid sites in Amberlyst 70 is approximately 50 % of the acid site concentration of the other resins (see Table 3.2). So, because of these reasons, the forward kinetic parameter obtained with A70 is similar to the values measured using the other catalysts. This is the resin able to be operated at the highest temperatures. A possible explanation could deal with an elaboration procedure implying higher temperature preparation stages. Thus, some reduction of acid site concentration takes place but each acid site of this resin ends up being more active.

Apart from this set of experiments, all the other ones were carried out using A47 as catalyst since its mechanical resistance makes this resin, a priori, the most suitable one to operate in slurry reactors or structured packings. It must be remembered that the aim of this kinetic study in a batch reactor is to collect as much information as possible to develop advanced reaction systems such as reactive distillation and membrane reactors.

3.2.5 Effect of the temperature

Three different temperatures were tested: 293 K, 313 K and 333 K. For each temperature, at least four different experiments were performed being the definitive kinetic parameters the arithmetic average value of the calculated parameters for each experiment.

Figure 3.5 shows the evolution of the conversion of the butanal at the three different temperatures. As it can be observed an increase of the temperature implies a decrease in the equilibrium conversion (it is an exothermic reaction) and an increase of the reaction rate.

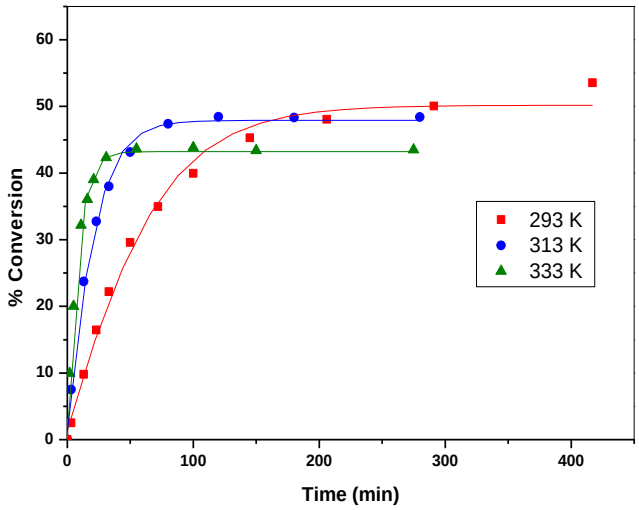

Figure 3.5 Effect of the temperature. Conditions: EtOH:BHO rate 2:1, catalyst loading 0.5 % w/w A47, 500 rpm. Solid lines indicate just trends.

Table 3.4 shows the forward and reverse kinetic parameters obtained from fitting experimental data to the acetal mass balance differential equation. All the experiments were repeated at least three times in order to get accurate enough parameter values within a predeterminated tolerance range for a confidence interval of 95% according to the "*T-Student*" distribution

Table 3.4 Kinetic parameters and equilibrium conversion at different temperatures.

Temp. (K)	**k ($mmol^{-2}·L^{3}·min^{-1}·g.cat^{-1}$)**	**k_4 ($mmol^{-1}·L^{2}·min^{-1}·g.cat^{-1}$)**	**% Conv.**
293	30.1 ± 2.2	0.14 ± 0.02	51-53
313	79.4 ± 11.5	0.70 ± 0.09	46-48
333	173.0 ±11.5	2.69± 0.30	42-43

Plotting all these data following Arrhenius' correlation (Ln k vs 1/T), activation energy was obtained.

$$Ln(k) = Ln(A) + \left[\frac{-E_a}{RT}\right] \tag{3.10}$$

Where: E_a is the activation energy (J/mol)

R is the universal gas constant (J/(mol K))

T is the temperature in Kelvin

A is the pre-exponential factor

k is the kinetic constant

Arrhenius' correlation for the forward reaction is shown in Figure 3.6

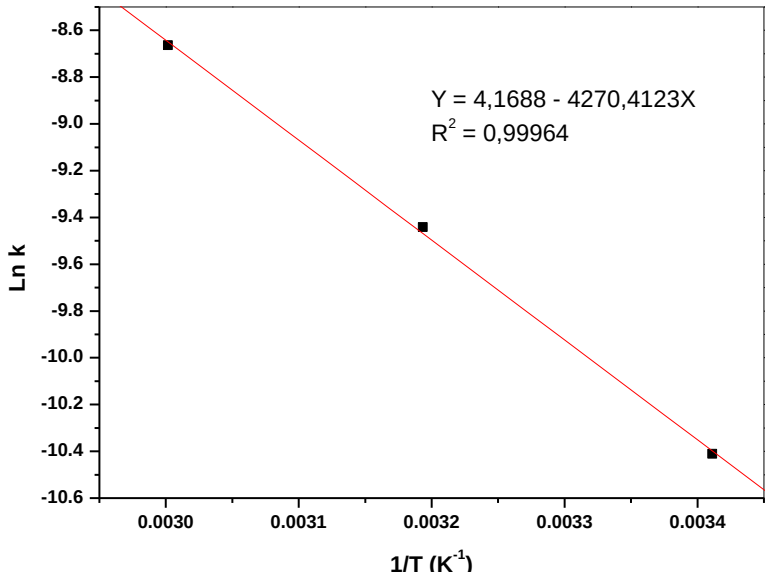

Figure 3.6 Arrhenius correlation for the forward reaction.

From the linear trend line activation energy and pre-exponential factor can be calculated:

- E_a = 35.5 (kJ mol^{-1})
- A = 64.7 (mol^{-2} L^3 min^{-1} $g.cat^{-1}$)

Arrhenius' correlation for the reverse reaction is shown in Figure 3.7.

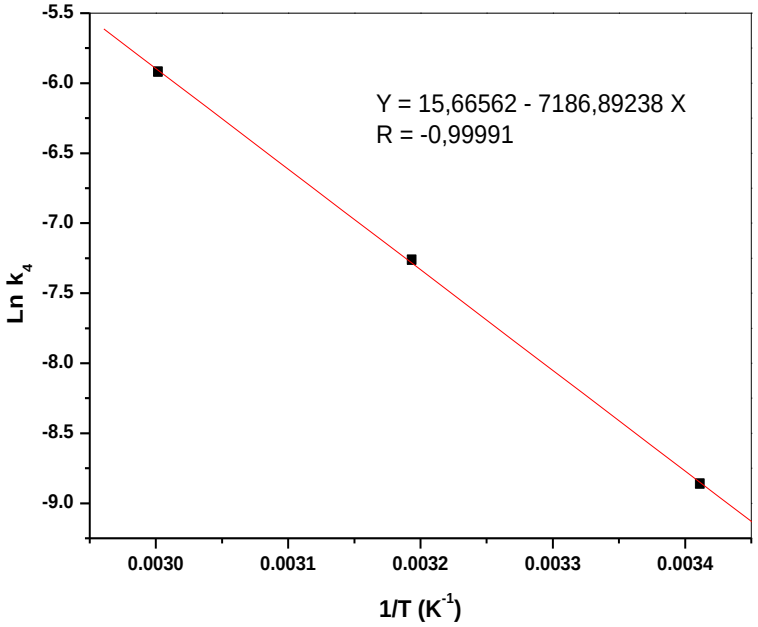

Figure 3.7 Arrhenius correlation for the reverse reaction.

From the linear trend line activation energy and pre-exponential factor can be calculated:

- E_a = 59.8 (kJ mol^{-1})
- A = 6.4 E+6 (mol^{-1} L^2 min^{-1} $g.cat^{-1}$)

In terms of equilibrium constant, it is already known that it is inversely proportional to the temperature following the next relation:

$$-Ln\,K = \frac{\Delta G^0}{RT} \tag{3.11}$$

Equilibrium constant can be calculated as the ratio of the forward and reverse kinetic parameters (k/k_4). Once K is calculated, plotting Ln K versus 1/T free energy of Gibbs can be estimated.

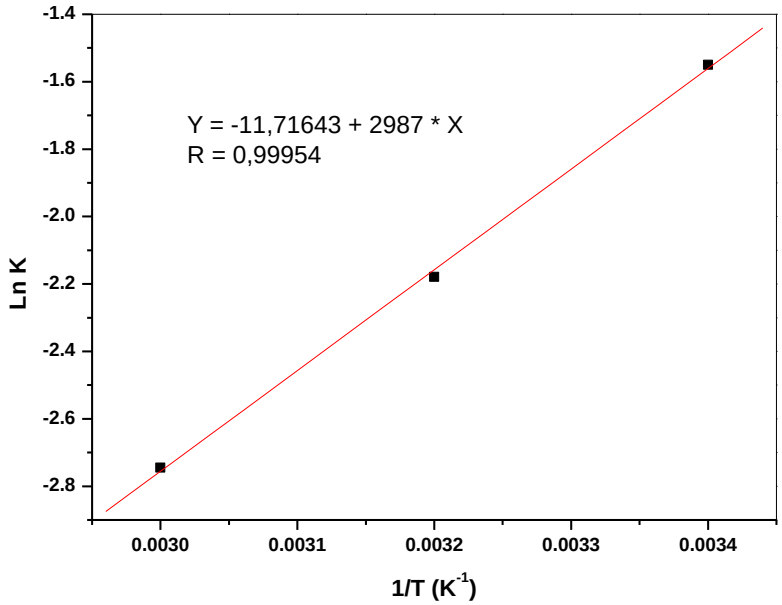

Figure 3.8 Variation of the equilibrium constant with temperature

As the independent term of the equation relating the equilibrium constant to temperature can be considered negligible comparing to its slope, an estimation of the ΔG_r^0 average (in the temperature range used) can be estimated.

- ΔG^0 = -24.2 (kJ/mol)

3.2.6 Effect of catalyst loading

Catalyst loading was varied from 0.5 % w/w to 1.5 % w/w. As it can be seen in Figure 3.9 the reaction rate is faster with higher catalyst loading due to the increase of the total number of acid sites available in the medium.

In Table 3.5 it can be seen easily that *wk* is directly proportional to the catalyst loading and how the kinetic constant per catalyst gram is independent of the catalyst loading. The differences in conversion for long reaction times (< 3%) are due to experimental errors since the catalyst amount cannot influence the final conversion (equilibrium).

Table 3.5 Effect of catalyst loading on the kinetic parameters.

Cat. load	**w** (g.cat/L)	**wk** ((mol/L)$^{-2}$·min^{-1})	**wk$_4$** ((mol/L)$^{-1}$min^{-1})	**k** (mol^{-2}·L^3·min^{-1}·g.cat^{-1})	**k$_4$** (mol^{-1}·L^2·min^{-1}·g.cat^{-1})
0.5 %	45-47	319.9 ± 41.1	2.8 ± 0.3	7.9E-5 ±1.1E-5	7.0E-4 ± 8.7E-5
1.0 %	45-47	629.9 ± 21.5	7.2 ± 0.8	7.9E-5 ± 2.6E-6	9.0E-4 ± 1.1E-4
1.5 %	45-47	974.6 ± 94.6	9.0 ± 1.6	8.1E-5 ± 7.8E-6	7.5E-4 ± 1.3E-4

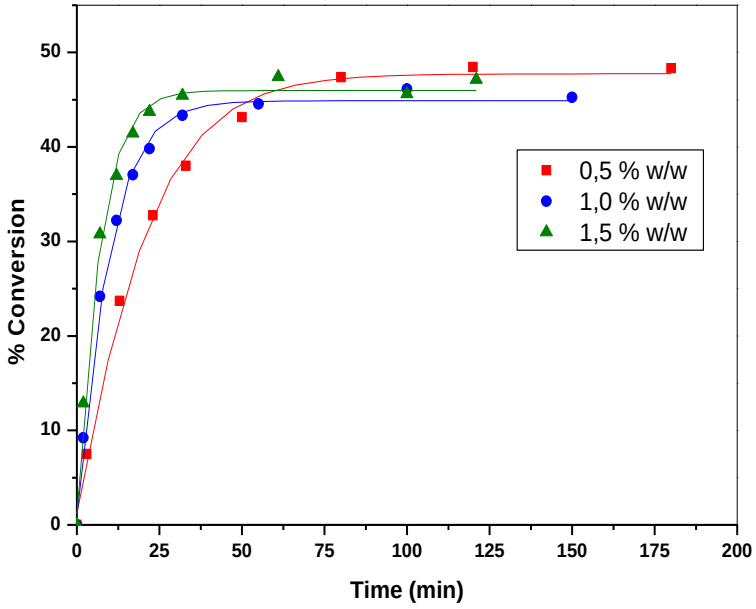

Figure 3.9 Effect of catalyst loading on the reaction rate. Conditions: EtOH:BHO 2:1; temperature: 313 K; catalyst: A47; 500 rpm. Solid lines indicate just trends.

3.2.7 Effect of the feed composition

Three different feed mole ratios were tested (EtOH:BHO from 2:1 to 3:1 and further to 4:1) in order to check the order of reaction and estimate equilibrium conversions.

Two different order of reactions were tested; the explained one in section 3.2.2 as the most probable one and the other possible one (order one for ethanol).

$$\frac{d[Ac]}{dt} = wk[BHO][EtOH] - wk_4[AC][W] \tag{3.12}$$

Kinetic parameters (wk & wk_4) were estimated by minimizing the sum of squares of the difference between the experimental and the calculated concentration for each component. For this purpose Matlab "Nelder-Mead simplex direct search" algorithm was used. The parameter "sum_square" shows the sum of squares of the difference between the experimental and the calculated concentration giving an estimation of the adequacy of each kinetic equation proposed.

All the experiments were repeated at least three times and in every single case the curve fits slightly better when 2nd order with respect to ethanol(this order is also the one derived –see section 3.2.2- in the mechanistic discussion) is used. In some cases, as it is showed in Table 3.6, the algorithm was unable to meet the integration tolerances without reducing the step size below the smallest value allowed (2.273737e-013) at time "t".

Table 3.6 Fitting of the experimental points to the reaction model.

EtOH:BHO mole ratio	**Sum_square for order 2 for EtOH**	**Sum_square for order 1 for EtOH**
2:1 (a)	1.69 E-9	Fitting error
2:1 (b)	9.96 E-9	3.23 E-8
2:1 (c)	2.46 E-9	Fitting error
3:1 (a)	1.37 E-7	1.59 E-7
3:1(b)	1.77 E-8	1.74 E-8
3:1 (c)	2.67 E-8	4.81 E-8
4:1 (a)	7.33 E-8	1.11 E-7
4:1 (b)	1.77 E-8	4.55 E-8
4:1 (c)	3.55 E-9	1.23 E-8

In Figure 3.10 it can be observed, as it was expected, that increasing the ethanol/butanal mole ratio the equilibrium conversion with respect to butanal is increased. The excess of one of the reactants implies higher conversions according to Le Chatelier principle.

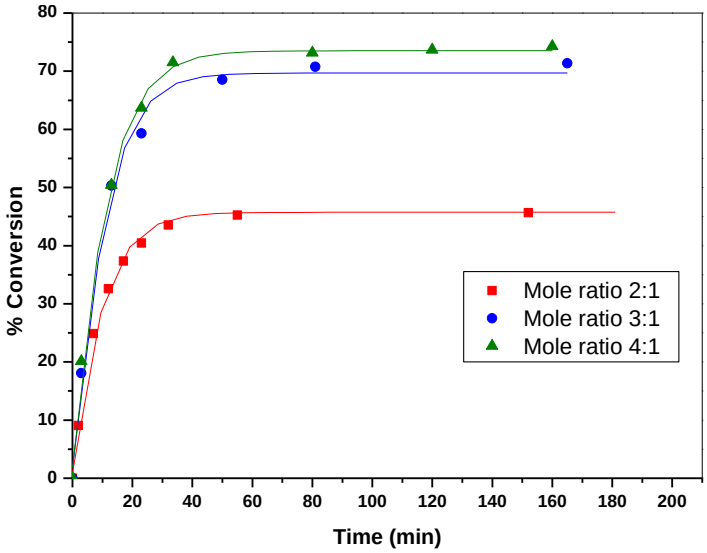

Figure 3.10 Effect of the ethanol/butanal feed mole ratio on the equilibrium conversion. Conditions: Temperature 313 K, Catalyst loading: 1.0 % w/w A47, 500 rpm. Solid lines indicate just trends.

3.3 Summary of the estimated kinetic parameters

Table 3.7 Estimated kinetic parameters. Conditions: temperature: 313 K; 500 rpm; catalyst: A47 1.0 % w/w.

EtOH: BHO	**% conv.**	**wk** **((mol/L)$^{-2}$min^{-1})**	**wk$_4$** **((mol/L)$^{-1}$min^{-1})**	**k** **(mol^{-2} L^3 min^{-1} g.cat^{-1})**	**k$_4$** **(mol^{-1} L^2 min^{-1} g.cat^{-1})**
2:1	45-47	629.9 ± 21.5	7.2 ± 0.8	7.9E-5 ± 2.6E-6	9.0E-4 ± 1.1E-4
3:1	70-72	674.7 ± 38.5	3.4 ± 0.3	8.5E-5 ± 4.9E-6	4.3E-4 ± 3.8E-5
4:1	74-76	556.9 ± 29.7	5.6 ± 0.9	7.0E-5 ± 3.7E-6	7.1E-4 ± 1.2E-4

Table 3.8 Estimated kinetic parameters. Conditions: 500 rpm; catalyst: A47 0.5 % w/w; EtOH/BHO 2:1

Temp (K)	**% conv.**	**wk** **((mol/L)$^{-2}$min^{-1})**	**wk$_4$** **((mol/L)$^{-1}$min^{-1})**	**k** **(mol^{-2} L^3 min^{-1} g.cat^{-1})**	**k$_4$** **(mol^{-1} L^2 min^{-1} g.cat^{-1})**
293	51-53	119.9 ± 8.8	0.6 ± 0.1	3.0E-5 ± 2.2E-6	1.4E-4 ± 2.3E-5
313	46-48	319.9 ± 42.1	2.8 ± 0.3	7.9E-5 ± 1.1E-5	7.0E-4 ± 8.7E-5
333	42-43	689.8 ± 46.0	10.7 ± 1.2	1.7E-4 ±1.1E-5	2.7E-3 ± 3.0E-4

Table 3.9 Estimated kinetic parameters. Conditions: temperature: 313 K; 500 rpm; catalyst: loading 0.5 % w/w; EtOH/BHO 2:1.

Cat.	**% conv.**	**wk** **((mol/L)$^{-2}$min^{-1})**	**wk$_4$** **((mol/L)$^{-1}$min^{-1})**	**k** **(mol^{-2} L^3 min^{-1} g.cat^{-1})**	**k$_4$** **(mol^{-1} L^2 min^{-1} g.cat^{-1})**
A15Wet	45-47	889.0 ± 58.4	7.8 ± 1.1	1.1E-4 ± 7.5E-6	9.7E-4 ± 1.4E-4
A35Wet	45-47	823.2 ± 46.8	7.2 ± 0.6	1.0E-4 ± 5.9E-4	8.9E-4 ± 8.0E-5
A70	45-47	744.6 ± 109.8	7.4 ± 1.0	9.3E-5 ± 1.3E-5	9.2E-4 ± 1.2E-4
A47	45-47	629.9 ± 21.5	7.2 ± 0.8	7.9E-5 ± 2.6E-6	9.0E-4 ± 1.1E-4

Table 3.10 Estimated kinetic parameters. Conditions: temperature: 313 K; 500 rpm; catalyst A47; EtOH/BHO 2:1.

Cat. loading	**% conv.**	**wk** **((mol/L)$^{-2}$min^{-1})**	**wk$_4$** **((mol/L)$^{-1}$min^{-1})**	**k** **(mol^{-2} L^3 min^{-1} g.cat^{-1})**	**k$_4$** **(mol^{-1} L^2 min^{-1} g.cat^{-1})**
0.5 %	45-47	319.9 ± 41.1	2.8 ± 0.3	7.9E-5 ±1.1E-5	7.0E-4 ± 8.7E-5
1.0 %	45-47	629.9 ± 21.5	7.2 ± 0.8	7.9E-5 ± 2.6E-6	9.0E-4 ± 1.1E-4
1.5 %	45-47	974.6 ± 94.6	9.0 ± 1.6	8.1E-5 ± 7.8E-6	7.5E-4 ± 1.3E-4

Chapter IV

Reactive distillation. Experimental part

4 Reactive distillation. Experimental part

The aim of the present chapter is to demonstrate that using reactive distillation systems the thermodynamic limitations that the reaction under study shows can be overcome achieving higher conversions than the obtained ones in conventional reaction systems (Chapter III).

As experimental data for 1,1 diethoxy butane were not found in the literature, important experimental work was required in order to get enough knowledge about the interactions between the catalytic reaction and the distillation process taking place in the same unit.

A semi-pilot plant was used in order to study the effect of different parameters. The experimental work was focused on finding the best column configuration in order to achieve the highest possible process conversion (above the ones achievable in a conventional reaction system). For this purpose different column configurations were tested varying the main parameters: pressure drop, catalyst amount, feed temperature, location of the catalytic section and different feed configurations.

4.1 Experimental procedure

4.1.1 Materials

All the reactants used in this part of the project are described in Section 3.1.1. In terms of catalyst, only Amberlyst 47 was tested since the performance of other similar catalysts like A15W, A35W and A70 is very similar for the studied reaction as it is shown in Chapter III; A47 is the most suitable one to use in reactive distillation systems due to its higher mechanical resistance.

4.1.2 Product analysis

Both the reactants (ethanol and butanal) and reaction products (1,1 diethoxy butane and water) were analyzed by gas chromatography (Agilent 6890N) using a flame ionization detector (FID) and a thermal conductivity detector (TCD). An Agilent 125-1065 DB-1 capillary column was used (60m x 530μm x 5μm) with helium as the carrier gas. More details of the method are shown in Table 4.1.

Table 4.1 GC method conditions.

GC: Agilent 6890 N
Sample Injection
Diluted 1.5 mL of sample to 10 mL with Dimethyl sulfoxide
Using an autosampler (Agilent 7683)
Injection temperature: 200 ºC
Injection mode: Split
Split ratio: 4:1
Carrier gas pressure: 20 psig
Carrier gas: He (99.999 %)
Column: DB-1 60 m x 0.53 mm x 5 μm capillary column
Temperature ramps:
Initial temperature: 50 ºC along 4 min
Rate: 30 ºC/min until 180 ºC
50 ºC/min until 240 ºC and keep 1 min
Detectors: FID & TCD
Detector temperatures
FID: 250 ºC
TCD: 250 ºC

4.1.3 Reaction apparatus and procedure

The experiments were carried out in a semi-pilot continuous distillation plant where some conventional structured packing modules (multiknit) were replaced by structured catalytic packings (Katapak SP-11).

A schematic diagram is shown in Figure 4.1. The main parts and characteristics are described in the following points:

1. Feed

Both reactants are introduced to the system by a couple of dosing pumps and the feed can be pre-heated using two different electric heat interchangers (1000 Watt). Besides, as the distillation column has 3 different feeding points, the installation incorporates a valve system in order to choose a particular feeding configuration.

The pre-heating system incorporates PID control loops to ensure that the feeding temperatures are the desired ones.

2. Distillation column

The distillation column is the heart of the installation. Its inner diameter is 50 mm and a maximum height of 750 mm. It has 3 intermediate plates with 3 different temperature measurement points and 3 valves to withdraw samples from them; thus, temperature and composition profiles along the column can be obtained.

The set up was also provided with a reboiler, a total condenser and a reflux divider. The reboiler operates with a stainless steel resistance (2000 Watt) and the liquid level of the reboiler is controlled by a stainless steel level float. In order to control the required power a pressure drop PID controller is installed between the reboiler and the top of the column.

The total condenser works with water as refrigerant and it has a couple of Pt100 thermowells in order to measure the temperature variation of the cooling water; a flow controller is incorporated in order to measure the water flow. Thus, the condenser heat duty can be estimated.

The reflux divider works with a timer and an on-off valve.

3. Output

The distillate and the bottoms, after being cooled down, are collected in 2 different drums.

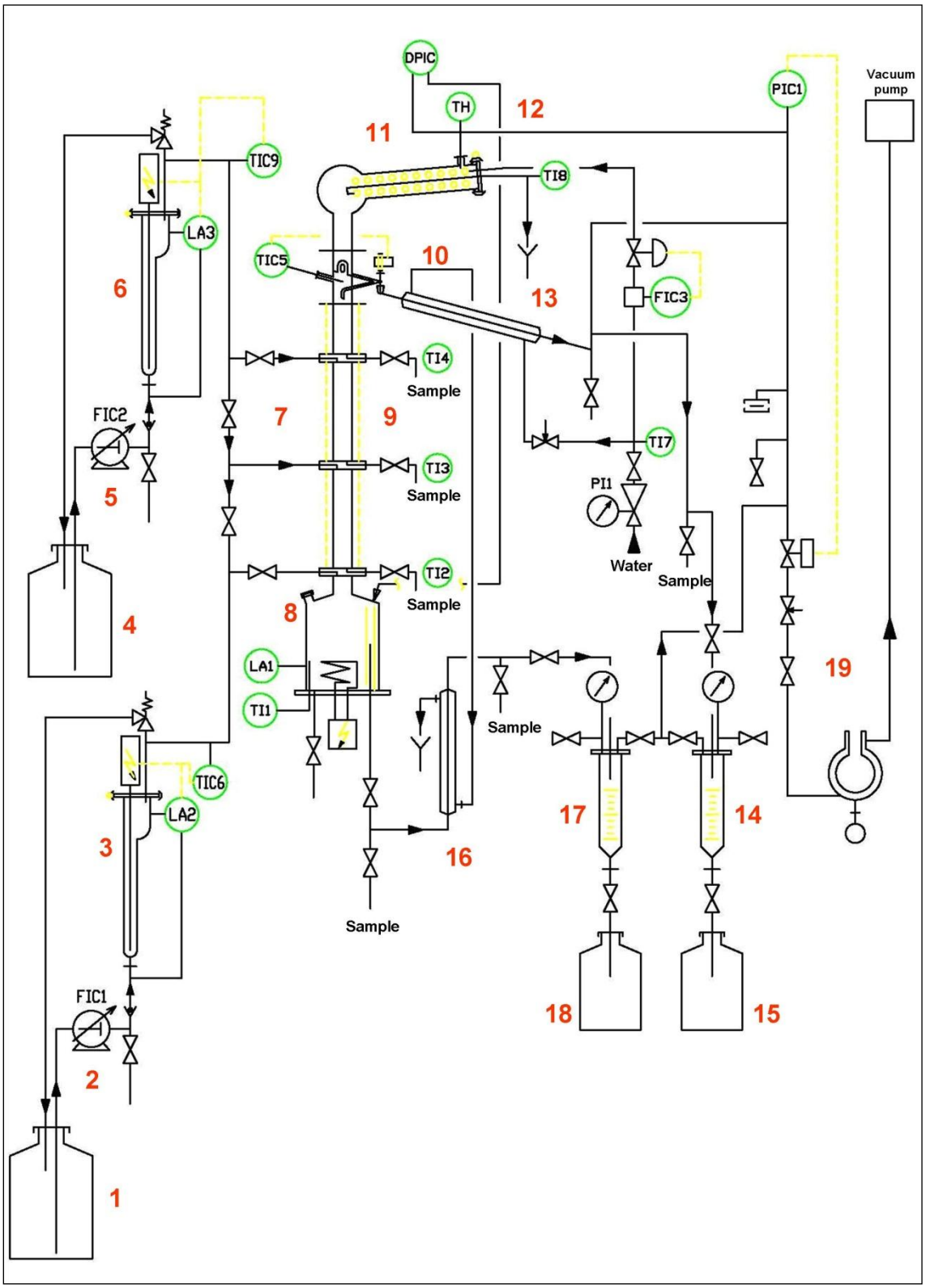

Figure 4.1 Schematic diagram of the reactive distillation installation.

Table 4.2 Description of the different parts of the reactive distillation installation.

1	Storage drum 1. Capacity: 20 L
2	Dosing pump 1. Adjustable flow between 0 – 25 L/h
3	Pre-heater 1 (1000 Watt). T measurement. Level detector
4	Storage drum 2. Capacity: 20 L
5	Dosing pump 2. Adjustable flow between 0 – 25 L/h
6	Pre-heater 2 (1000 Watt). T measurement. Level detector
7	Valve system to choose the feeding points
8	Reboiler (2000 Watt). Total capacity: 6 L T measurement Entry neck Discharge valve Level float
9	Distillation column ID: 50 mm Height: 750 mm (300 mm + 300 mm + 150 mm) Packing: multiknit (non catalytic) & Katapak SP-11 (catalytic packing) Pressure drop controller Removable heat insulation blanket
10	Reflux system by an electromagnetic valve T measurement
11	Glass condenser with an inner stainless steal coil T measurement in the refrigerant (water) input and output. Water flow measurement
12	Air vent T measurement dP measurement
13	Coil to cool down the distillate
14	Measuring cylinder of 1L
15	Storage drum (10 L)
16	Coil to cool down the bottoms. Sample valve
17	Measuring cylinder of 1L
18	Storage drum (10 L)
19	Vacuum circuit

Table 4.3 Indicators

Temperatures	
T11	Temperature of the reboiler
T12	Temperature in the bottom side of the column
T13	Temperature in the middle of the column
T14	Temperature in the top side of the column
TIC5	Temperature controller in the head of the column
TIC6	Pre-heating temperature (1) controller
TIC9	Pre-heating temperature (2) controller
TI7	Cooling water temperature
TI8	Condenser output water temperature
THI	Temperature in the air vent of the condenser
Flow measurements	
FIC1	Flow controller of the 1st feeding pump
FIC2	Flow controller of the 2nd feeding pump
FIC3	Condenser water flow controller
Pressure transmitter	
DPIC1	dP controller
Level detectors	
LA1	Alarm level in the reboiler
LA2	Alarm level in the 1st pre-heater
LA3	Alarm level in the 2nd pre-heater
Pressure	
PIC	Absolute pressure controller in the column

The installation, apart from all these characteristics, includes different safety systems. There are 3 level alarms: 2 in the pre-heaters and another one in the reboiler. If liquid is not detected, the heating power is deactivated. Moreover, the cooling water of the condenser must be set up above 100 L/h in order to allow the controlling system to supply power to the reboiler. There is another security system in order to avoid risky situations. There is an extra Pt100 thermowell located in the air vent of the condenser; if an abnormal high temperature (> 60 ºC) is detected the power supply is deactivated in the reboiler; this fact may happen when not all the vapor is condensed and an over pressure situation takes place, and therefore an explosion risk starts being possible.

In order to get better measurements of all the variables and a better control, the installation is connected to a computer where all the variables are depicted, registered and controlled.

- Procedure

Before starting any set of experiments, the desired column configuration was fixed, i.e. the desired catalyst amount in a particular height of the column. Once the column was rebuilt a leak test was performed (with the vacuum pump of the system) in order to make sure that everything was correctly assembled. Besides, the pumps were calibrated for different frequencies and different pump strokes for each reactant in order to know the ratio between the frequencies (or strokes) and the desired pumped liquid flow (in volume).

Once the installation was ready, the reactants were charged into the reboiler using its entry neck (2.5 L aprox). Then, all the valves were closed, also de reflux valve, and the reboiler power was switched on (after switching on the condenser). Thus, the installation works in a batch mode and the column is pre-heated and stabilized.

When all the variables were stabilized (15 min aprox.) the feeding pumps were switched on, the reflux ratio was fixed and the reboiler output valve was also opened. This time was considered as the experiment starting time. Then, at certain specific time intervals (every 35 minutes, more or less) different samples were withdrawn (≈ 2 mL) in order to analyze them in a GC; moreover, distillate and bottoms flow rates were measured. Every sampling time 5 different samples were withdrawn; 1 from the bottoms, 1 from the distillate and 3 samples from the 3 different plates located at different column heights.

It was observed that, in most of the cases, in 4 hours the process was fully stabilized. At high reflux ratios in 2-3 hours everything was quite stabilized whilst at low reflux ratios (<R=2) 4 hours were necessary in order to have a steady-state operation.

Once the experiments were finished, the power was switched off and everything was left to cool down before discharging the reboiler.

4.2 Results & Discussion

This section contains all the information from all the experiments that were performed with the semi-pilot reactive distillation installation. Different experiments were carried out in order to study the effect of different parameters. First of all some initial experiments were done without any catalyst (simple continuous distillation) to check possible non catalytic reactions taking place and then other catalytic experiments were performed.

4.2.1 Initial experiments

Some initial experiments were carried out in the absence of catalyst in order to check if the acetalization reaction takes place in the system. Besides, these experiments were also valid to learn how to manage the plant and observe the hydrodynamics of the column adjusting the feed flows.

The chosen experimental conditions for these very first tests were the next ones:

- Stoichiometric feed ratio. (2 EtOH : 1 Butanal in moles)
- Feeding positions (see Figure 4.2):
    - From the top intermediate stage: ethanol (the less volatile reactant)
    - From the middle intermediate stage: butanal (the most volatile reactant)
- Low pressure drops (0.5 & 1.2 mbar)
- Reflux ratio equal to 2 (R=2)

In principle, as a first approximation, the feed temperature was chosen equal to 60 ºC for both of the reactants because in the column stabilization process (operating in batch mode) it was observed that the column temperature in the feed points was around 70 ºC. Thus, the objective was to avoid perturbations to the system.

Regarding the feed flows, the following criteria were used to select them: not to spend too much reactant amounts, have good pump performance and good column fluid dynamics. According to these criteria, the chosen flows are shown in Table 4.4.

Table 4.4 Feed flows with their corresponding pump characteristics.

	Flow (L/h)	**% stroke**	**% frequency**
Butanal	3.10	100 %	10 %
Ethanol	4.15	100 %	12 %

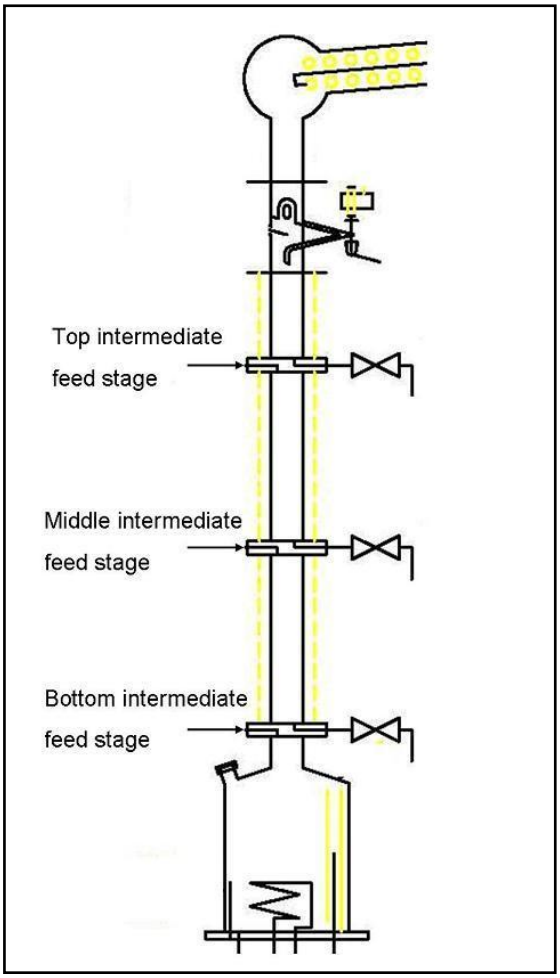

Figure 4.2 Feed points and sampling stages in the distillation column.

A couple of experiments were carried out in the mentioned conditions and the measured acetal concentration in these tests was absolutely negligible. The achieved conversions in these experiments were around 0.1 %.

In terms of separation, the ethanol – butanal ratio in the reboiler does not change too much (it remains 2:1) while the distillate is much richer in ethanol. The concentration profile along the column is shown in Table 4.5.

Table 4.5 Achieved concentration profile in one of the "initial experiments"

	mol/L Butanal	mol/L EtOH
Distillate	2.2338	15.6674
Top intermediate stage	0.5529	17.6435
Middle intermediate stage	1.6546	15.3465
Bottom intermediate stage	6.6148	7.5928
Bottoms	5.2122	10.0698

The effect of the distillation in this case is not really strong due to the column height and because there are two different feed points (feeding the most volatile one from the bottom stage while the least volatile one is fed from the top stage); the effect of the feed disturbs the trends of the concentration profile along the column. However, in the last part of the column, it can be observed how the liquid was enriched in ethanol and was depleted in butanal when the liquid goes down from the head of the column to the top-intermediate stage. Thus, it is confirmed that despite having a longer chain, the butanal is more volatile than the ethanol (also the normal boiling point of butanal is lower than the boiling point of ethanol).

4.2.2 Pressure drop effect

The pressure drop (ΔP) is a critical variable in order to have good fluid dynamics inside the column and therefore, good liquid–vapor contact. For certain experimental conditions, a higher pressure drop is obtained supplying more power in the reboiler so, higher vapor and liquid flows are got along the column.

Two set of experiments were performed at different ΔP values and at different reflux ratios, keeping constant all the other parameters. As it can be observed in Figure 4.3, at higher pressure drops higher conversions are achieved. Also, it can be observed that the effect of the reflux ratio is much more significant than the pressure drop effect.

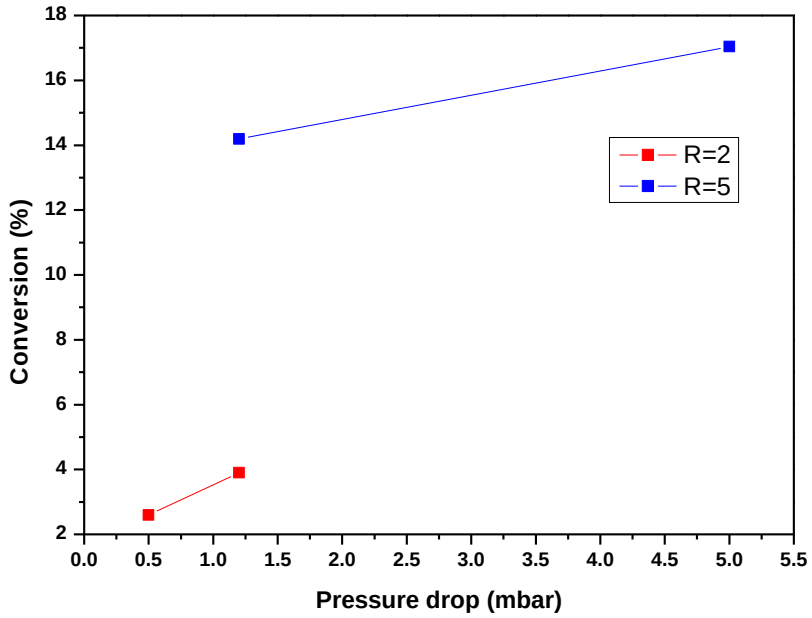

Figure 4.3 Effect of the pressure drop in the conversion. Conditions: stoichiometric feed at 60ºC (ethanol from the top side, 4.15 L/h & butanal from the bottom side, 3.10 L/h), 1 Katapak SP-11 module.

From this point forward, the maximum possible power of the reboiler was used in order to get a pressure drop as high as possible. It must be pointed out that depending on the number of Katapak modules and the reflux ratio, the highest achievable pressure drop changes. Katapak SP-11 modules produce much less pressure drop than the multiknit structured packings.

These first experiments were carried out using only one Katapak SP-11 module but it is clear that more modules are required in order to get higher conversions.

4.2.3 Feed temperature effect

In principle, as a first approximation, the feeding temperature was chosen equal to 60 ºC for both reactants because in the column stabilization process (operating in batch mode) it was observed that the column temperature in the feeding points was around 70 ºC. It is known that at higher temperatures reactions carry out faster but in this case, dealing with an exothermic reaction, at higher temperatures the equilibrium conversion is lower. In order to see which of the effects was the predominant one, another experiment was performed feeding the reactants as close to their saturation point as possible (65 ºC for butanal and 70 ºC for ethanol). It was not possible to feed them at higher temperatures since the liquid located next to the resistance started boiling.

Both of the experiments were carried out with a stoichiometric feed ratio (ethanol from the top side, 4.15 L/h & butanal from the bottom side, 3.10 L/h), 1 Katapak SP-11 module and at total reflux ratio. The achieved conversions are shown in Table 4.6.

Table 4.6 Achieved conversions with different feeding temperatures.

	% Conversion
Ethanol & Butanal at 60 ºC	17.04 %
Ethanol at 70 ºC & Butanal at 65 ºC	18.35 %

It can be observed that if the reactants are introduced at higher temperatures, slightly better conversions are obtained. For this reason, all the following experiments were carried out feeding ethanol at 70 ºC and feeding butanal at 65 ºC being the standard operating conditions the following ones:

- The maximum possible pressure drop
- Stoichiometric feed ratio
    - Ethanol: 4.15 L/h, at 70 ºC, fed from the top-intermediate stage.
    - Butanal: 3.10 L/h, at 65ºC, fed from the middle-intermediate stage.

The number and the position of Katapak SP-11 modules and the reflux ratio will be the variables that are going to be changed in order to get the best column configuration.

4.2.4 Catalyst loading effect

According to the previous experiments, it is clear that the catalyst amount is a critical parameter in order to achieve high conversions. Three different column configurations were experimentally tested: 3 Katapak SP-11 modules, 4 modules and 5 modules placed in different ways as it is shown in Figure 4.4.

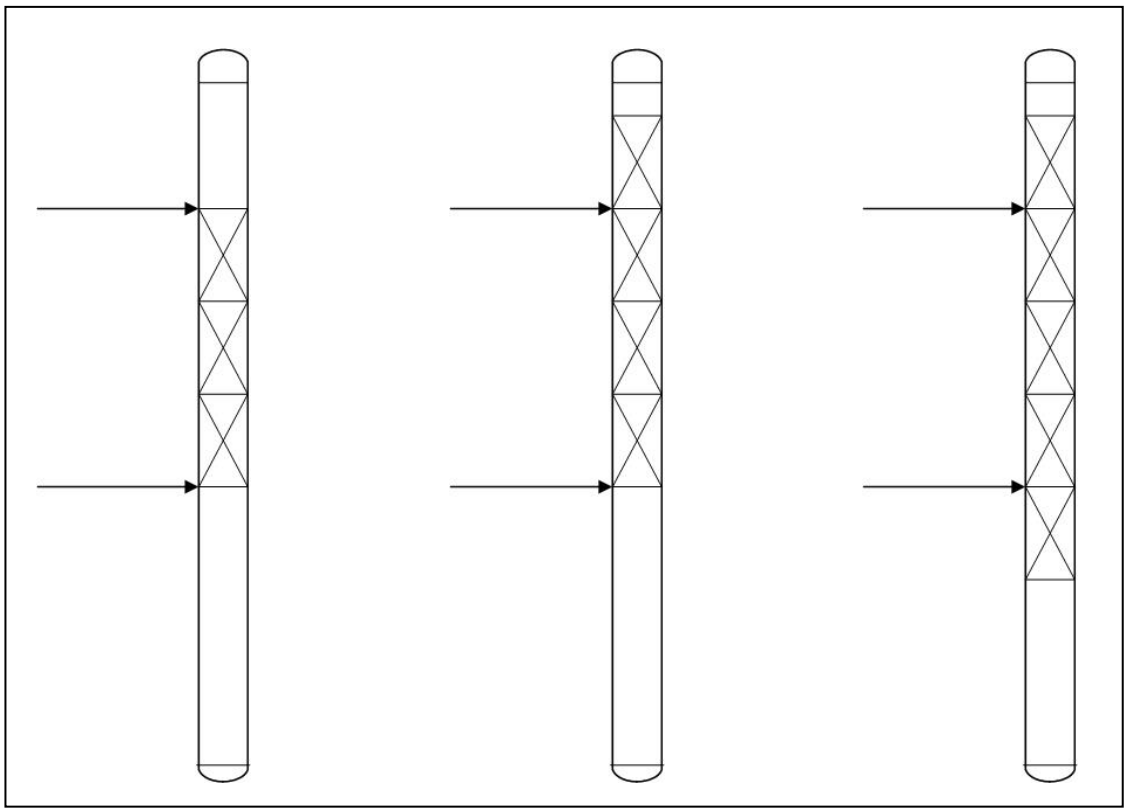

Figure 4.4 Schematic diagram showing the used 3 column configurations.

The height of each Katapak SP-11 module is 10 cm and each one contains 20 g of catalyst (A47).

First of all some batch tests were carried out. For this purpose a stoichiometric feed composition was introduced to the reboiler from its neck entry keeping closed all the output valves. The difference with a batch stirred reactor lies in that in a BSTR reactor the reaction takes place in the bulk of the reactor while in this system, the reaction takes place in the distillation column where the liquid is enriched in the reactants due to the volatility difference between the reactants and the reaction products. The obtained conversions are depicted in Figure 4.5.

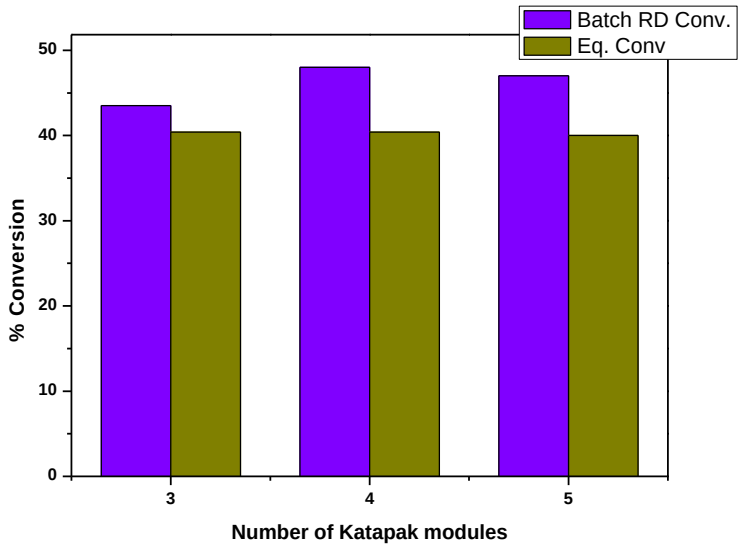

Figure 4.5 Achieved conversions in batch mode and their comparison with the equilibrium conversions at their corresponding T.

As it can be seen, the measured conversions are a bit higher than the equilibrium conversions for these conditions. There is no significant difference between the achieved conversions with 4 and 5 Katapak modules. It seems that the last Katapak module, which is placed just below the middle-intermediate feed stage, does not have a significance effect. This fact could be explained since acetal concentration in this point of the catalytic section is the highest one and thus, the reverse reaction could be significant.

In order to get more data, several experiments were carried out in continuous mode varying the reflux ratio with all the rest operation conditions maintained without any variation. The obtained results are depicted in Figure 4.6.

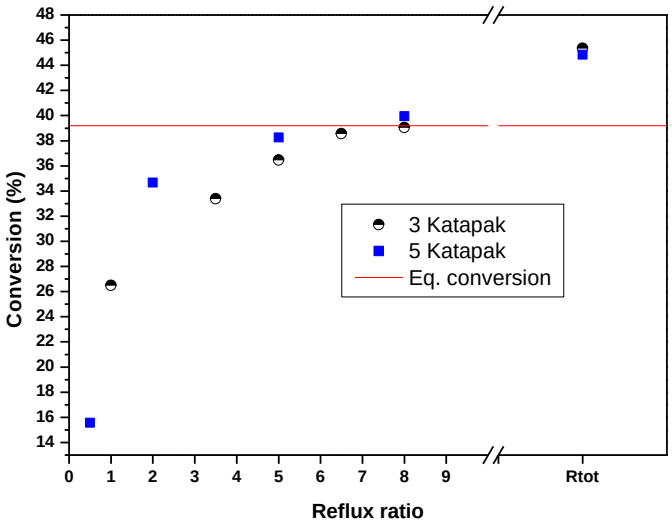

Figure 4.6 Catalyst loading effect for different reflux ratios.

As it was expected at higher reflux ratios, greater conversions were achieved in both cases, with 3 and 5 Katapak modules. This fact is logical since at high reflux ratios, the reactant molecules have more opportunities to react because they pass through the catalyst more times.

It seems that at very low and very high reflux ratios, the amount of catalyst is not so critical since the achieved conversions are quite similar. However, the equilibrium conversion was overcome working only with total reflux. This can be explained by the limited achievable separation among water and non-reacted ethanol and butanal in the rectification section. As a result, significant amounts of ethanol and butanal left the column before they can react except in the case of total reflux ratio. Furthermore, at low reflux ratios the concentrations in the downflow reaching the reactive section are not far away from the equilibrium ones except for the acetal (Table 4.7). Reactive distillation systems would overcome more efficiently thermodynamic limitations operating with reactants that can be separated from water more easily by distillation.

Table 4.7 Distillate composition at R=0.5 and the corresponding equilibrium composition in a conventional reactor.

	Molar %			
	Acetal	**Water**	**Ethanol**	**Butanal**
R=0.5	2.5	14.6	57.2	25.7
Equilibrium	15.4	15.4	46.0	23.0

Another important aspect is the acetal concentration in the output. At low reflux ratios high acetal concentrations are obtained in the bottoms as it is shown In Figure 4.7 & Figure 4.8.

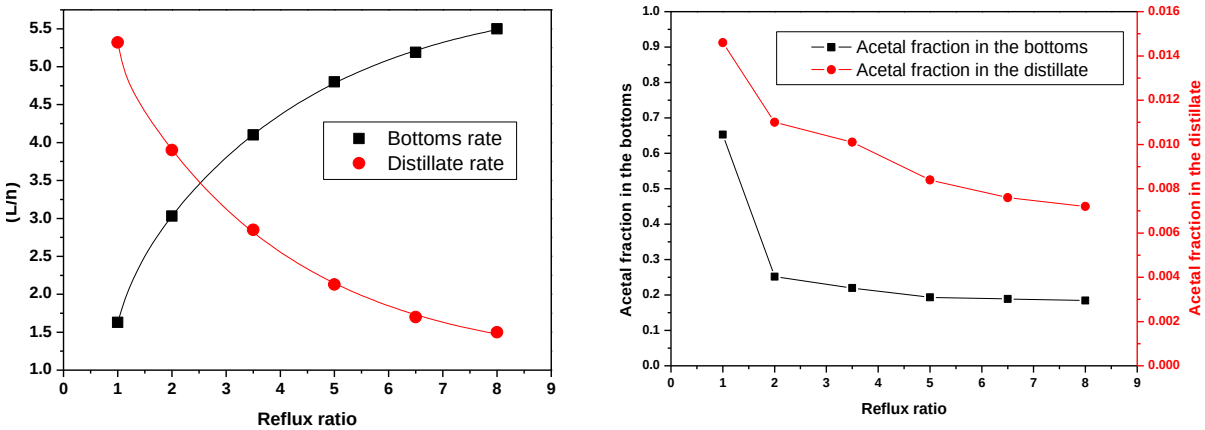

Figure 4.7 Volumetric flow rate and acetal concentration in the outputs. Catalyst loading: 3 Katapak SP-11 modules.

In spite of having very low conversions at low reflux ratios, it can be seen that working only with 3 Katapak modules, 65 molar % of acetal can be achieved in the reboiler, facilitating its later purification.

Further experiments were carried out with 5 Katapak modules. In this case, one test was performed at R=0.5 and the acetal concentration obtained was slightly more than 80 % as it can be seen in Figure 4.8. Working at low reflux ratios the distillate rate is much higher than the bottoms rate. Thus, the lighter compounds (ethanol and butanal) were extracted from the head of the column while the heavy compounds (basically 1,1 diethoxy butane) concentrate in the reboiler.

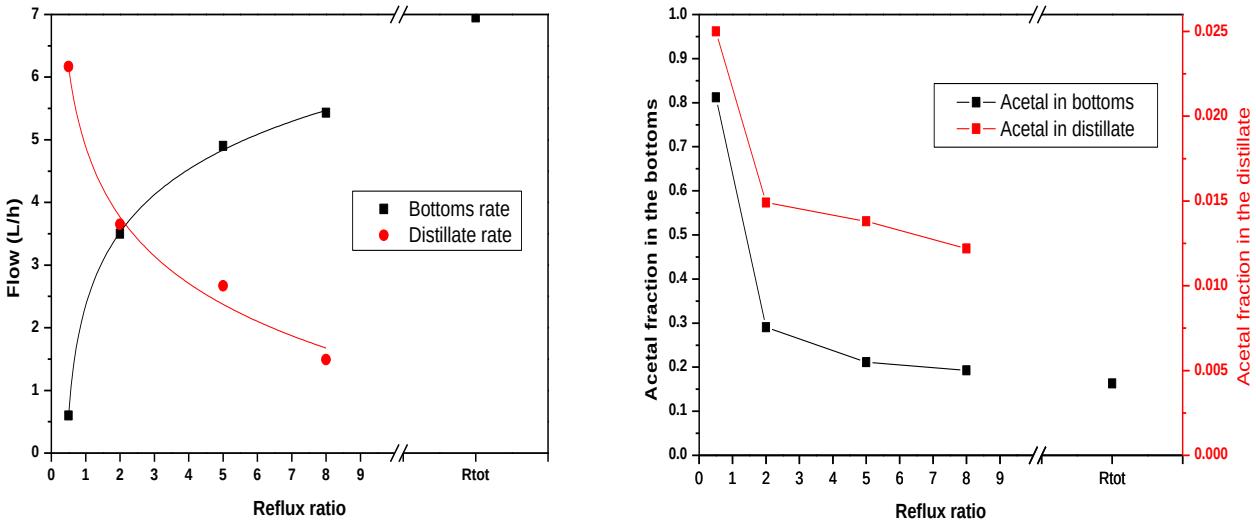

Figure 4.8 Volumetric flow rate and acetal concentration in the outputs. Catalyst loading: 5 Katapak SP-11 modules.

However, a couple of secondary reaction products were observed in the experiment carried out at 0.5 reflux ratio. Gas chromatography with mass spectroscopy (GC/MS) technique was used in order to identify these new components and it was concluded that the unknown products were cis-1-ethoxy-1-butene and trans-1-ethoxy-1-butene. The most probable explanation is that the acetal (1,1-dithoxy butane) was converted in cis(trans)-1-ethoxy-1-butene and ethanol (see Figure 4.9) as a result of the high temperatures achieved in the reboiler when operating at so low reflux ratio.

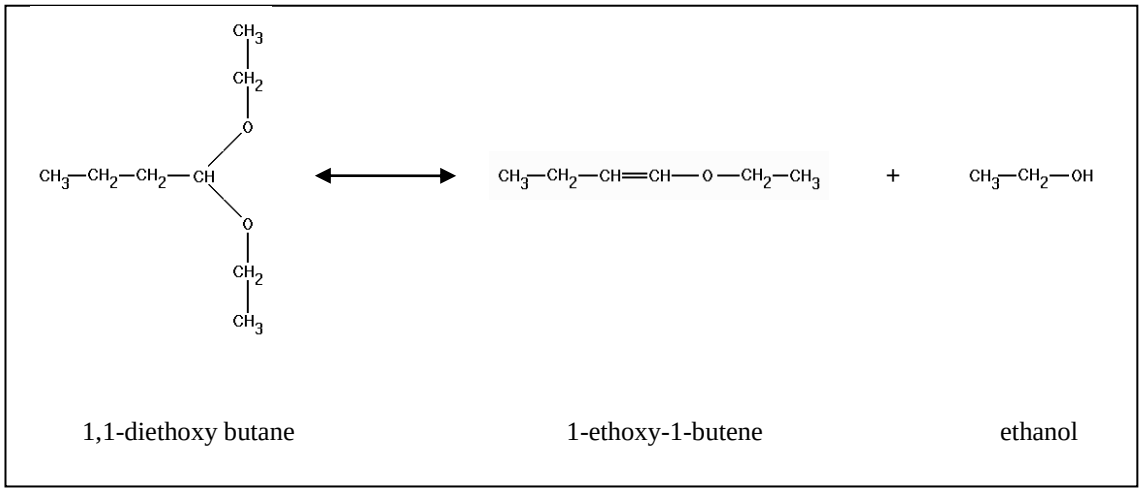

Figure 4.9 1-ethoxy-1-buene production reaction from 1,1-diethoxy butane.

In the reactive section the temperature was 74.15 ºC, which is slightly higher than the temperatures observed in those experiments carried out at higher reflux ratios (see Table 4.8). However it does not seem to be the reason to have this side reaction since the temperature increase is not significant and in some other experiments higher temperatures were observed.

In terms of concentrations and temperatures in the reboiler, it must be pointed out the great increase of acetal concentration, and thus of the temperature, when experiments were carried out at R=0.5 (see Table 4.9). It seems that this is the most probable reason to have the mentioned side reaction.

Table 4.8 Achieved temperatures in the reactive section in different experiments performed at different reflux ratios.

R	T (ºC)	
	3 Katapak	**5 Katapak**
0.5	-	74.15
1	74.85	-
2	-	73.25
3.5	73.75	-
5	72.80	73.07
6.5	73.07	-
8	72.35	72.50
Rtot	72.27	72.15

Table 4.9 Temperature and concentrations in the reboiler at different reflux ratios. Experiments performed with 5 Katapak modules.

R	T (ºC)$_{reb}$	(Acetal fraction)$_{reb}$
0.5	136.0	0.789
2	79.4	0.291
5	77.0	0.211
8	76.4	0.193
Rtot	75.1	0.163

The boiling point of 1-ethoxy-1-butene is around 94 ºC; moreover, according to a brief thermodynamic study performed by ASPEN PLUS using RGIBBS module , acetal decomposition in 1-ethoxy-1-butene, which is an endothermic reaction, is thermodynamically favored only at reboiler conditions when R≤0.5 (temperature around 413.15-416.15 K and high acetal concentrations).

As it is previously mentioned, in these tests, due to the high acetal concentration obtained in the bottoms, the temperature in the reboiler is really high and the stabilization of the operation takes 4 hours approximately. In those experiments carried out at higher reflux ratios, the column stabilization is much faster. (see Figure 4.10 & Figure 4.11)

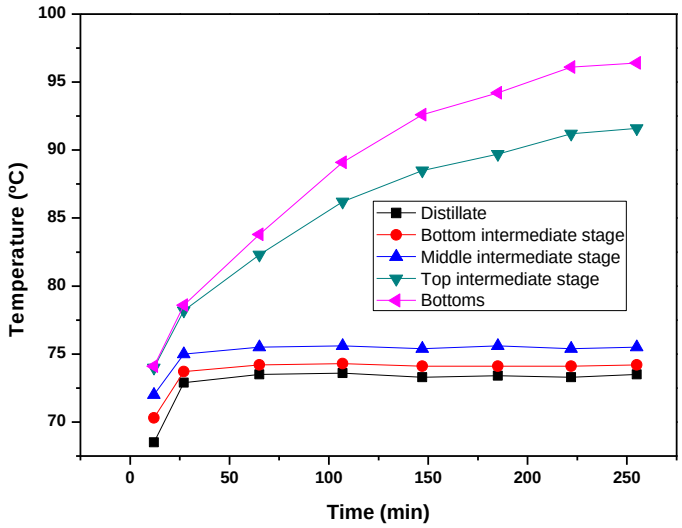

Figure 4.10 Temperature profile along the column. Experiment carried out with 3 Katapak modules and R=1

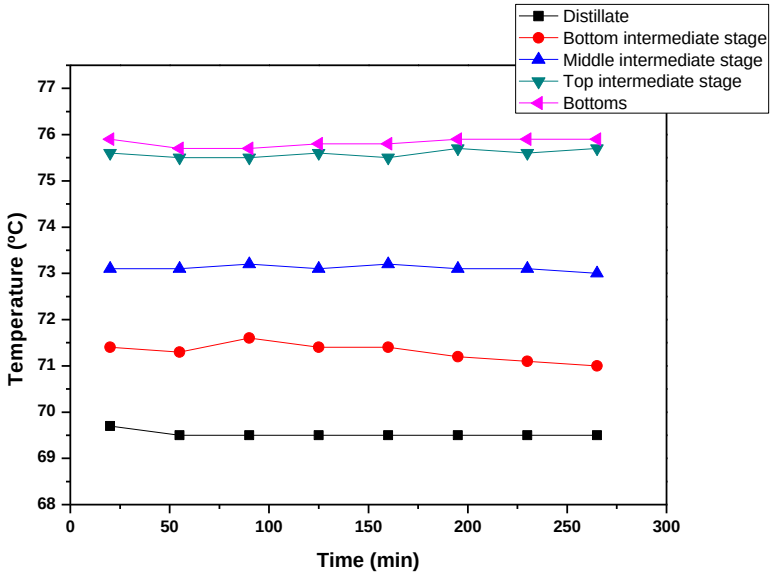

Figure 4.11 Temperature profile along the column. Experiment carried out with 3 Katapak modules and Rtotal

4.2.5 Location of the catalytic section

In this section, the effect of the stripping stages will be discussed. For this purpose 2 different column configurations were used as it is indicated in Figure 4.12.

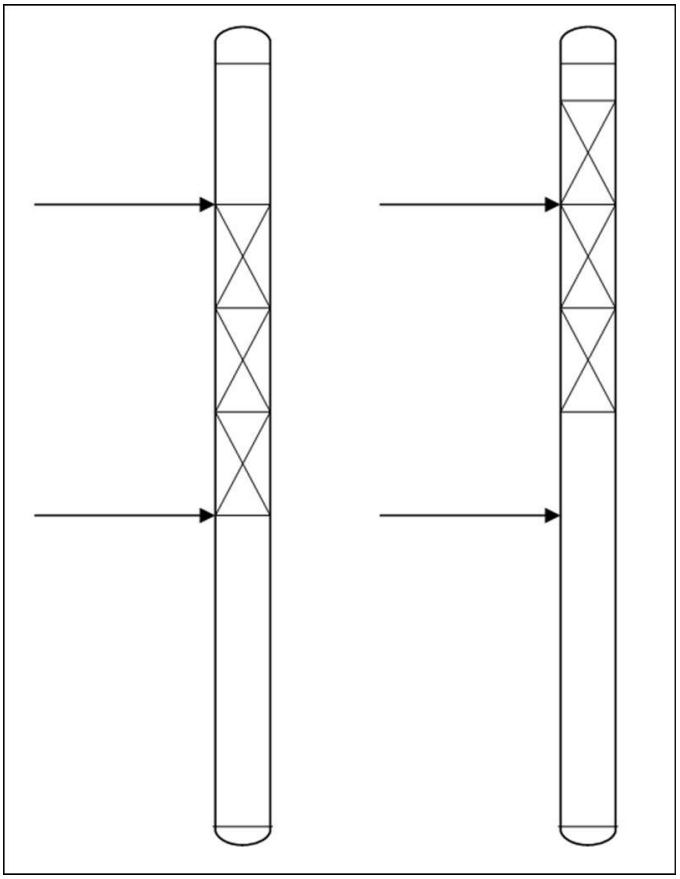

Figure 4.12 Schematic diagram showing the used 2 column configurations.

As it can be seen, in both of the cases 3 Katapak SP-11 modules were used and the variation stems from the modification of stripping height, and therefore, the rectification height.

Figure 4.13 shows the variation of the conversion with the reflux ratio. It can be observed that at low reflux ratios the conversion with additional stripping height is higher, but at higher reflux ratios this trend changes being the achieved conversion lower with this column configuration.

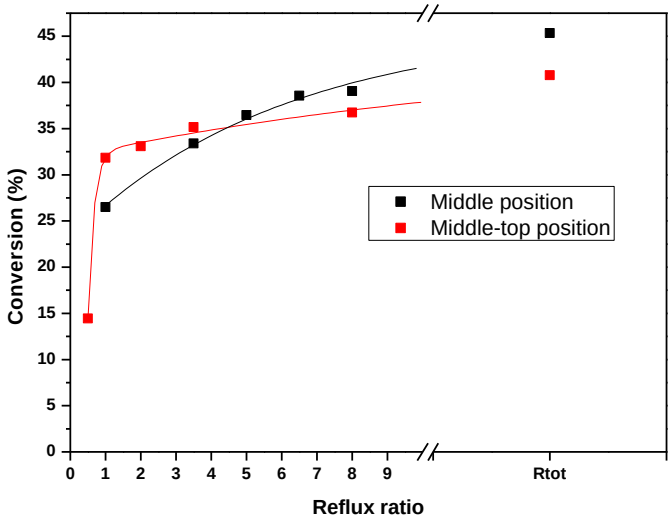

Figure 4.13 Conversion vs R with the two column configurations.

In principle, more stripping height implies higher concentration of the volatile compounds (the reactants) and lower acetal concentrations in the reactive section. According to this explanation the achieved conversion should have been higher with the second column configuration for all the reflux ratios but this is not true for high reflux ratios.

Theoretically, working with high reflux ratios and with the same separation stages, the achieved separation must be higher due to a better vapor-liquid contact. Thus, the liquid mixture which reacts in the catalytic section is even more enriched in the reactants leading to really high conversions. This fact can be explained in the following way. As a consequence of having a higher stripping height, the top part of the catalytic section works better and therefore, more acetal is formed in this part. Due to its low relative volatility, the acetal goes towards the reboiler as soon as it is formed. Thus, acetal concentrations in the lowest part of the catalytic section could be important enough in order to have a significant influence of the reverse reaction and have lower conversions. This effect will be described in more detailed in Section 5.3 since the process mathematical model also predicts this effect.

Also in this case, it must be remarked that 1-ethoxy-1-butene was detected in the experiment which was carried out at R=0.5.

4.2.6 Different feeding configurations

In this section several aspects related to the feeding configuration like feed flow effect, feeding position and feed composition will be discussed.

4.2.6.1 Feed flow effect

In order to measure this effect, 3 different feed flows were used as it is shown in Table 4.10. Notice that the feed flows decrease, being in the second experiment the half of the first one (standard) and a quarter part in the third case. All the other parameters were kept constant and these experiments were carried out using 5 Katapak modules.

Table 4.10 Different feed flows tested.

	Exp 1	**Exp 2**	**Exp 3**
EtOH (L/h) – Top intermediate stage	4.15	2.05	1.12
Butanal (L/h) – Middle intermediate stage	3.10	1.60	0.83

In principle, as the catalyst loading does not change, decreasing the feed flow the conversion should increase. However, it must be taken into account that the fluid dynamics of the column also changes and the vapor-liquid contact and liquid-catalyst contact could be a bit worse.

The achieved conversions are depicted in Figure 4.14:

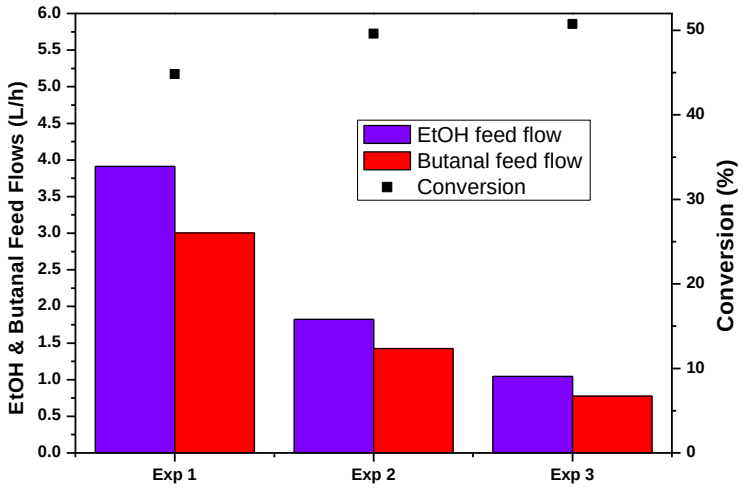

Figure 4.14 Relation between feed flows and the achieved conversion

As it can be seen in Figure 4.14, the conversion increases if the feed flows are decreased. However, it seems that it is difficult to achieve higher conversions decreasing the feed flows since a very low enhancement was obtained between the second and the third experiment.

4.2.6.2 Feed position

Two different feeding configurations were tested; the first one introducing the ethanol from the top-intermediate feed stage and the butanal from the middle-intermediate feed stage and the second one, introducing a stoichiometric feed composition through the top-intermediate feed stage (see Figure 4.15). All the experiments were carried out with 5 Katapak SP-11 modules.

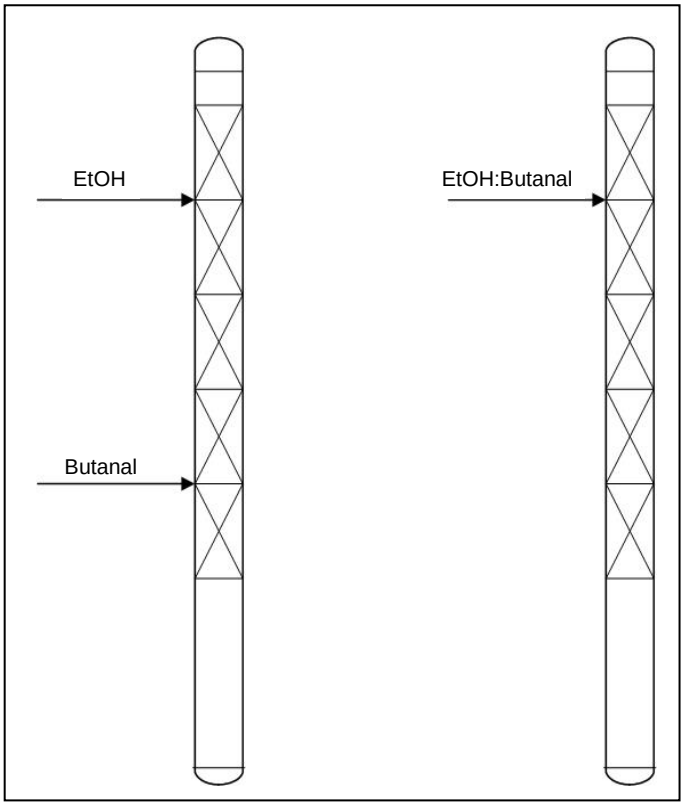

Figure 4.15 Schematic diagram of the tested feeding configurations

Butanal is a bit more volatile than the ethanol and that is the reason why ethanol was fed from the top-intermediate feed stage and butanal from the middle-intermediate stage. However, the volatility difference between them is not really big ($T_{b,EtOH}$=78 ºC & $T_{b,but}$=74 ºC) and that is why the second configuration was tested.

In order to test the second configuration, the feed was prepared in the corresponding storage drum and, before introducing it to the column, it was pre-heated to 68 ºC. The

used feed flow was 7.3 L/h, the sum of the standard flows (3.1 L/h of butanal + 4.15 L/h ethanol), in order to maintain the same fluid dynamics in the distillation column. The achieved conversions with both configurations are depicted in Figure 4.16.

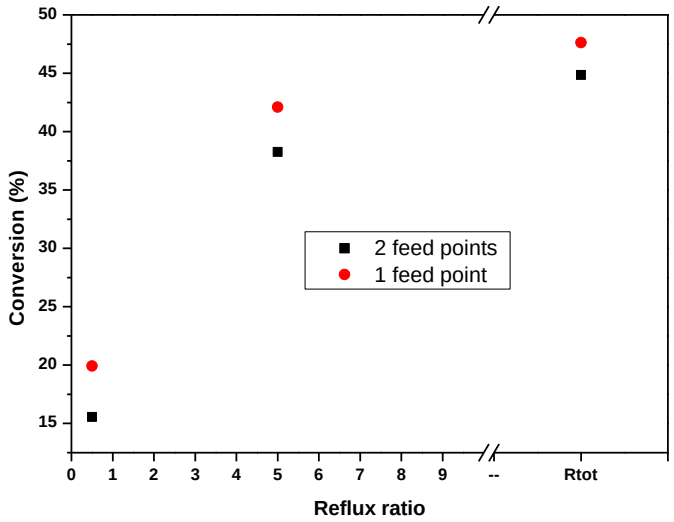

Figure 4.16 Achieved conversion with both of the feeding configurations at 3 different reflux ratios. Experiments carried out using 5 Katapak SP-11 modules.

It is clear that introducing the feed in one unique point enhances considerably the conversion; so, it seems that the volatility difference between the reactants is not high enough in order to use two different feed points. Besides, for further developments at industrial scale, having one feed point is much cheaper since it is not necessary to separate the ethanol from the butanal that have not react before recycling them.

4.2.6.3 Feed composition

In this section the effect of the feed composition was tested. For this purpose 2 different compositions were tested: 2:1 and 4:1 in EtOH:Butanal. In this case, the reactants were fed only from the top-intermediate feed stage since, as it is demonstrated in the previous section, with this configuration the achieved conversions are higher than the conversions achieved having 2 different feed points.

For each feed composition 3 different reflux ratios were tested; the obtained results are shown in Figure 4.17. All the experiments were carried out using 5 Katapak SP-11 modules and the feed flow were 7.3 L/h in all the cases.

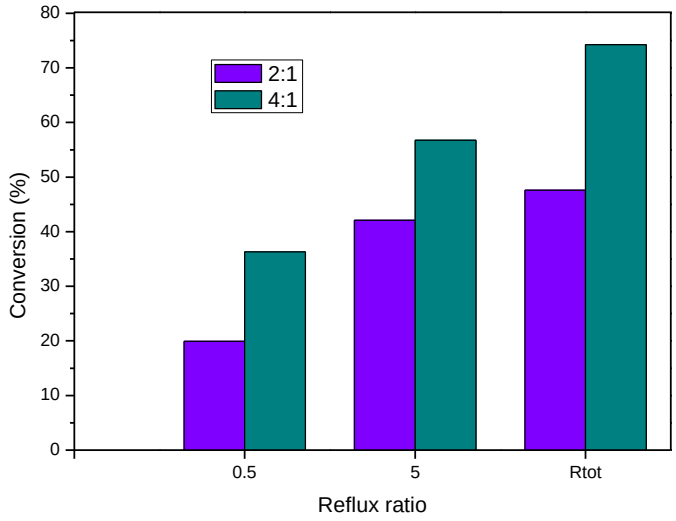

Figure 4.17 The obtained conversions with 2 different feed compositions for 3 different reflux ratios.

As it was expected, when working with an excess of one of the reactants (ethanol in this case) higher conversions are achieved.

In the following graphs the difference between the experimental conversions and the equilibrium ones are depicted.

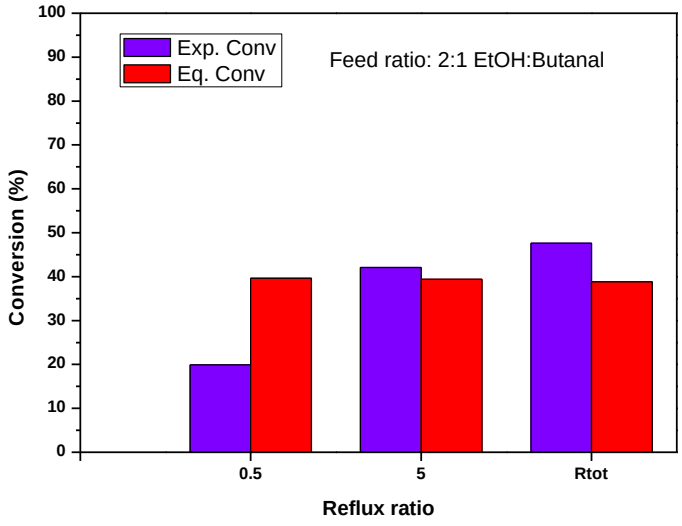

Figure 4.18 Achieved experimental conversion vs equilibrium conversion for a stoichiometric feed ratio (2:1). 5 Katapak SP-11 modules. One feed point: top-intermediate feed stage.

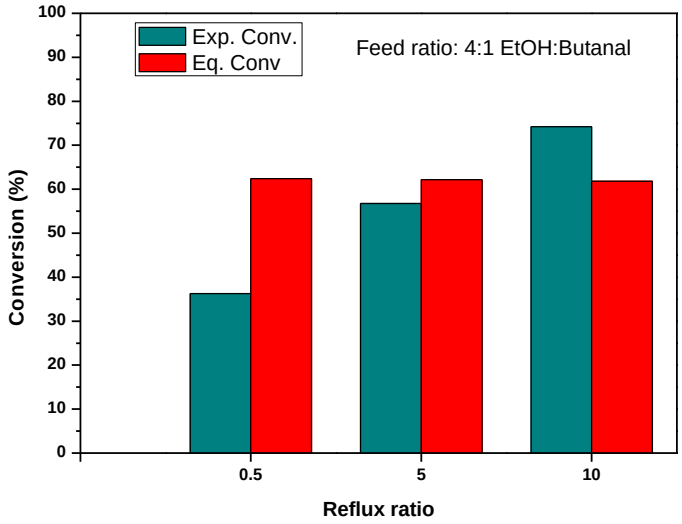

Figure 4.19 Achieved experimental conversion vs. equilibrium conversion. Feed ratio: 4:1; 5 Katapak SP-11 modules; one feed point: top-intermediate feed stage.

Comparing Figure 4.18 & Figure 4.19 it can be observed that working with an stoichiometric feed ratio, the equilibrium conversion was overcame at R=5 and Rtotal. On the other hand, with a 4:1 feed ratio, only working at total reflux equilibrium conversion was overcame. However, in this last case, the difference between the experimental and equilibrium conversion is 12.41% while in the stoichiometric case the differences are 8.78% and 2.71% (for total reflux and R=5 respectively).

4.3 Conclusions

After studying all these effects several conclusions and observations were made. The first evidence was that in the absence of catalyst, the reaction does not carry out.

In the initial experiments, which were carried out with a unique Katapak module, it was observed that with higher pressure drops in the columns, higher conversions were achieved due to a better liquid-catalyst contact. As a drawback, a higher pressure drop implies more power supply in the reboiler which makes the process more expensive from the energetic point of view.

Another tested effect was the feed temperature and working with one Katapak module, it was observed that with higher feed temperatures, higher conversions were achieved. As same as in the previous tests, the drawback is the energy consumption that it implies.

Same more experiments were carried out varying the catalyst loading. It was observed that higher conversions were achieved with more Katapak modules, especially operating at low reflux ratios. At high reflux ratios the catalyst amount is not so critical. On the other hand, the variation of the stripping height showed that more separation stages implies higher conversions at low reflux rates but, depending on the configuration of the catalytic section, lower conversions could be achieved at high reflux ratios.

The variation of the stripping section height showed that more separation stages implies higher conversions at low reflux rates but, depending on the configuration of the catalytic section, lower conversions could be achieved at high reflux ratios. In principle, more stripping height implies higher concentration of the volatile compounds (the reactants) and lower acetal concentrations through the reactive section. According to this explanation, the achieved conversion should have been higher with higher stripping section for all the reflux ratios but this is not true for the highest ones. This fact can be explained in the following way: as a consequence of having a higher stripping height, the top part of the catalytic section works better and therefore, more acetal is formed there. Due to its low relative volatility, the acetal goes down towards the reboiler as soon as it is formed. Thus, acetal concentrations in the lowest part of the catalytic section could be important enough in order to favor the reverse reaction and as a result reach lower conversions.

Regarding the different feed configurations, the main conclusion is that feeding the reactants mixture from the top side of the reactive section, the achieved conversion increases significantly due to the low volatility difference between butanal and ethanol. On the other hand, it was observed that working with lower feed flows (keeping 5 Katapak modules) higher conversions were obtained being the optimal one 3.5 L/h approximately. Besides, introducing a 4:1 EtOH: Butanal mixture, conversions up to 75% were achieved working with R=5.

To sum up, it can be said that the optimum column configuration is the following one:

- 5 Katapak SP-11 modules
- One unique feed point, at the top side of the catalytic section.
- Feed composition: 4:1 EtOH:Butanal
- Feed flow: 3.5 L/h
- Feed temperature: as close as possible to the saturation conditions of the mixture.
- High pressure drops

Chapter V

Reactive distillation. Modeling part

5 Reactive distillation. Modeling part

In this chapter, the development of a mathematical model for the reactive distillation will be presented. As the experimental semi-pilot plant used in the experimental work (Chapter IV) had some limitations (e.g., the column height) the model developed in the present chapter will help to understand the process more accurately when e.g. the column height or other parameters are varied. First of all the model will be checked and tuned with experimental data presented in Chapter IV and then an initial process design work will be presented.

This model is based on a steady-state equilibrium model for the production of 1,1 diethoxy butane from ethanol and butanal and the model takes into account only the global reaction:

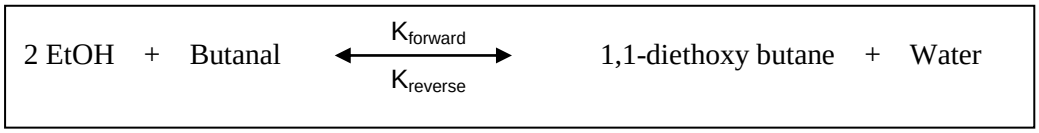

MATLAB was chosen as the software package used to solve the resulting mathematical system due to its friendly manipulation when programming mathematical algorithms.

The model works with N stages in which a reboiler and a total condenser are included. 2 different feed streams at 2 different stages can be considered. The acetalization reaction is carried out only in the liquid phase and this phase is thermodynamically modeled as a non ideal mixture; the activity coefficients (γ_j) are calculated using the NRTL equation.

5.1 The model and its simplifications

One of the objectives of the model is the prediction of the experiments performed in the semi-pilot plant described in Chapter IV. It must be mentioned that the experimental column is a packed one while the model considers discontinuous equivalent stages.

A schematic diagram of an equilibrium stage is shown in Figure 5.1. For a generic *i* stage, the vapor from *i+1* stage and the liquid from *i-1* stage are brought into contact on the *i* stage together; the leaving streams are supposed to be in equilibrium. Each stage is

considered as an adiabatic system. The complete separation process is modeled as a sequence of N of these equilibrium stages (Figure 5.2).

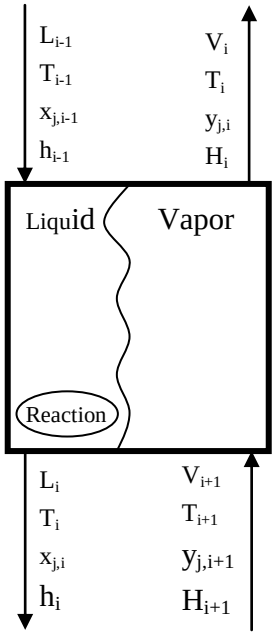

Figure 5.1 The equilibrium stage.

The equilibrium model used in this model consists on the conventional MESH equations (**M**aterial balances, phase **E**quilibrium relations, **S**ummation equations and enthalpy balances -**H**-).

As it can be seen in Figure 5.2, the column consists on N-1 equilibrium stages and a total condenser. It has 2 different possible feed stages (NFT & NFB) and the reactive zone is located between these two stages. It is assumed that there is no reaction in the feed stages, i.e., the reaction takes place between NFT+1 and NFB-1 stages only in the liquid phase.

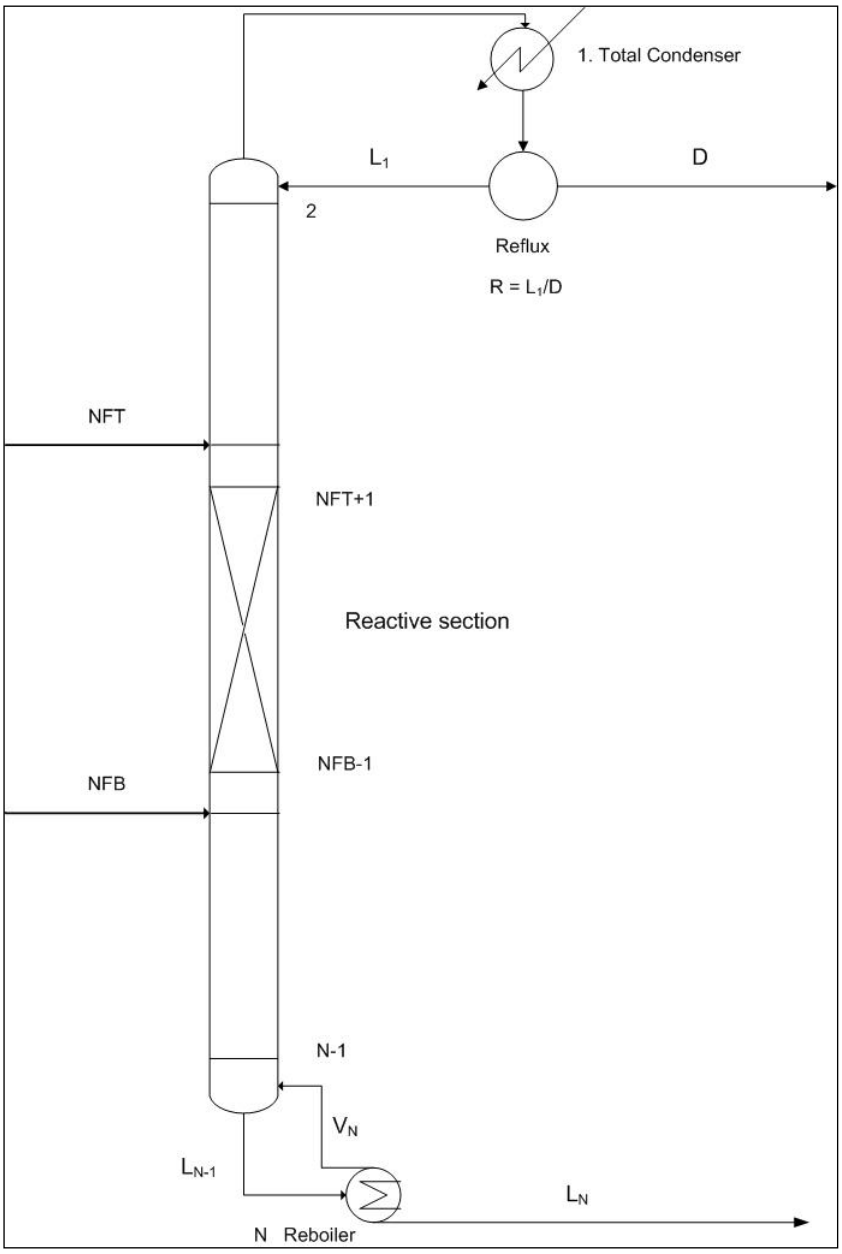

Figure 5.2 The modeled reactive distillation column.

5.1.1 The algorithm

The algorithm consists of a non linear equation system, where all the material and energy balances are included. Apart from these equations, phase equilibrium and summation equations with all the required equations to define the specific heat, saturation pressure and other thermodynamic properties are also defined and included.

First of all, ideal liquid mixture behavior is assumed ($\gamma_i = 1$). With the compositions and temperatures calculated using this assumption a new set of activity coefficients is

calculated. A *while* loop is used in order to converge to the correct values. A scheme of the algorithm is shown in Figure 5.3.

In order to calculate the activity coefficients, Wilson, NRTL and Uniquac models are used for polar compounds. All of them can handle azeotropes, but Wilson cannot handle two liquid phases. After analyzing mixtures of ethanol, butanal, acetal and water with Wilson, NRTL and Uniquac models, NRTL model was chosen, a priori, as the most suitable one (55).

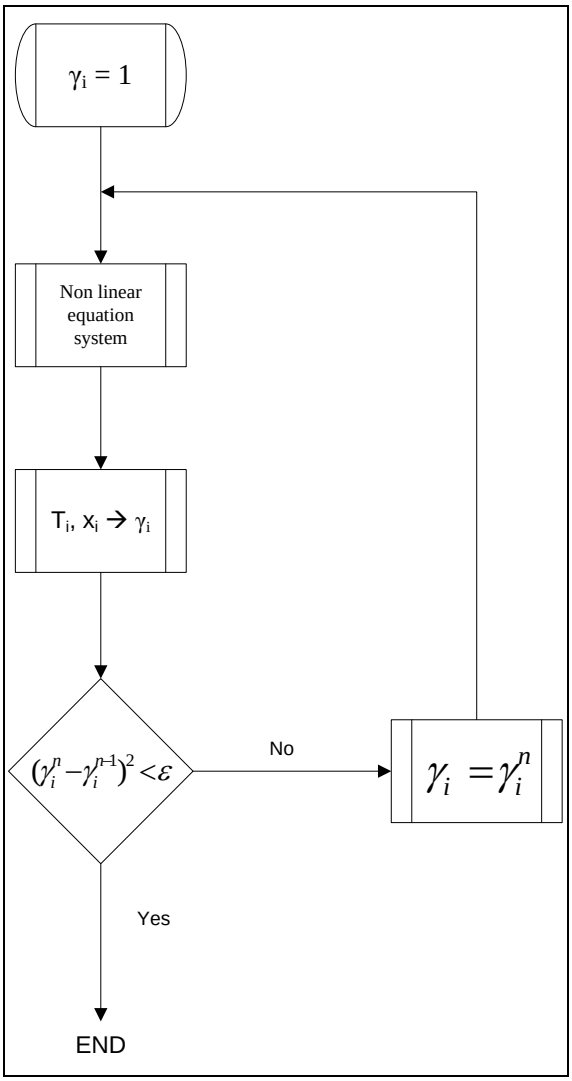

Figure 5.3 The scheme of the algorithm used to solve the model.

5.1.2 Degrees Of Freedom (DOF) analysis

As the first step of the modeling, a study of degrees of freedom was performed. This study is essential in order to know if the mathematical model can be solved or not.

In order to define all the stages correctly, the stage variables of a certain stage are considered the output variables of this stage; i.e. in the reboiler only one liquid flow is considered (L_N) since the input liquid flow (L_{N-1}) is considered a parameter from (N-1) stage.

Three different sections were taken into account; on the one hand the equilibrium stages of the column and on the other hand the total condenser and the reboiler. In Table 5.1, Table 5.2 and Table 5.3 all the required variables and equations are shown.

Table 5.1 Variables and equations for the total condenser.

Variables		**Equations**	
Liquid fractions	4	Material balance	4
Liquid flow	1	Energy balance	1
Condenser duty	1	Summation equations	1
Temperatures	1		
TOTAL	7	TOTAL	6

In a total condenser there is not any equilibrium so the corresponding equations are not required. It can be observed that there are more variables than equations so one of them must be specified in the model.

Table 5.2 Variables and equations for the reboiler.

Variables		**Equations**	
Liquid fractions	4	Material balance	4
Vapor fractions	4	Energy balance	1
Liquid flows	1	Summation equations	2
Vapor flows	1	Equilibrium equations	4
Reboiler duty	1		
Temperatures	1		
TOTAL	12	TOTAL	11

As in the condenser, one variable must be specified in order to solve the reboiler.

Table 5.3 Variables and equations for the i=N-2 stages.

Variables		**Equations**	
Liquid fractions	4i	Material balance	4i
Vapor fractions	4i	Energy balance	1i
Liquid flows	1i	Summation equations	2i
Vapor flows	1i	Equilibrium equations	4i
Temperatures	1i		
TOTAL	11i	TOTAL	11i

In this case the number of variables is the same as the number of equations. So, in order to solve all the equations 2 parameters must be defined: 1 in the reboiler and another one in the condenser. The chosen variables were the temperature in the condenser and the liquid flow rate in the reboiler. Specifying these 2 parameters, all the equations can be solved.

In the case of the condenser temperature a specific relation was imposed to the system: the temperature in the input and in the output of the condenser must be the same. Thus, the condenser duty value is just the condensation heat of the mixture that arrives to the condenser. On the other hand, the liquid flow rate in the reboiler is specified as an input data.

5.1.3 Equations

As it is indicated in Section 5.1, this model consists on the conventional MESH equations. In the following sections *i* will be the counter for the different stages while *j* will be the subscript which will refer to each component.

- Material balance

$$L_{i-1}x_{j,i-1} + V_{i+1}y_{j,i+1} - L_i x_{ji} - V_i y_{ji} + r_j \upsilon = 0 \tag{5.1}$$

Where:

	L	liquid molar flow (mol/s)
	V	vapor molar flow (mol/s)
	x	liquid molar fraction
	y	vapor molar fraction
	r	reaction rate (mol/(s L))
	υ	reaction volume (L)

- Enthalpy balance

$$L_{i-1}h_{j,i-1} + V_{i+1}H_{j,i+1} - L_i h_{ji} - V_i H_{ji} + \Delta H_r r_j \upsilon + Q_i = 0 \quad (5.2)$$

Where:

$$h_i = c_{p_m}^L \left(T_i - T_{ref}\right) \quad (5.3)$$

$$H_i = c_{p_m}^V \left(T_i - T_{ref}\right) \quad (5.4)$$

c_p	specific heat (J/(mol K))
T	Temperature (K)
ΔH_r	Enthalpy of reaction
Q	Heat (J/s)

NOTE: In this model the used reference temperature is 298.15 K for every thermodynamic property.

- Equilibrium equation

$$y_{ji} = K_{ji} x_{ji} \quad (5.5)$$

Where:

$$K_{ji} = \frac{\gamma_{ji} P_j^{sat}}{P_i} \qquad \text{where } P_i = P_{atm} = \text{Constant} \quad (5.6)$$

P	total pressure (bar)
P^{sat}	saturation pressure (bar)
γ	activity coefficient

- Summation equations

$$\sum_{j=1}^{c} x_{ji} = 1 \quad (5.7)$$

$$\sum_{j=1}^{c} y_{ji} = 1 \quad (5.8)$$

In order to solve this system of equations additional equations must be implemented.

5.1.3.1 Reaction rate

A kinetic law must be implemented in both, material and enthalpy balances. The studied reaction was the next one:

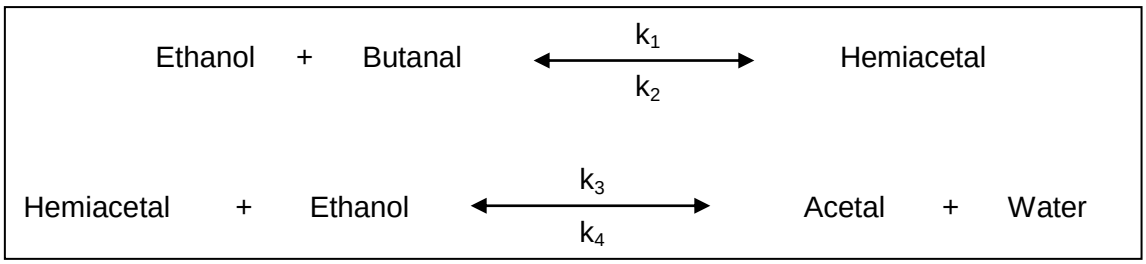

According to the results of the kinetic study previously reported, a reaction mechanism was proposed in Chapter III. The global reaction can be symbolized as:

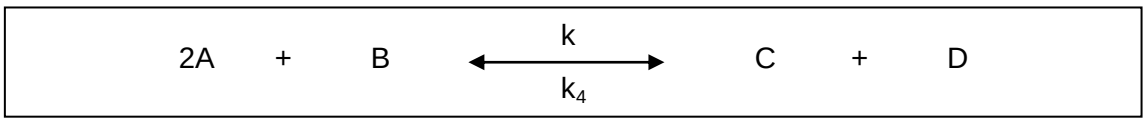

$$\frac{d[C]}{dt} = wkC_A^2C_B - wk_4C_CC_D \tag{5.9}$$

Where: w catalyst loading (g cat/L)

C_j concentration of "j" (mol/L)

$k = k_3K$ & $K = \frac{C_{HA}}{C_AC_B}$;

The relationship among all the component rates is given in the next equation:

$$\frac{r_A}{-a} = \frac{r_B}{-b} = \frac{r_C}{c} = \frac{r_D}{d} \tag{5.10}$$

Based on this equation, rate laws for all the components are:

$$r_A = -2wkC_A^2C_B + 2wk_4C_CC_D \tag{5.11}$$

$$r_B = -wkC_A^2C_B + wk_4C_CC_D \tag{5.12}$$

$$r_C = wkC_A^2C_B - wk_4C_CC_D \tag{5.13}$$

$$r_D = wkC_A^2C_B - wk_4C_CC_D \tag{5.14}$$

In order to calculate the concentration of each component in mol/L the volumetric flow must be calculated using the following equation:

$$Q_V = \sum_{j=1}^{c} \frac{L_i x_{ji} MW_j}{\rho_j} \quad [\text{L/s}] \tag{5.15}$$

Where: MW molecular weight
ρ density of the liquid mixture

Dividing the molar flows by the volumetric flow, the concentrations in mol/L are obtained.

$$C_j = \frac{L_j x_j}{Q_v} \quad [\text{mol}_j/\text{L}] \tag{5.16}$$

Kinetic constants follow Arrhenius' Correlation:

$$Ln(k) = Ln(A) + \left[\frac{-E_a}{RT}\right] \tag{5.17}$$

Where: E_a is the activation energy (J/mol)
R is the universal gas constant (J/(mol K))
T is the temperature in Kelvin
A is the pre-exponential factor
k is the kinetic constant

In Table 5.4 the activation energy and the pre-exponential factor obtained in the kinetic study (Chapter III) are showed. These values were implemented in the model.

Table 5.4 Arrhenius' Correlation's parameters for the global reaction.

	Forward reaction	**Reverse reaction**
E_a (kJ/mol)	35.5	59.8
A	$64.7 \left(\frac{L^3}{mol^2 \min\ gcat}\right)$	$6.4E+6 \left(\frac{L^2}{mol \min\ gcat}\right)$

5.1.3.2 Specific heat

For liquids, an average specific heat was used for each component

Table 5.5 Specific heat for each component in the liquid phase.

Component	C_p (25 ºC) (J/(mol K))
Ethanol	112.0 (56)
Butanal	164.00 (56)
1,1 Diethoxy butane	239.551 (Aspen)
Water	75.38 (56)

For the vapor phase, a T dependant expression was used:

$$C_P = A + BT + CT^2 + DT^3 \qquad \text{[J/(mol K)]} \tag{5.18}$$

Table 5.6 Different coefficients to calculate the specific heat of each component as an ideal gas.

Component	A	B	C	D
Ethanol	9.014	2.141 E-1	-8.390 E-5	1.373 E-9
Butanal	1.408 E+1	3.457 E-1	-1.723 E-4	2.887 E-8
1,1 Diethoxy butane	-39.726	1.063	-0.788 E-3	2.416 E-7
Water	3.224 E+1	1.924 E-3	1.055 E-5	-3.596 E-9

For ethanol, butanal and water the coefficient were obtained from Prausnitz (57) while the coefficients of the acetal were estimated with ASPEN PLUS.

In the enthalpy balance an average specific heat was used, so:

$$\overline{C_{pi}} = \frac{\int_{Tref}^{T} C_{pi}}{T - T_0} = \frac{A_i(T - T_0) + (B_i/2)\left(T^2 - T_0^2\right) + (C_i/3)\left(T^3 - T_0^3\right) + (D_i/4)\left(T^4 - T_0^4\right)}{T - T_0} \tag{5.19}$$

5.1.3.3 Enthalpy of reaction

As the reaction is supposed to take place only in the liquid phase the reaction enthalpy must be calculated from enthalpies of formation in the liquid phase. Formation enthalpies of ethanol, butanal and water are presented in Table 5.7.

Table 5.7 Enthalpies of formation at 25 ºC in liquid phase for ethanol, butanal and water (56).

Component	**$\Delta H_{f,j}$ (25 ºC) in [kJ/mol]**
Ethanol	-277.6
Butanal	-240.0
Water	-285.83

For 1,1 diethoxy butane no enthalpy of formation in liquid phase was found but with the enthalpy of formation as an ideal gas and the vaporization enthalpy (both estimated using ASPEN PLUS) it was possible to calculate its formation enthalpy as liquid:

Table 5.8 Enthalpies of formation and vaporization of the acetal.

Component	**ΔH_f (IG) [kJ/mol]**	**ΔH_{vap} (1 bar) [kJ/mol]**
1,1 Diethoxy butane	-496.788	43.68

$$\Delta H_f^{\circ}(liq) = \Delta H_f^{\circ}(IG) - \Delta H_{vap} = -540.468 \quad [\text{kJ/mol}] \tag{5.20}$$

Thus, the enthalpy of reaction is defined as:

$$\Delta H_r(T) = \sum_j \nu_i \Delta H_f^{\circ}(liq) + \int_{T_0=298.15}^{T} \Delta C_p dT \tag{5.21}$$

$$\Delta H_r^{\circ}(T_0) = \sum_j \nu_i \Delta H_f^{\circ}(liq) = -31.098 \ [kJ/mol] \tag{5.22}$$

$$\Delta C_p = \sum \nu_j C_{p_j}(liq) = -73.069 \quad [J/(mol\,K)] \tag{5.23}$$

The final expression for the enthalpy of reaction is given in the next equation. Remark that as it is a function of temperature, it changes from one stage to another.

$$\Delta H_r(T_i) = -31098 + (-73.069) * (T_i - 298.15) \tag{5.24}$$

5.1.3.4 Saturation pressure

In order to calculate the saturation pressure of each component at any temperature an amplified Antoine's equation (eq. (5.25) was used for ethanol, butanal and water (57) and a simplified equation (eq. (5.26) based on their two available points (critical point and normal boiling point, estimated with Aspen) for the acetal.

$$Ln\frac{P_j^{sat}}{P_{c,j}} = \frac{T_{c,j}}{T}\left[Ax + Bx^{1.5} + Cx^3 + Dx^6\right] \quad (5.25)$$

Where $x = 1-T/T_c$ T in K & P in bar

$$Ln\, P_j^{sat} = A - \frac{B}{T} \quad (5.26)$$

In Table 5.9 all the parameters are indicated

Table 5.9 Parameters for the calculation of P^{sat} (57) & Aspen.

Comp.	A	B	C	D	P_c (bar)	T_c (K)	T range
Ethanol	-8.51838	0.34163	-5.73683	8.32581	61.4	513.9	293-513.9
Butanal	-7.01403	0.12265	-0.00073	-8.50911	53.8	545.4	304-545.4
Acetal	11.38	4735.9	-	-	24.7	579.52	
Water	-7.76451	1.45838	-2.77580	-1.23303	221.2	647.3	275-647.3

Apart from the critical point, the normal boiling point of the acetal was also used in order to calculate its A and B. ($T_{nb,acetal}$ = 416.2 K).

5.1.3.5 Holdup

The liquid holdup correlation for each Katapak SP-11 module was kindly provided by Sulzer, the supplier. The liquid load data were transformed from $m^3/(m^2h)$ to L/s using the column section of the semi-pilot plant. Fitting the data, a second degree polynomial was obtained.

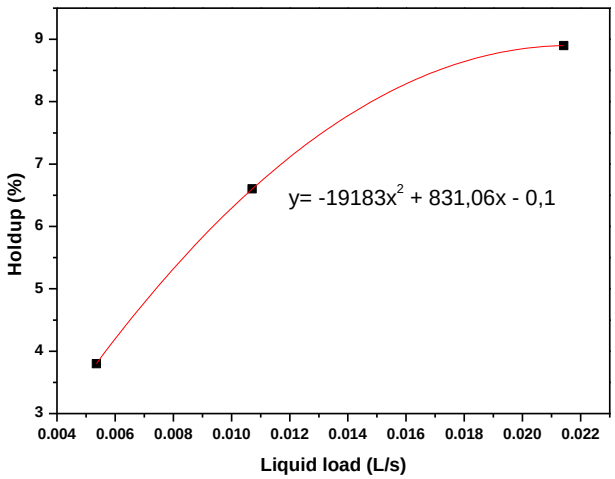

Figure 5.4 Correlation between the liquid loads of the column with the holdup in a Katapak SP-11.

5.1.4 Input data

Any mathematical model requires some input data in order to be solved. For this model, the required input data are the next ones:

- Number of stages (N)
- Location of the top feed stage (NFT) and the bottom feed stage (NFB)
- Feed rate in the top feed stage (mol/s) (FT)
- Feed rate in the bottom feed stage (mol/s) (FB)
- Composition of the feed streams
- Temperature of the feed streams (K)
- Reflux ratio
- Total pressure (bar)
- Molecular weight (g/mol) and density (g/mL) of the components (in liquid phase)
- Different parameters to calculate thermodynamic parameters like saturation pressure and specific heat as a function of temperature for each component
- Catalyst amount of each Katapak module. It is estimated that there are 20 g in each Katapak (52;58)

Apart from all these data, as it is explained in Section 5.1.2, the liquid rate (L/h) must be specified in the reboiler, as well as an additional restriction in the condenser ($T_{in}=T_{out}$).

As all the computers operate with numeric methods, the model needs some guess values to start iterating to solve the equation system. Matlab *Fsolve* function was used in order to solve the system. This function forces to insert all these guess values in a unique vector (*x0*). The variable will be one or another depending on the position of the variable *x* in the vector. However, just before the equations a variable change is done in order to have readable equations.

x_A	x(1) ⋮ x(N)	P_A^{Sat}	x(13N-6) ⋮ x(14N-8)
x_B	x(N+1) ⋮ x(2N)	P_B^{Sat}	x(14N-7) ⋮ x(15N-9)
x_C	x(2N+1) ⋮ x(3N)	P_C^{Sat}	x(15N-8) ⋮ x(16N-10)
x_D	x(3N+1) ⋮ x(4N)	P_D^{Sat}	x(16N-9) ⋮ x(17N-11)
y_A	x(4N+1) ⋮ x(5N-1)	$C_{P,A}$	x(17N-10) ⋮ x(18N-11)
y_B	x(5N) ⋮ x(6N-2)	$C_{P,B}$	x(18N-10) ⋮ x(19N-11)
y_C	x(6N-1) ⋮ x(7N-3)	$C_{P,C}$	x(19N-10) ⋮ x(20N-11)
y_D	x(7N-2) ⋮ x(8N-4)	$C_{P,D}$	x(20N-10) ⋮ x(21N-11)
L	x(8N-3) ⋮ x(9N-5)	Q_V	x(21N-10) ⋮ x(21N-12+NFB-NFT)
V	x(9N-4) ⋮ x(10N-6)	Q_C	x(21N-11+NFB-NFT)
		Q_R	x(21N-10+NFB-NFT)
T	x(10N-5) ⋮ x(10N-6)	*k1*	x(21N-9+NFB-NFT) ⋮ x(21N-11+2NFB-2NFT)
h	x(11N-5) ⋮ x(12N-6)	*k2*	x(21N-10+2NFB-2NFT) x(21N-12+3NFB-3NFT)
H	x(12N-5) ⋮ x(13N-7)	*Holdup*	x(21N-11+3NFB-3NFT) x(21N-13+4NFB-4NFT)
		DHR_ra	x(21N-12+4NFB-4NFT) x(21N-14+5NFB-5NFT)

Figure 5.5 The guess values vector with its relative positions.

The output data of the model is the same vector but with the optimum values that predicts the performance of the specified reactive distillation system operating at the specified conditions.

5.2 Model validation

5.2.1 Model tuning

In order to get model predictions matching experimental results within acceptable ranges some parameters had to be adjusted. One of the most important one is the number of stages: on the one hand the reaction stages and on the other hand the separation stages (stripping & rectification ones).

According to the model structure, the used experiments for the tuning were those ones carried out with 3 Katapak modules. The column configuration of these experiments is depicted in Figure 5.6.

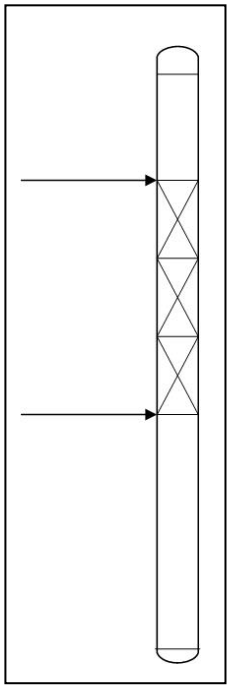

Figure 5.6 Used experimental column configuration for model tuning.

Besides, the model incorporates some simplifications, e.g. the assumption that the column is adiabatic and in every single stage the equilibrium is achieved. Actually, these hypotheses are not fully true and an additional *tuning factor* was used.

At first, one reacting stage was assigned to 3 Katapak modules and then stripping stages were varied (rectification stages were not changed since the height of the rectification section in the experimental semi-pilot plant is really low; only one stage was assigned, the top feed stage). According to the literature 0.3 m of Katapak SP-11 modules are equivalent to 0.66 stages as the NTSM number (Number of Theoretical Stages per Meter) for this type of structured packing is 2 (58).

An optimum *tuning factor* was found in each case and it was checked if the factor was constant or it presented any specific trend. This *tuning factor* includes several factors apart from the ones mentioned above: like the equivalent plate efficiencies and a wetting factor of the catalyst since all the catalyst may not have taken part in the reaction; moreover, the model assumes that the column is completely adiabatic when in reality it was not. Because of all these reasons this factor was applied to the kinetic expressions of the reactive stages.

Thus, 3 different column configurations were checked as it is shown in Table 5.10.

Table 5.10 Tested 3 column configurations for model tuning.

Configuration		Different stages
1	N=5 NFT=2 NFB=4	1 reaction stage + 1 stripping stages + 1 rectification stages
2	N=6 NFT=2 NFB=4	1 reaction stage + 2 stripping stages + 1 rectification stages
3	N=7 NFT=2 NFB=4	1 reaction stage + 3 stripping stages + 1 rectification stages

These three column configuration were tested choosing an appropriate *tuning factor* in each case. In all these cases conversion was used as checking parameter. Table 5.11 shows the experimental and the predicted data in each case as well as the optimum *factor* which adjusts the reaction performance.

Table 5.11 Experimental and predicted data for each experiment.

Exp. Reflux ratio	**Exp. Conv**	**Conf 1**		**Conf 2**		**Conf 3**	
		Pred. Conv.	***Tuning Factor***	***Pred. Conv.***	***Tuning Factor***	***Pred. Conv.***	***Tuning Factor***
R=1	26.5%	26.4%	0.363	26.5%	0.145	26.5%	0.151
R=3.5	33.4%	33.4%	0.131	33.5%	0.114	33.5%	0.118
R=5	36.5%	36.4%	0.145	36.4%	0.125	26.5%	0.131
R=6.5	38.6%	38.5%	0.178	38.5%	0.154	38.6%	0.160
Rtot	45.3%	45.4%	0.083	45.7%	0.091	45.3%	0.105

Regarding the performance of the *tuning factor* it seems that the second and third configurations are the most suitable ones; in these two configurations the factor is more stable. After checking this aspect, the separation of the compounds was checked. For this purpose acetal concentration in the distillate and in the bottoms was the checked parameter since its measurement is the most reliable one as it is explained in Section 3.2.

Table 5.12 shows the acetal fractions in the distillate as well as in the bottoms for both, the experimental results and for the predicted values.

Table 5.12 Acetal fractions in the distillate and in the bottoms. Experimental results and predicted results for each model configurations.

	Experiments		**Predictions**					
			Conf 1		**Conf 2**		**Conf 3**	
R	**Acetal fraction**		**Acetal fraction**		**Acetal fraction**		**Acetal fraction**	
	Bottoms	**Distilate**	**Bottoms**	**Distilate**	**Bottoms**	**Distilate**	**Bottoms**	**Distilate**
1	0.65	0.014	0.75	0.0065	0.76	0.0053	0.8	0.0053
2	0.25	0.010	0.28	0.0047	0.28	0.0042	0.29	0.0041
3.5	0.22	0.010	0.23	0.0045	0.23	0.004	0.24	0.0038
5	0.19	0.0084	0.22	0.0044	0.22	0.0039	0.22	0.0036
6.5	0.19	0.0076	0.2	0.0045	0.2	0.0039	0.2	0.0037
Total	0.17		0.18		0.18		0.18	

According to these results, it is clear that the best column configuration for the model is the second one. In terms of separation there are hardly differences between the first and second configurations and the predicted acetal molar fraction of these two configurations are closer to the real ones than the predicted ones by the third configuration. Taking into account that the *tuning factor* performs better in the second configuration, this one was the chosen configuration as the best one.

From this point on, the average value of the *tuning factor* values obtained with the 2nd configuration was used for all the simulations (F=0.13). The order of magnitude of this number was the expected one.

The *tuning factor* includes several factors like the equivalent plate efficiencies and a wetting factor of the catalyst. According to the literature 0.3 m of Katapak SP-11 modules are equivalent to 0.66 stages as the NTSM number for this type of structured packing is 2 (58). On the other hand all the catalyst may not have taken part in the reaction and moreover, the model assumes that the column is completely adiabatic when in reality it was not.
However, the existence of external mass transfer was studied in order to check if it limits the process; for this purpose a first approximation was done using the Frössling correlation.

$$Sh = 2 + 0.6\,\mathrm{Re}^{1/2}\,Sc^{1/3} \tag{5.27}$$

Where:

$$Sh = \frac{k_c d_p}{D_{AB}} \text{ ; (Sherwood)} \tag{5.28}$$

$$\mathrm{Re} = \frac{d_p U \rho}{\mu} \text{ ; (Reynolds)} \tag{5.29}$$

$$Sc = \frac{\mu}{\rho D_{AB}} \text{ ; (Schmidt)} \tag{5.30}$$

Where:

d_p	Catalyst particle size (m)
U	Liquid speed in the catalytic section (m/s)
μ	Dynamic viscosity (Pa s)
ρ	Density of the liquid mixture (kg/m^3)
D_{AB}	$D_{but,mix}$ butanal diffusivity in the mixture

In order to perform these calculations, the observed conditions of an experiment carried out at low reflux ratio were chosen (3 Katapak modules, R=0.5). The lowest liquid flows in the column are obtained operating at total distillate but the distillate rate is necessary in order to calculate them; therefore, R=0.5 was chosen. The lower liquid flows in the column, the lower liquid speed in the reactive section and if in these

conditions the external mass transfer is negligible it can be considered insignificant in all the cases.

Therefore, the used column conditions for all the calculations were the following ones:

- Composition (molar fraction):
  - X_{but} = 0.15
  - X_{EtOH} = 0.67
  - X_{acetal} = 0.05
  - X_{H2O}=0.12
- Temperature in the reactive section: 75 ºC
- R=0.5 ; Distillate rate: 0.61 L/h

ASPEN PLUS was used to calculate the viscosity, the density and the diffusivity. Finally, the acetal concentration was not introduced in ASPEN since with its presence ASPEN reports several errors. However, the acetal concentration is very low and it is supposed that its presence does not affect too much to the properties of the mixture.

Notice that the particle size of Amberlyst 47 is not supplied by Rohm & Haas. However, knowing the particle sizes of Amberlyst 15Wet, Amberlyst 35Wet and Amberlyst 70 (see Table 3.2 of Chapter III) and observing that the A47 particle size is slightly bigger than A35W's size, 1 mm diameter value was used for the calculations. In Chapter VI this value was checked and confirmed (see Figure 6.18).

In order to calculate the liquid speed, the full column section (ø = 50 mm) was used instead of taking away the section of the catalyst bags. If with this simplification the external mass transfer is not relevant, it will not be relevant in reality since the actual liquid speed is higher. The estimation of all these parameters is shown in Table 5.13.

Table 5.13 Estimation of all the parameters in order to calculate k_c.

d_p = 1E-3 m	
U = 6.101E-4 m/s	Re = 1.08;
μ = 4.237E-4 (Pa s)	Sc = 195.48;
ρ = 753.53 (kg/m^3)	Sh = 347826.087 k_c
$D_{but,mix}$ = 2.875E-9 (m^2/s)	

Applaying Frössling's correlation the "k_c" value is obtained:

$$k_c = 1.618E\text{-}5 \text{ (m/s)}$$

In order to know if the reaction is controlled by the kinetics or by the external mass transfer, the kinetic low and the average molar flux from the liquid bulk to the catalyst surface are matched.

$$-r = k'\left(C_A^S\right)^2 C_B^S = \left(k_c a_c\right)_B \left(C_{BL} - C_B^S\right) = 0.5\left(k_c a_c\right)_A \left(C_{AL} - C_A^S\right) \tag{5.31}$$

Where "a_c" is the surface area per kg of catalyst. (for A47 a_c = 50000 m^2/kg; see Table 3.2 of Chapter III)

C_B^S can be expressed like:

$$C_B^S = \frac{\left(k_c a_c\right)_B C_{BL}}{k'\left(C_A^S\right)^2 + \left(k_c a_c\right)_B} \tag{5.32}$$

Substituting (5.32) in (5.31) and assuming that $(k_c a_c)_A \approx (k_c a_c)_B$

$$-r = k'\left(C_A^S\right)^2 \frac{\left(k_c a_c\right) C_{BL}}{k'\left(C_A^S\right)^2 + \left(k_c a_c\right)} = \frac{C_{BL}}{\frac{1}{k_c a_c} + \frac{1}{k'\left(C_A^S\right)^2}} \tag{5.33}$$

Comparing the values of $\frac{1}{k_c a_c}$ and $\frac{1}{k'\left(C_A^S\right)^2}$ it is possible to assert if the process is controlled by the kinetics or by the mass transfer.

$k_c a_c$ = 0.809 (L/(g s))

As the value of C_A^S is unknown, the value of $(k' C_{AL})$ will be estimated as a first approximation.

C_{AL} = 7.43 mol/L (concentration of EtOH in the reactive section; experimental value).

k' (73 ºC) = 2.835E-4 (L^3/(mol^2 s gcat)) (see Chapter III, Section 3.5)

(C_{AL} k') = 0.01565 (L/(s gcat))

Therefore:

$$\frac{1}{k_c a_c} < \frac{1}{k'(C_{AL})^2} \tag{5.34}$$

And, as (k' $(C_A^S)^2$) < (k' $(C_{AL})^2$):

$$\frac{1}{k_c a_c} << \frac{1}{k'(C_A^S)^2} \tag{5.35}$$

Therefore, the external mass transfer is negligible with regards to the kinetics.

5.2.2 Comparison of experimental results versus model predictions

In order to check that all the model predicted parameters are comparable to the experimental values, some graphs and tables will be shown in this section.

In Figure 5.7 it can be observed that the achieved experimental conversion and the predicted ones correspond quite well. Moreover, there are some other parameters like temperatures or bottoms and distillate flow rates that are also quite similar as it is shown in Table 5.14.

All the simulations were performed using 3.1 L/h of butanal and 4.15 L/h of ethanol, as feeding flow rates, as same as in the experiments.

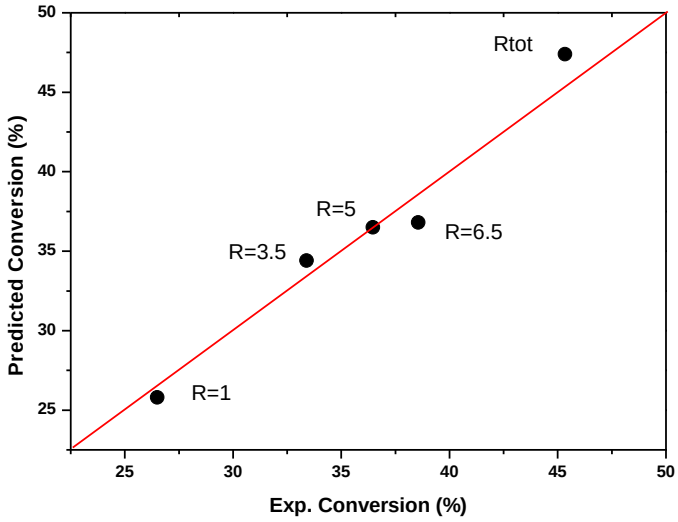

Figure 5.7 Experimental conversions vs. predicted conversions. Factor: 7E-4.

Table 5.14 Comparison of some other experimental and predicted parameters.

R	Distillate rate (L/h)		Bottoms rate (L/h)		T in the reboiler (ºC)	
	Exp.	Predicted	Exp.	Predicted	Exp.	Predicted
1	5.32	5.45	1.63	1.69	96.4	96.7
3.5	2.85	2.87	4.10	4.24	78.3	78.66
5	2.13	2.28	4.80	4.81	76.7	78.34
6.5	1.7	1.77	5.19	5.32	77.0	77.82
Rtot	-	-	7.05	7.05	75.9	77.62

In order to conclude this section, it can be said that the model predictions agree with the experimental results using a *tuning factor* of 0.13, with 4 column stages (+ a total condenser & a reboiler) and the two feed stages placed at N=2 and N=4.

5.3 Model application for initial process design

In this section several column configurations were tested in order to study the effect of each parameter and establish an appropriate column configuration. For this purpose the number of different stages (reaction, rectification and stripping stages) were varied as well as different feed parameters like flow rate, temperature, composition and position.

For each reflux ratio experimentally obtained feed-bottom flow rate ratios were used for the simulation calculations.

5.3.1 Variation of equivalent stage numbers

First of all, one kind of stages was varied while the rest of the column configuration was kept constant. Then some combinations were performed.

5.3.1.1 Rectification stages

As it is proved in Section 5.2 the optimum column configuration that better agrees with the experimental results has 6 stages (included a total condenser as well as a reboiler) where the feed stages are placed in N=2 and N=4. This column configuration will be considered as the base in order to get the best column configuration.

Three different column configurations (see Table 5.15) were simulated for different reflux ratios, in order to see the effect of the rectification stages in the column performance.

Table 5.15 Tested 3 column configurations. Variation of rectification stages having 1 reaction stage and 2 stripping stage.

Conf. 1	N=6 NFT=2 NFB=4	1 rectification stages
Conf 2.	N=7 NFT=3 NFB=5	2 rectification stages
Conf 3	N=8 NFT=4 NFB=6	3 rectification stages

Figure 5.8 shows the effect of the effect of the rectification stages.

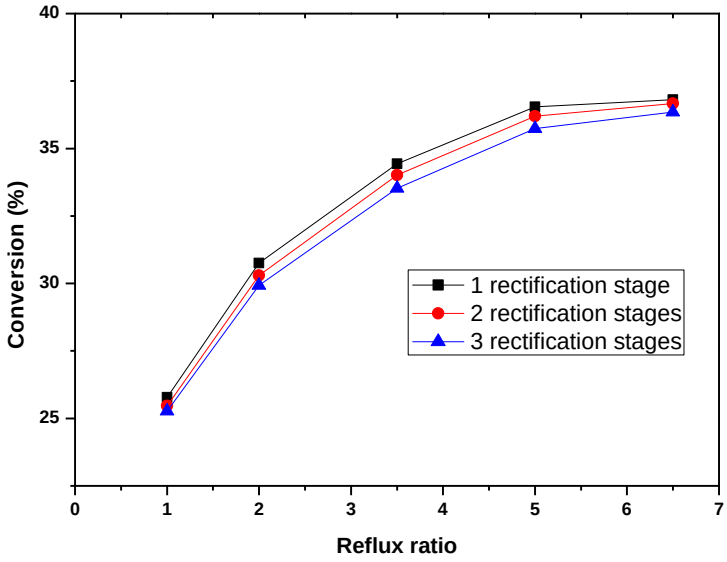

Figure 5.8 Reflux vs. conversion at several number of rectification stages.

As it was expected, it can be seen in Figure 5.8 how the conversion decreases increasing the number of rectification stages. With more rectification stages, there is less acetal in the distillate and therefore, there is more acetal in the reactive sections so the conversion decreases.

Table 5.16 shows the effect of the number of rectification stages in the acetal concentration of the distillate. It can be seen that each added rectification stages decreases a 50% the acetal fraction.

Table 5.16 Acetal concentrations in the distillate for different rectification stages.

Reflux ratio	Number of rectification stages	Acetal molar fraction in the distillate
1	1	5.2E-3
	2	2.8E-3
	3	1.7E-3
2	1	4.6E-3
	2	2.1E-3
	3	1.0E-3
3.5	1	4.2E-3
	2	1.6E-3
	3	6.9E-4
5	1	3.9E-3
	2	1.4E-3
	3	5.3E-4
6.5	1	3.7E-3
	2	1.2E-3
	3	4.3E-4

In the overall, it seems that only one rectification stage is enough in order to have really low acetal concentrations in the distillate and not to decrease the conversion too much.

5.3.1.2 Stripping stages

In principle, more stripping stages imply a higher concentration in volatile compounds (the reactants) in the reactive section and as a results higher conversion. However, it must be remembered that in the experimental part (Section 4.2.5) this effect was not fully found. Having more stripping height, it was observed that at high reflux ratios lower conversions were achieved.

Five different column configurations (see Table 5.17) were simulated for different reflux ratios, in order to see the effect of the stripping stages in the column performance.

Table 5.17 Tested 5 column configurations. Variation of stripping stages having 1 reaction stage and 1 rectification stage.

Conf. 1	N=5 NFT=2 NFB=4	1 stripping stages
Conf 2.	N=6 NFT=2 NFB=4	2 stripping stages
Conf 3	N=7 NFT=2 NFB=4	3 stripping stages
Conf 4	N=9 NFT=2 NFB=4	5 stripping stages
Conf 5	N=11 NFT=2 NFB=4	7 stripping stages

In Figure 5.9 the same behavior as in the experimental part is observed: with 2 stripping stages higher conversions than with 1 stripping stages were achieved for every reflux ratio but with 3, 5 and 7 stripping stages lower conversions are achieved when operating at high reflux ratios.

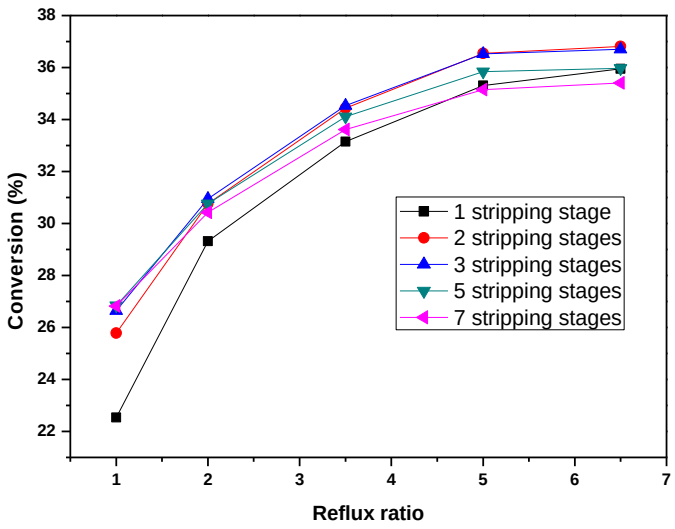

Figure 5.9 Reflux vs. conversion at several number of stripping stages.

As it is explained in Section 4.2.5, it is possible that the top part of the catalytic section works better but it may happen that in the lower part of the catalytic section, acetal concentration is important enough (because of the acetal produced in the upper catalytic

section goes down) in order to have an important effect of the reverse reaction, being the overall conversion lower than the expected one.

However, more evidences are shown in the following sections that can explain more accurately this effect.

5.3.1.3 Reaction stages

As well as rectification and stripping stages were varied, in this case reaction stages will be modified. 4 column configurations were simulated as it is shown in Table 5.18.

Table 5.18 Tested 4 column configurations. Variation of reaction stages having 1 rectification stages and 2 stripping stage.

Conf. 1	N=6 NFT=2 NFB=4	1 reaction stage
Conf 2.	N=7 NFT=2 NFB=5	2 reaction stages
Conf 3	N=8 NFT=2 NFB=6	3 reaction stages
Conf 4	N=10 NFT=2 NFB=8	5 reaction stages

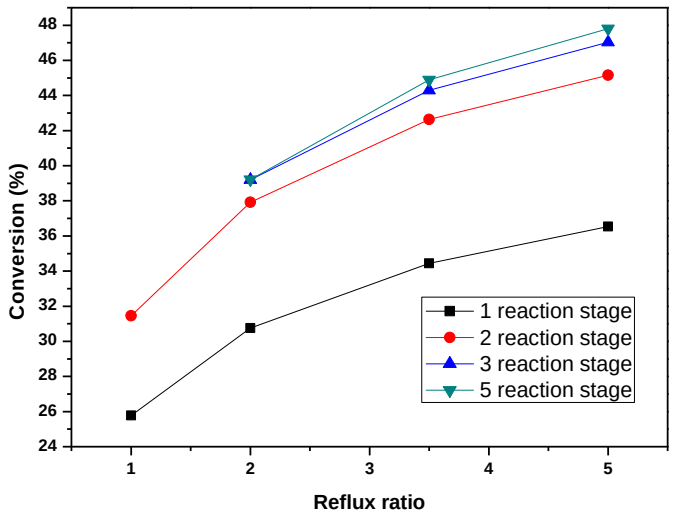

Figure 5.10 Reflux ratio vs. conversion for different number of reaction stages.

In Figure 5.10 it can be observed that the effect of increasing the number of reaction stages is more noticeable at high reflux ratios. However, it seems that from 3 reaction stages on an insignificant enhancement of conversion can be achieved.

In Table 5.19 it can be observed that with the addition of reaction stages, those stages placed in the down part of the reactive section hardly work. It seems that the acetal and water created in the top reaction stages go down and they avoid the reaction in the lower reaction stages.

Table 5.19 Predicted values of enthalpy of reaction times reaction rate times volume ($\Delta H_r r_j \upsilon$) in each reaction stage in each column configuration for R=5.

Configuration	**Reaction stage**	$-\Delta H_r r_c \upsilon$ **(J/s)**
1 reaction stage	1	121.67
2 reaction stages	1	119.59
	2	31.016
3 reaction stages	1	112.63
	2	34.616
	3	9.746
5 reaction stages	1	104.58
	2	32.353
	3	13.526
	4	8.205
	5	1.069

According to all these results, it seems that the appropriate column configuration would have 3 reaction stages, 3 stripping stages and 2 rectification stages. However, further simulations were performed varying simultaneously the stripping stages and the reaction stages in order to see if there is any kind of relation between them.

5.3.1.4 Simultaneous variation of reaction and stripping stages

In order to check if any relation between the reaction stages and stripping stages exists, further simulations were performed varying simultaneously these two kinds of stages. The reaction stages were varied from 1 to 5 and the tested stripping stages 3, 4 and 5 for each number of reaction stages. Thus, the obtained predictions are depicted in Figure 5.11, Figure 5.12 and in Figure 5.13.

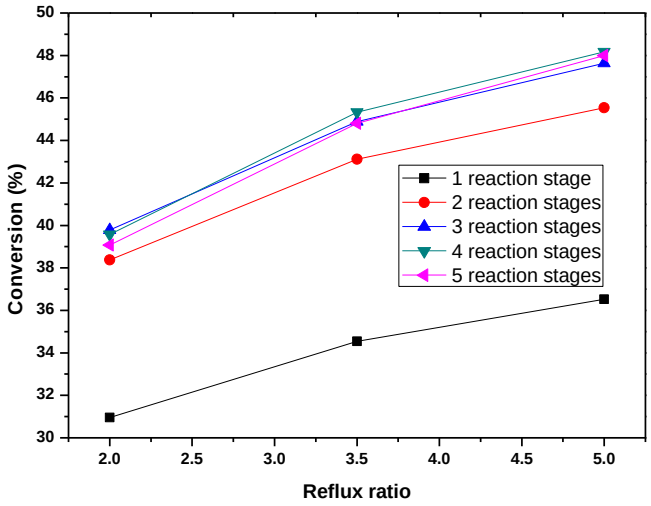

Figure 5.11 Conversion vs. reflux ratio for several reaction stages with 3 stripping stages.

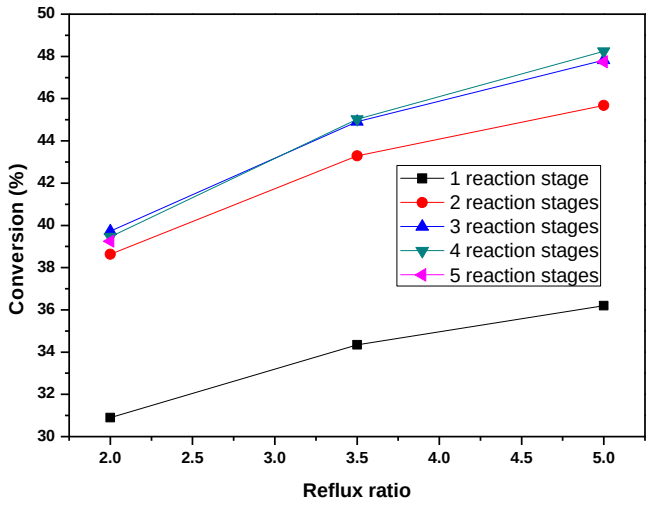

Figure 5.12 Conversion vs. reflux ratio for several reaction stages with 4 stripping stages.

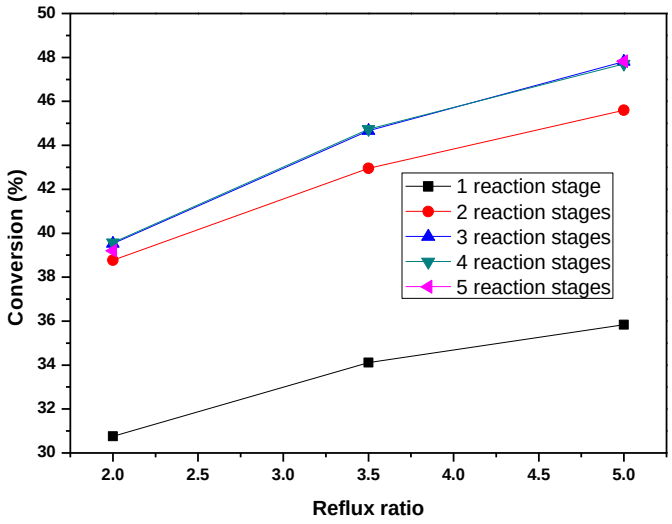

Figure 5.13 Conversion vs. reflux ratio for several reaction stages with 5 stripping stages.

It is clear that from the 3rd reaction stage no significant improvement can be achieved. Moreover, having more stripping stages the improvement from the 3rd reaction stage on is almost zero.

For R=5, the $-\Delta H_r r_c \upsilon$ values for each case are shown in Table 5.20.

Table 5.20 Predicted values of enthalpy of reaction times reaction rate times volume ($\Delta H_r r_j \upsilon$) in each reaction stage for each stripping stage (R=5).

Configuration	**Reaction stage**	$-\Delta H_r r_c \upsilon$ **(J/s)**		
		3 stripping stages	**4 stripping stages**	**5 stripping stages**
1 reaction stage	1	121.54	120.44	119.2
2 reaction stages	1	120.63	121.11	120.96
	2	31.175	31.108	30.972
3 reaction stages	1	114.11	115.17	115.79
	2	34.684	34.553	34.347
	3	10.134	9.7629	9.2838
4 reaction stages	1	110.62	112.4	112.02
	2	32.479	32.324	31.536
	3	13.945	13.223	12.656
	4	3.7574	3.05553	2.9723
5 reaction stages	1	106.38	108.25	109.95
	2	31.777	31.467	31.657
	3	12.731	11.894	11.65
	4	7.7513	6.7922	6.2131
	5	1.6914	1.023	0.17468

It can be observed in all the cases that increasing the stripping stages, the enthalpy of reaction of the bottom side reaction stages decreases probably due to the acetal amount that comes from the upper stages.

Another important conclusion is that operating at low reflux ratios, the enthalpy of reaction can change its sign as it can be seen in Table 5.21. This sign change means that the reverse reaction is more important than the forward reaction. Therefore, adding more catalyst (or reaction stages) does not mean that higher conversions will be always achieved in this kind of systems.

Table 5.21 $\Delta H_r r_j \upsilon$ predicted values for R=2, 5 stripping stages and 7 reaction stages.

Reaction stages	$-\Delta H_r r_j \upsilon$ (J/s)
1	96.691
2	24.226
3	7.309
4	3.6247
5	-1.0402

With these series of simulations it is confirmed that, regarding the stages and reflux ratios, the optimum column configuration for the used superficial feed flows (1.578 $m^3/(h\ m^2)$ of butanal & 2.124 $m^3/(h\ m^2)$ of ethanol) has the following characteristics:

- 3 reaction stages
- 3 stripping stages
- 1 rectification stages
- R=5

In terms of concentration, as well as in the experimental part, the model predicts that high acetal concentrations can be achieved operating at low reflux ratios. The model predicts that acetal molar fractions up to 90 % can be achieved in the reboiler operating with 2 reaction stages, 2 stripping stage and 1 rectification stages. However, the model does not take into account the effect of side reactions i.e. the 1,1 diethoxy butane conversion to 1-etoxy-1-butene and water that happens when high acetal concentration and thus, high temperatures are achieved in the reboiler; so, these data could not be really trustworthy.

5.3.2 Effect of the bottoms flow rate

In this section bottoms flow rate will be varied. For each simulation experimentally obtained feed-bottoms rate ratio was used so far. Varying the bottoms rate it will be checked if any enhancement can be achieved.

For the following simulations the optimum column configuration achieved in the previous section was used (see Figure 5.14):

- 3 reaction stages
- 3 stripping stages
- 1 rectification stages
- R=5
- 3.1 L/h of butanal fed from the bottom side of the catalytic section (65 ºC)
- 4.15 L/h of ethanol fed from the top side of the catalytic section (70 ºC) (stoichiometric feed)

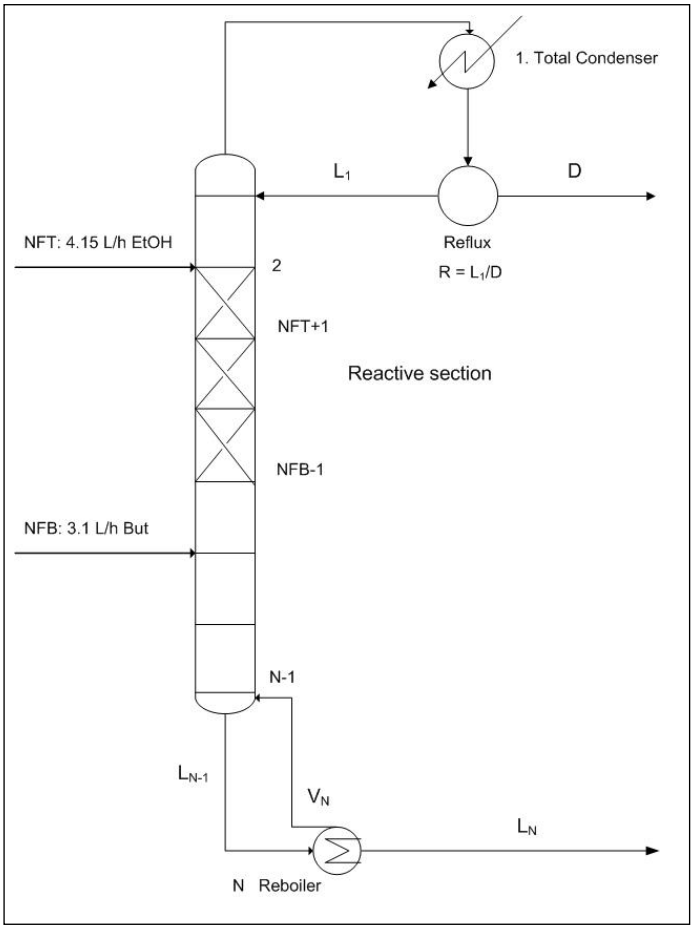

Figure 5.14 Schematic diagram of the optimum column configuration

The achieved conversions varying the bottoms rate are depicted in Figure 5.15.

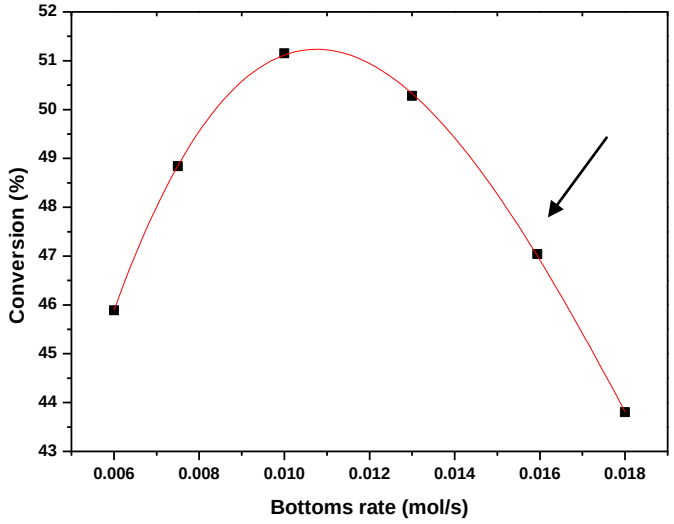

Figure 5.15 Conversion vs. bottoms rate

Mention that 0.0159 mol/s is the experimental bottom rate value. It is clear that extracting 0.011 mol/s from the bottoms, a maximum conversion is achieved. In term of concentrations, interesting acetal molar fractions are achieved in the reboiler decreasing the bottoms rate (see Table 5.22).

Table 5.22 Acetal molar fractions achieved in the reboiler for different bottoms rate.

Bottoms rate (mol/s)	Acetal molar fraction
0.006	0.72
0.0075	0.61
0.010	0.48
0.013	0.37
0.0159	0.28
0.018	0.23

5.3.3 Different feeding configurations

In this section different feeding configurations will be discussed in order to see which one offers the best column performance. For this purpose feed flow, feed temperature, feed composition and feed position will be varied.

5.3.3.1 Effect of the feed flow rate

In order to measure this effect, 3 different feed flows were used as it is shown in Table 4.10. Notice that the feed flow decreases, being in the second experiment the half of the first one (standard) and a quarter part in the third case. All the other parameters were kept constant.

Table 5.23 Different feed flows tested.

	Exp 1	**Exp 2**	**Exp 3**
EtOH (L/h) – NFT	4.15	2.05	1.12
Butanal (L/h) – NFB	3.10	1.60	0.83

It must be taken into account that the fluid dynamics of the column changes and the *tuning factor* probably would be different but even though the simulation results can give an idea of the column performance.

The achieved conversions are depicted in Figure 4.14:

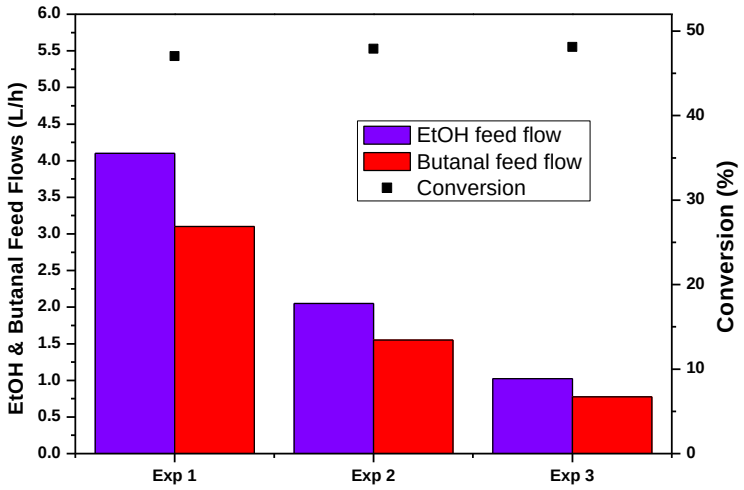

Figure 5.16 Relation between feed flows and the achieved conversion

As well as in the experimental part (Section 4.2.6.1), it can be seen in Figure 4.14 that the conversion increases if the feed flows are decreased. However, it seems that it is difficult to achieve higher conversions decreasing the feed flows since a very low enhancement was obtained between the second and the third experiment.

5.3.3.2 Effect of the feed temperature

As well as in the experimental part, the effect of the feed temperature was checked with the model. All the simulations were performed in the column conditions described in Section 5.3.2. The feed temperatures of both feed streams were the same except at the highest temperature which were 65 ºC for butanal and 70 ºC for ethanol.

Figure 5.17 shows the effect of the feed temperature. In this case, contrary to the experimental evidence, it is clear that increasing the feed temperature decreases the conversion.

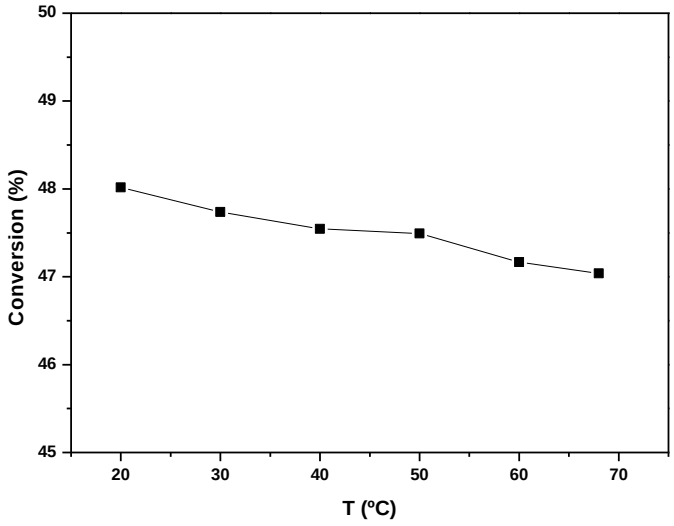

Figure 5.17 Conversion vs. feed temperature with 3 reaction stages.

It is known that at higher temperatures reactions run faster but in this case, dealing with an exothermic reaction, at higher temperatures the equilibrium conversion is lower. In this case it seems that the effect of being an exothermic reaction is more important. However, some other simulations were performed in order to study the same effect but with lower catalyst amount. For this purpose, 2 more simulations were performed, with a unique reaction stage and with "0.3 reaction stages".

In principle, it is not possible to model 0.3 reaction stages but this simulation was done in order to simulate the system with only one Katapak module (which was the catalyst loading used in the experimental part when feed temperature effect was measured). Remember that 1 reaction stage was defined as an equivalent of 3 Katapak SP-11 modules. Instead of introducing 0.3 reaction stages, which is not possible, the *tuning factor* was divided by 3.

Thus, the effect of the feed temperature having 1 reaction stage and "0.3 reaction stages" is depicted in Figure 5.18.

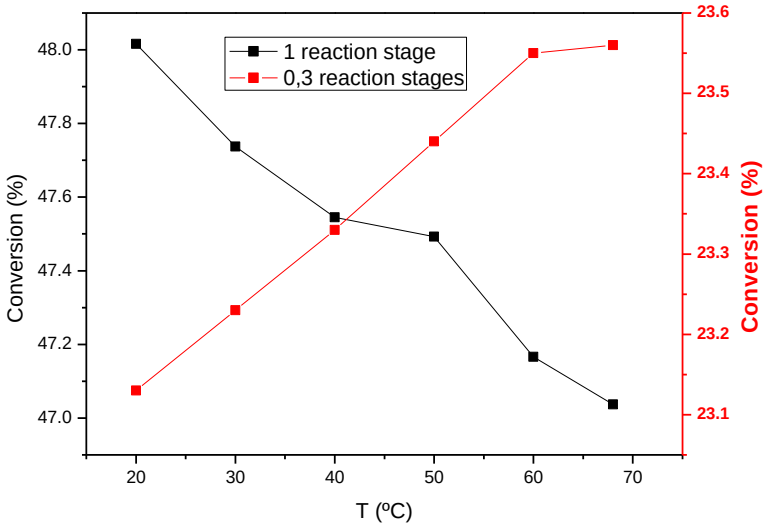

Figure 5.18 Effect of the feed temperature with 1 reaction stage and "0.3 reaction stages".

It can be observed that both trends are really different. In the case of "0.3 reaction stages", the followed trend agrees with the effect observed in the experimental part (Section 4.2.3). Probably, when the catalyst amount is really low, increasing the feed temperature increases the conversion because the residence time is low enough and equilibrium limitations have not important influence. But, when the catalyst amount is high enough, the residence time is higher and the effect of the reverse reaction becomes significant decreasing the conversion.

5.3.3.3 Effect of the feed composition

In this section the effect of the feed composition will be studied. Three different feed composition were tested: 2:1, 3:1 and 4:1 of EtOH:Butanal mol ratio. All the simulations were performed in the column conditions described in Section 5.3.2.

The achieved conversions as well as the equilibrium conversions are shown in Figure 5.19.

As it was expected, when working with an excess of one of the reactants (ethanol in this case) higher conversions are achieved. It can be observed that in all the cases the difference between the predicted and the equilibrium conversions is approximately constant and very similar to the differences obtained experimentally (Section 4.2.6.3)

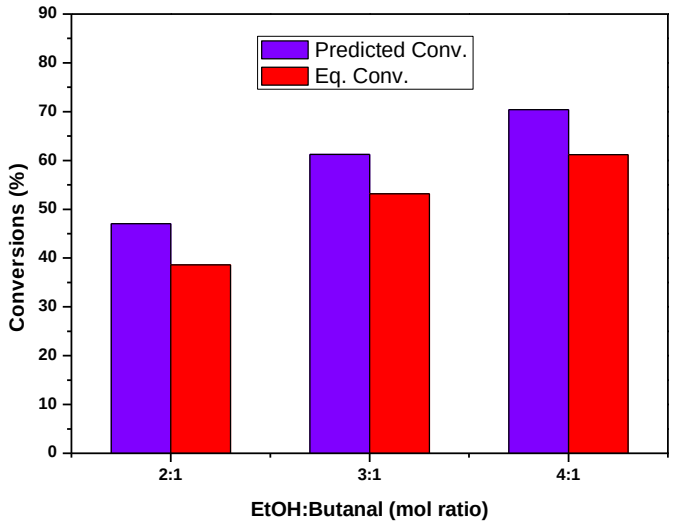

Figure 5.19 Predicted conversions for different feed compositions and their comparison with the corresponding equilibrium conversion.

The equilibrium conversions for 3:1 and 4:1 feed mixtures were obtained from the equilibrium constant. As K_c only depends on the temperature, the equilibrium conversion can be worked out from equation (5.37).

$$K_c = \frac{C_{ac} C_W}{\left(C_{EtOH}\right)^2 C_{But}} \tag{5.36}$$

In term of conversion:

$$K_c = \frac{\left(C_{But,0} X\right)^2}{\left(C_{EtOH,0} - 2C_{But,0} X\right)^2 \left(C_{But,0} - C_{But,0} X\right)} \tag{5.37}$$

5.3.3.4 Effect of the feed position

Three different feeding configurations were predicted; the first one introducing ethanol from the top side of the catalytic section (NFT) and butanal from the bottom side of the catalytic section (NFB); the second one, introducing a stoichiometric feed composition through the top side of the catalytic section (NFT); and the third one introducing a stoichiometric feed composition through the bottom side of the catalytic section (NFB) (see Figure 5.20).

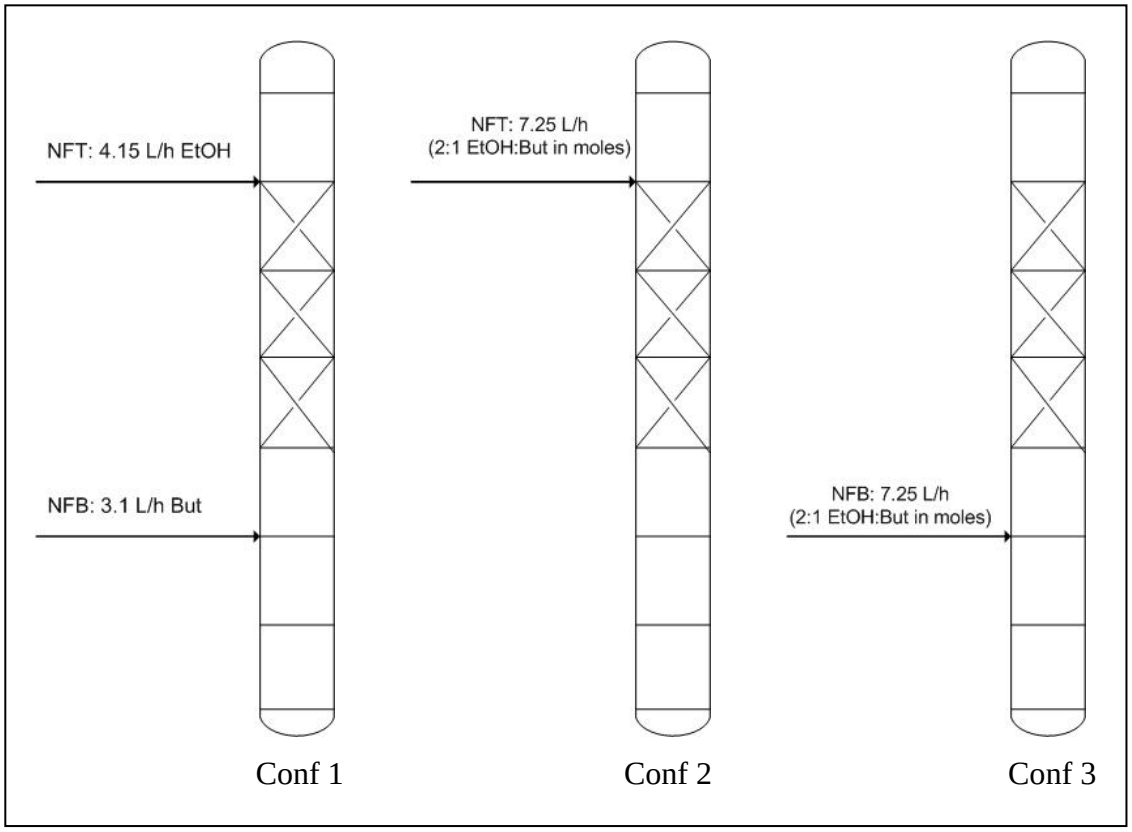

Figure 5.20 Schematic diagram of the predicted feeding configurations.

In Figure 5.21 it is observed that the 2nd configuration offers better conversions and the 3rd configuration offers the worst ones. This effect was also checked experimentally so it is confirmed that the volatility difference between ethanol and butanal is not high enough in order to feed them through different feed heights.

In those configurations with a unique feed point, a feed rate of 7.25 L/h was used in order to simulate similar fluid dynamics within the column.

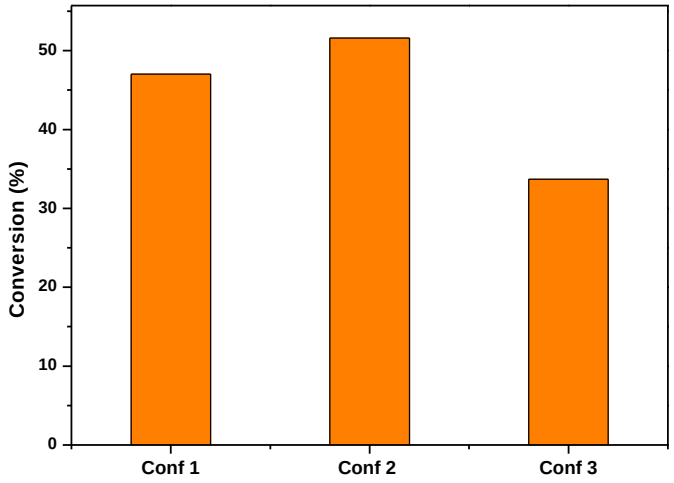

Figure 5.21 Conversions with different feed configurations.

5.4 Conclusions

It was demonstrated that a reactive distillation mathematical steady-state model based can predict quite accurately the experimental results. A *tuning factor* was used in order to adjust the model with the results and it can be considered constant for similar fluid dynamics behavior. This *tuning factor* includes several factors like, plate efficiency, and catalyst wet factor. It was checked that there is not any resistance to the external mass transfer and thus, the reaction is controlled by the kinetics.

The optimum number of stages was found and it was concluded that increasing the number of reaction stages does not imply higher conversions. Depend on the operating conditions it may happen that in the lower side of the catalytic section the reverse reaction is more important than the forward reaction, which implies a conversion decrease.

It was also concluded that the conversion is not increased rising the number of stripping stages. Besides that, operating at high reflux ratios, an increase in the number of stripping stages implies a conversion decrease. This effect was also observed experimentally.

In terms of rectification stages, the great volatility difference between acetal and the reactants was demonstrated since one rectification stage seems to be enough.

Regarding the different effects checked varying different parameters, in all the cases could be verified that the experimentally observed trends agree with the model predicted trends. Thus, it was proved that feeding a stoichiometric mixture from the top of the catalytic section, higher conversions than feeding through 2 different feed heights are achieved.

Moreover, it was observed that modifying the bottoms flow rate, different conversions can be achieved and an optimal rate can be found.

Another interesting conclusion is that depending on the catalyst loading or the number of reaction stages, an increase in the feed temperature can imply a decrease in the conversion. In this effect, the most important parameter is the residence time. With low residence times (low catalyst amounts) an increase of the feed temperature increases the conversion but at higher residence times (higher catalyst amounts) an increase of the feed temperature implies a conversion decrease.

To sum up it can be said that the optimum column configuration for the treated feed flow (7 L/h) is the following one:

- 3 reaction stages
- 3 stripping stages
- 1 rectification stages
- Reflux ratio = 5
- Bottoms flow rate = 0.011 mol/s
- Feed: one unique feed (stoichiometric mixture of both reactants) to the top part of the catalytic section

Chapter VI

Membrane reactors. Experimental part

6 Membrane reactors. Experimental part.

The aim of the present chapter is to demonstrate that using dehydration membrane reactors the thermodynamic limitations that the studied reaction shows can be overcome achieving high conversions. In order to fulfill this objective lab scale semi-batch experiments were performed. The experimental work was divided in four different parts:

- Choose an appropriate membrane and test it with standards mixtures.
- Test the membrane to the catalyst impacts.
- Perform dehydration experiments without any reaction with ethanol/butanal/1,1 dithoxy butane/water mixtures.
- Perform semi-batch experiments were reaction and separation are carried out in the same unit.

The work presented in the present chapter and in Chapter VII was performed in the facilities of the "Membrane Technology Group" of ECN

6.1 Theoretical background of pervaporation membrane transport

In this section only the background of pervaporation is described. The background of the acetalization reaction is described in Chapter III.

6.1.1 Fick's Law

Pervaporation processes can be described following a Solution-Diffusion Model since two different mechanisms, diffusion and sorption-desorption, are present. R.W. Baker (38) demonstrates, starting from Fick's Law (eq. (6.1), that the flux of a component *i* through a pervaporation membrane can be expressed in terms of the partial vapor pressures in the feed and in the permeate sides of the membrane (eq. (6.2).

$$J_i = -D_i \frac{dc_i}{dx} \tag{6.1}$$

Where:

J_i	is the flux of component *i* in g/(cm^2·s)
$\frac{dc_i}{dx}$	is the concentration gradient of component *i* (g/(cm^3·cm))
D_i	is the diffusion coefficient (cm^2/s)

$$J_i = Q_i(P_i^{feed} - P_i^{permeate}) \tag{6.2}$$

Where:

J_i	is the flux of component *i* in g/(cm^2·s)
Q_i	is the permeance value for component *i* in g/(cm^2·s·bar)
P_i	is the partial vapor pressures of component *i* in bar

Equation (6.2) is the preferred method of describing membrane performance because it separates the two contributions to the membrane flux: the permeance (membrane characteristic) and the driving force (process characteristic).

6.1.2 Driving forces

The vapor pressures in the permeate side can be easily obtained by measuring the total permeate pressure and the permeate composition. However, the partial vapor pressures of each component in the feed liquid side are not so easy to calculate (to measure). For this purpose, equation (6.2) was modified in the following way (59).

It is assumed that in the feed liquid phase the liquid is in equilibrium with the vapor so the fugacity of component *i* in a mixture in the liquid phase and in the vapor phase is the same.

$$\hat{f}_i^L = \hat{f}_i^V \tag{6.3}$$

The fugacity of component *i* in a vapor phase mixture is equal to the partial pressure of component *i* (at low or moderate pressures).

$$\hat{f}_i^V = y_i \hat{\phi}_i P = y_i P \tag{6.4}$$

Where:

$\hat{f}_i$ fugacity of component *i* in a mixture in bar.

y_i is the molar fraction of component *i*

$\hat{\phi}_i$ is the fugacity coefficient of component *i*. (at low or moderate pressures $\hat{\phi}_i \sim 1$)

P is the total pressure in bar.

On the other hand, the fugacity of component *i* in a liquid mixture is equal to its molar fraction times its fugacity as a pure component times its activity coefficient.

$$\gamma_i = \frac{\hat{f}_i^{\,L}}{\hat{f}_i^{\,Ideal\ Mixture}} \tag{6.5}$$

$$\hat{f}_i^{\,Ideal\ Liquid} = x_i\ f_i \tag{6.6}$$

$$\hat{f}_i^{\,L} = x_i\ \gamma_i\ f_i \tag{6.7}$$

Where:

$\hat{f}_i^{\,L}$ is the fugacity of component *i* in liquid phase mixture; in bar

$\hat{f}_i^{\,Ideal\ Liquid}$ is the fugacity of component *i* in liquid phase (ideal mixture); in bar

γ_i is the activity coefficient of component *i*

x_i is the liquid molar fraction of component *i*

f_i is the fugacity of component *i* as a pure component in bar

The fugacity of component *i* as pure component is expressed in equation (6.8)

$$f_i(T,P) = f_i^{\,sat}(T, P_i^{\,sat}(T)) \cdot Py \tag{6.8}$$

Where:

$f_i^{\,sat}(T, P_i^{\,sat}(T))$ is the saturation fugacity of component *i* in bar

Py is the Pointing factor

By definition, the Pointing factor is function of (P- $P_i^{\,sat}$).

$$Py = EXP\left[\frac{\bar{v}_i^{L}\,(P - P_i^{sat})}{RT}\right] \tag{6.9}$$

Where:

$\bar{v}_i^{L}$	is the specific molar volume of component *i* in liquid phase in L/mol
P	is the total pressure in kPa
P_i^{sat}	is the saturation pressure of component *i* in kPa
R	is the universal gas constant in J/(mol·K)
T	is the temperature in Kelvin

The specific volume *i* of a component *i* in liquid phase is much lower than in vapor phase ($\bar{v}_i^{L} << \bar{v}_i^{V}$) so, unless the ($P - P_i^{sat}$) term is huge, the pointing factor can be considered equal to 1. In pervaporation, the total pressure is atmospheric, so the pointing factor can be assumed equal to one.

The saturation fugacity of component *i*, by definition, is equal to the its saturation pressure times its fugacity coefficient; at low or moderate pressures the fugacity coefficient can be assumed equal to 1 so, equation (6.7) can be written in the following way:

$$\hat{f}_i^{L} = x_i\,\gamma_i\,P_i^{sat} \tag{6.10}$$

Therefore, in the equilibrium, the partial vapor pressure of component *i* is equal to the product among the liquid molar fraction, the activity coefficient and the saturation pressure of component *i*.

$$y_i P = x_i\,\gamma_i\,P_i^{sat} \tag{6.11}$$

Substituting equations (6.11) and (6.4) in (6.2) the pervaporation main transport equation is obtained.

$$\boxed{J_i = Q_i\,(x_i\,\gamma_i\,P_i^{sat} - y_i P^{perm})} \tag{6.12}$$

6.1.2.1 Saturation pressures

In order to calculate the saturation pressure of each component at any temperature an amplified Antoine's equation (eq. (5.25) was used for ethanol, butanal and water (57) and a simplified equation (eq. (5.26) based on their two available points (critical point and normal boiling point, estimated with ASPEN PLUS) for the acetal (see Section 5.1.3.4).

6.1.2.2 Activity coefficients

In order to calculate the activity coefficients, Margules activity coefficient model was used for ethanol-water and butanol-water binary mixtures (eq. (6.13) & (6.14). Wilson, van Laar, UNIQUAC, UNIFAC and NRTL methods were tested at ECN and all of the methods show a similar behavior except Wilson so Margules was chosen because of it is the easiest one to be used.

For multi-component mixtures where ethanol, butanal, 1,1 diethoxy butane and water are involved Wilson, NRTL and UNIQUAC can be used as the most common methods for polar compounds. All of them can handle azeotropes, but Wilson cannot handle two liquid phases. After analyzing mixtures of ethanol, butanal, acetal and water with Wilson, NRTL and UNIQUAC models, the NRTL model was chosen, a priori, as the most suitable one (55) (eq. (6.15).

- Margules activity coefficient model

$$Ln\,\gamma_1 = A_{12} + 2[(A_{21} - A_{12})\,x_a]\,x_b^2 \tag{6.13}$$

$$Ln\,\gamma_2 = A_{21} + 2[(A_{12} - A_{21})\,x_b]\,x_a^2 \tag{6.14}$$

Where:

Table 6.1 Binary iteration parameters for Margules activity coefficient model. (60)

A_{12} / A_{21}	**Water**	**Ethanol**	**Butanal**
Water	X	1.6022	3.2051
Ethanol	0.7947	X	-0.0120
Butanal	0.8608	0.0369	X

- Non-random two-liquid (NRTL) activity coefficient model for multi-component mixtures:

$$Ln\,\gamma_i = \frac{\sum_j x_j\,\tau_{ji}\,G_{ji}}{\sum_k x_k\,G_{kj}} + \sum_j \frac{x_j\,G_{ij}}{\sum_k x_k\,G_{kj}}\left(\tau_{ij} - \frac{\sum_m x_m\,\tau_{mj}\,G_{mj}}{\sum_k x_k\,G_{kj}}\right) \qquad (6.15)$$

Where: $G_{ij} = EXP\,(\alpha_{ij}\,\tau_{ij})$

$\tau_{ij} = a_{ij} + b_{ij}/T + (e_{ij}\,Ln\,T + f_{ij}\,T)$

$\alpha_{ij} = c_{ij} + d_{ij}\,(T\text{-}273.15K)$

$\tau_{ii} = 0$

$G_{ii} = 1$

a_{ij}, b_{ij}, e_{ij} and f_{ij} are unsymmetrical. (a_{ij} may not be equal to a_{ji}, etc.)

In Table 6.2 binary iteration parameters for the NRTL activity coefficient model are shown. 1,1 diethoxy butane (= the acetal) data were not found in the bibliography and as this compound is not in the ASPEN PLUS database, its properties were estimated using the UNIFAC method

Table 6.2 Binary iteration parameters for NRTL activity coefficient model (ASPEN PLUS). d_{ij}, e_{ij}, e_{ji}, f_{ij} & f_{ji} values were equal to zero.

Comp. i **Comp. j**	**Ethanol** **Butanal**	**Ethanol** **Water**	**Butanal** **Water**	**Acetal** **Ethanol**	**Acetal** **Butanal**	**Acetal** **Water**
Temp.	**ºC**	**ºC**	**ºC**	**ºC**	**ºC**	**ºC**
$\mathbf{a_{ij}}$	0	-0.8009	0	0	0	0
$\mathbf{a_{ji}}$	0	3.4578	0	0	0	0
$\mathbf{b_{ij}}$	-94.1633	246.18	631.1153	112.58564	-230.4113	86.741559
$\mathbf{b_{ji}}$	288.1581	-586.0809	969.4386	338.54192	408.78426	2323.161
$\mathbf{c_{ij}}$	0.3	0.3	0.47	0.3	0.3	0.3
$\mathbf{T_{lower}}$	72.75	24.99	50	25	25	25
$\mathbf{T_{upper}}$	78.3	100	93.1	25	25	25

As ASPEN PLUS estimated d_{ij}, e_{ij}, e_{ji}, f_{ij} & f_{ji} binary parameters equal to zero, τ_{ij} and α_{ij} functions can be simplified. Thus, G_{ij} is function of T^{-1}.

$\tau_{ij} = a_{ij} + b_{ij}/T$

$\alpha_{ij} = c_{ij}$

$G_{ij} = EXP\,[c_{ij}\,(a_{ij} + b_{ij}/T)]$.

6.2 Experimental procedure

As it is demonstrated in Chapter III, this reaction shows important thermodynamic limitations achieving low equilibrium conversions. In this Chapter, the effect of the pervaporation process to the reaction will be studied. For this purpose HybSi® dehydration membranes were used. According to the Le Chatelier law, continuous water removal from the reaction mixture shifts the reaction to the forward direction achieving higher conversions than the equilibrium ones.

In order to fulfill this goal, the experimental part was divided in four different tasks:

1. Find a selective membrane.
2. Check if the impact of catalyst particles can damage the membrane surface when a slurry reactor is used.
3. Perform separation experiments (without reaction) of all the components that take part in the reaction.
4. Perform reaction + pervaporation experiments in the same unit.

6.2.1 Materials

The used reagents were ethanol (99.9 % w/w for synthesis) and butanal (99 % w/w) both from Merck. 1,1 diethoxy butane (97%) from Acros Organics was used to prepare different standards for GC calibration. In terms of catalyst, Amberlyst 47 (sulphonic ion exchange resin), kindly provided by Rohm & Haas, was the used one. Hybrid silica membranes based upon BTESE and BTESM (see Section 6.2.4.1) as precursor were used for the pervaporation experiments.

6.2.2 Product analysis

In case of the standard binary mixture tests, both, feed and permeate sides were analyzed by refraction index at 20 ºC.

When all the reaction compounds were involved in the experiments, both the reactants (ethanol and butanal) and the reaction product (1,1 diethoxy butane) were analyzed by gas chromatography (Shimadzu GC-17A) using a flame ionization detector (FID). A Phenomenex ZB-Wax plus capillary column was used (30m x 0.25 mm x 0.25 µm) with helium as the carrier gas. More details of the method are shown in Table 3.1.

Table 6.3 GC method conditions.

GC: Shimadzu GC-17A
Sample Injection
Dilution
Permeate samples: approx. 15 and 450 times
Feed samples: approx. 450 times
Using an autosampler: 0.5 µL
Injection temperature: 240 ºC
Injection mode: Split
Split flow: 1:200
Carrier gas flow: 1 mL/min
Carrier gas: He (99.999 %)
Column: Phenomenex ZB-Wax plus 30m x 0.25 mm x 0.25 µm capillary column
Temperature ramps:
Initial temperature: 50 ºC along 1 min
Rate: 30 ºC/min until 200 ºC
keep 5 min at 200ºC
Detectors: FID
Detector temperatures
FID: 250 ºC

Water content of the feed side was measured using Karl Fisher titration method. In this case, a volumetric titration method was used. The general reactions behind Karl Fischer titration are as follows:

$$CH_3OH + SO_2 + RN \rightarrow [RNH]SO_3CH_3$$

$$H_2O + I_2 + [RNH]SO_3CH_3 + 2\ RN \rightarrow [RNH]SO_4\ CH_3 + 2\ [RNH]I$$

(RN = Base)

The sulphur dioxide reacts with the alcohol to from an ester which is neutralized by the base. The anion of the alkyl sulphurous acid is the reactive component and is already present in the KF reagent. The titration of water constitutes the oxidation of the alkyl-sulfite anion to alkyl sulphate by the iodine. This reaction consumes water.

However, the presence of butanal (aldehyde) in the titration media involves some inconveniences since it can react giving acetals using conventional reagents. In this reaction water is formed which is then also titrated. This results in abnormal high water contents. In order to avoid these problems, a special titration reagent was used: HYDRANAL composite 5K supplied by Sigma-Aldrich.

The water concentrations in the permeate side (for multi-component experiments) was estimated with refraction index measurement, in order to have a first and quick indication about the water content. Basically, as it is shown in Section 6.2.4.3, the main permeating compounds are ethanol and water. The presence of small amounts of butanal and acetal do not affect significantly to the EtOH/Water refraction index values. Some samples were prepared and measured in order to check if the assumption of a binary mixture is correct. The results are presented in Table 6.4. Moreover, afterwards it was checked that the water concentration estimated with the refraction index is in a good agreement with the water concentration calculated as the difference to 100% of the organics sum.

Table 6.4 Effect of the presence of butanal and acetal in the refraction index measurements

Water wt%	EtOH wt%	Butanal wt%	Acetal wt%	RI (nd)	Calculated water wt%	Remarks
90.0	10	-	-	1.33963	90.2%	-
88.4	10.4	0.5	0.63	1.34109	88.1%	-
90	8	1	1	1.34066	-	2 liq. phases

6.2.3 Apparatus, procedure and working principle

The experiments were carried out in a semi-batch lab scale glass pervaporation unit. The glass pervaporation equipment is made up of three parts:

- Feed system consisting of a feed vessel (2L), heating/stirring plate, stand and membrane immersed in the feed mixture. There is also an option to use a feed pump to add material to the feed.
- Continuous permeate system which consists of connection to permeate glass manifold, large chilled water spiral glass condenser and permeate pot, HX-300chilled water unit, pressure sensor and vacuum pump.
- Sampling permeate system consisting of a connection to permeate glass manifold, connection to permeate crane and sample vials, pressure sensor, liquid nitrogen cold trap and vacuum pump

The vacuum pressure sensors are connected to a central display unit. A schematic diagram is shown in Figure 6.1.

.

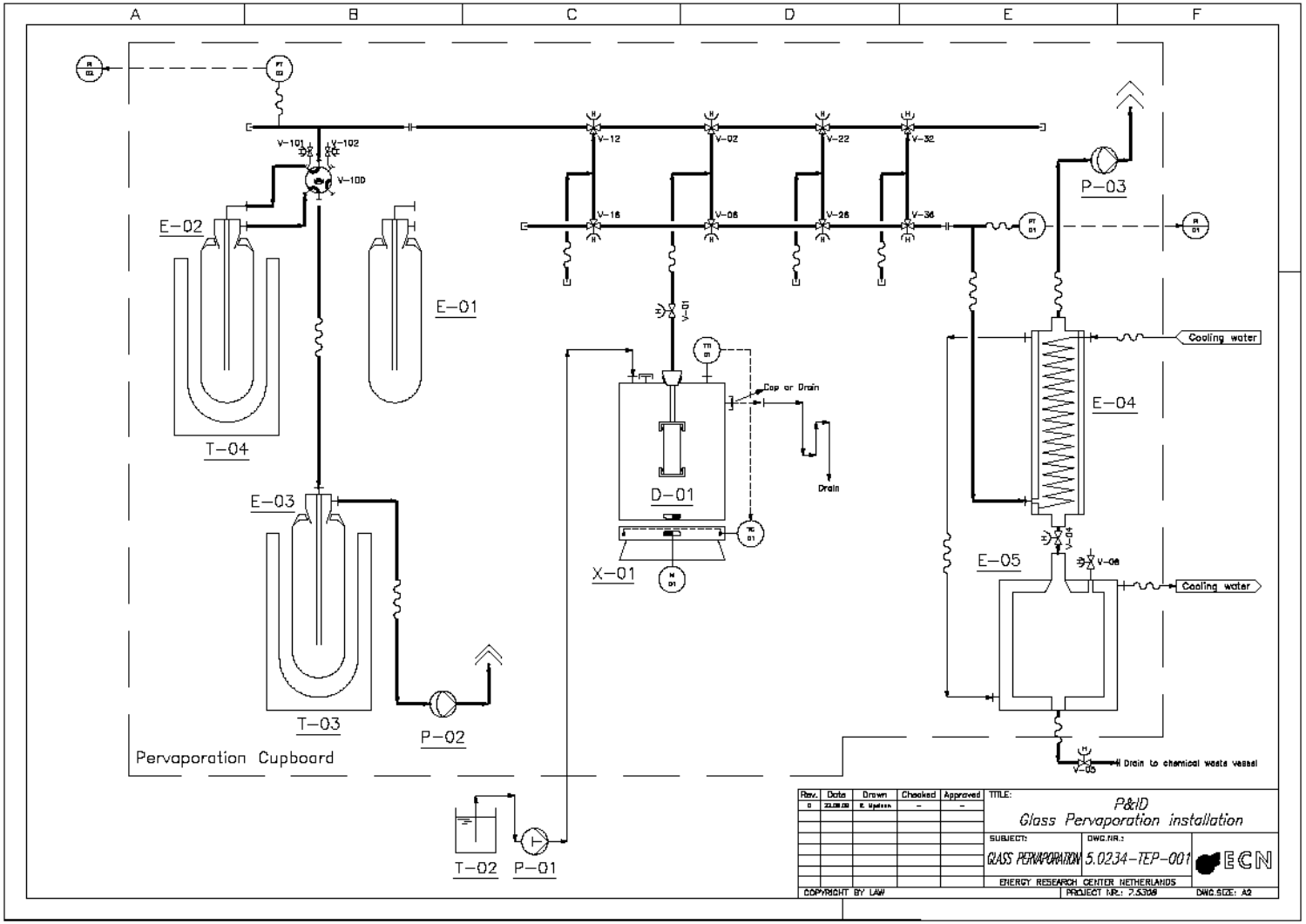

Figure 6.1 Schematic diagram of the glass pervaporation unit.

Several feed vessels and membranes can be connected to the permeate manifold at any one time. When not measuring the performance of a membrane, all the permeate vapors obtained from the membranes are directed into the continuous permeate system (E-05). The vapors are condensed and collected in the permeate pot, which is then emptied periodically. This condensation is operated using a chilled water supply. The cooling water system consists of the HX-300 unit and insulated cooling water piping. The HX-300 can supply 11 L/min of 0°C cold water. The flow rate is controlled via the use of variable area rotameters. The system contains a mixture of glycol/water (~ 40% glycol).

When the performance of a particular membrane (D-01) must be studied its permeate vapors are directed towards the sampling permeate system (E-01, E-02 or E03) again by opening or closing the appropriate valves and directing the vapors from that particular membrane to the upper part of the manifold. Here samples can be collected using liquid nitrogen to condense the vapors in one of the sample vials. The purpose of the cold trap is to ensure no vapors reach the vacuum pump (P-02) and/or the atmosphere.

- Working principle

A membrane is placed in a feed mixture with the outer surface of the tubular membrane in contact with the feed (see Figure 6.3). The inside membrane bore is sealed using o-rings and end caps preventing the contact with the feed (see Figure 6.2). This inner bore is the permeate side of the membrane. The permeate side is evacuated to a pressure of 0-10 mbara via the use of a refrigerated condenser and vacuum pump system. The feed is heated (max temperature is the boiling point of the mixture) and magnetically stirred via the heating plate.

Due to the vacuum, part of the feed diffuses through the pores in the membrane while the other components remain in the feed mixture. The permeate stream that passes through the membrane is a vapor due to the applied pressure. It travels through the refrigerated condenser where any condensable vapors are condensed and stored in the permeate pot. Non condensable gases are then removed from the system by the vacuum pump. These permeate flow-rate and concentration along with the feed concentration can be measured so as to ascertain the performance of the membrane. Also the membrane area is calculated from its length and diameter.

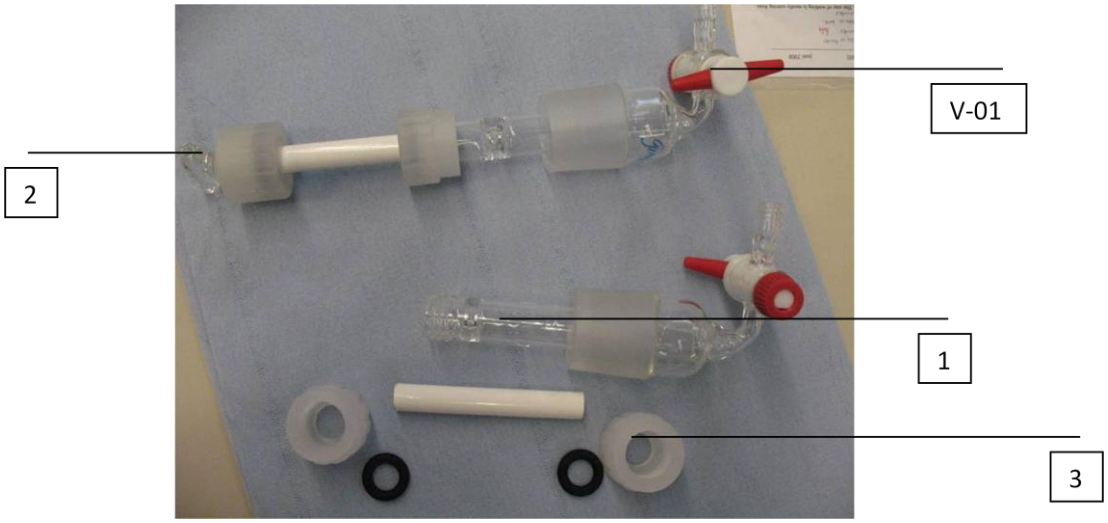

Figure 6.2 Sealing of a glass pervaporation membranes

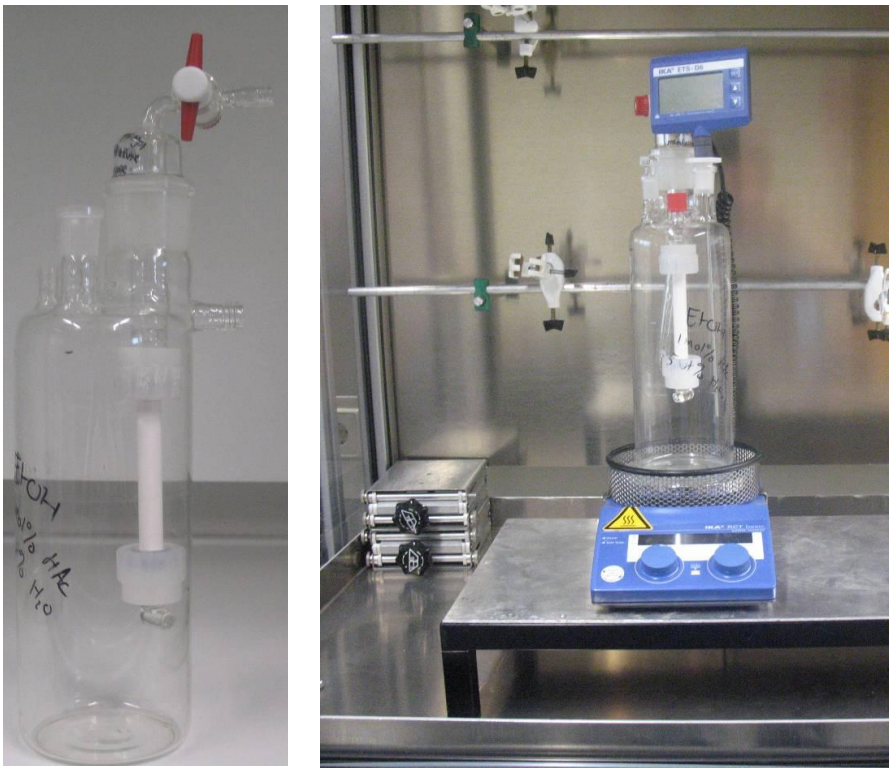

Figure 6.3 Reactor or feed vessel.

Depending on the type of experiment, the operating procedure was different. Because of this reason, in the beginning of each experiment type section the followed procedure will be explained shortly.

6.2.4 Results & Discussion

This section contains all the information from all the experiments that were performed with the glass pervaporation installation. Different types of experiments were carried out in order to study different aspects of the process:

1. Standard tests to choose a selective membrane.
2. Check if the impacts of catalyst particles damage the membrane surface.
3. Perform separation experiments (without reaction) of all the components that take part in the reaction.
4. Perform reaction + pervaporation experiments in the same unit

6.2.4.1 Membrane selection

In the beginning some butanol/water (95:5 wt% at 95 ºC) and ethanol/water (95:5 wt% 70 ºC) standard tests were performed with three different membranes. The aim of these tests was to choose a suitable membrane to perform all the experiments. The tested membranes were the following ones:

1. BTESE_1
2. BTESM
3. BTESE_2

The operating procedure in the standard tests was the following one:

- Assemble the membrane to the holders.
- Prepare the specific binary mixture.
- Place the membrane and the thermocouple in the feed vessel.
- Warm up the mixture to the desired temperature, connect the vacuum and set the stirring speed (1000-1100 rpm) meanwhile.
- Set up the peristaltic feed pump in order to keep the water concentration in the vessel constant.
- Leave 2-3 hours stabilizing.
- Open and close the corresponding valves in order to direct the permeate to the sampling side. Wait 2 minutes approximately to homogenize all the vapors.
- Measure the feed concentration with the refraction index just before starting a pervaporation measurement and then start it placing a liquid nitrogen vessel around the sampling trap and opening the corresponding valve.
- After a certain period of time (between 20 and 45 minutes) stop the measurement and again measure the feed concentration with the refractive

index. The feed concentration of the measurement will be the average between the start and end values.

- Wait some minutes to defrost the permeate sample, weight the sample and measure its composition using refraction index.
- Do two composition measurements per day during 2-3 days.

6.2.4.1.1 BTESE_1

In order to check if the membrane is selective or not for our process a Butanol/Water (95:5 wt %) standard test was performed at 95 ºC. The results of this experiment are shown in Figure 6.4 and Figure 6.5. The water feed concentration was around 5 wt% in all the measurements but all the flux and permeance values were corrected to exactly 5.0 wt% of water in the feed side. The membrane geometrical characteristics are shown in Table 6.5.

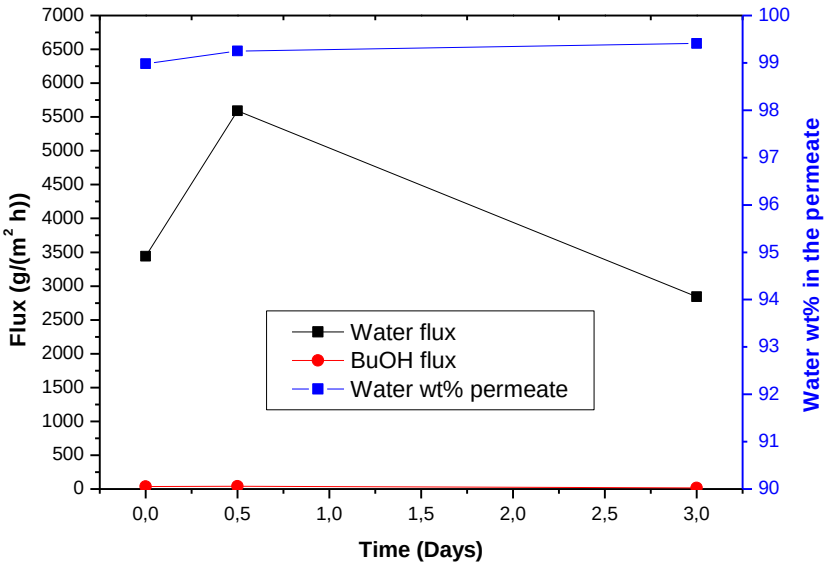

Figure 6.4 Membrane performance in a Butanol/Water (95:5 wt%) test at 95 ºC.

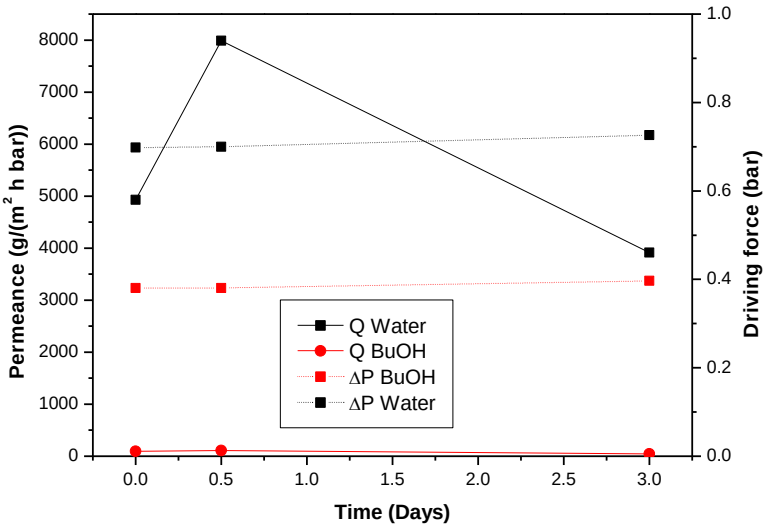

Figure 6.5 Membrane performance in a Butanol/Water (95:5 wt%) test at 95 ºC.

Table 6.5 Membrane geometrical characteristics.

Membrane	BTESE_1
Diameter (cm)	7.0
Length (cm)	1.4
Membrane area (cm^2)	30.8
He flow [ml min^{-1} (3 bar)$^{-1}$(10 cm)$^{-1}$]	15

As it can be seen in Figure 6.4 and Figure 6.5, the membrane performance (mainly flux and thus permeance) is not really stable but it must be mentioned that this behavior is normal during the first days for a new membrane. The membrane is selective for Butanol/Water mixtures since the water concentration in the permeate is above 99 wt%. The next step was to check if it was also selective for Ethanol/Water mixtures. An ethanol molecule is smaller than butanol molecule so, the separation is more difficult in this case. Therefore, the selectivity of the process should decrease in this case.

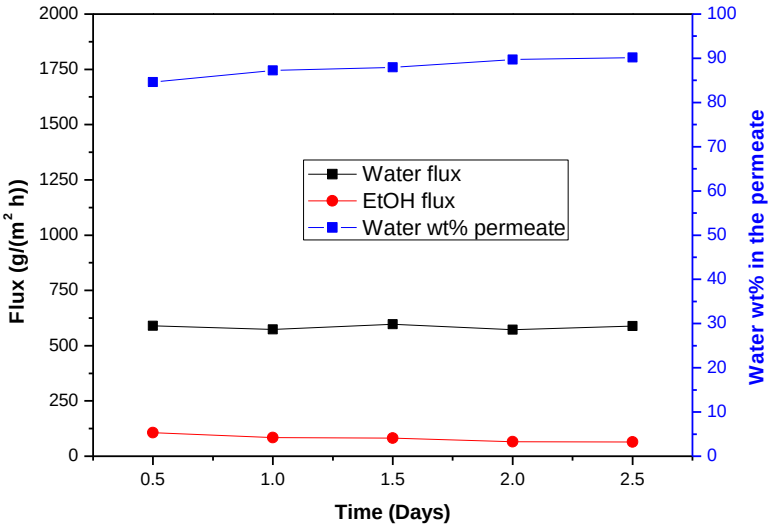

Figure 6.6 Membrane performance in an Ethanol/Water (95:5 wt%) test at 70 ºC.

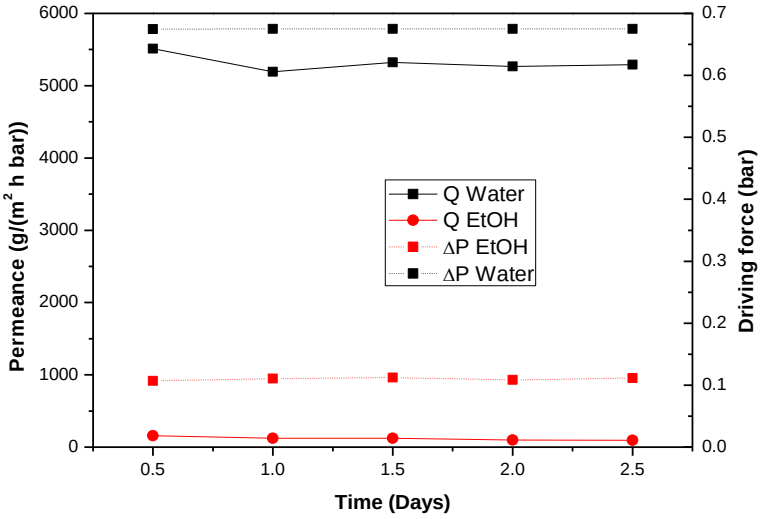

Figure 6.7 Membrane performance in an Ethanol/Water (95:5 wt%) test at 70 ºC.

In Figure 6.6 as compared to Figure 6.4 it can be seen that the water concentration in the permeate has decreased in the ethanol/water tests. However the membrane is selective and meets the criteria set that the permeate should contain at least 85 wt% water. The only inconvenient that this membrane shows in the ethanol/water test is the low water flux (typical water flux values for this kind of membrane with ethanol/water tests at 70 ºC are between 1000 and 1500 g/(m^2 h)).

As an observation, it should be mentioned that after the butanol/water test the membrane showed some brownish spots on its surface. After the ethanol/water test all the sports disappeared as it is shown in Figure 6.8.

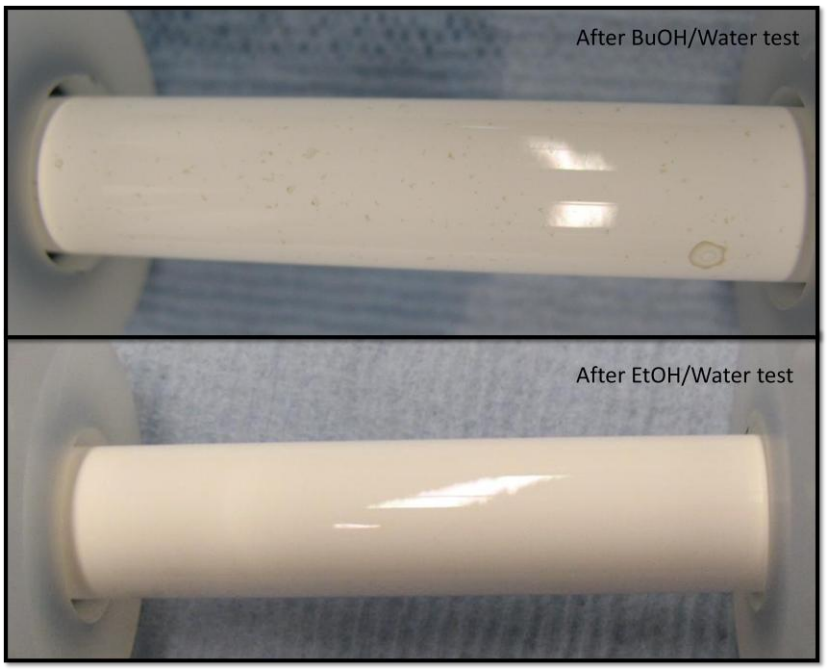

Figure 6.8 Membrane appearance after BuOH/Water test and after EtOH/Water test.

6.2.4.1.2 BTESM

With this membrane only an ethanol/water test was performed. In order to find a selective membrane for ethanol/butanal/1,1 diethoxy butane/water mixture, the membrane must be selective for ethanol/water mixtures (it is assumed that if the membrane is selective for EtOH/Water mixtures, it is also selective for BuOH/Water mixtures). The membrane geometrical characteristics are shown in Table 6.6.

Table 6.6 Membrane geometrical characteristics.

Membrane	BTESM
Diameter (cm)	7.5
Length (cm)	1.4
Membrane area (cm^2)	33.0
He flow [ml min^{-1} (3 bar)$^{-1}$(10 cm)$^{-1}$]	40

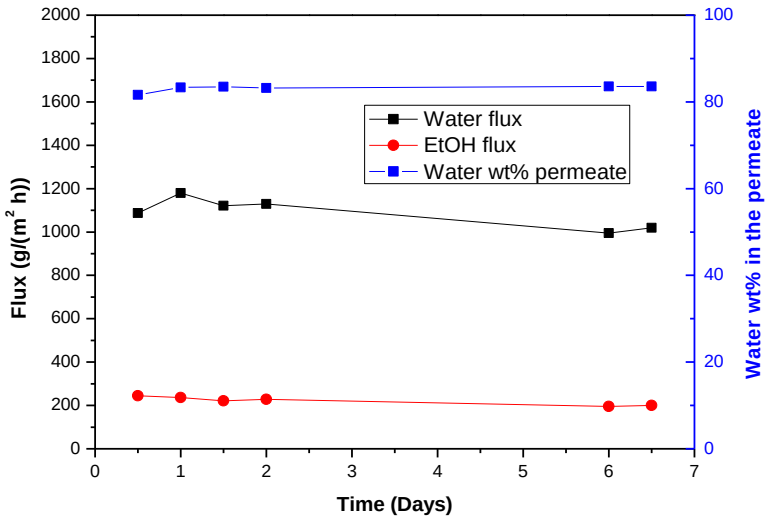

Figure 6.9 Membrane performance in an Ethanol/Water (95:5 wt%) test at 70 ºC.

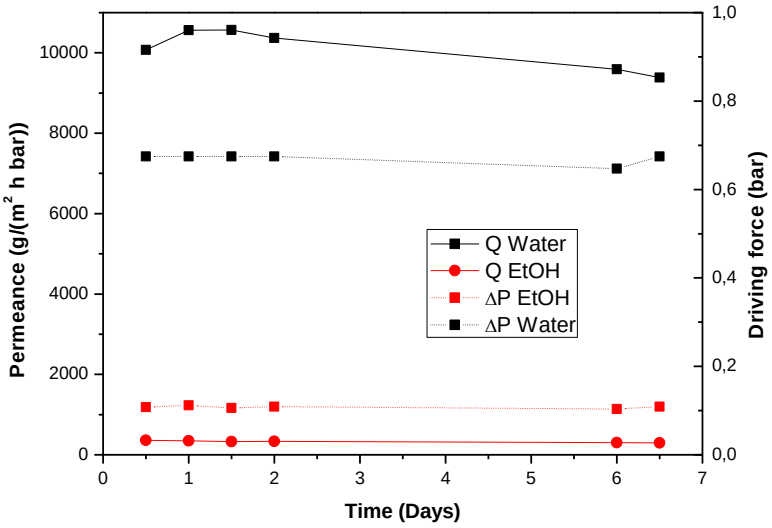

Figure 6.10 Membrane performance in an Ethanol/Water (95:5 wt%) test at 70 ºC.

In Figure 6.9 and in Figure 6.10 it can be observed that with the BTESM membrane the water concentration in the permeate side is a bit lower (around 83 wt%) than the previous membrane but the water flux is around 1100 – 1200 g/(m^2 h), which is good.

6.2.4.1.3 BTESE_2

Also in this case only an ethanol/water test (95:5 wt%) at 70 ºC was performed. The membrane behavior is depicted in Figure 6.11 and Figure 6.12. It can be observed that in this case both, water concentration in the permeate and the water flux are lower than

the previous membranes. The membrane geometrical characteristics are shown in Table 6.7.

Table 6.7 Membrane geometrical characteristics.

Membrane	BTESE_2
Diameter (cm)	7.5
Length (cm)	1.4
Membrane area (cm^2)	33.0
He flow [ml min^{-1} (3 bar)$^{-1}$(10 cm)$^{-1}$]	55

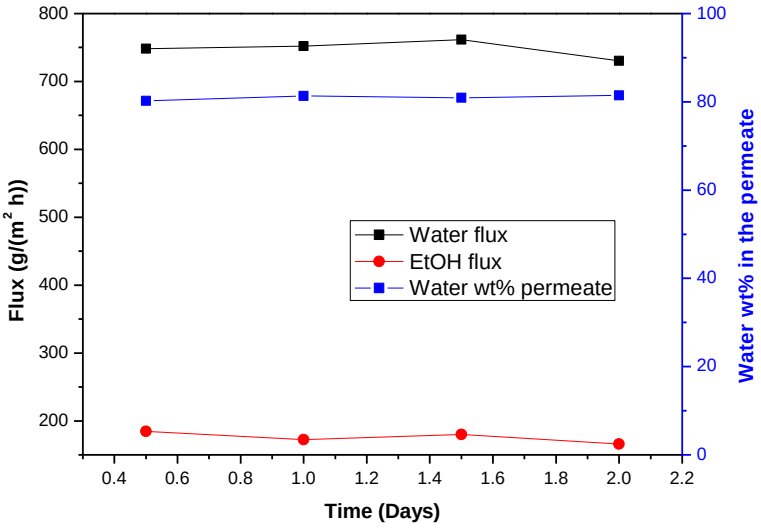

Figure 6.11 Membrane performance in an Ethanol/Water (95:5 wt%) test at 70 ºC.

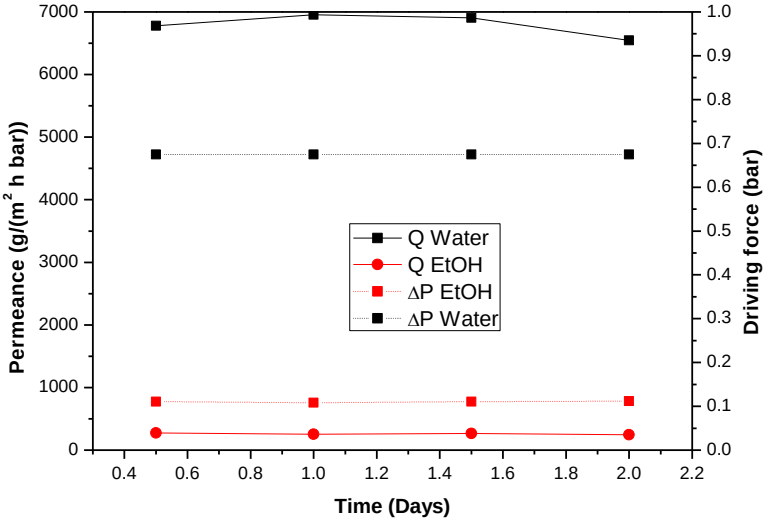

Figure 6.12 Membrane performance in an Ethanol/Water (95:5 wt%) test at 70 ºC.

6.2.4.1.4 Comparison of the tested membranes

Figure 6.13 shows a comparison of the binary pervaporation test results of the three tested membranes with a binary Ethanol/Water binary mixture (95:5 wt%) at 70 ºC.

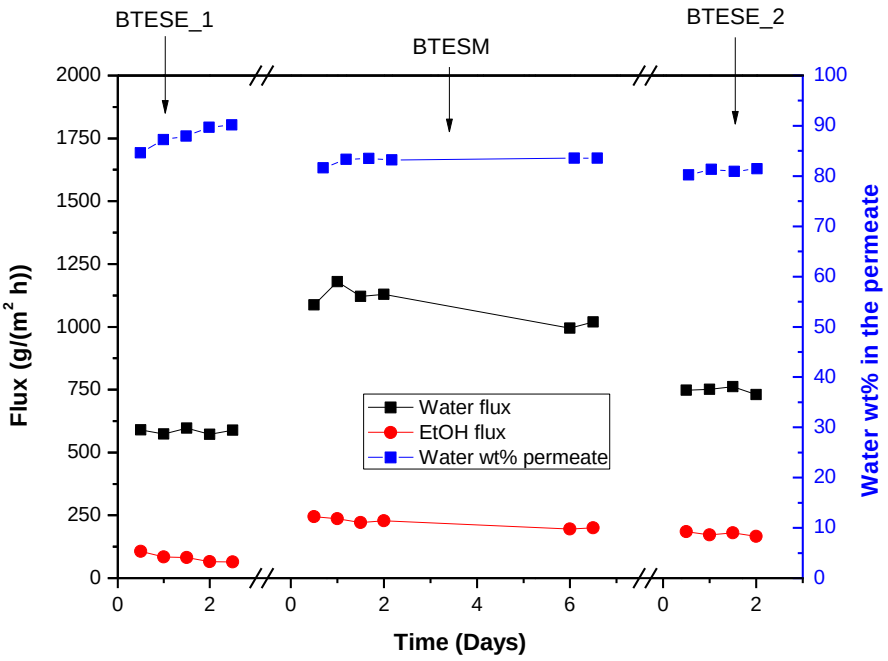

Figure 6.13 Comparison of the tested membranes in EtOH/Water mixture at 70ºC.

As it can be observed, the most selective membrane is the first one (B32 BTESE 07 BFS0912) and the third one (BTESE_2) is the least selective one. In terms of the water flux the first and third membranes show quite a low flux, below 900 g/(m^2 h), while the second membrane (BTESM) is the only one offering a relatively high water flux.

The third membrane (BTESE_2) was chosen to test if catalyst particle impacts damage the membrane surface. Between the first 2 membranes the first one (B32 BTESE 07 BFS0912) was chosen to perform all the pervaporation experiments because of its higher selectivity. However, it was observed that the membrane behavior suddenly changed. In a preliminary ethanol/butanal/acetal/water mixture dehydration experiment, it was observed that water concentration in the permeate was surprisingly low (around 65 wt% with 5 wt% of water in the feed side). In order to check if it was a membrane problem or a mixture problem, an ethanol/water standard test was performed. Figure 6.14 shows the difference between the membrane performance in an ethanol/water mixture before and after this quaternary mixture dehydration experiment. It is clear that water concentration in the permeate has decreased dramatically due to the ethanol flux increase and the water flux decrease.

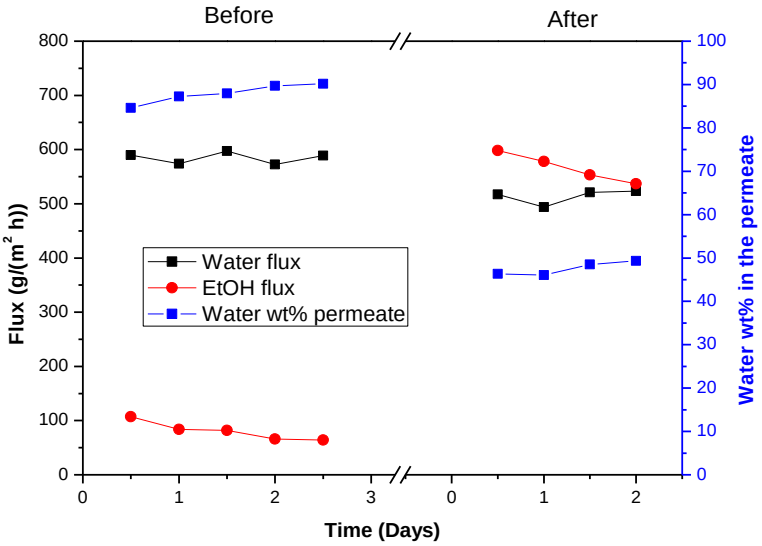

Figure 6.14 Comparison of the membrane behavior in an EtOH/Water mixture at 70ºC before and after performing the preliminary quaternary mixture dehydration experiment.

The most probable explanation of this behavior is that the membrane was damaged during the attaching/detaching process of the holders. For this reason, the second membrane, (BTESM) which was quite a good membrane, was chosen to perform all the experiments.

6.2.4.2 Effect of catalyst impacts on the membrane surface

One important test was to check if the impacts of Amberlyst 47 resin particles can damage the membrane surface and change the membrane performance. Depending on the membrane behavior, the experimental setup (a slurry reactor) could be modified for this or not. For this purpose, as it is indicated in Section 6.2.4.1.4, BTESE_2 membrane was chosen to perform this specific test.

Sommer & Melin (44) observed a selectivity drop after some small metal particles crashed over a silica membrane. Abrasion of the membrane top-layer was determined and they recommend installing a filter in order to avoid particle impacts over the membrane surface.

The test done now was carried out with butanol/water binary mixture at 95 ºC and 1200 rpm. The experiment was divided in 4 different sections. During the first few days no catalyst was added and the membrane behavior was checked and followed as function of time. In this region the flux decreases and water concentration in the permeate

increases. Most of the HybSi membranes show this behavior during the first 10 days. Afterwards 1 wt% of catalyst was added and after 18 days no change in the membrane behavior was observed (see Figure 6.15). What was observed was that catalyst particles broke down due to the magnetic stirring system.

The particle size decreased from 0.9 mm to some microns approximately (see Figure 6.18). In order to test the membrane resistance another 1 wt% of fresh catalyst was added. Also in this case, the membrane did not change and catalyst particles broke down again.

In order to test the membrane surface in a more aggressive way 1 wt% of alumina pellets where added. These alumina cylindrical pellets/extrudates are quite big and harder particles (length: 3.1 mm, diameter: 2.85 mm, see Figure 6.18). However, keeping 2wt% of Amberlyst 47 and 1 wt% of alumina pellets in suspension was impossible for the stirring system. For this reason a new butanol/water binary mixture was prepared and 1 wt% of alumina pellets were added. In this case a selectivity decrease was observed (see Figure 6.15). Also in this case, all the alumina pellets broke down, bringing the final particle size to around a few microns (see Figure 6.20).

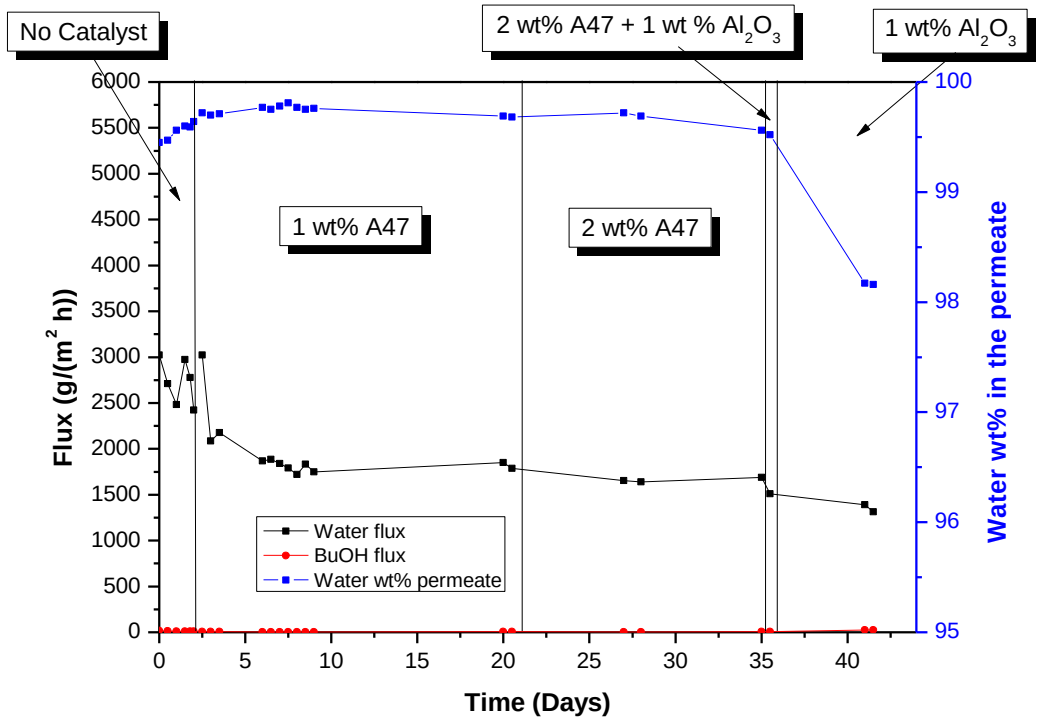

Figure 6.15 Performance of the membrane in butanal/water mixture at 95 ºC with different catalyst and alumina pellets loadings

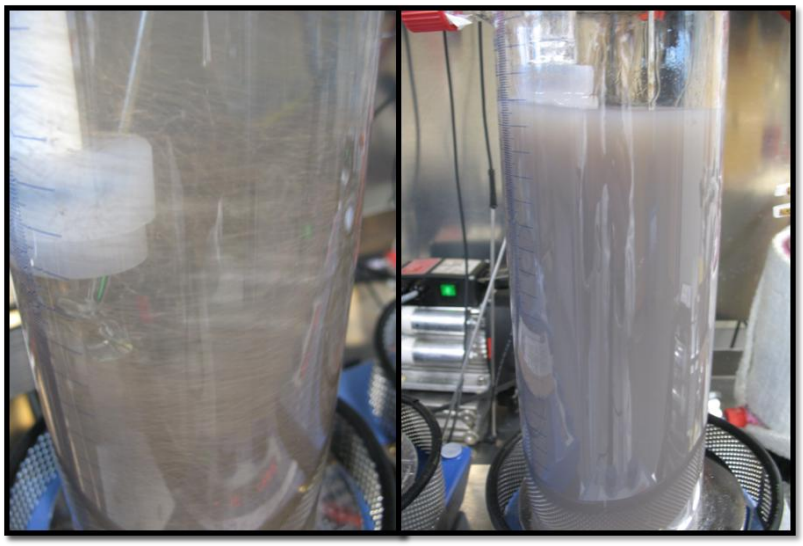

Figure 6.16 Appearance of the mixture with Amberlyst 47 at the beginning of the experiment and after some days.

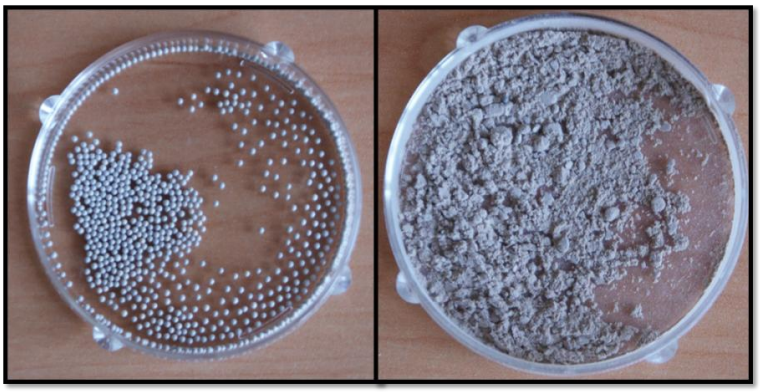

Figure 6.17 Appearance of Amberlyst catalyst particles before and after the experiment.

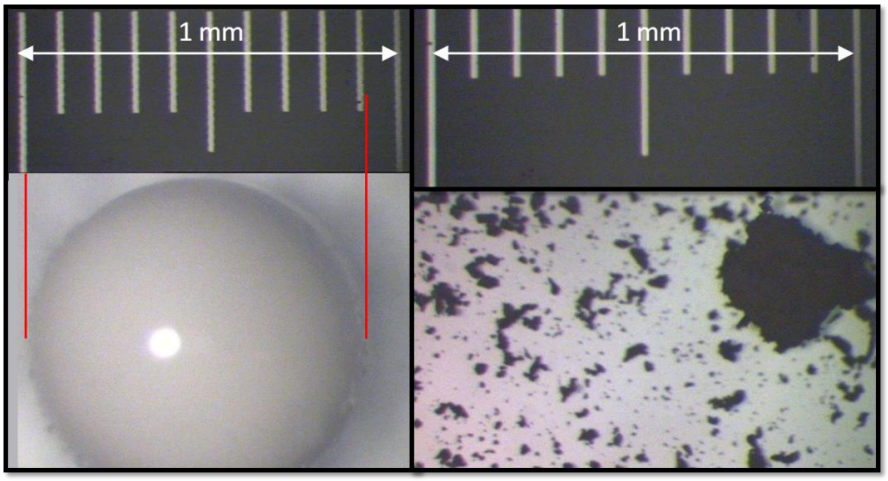

Figure 6.18 Optical microscope pictures of Amberlyst 47 resins before and after the experiment.

Figure 6.19 Appearance of the mixture with alumina pellets at the beginning of the experiment and after some days.

Figure 6.20 Appearance of alumina pellets before and after the experiment. The last picture shows the appearance of Al_2O_3 pellets after the experiment and it was taken with an optical microscope.

In terms of the membrane, in Figure 6.21 and Figure 6.22 some defects are visible with an optical microscope, which could explain the decrease in the selectivity. However, in Figure 6.22 it can be seen that before performing the experiment with catalyst particles and alumina pellets, the membrane also had some defects that can explain the performance explained in Sections 6.2.4.1.3 and 6.2.4.1.4.

Figure 6.21 Physical appearance of the membrane after performing the experiment with Amberlyst resins and alumina particles.

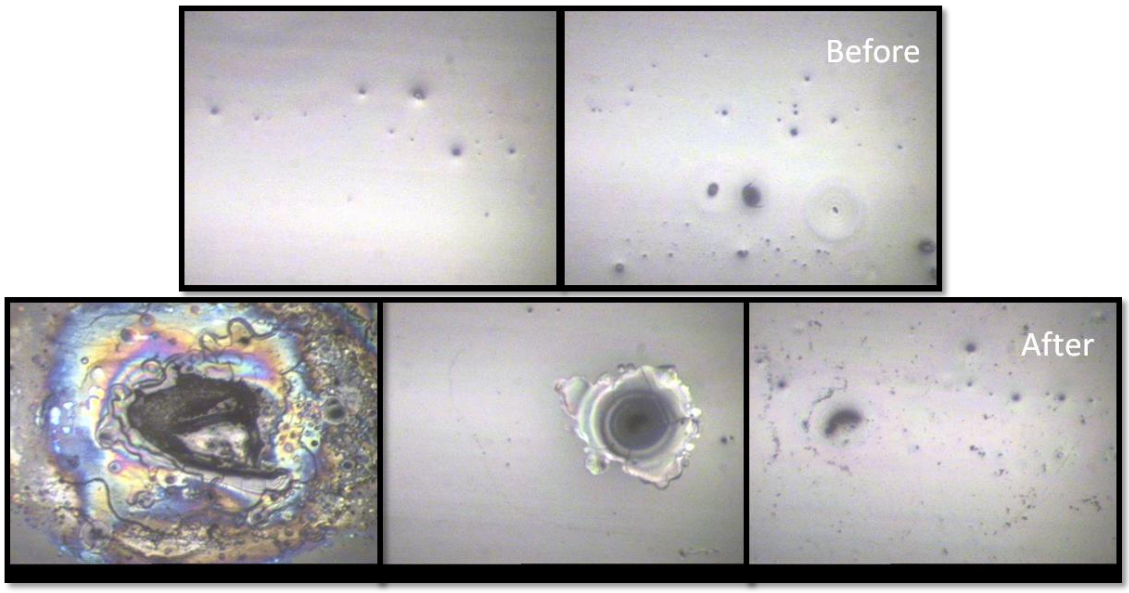

Figure 6.22 Optical microscope pictures of the membrane taken before and after the butanol/water experiment with Amberlyst resins and alumina pellets.

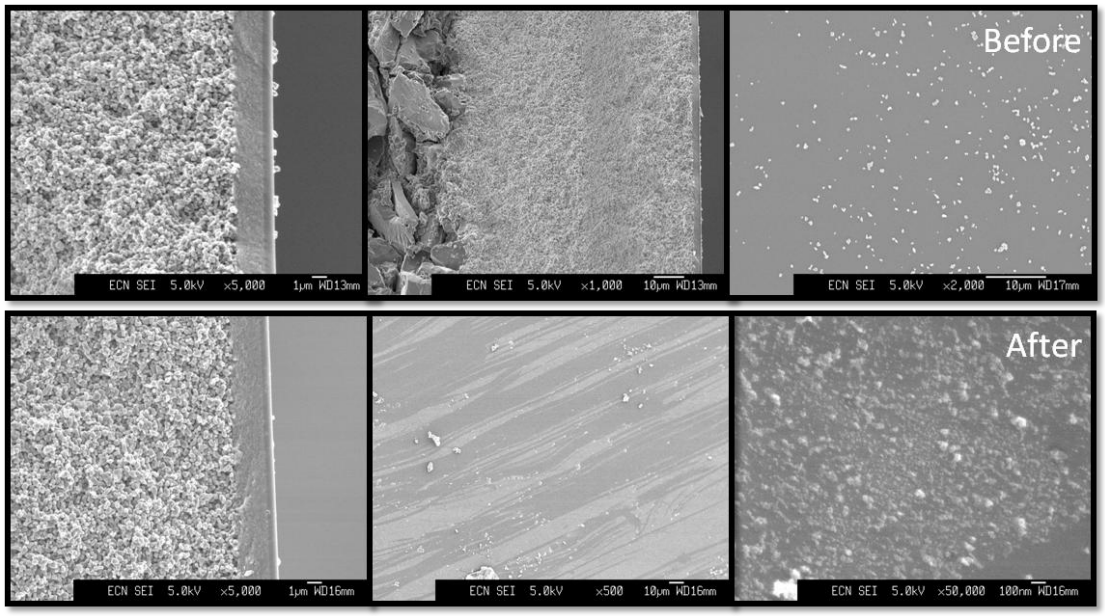

Figure 6.23 SEM pictures of the membrane surface and membrane layers. Pictures were taken before and after the butanol/water experiment with Amberlyst resins and alumina pellets.

SEM pictures (Figure 6.23) show that membrane layers are well defined both, before and after the experiment. However, in SEM pictures taken from the membrane surface an increase of some deposits or sediments can be observed, probably due to alumina pellets. Also some mechanical effects or scratches seem to have appeared.

It can be concluded that the membrane showed a great resistance to the impacts of the Amberlyst catalyst for a period of more than 30 days. Only when harder particles (alumina pellets) were added a selectivity decrease was observed.

6.2.4.3 Ethanol / Butanal / 1,1 diethoxy butane / Water dehydration experiments

The aim of these experiments was to check the membrane behavior and confirm if the membrane was selective enough for this specific mixture. Moreover, these experiments were used for calculation of the permeance of each compound and these permeances are then used as input into a mathematical model, which will be described later.

After performing the standard ethanol/water test, the next logical step would be to perform some butanal/water and 1,1 diethoxy butane/water dehydration tests but these two binary mixtures are completely immiscible. Thus directly the multi-component mixture was tested.

In this kind of tests, the used operating procedure was the following one:

- Carry out a reaction between ethanol and butanal at 50 ºC with 1 wt% of catalyst in a normal beaker. (It is known that in 1 hour approximately the reaction reaches the equilibrium, around 45 % of conversion).
- Remove all catalyst particles filtering the reaction mixture.
- Place the quaternary mixture in a pervaporation vessel and incorporate the membrane.
- Warm up the mixture up to the desired temperature.
- Once the temperature is stabilized connect the vacuum.
- Wait half an hour to stabilize the system.
- Open and close the corresponding valves in order to direct the permeate to the sampling side. Wait 2 minutes approximately to homogenize all the vapors.
- Withdraw a feed sample just before starting a pervaporation measurement and save it in a vial to be analyzed by GC. Part of the sample was used to analyze the water content by Karl Fischer. Start the measurement.
- After a certain period of time (between 45 and 120 minutes, depending on the temperature and water concentration in the feed side) stop the measurement and withdraw another feed sample and measure the water content by Karl Fischer. The feed samples taken just before and after each measurement were mixed in order to measure the average concentration.

- Wait some minutes to defrost the permeate sample, weight the sample and measure its water concentration using refraction index. The organics were analyzed by GC.

In these experiments the water concentration in the feed side is not constant since it is being removed by the membrane. In order to choose suitable temperatures for the measurements, the used criterion was based on the bubble point temperature of the initial equilibrium mixture. Table 6.8 shows an estimation of the initial composition. Aspen Plus was used to calculate the corresponding bubble point temperature: 77.8 ºC. The pervaporation tests were now performed at 3 different temperatures: 70 (just below the bubble point of the mixture), 55 and 40 ºC. A higher temperature step than 15 ºC was not convenient since the flux could be extremely low at the lowest temperature.

Table 6.8 Estimation of the equilibrium composition at 50 ºC.

Compound	**Concentration (wt %)**
Ethanol	30.8
Butanal	24.1
1,1 diethoxy butane	40.1
Water	5.0

As it is indicated in Section 6.2.4.1.4, M32 BTESM 08 BFS0912 membrane was used in all these experiments. However, in these cases the membrane area was 24.2 cm^2.

Figure 6.24 shows the typical behavior of this kind of experiments. In this case, Figure 6.24 shows the performance at 70 ºC. It can be seen how the water concentration in the feed side decreases considerably as function of time. The ethanol and butanal concentrations also decrease since they permeate a bit through the membrane. As the acetal does not permeate through the membrane, its concentration, expressed in wt%, increases.

At the permeate side, the water concentration is quite high, while the water concentration in the feed side is low. With 3 wt% of water in the feed side, its concentration in the permeate is around 90 wt%. With 1.5 wt% of water in the feed side, the corresponding water concentration in the permeate is 80 wt%; when the water concentration in the feed side is very low, the ethanol concentration in the permeate increases considerably although the flux is very low.

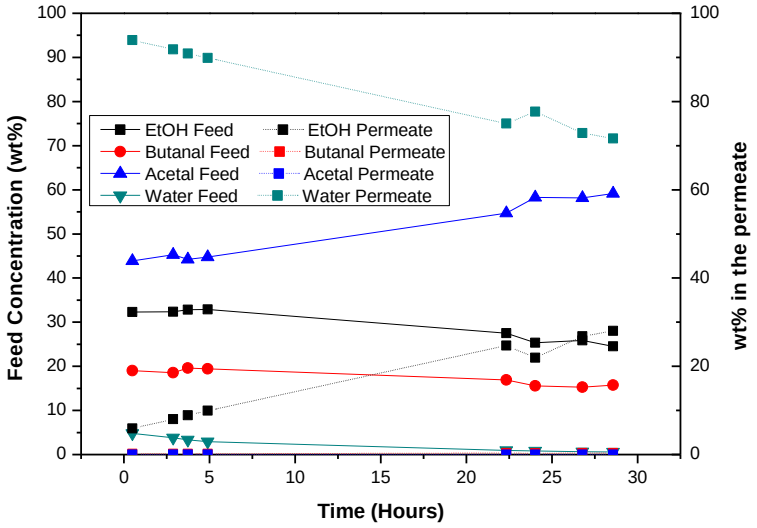

Figure 6.24 Concentration profile versus the time both, in the feed side and in the permeate side. T: 70 ºC.

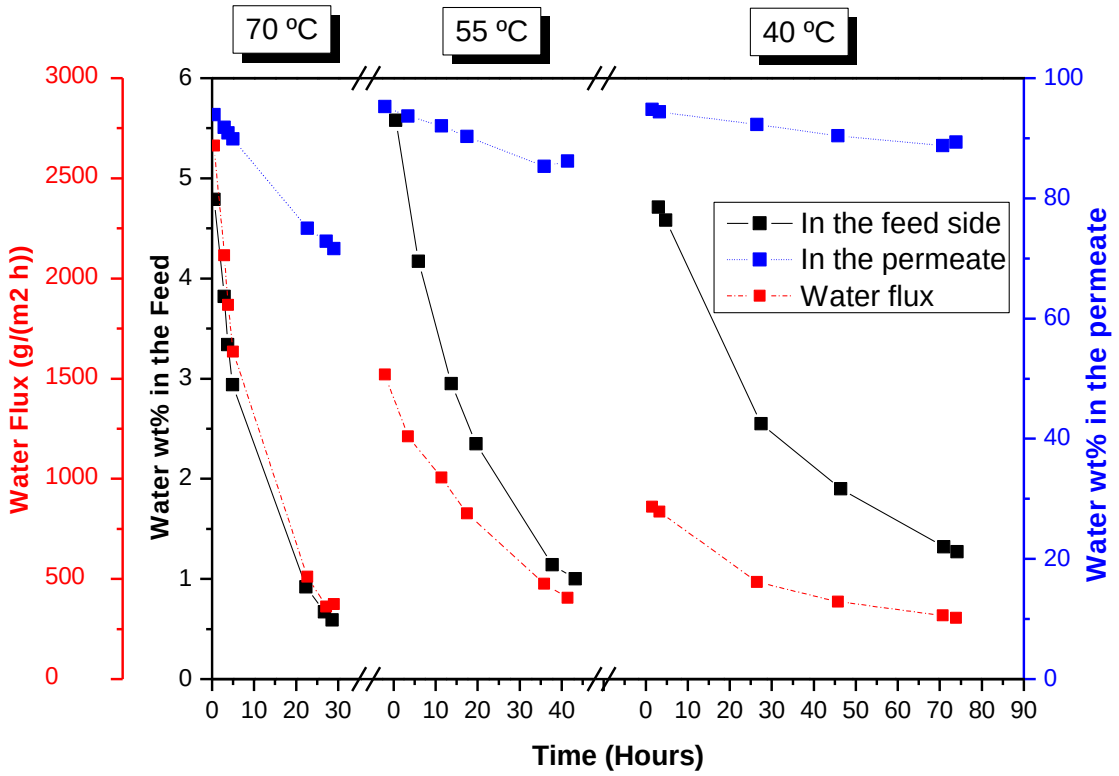

Figure 6.25 Water concentration profiles and water flux along the time for 3 different experiments performed at 70, 55 and 40 ºC.

Figure 6.25 shows that for similar water content in the feed side, the water flux decreases around 40 % decreasing the temperature by 15 ºC. It can be observed that at 70ºC it takes 20 hours to go from 5wt% of water to 1wt% while at 40 ºC it takes around

80 hours. The water concentration in the permeate does not change significantly with the temperature at the same feed water concentration.

Figure 6.26 shows permeance values for ethanol, butanal, 1,1 diethoxy butane and water. The acetal does not permeate through the membrane so its permeance value is equal to zero, while the permeance value of butanal is really low, almost zero. Ethanol permeance values are higher but comparing to water permeance values they are also quite low.

In case of the water, it is clear that water permeance value strongly depends on the temperature. The water permeance increases with decreasing temperature. A combination of different factors is believed to play a role here that influences the transport of species through the membrane: (1) sorption on the membrane, (2) diffusion through the membrane and (3) desorption from the membrane. Each of these effects has its own dependence on the temperature. With increasing temperature, sorption will become smaller while the diffusion rate increases. A decreasing permeance as function of temperature is observed when the heat of adsorption is larger than the respective activation energy for diffusion (61). This effect is more commonly observed in gas transport, where the permeance of a strongly adsorbing gas, e.g. CO2, decreases with temperature, while for a none adsorbing component its permeance increases (62).

The influence of the feed water concentration on the permeance is less clear. At 70 ºC the water permeance increases with increasing water content in the feed while at 55 ºC there is hardly any dependence and at 40 ºC the water permeance decreases with an increase of water content in the feed (see Figure 6.26). The most likely explanation for this behavior is the difference in competitive adsorption between water and the organic components at different temperatures and concentrations. At a higher temperature there is less adsorption for both water and the organic component and water transport is less hindered by competitive adsorption. At lower temperatures the competition between the adsorption of water and the organic is stronger and even though the water flux increases with concentration (as the driving force increases) the permeance decreases. As it will be explained in section 6.2.4.5, membrane changes as function of time are minimal and do not explain these permeance differences.

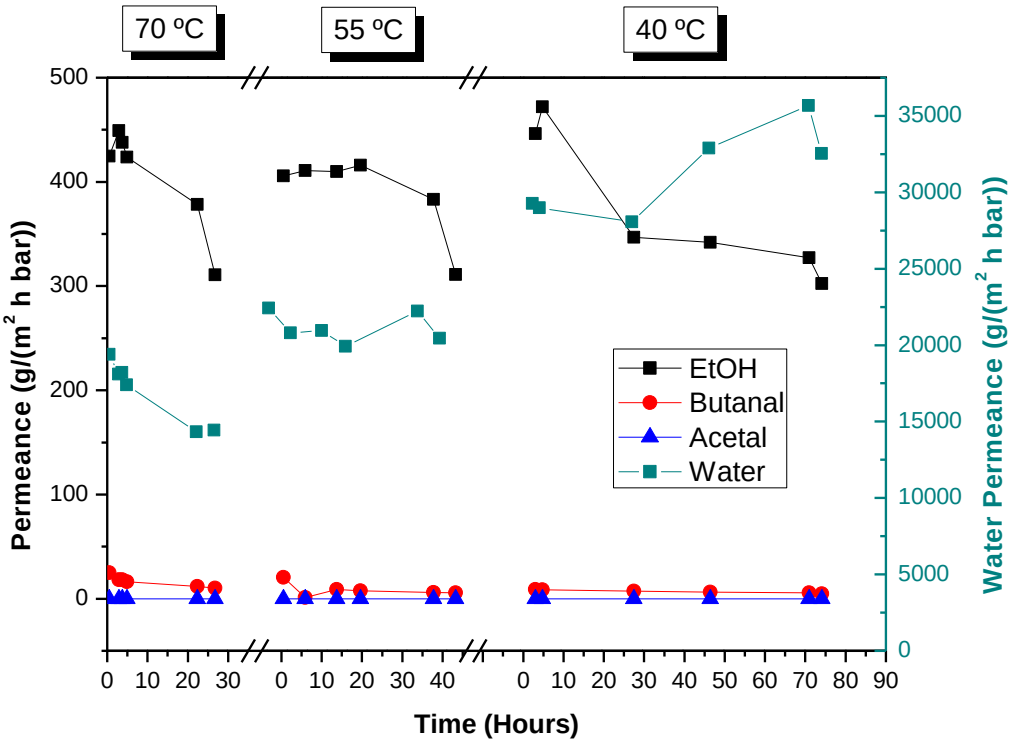

Figure 6.26 Permeance values at 70, 55 and 40 ºC.

For the modeling study average values for the permeances were taken at each temperature (see Table 6.9). As indicated in Figure 6.26 the permeance is a function of the feed concentration and by taking an average permeance an error of maximum 20% is introduced. The standard errors shown for butanal calculations are higher due to the measured small permeance values for this reactant as compared to the water permeance ones. For the acetal permeances, the indicated maxima were calculated from the detection limit of the analytic equipment for this compound. The acetal concentration in all the permeate samples was below this detection limit.

Table 6.9 Average permeance values at 70, 55 and 40 ºC for all the components

	Permeance [mol/(m².h.bar)]		
	70ºC	**55ºC**	**40ºC**
Q EtOH	8.3 ± 1.4	8.5 ± 0.9	8.1 ± 1.5
Q But.	0.2 ± 0.07	0.1 ± 0.1	0.1 ± 0.0
Q Acetal	< 0.17	< 0.19	< 0.18
Q Water	$(0.92 \pm 0.11)\cdot 10^3$	$(1.17 \pm 0.05)\cdot 10^3$	$(1.73 \pm 0.16)\cdot 10^3$

In order to study the permeance dependence on the temperature, the average values (over the measured range of concentration) were fitted to an Arrhenius type correlation (eq. (6.16).

$$Ln(Q) = Ln(A) + \left[\frac{-E_a}{RT}\right] \tag{6.16}$$

Where: E_a is the activation energy (J/mol)

R is the universal gas constant (J/(mol·K))

T is the temperature in Kelvin

A is the pre-exponential factor

Q is the permeance value (g/(m²·h·bar))

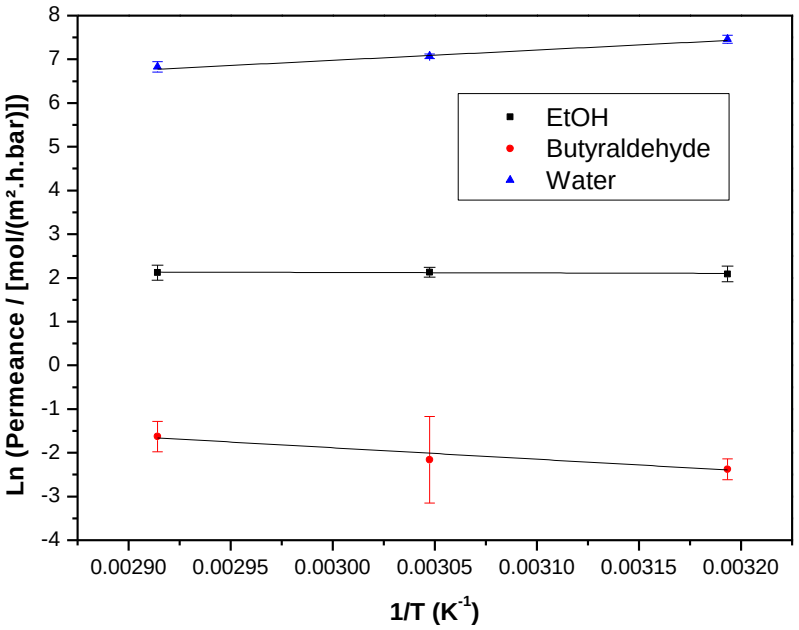

Figure 6.27 Permeance data fitted to an Arrhenius type correlation.

Figure 6.27 shows that the average permeance data at each temperature fit really well to an Arrhenius type correlation. Table 6.10 shows the pre-exponential factors as well as the activation energy of each compound.

By doing so, a simple empirical relation describing the performance of the used hybrid silica membranes within a rather small temperature and concentration range for the process under consideration is obtained. When using the model outside the concentration range tested here, the influence of feed concentration on the permeance will have to be taken into account. In the model validation section (section 7.1.2), it is shown that this straight forward approach leads to a model that very well describes the discontinuous process.

Table 6.10 Pre-exponential and activation energy values obtained fitting permeance values to an Arrhenius type correlation.

	A [mol/(m².h.bar)]	**E_a [kJ/mol]**
EtOH	10.92 ± 1.35	0.75 ± 0.7
Butanal	$(0.607 \pm 0.015) \cdot 10^3$	23.0 ± 7.5
Acetal	0	n.a.
Water	1.2 ± 2.1	-19.0 ± 2.1

The apparent activation energy (E_a) is the sum of the activation energy of diffusion (E_D) and the enthalpy of sorption (ΔH) as indicated above. While E_D is generally positive, ΔH is usually negative for the exothermic sorption process. When the negative ΔH dominates over the positive E_D, a negative value of E_a occurs. A negative Ea, and thus a decreasing permeance with increasing temperature, does not mean that the flux will decrease when the temperature is increased. Often (as in the studied case) the flux increases with temperature because the effect of temperature on the saturation pressure, and thus driven force, is more significant (63). The activation energy of -18,8 kJ/mol for water using HybSi® membranes is close to -16 kJ/mol as reported by Feng et al (63) using a polymeric membrane for ethanol-water dehydration experiments. Different activation energies for silica membranes for dehydration have been reported. Ten Elshof (64) has reported a value of -4 ±5 kJ/mol for water in methanol and -24 ± 7 kJ/mol for methanol in a system containing 15 wt% water. Bettens (65) has reported water activation energies of between 8.5 and 13.5 kJ/mol for 90% water in respectively methanol and ethanol. Sommer (66) has reported an activation energy of 13.3 kJ/mol for water and 12.6 kJ/mol for ethanol for mixtures of 5-15 wt% water in ethanol. Differences in the activation energies could have to do with the type of membranes, competitive temperature dependent adsorption effects, different mixtures and test conditions.

6.2.4.4 Reaction + pervaporation experiments

After checking that the chosen membrane is selective for ethanol/butanal/1,1 diethoxy butane/water mixtures and Amberlyst 47 particle impacts do not damage the membrane surface, reaction + pervaporation experiments were carried out in the same unit. Most of the authors use a separated pervaporation unit (31-33;67-69) instead of using one unique unit where the reaction and separation occur. However, as the suitable temperature range for the reaction and for pervaporation is in the same interval for the process under study and particle impacts do not damage the membrane surface, these experiments were carried out in the same unit.

The aim of these experiments was to prove that the thermodynamic limitations of the studied reactions can be overcome. Three different parameters were studied:

1. Temperature effect
2. Catalyst loading effect
3. Feed ratio effect.

In this kind of tests, the used operating procedure was the following one:

- Prepare the desired EtOH/Butanal mixture
- Warm up the mixture up to the desired temperature and connect the vacuum at the same time.
- Once the temperature is stabilized add the catalyst. Starting point of the experiment: t=0
- Open and close the corresponding valves in order to direct the permeate to the sampling side. Wait 2 minutes approximately to homogenize all the vapors.
- Withdraw a feed sample just before starting a measurement and save it in a vial to be analyzed by GC. Part of the sample was used to analyze the water content by Karl Fischer. Start the measurement.
- After a certain period of time (between 45 and 120 minutes, depending on the temperature and water concentration in the feed) stop the measurement and withdraw another feed sample and measure the water content by Karl Fischer.
- Wait some minutes to defrost the permeate sample, weigh the sample and measure its water concentration using refraction index. The organics were analyzed by GC.
- Go on withdrawing feed samples and measuring the permeate in the reactive system until the water concentration in the feed side was below 1 wt%.

No side reactions were observed in the experiments.

6.2.4.4.1 Effect of the temperature

In Section 6.2.4.3 it was shown that at lower temperatures the permeation flux decreases considerably. Because of this, from the pervaporation point of view, it seems that high temperatures should enhance the process. However, the acetalization reaction is an exothermic reaction, so, from the reaction point of view, at higher temperatures the reaction rate increases but the achievable conversions decrease. The objective of these experiments was to see which the predominant effect is and thus, to see which the optimum process temperature would be. For these purpose, three different temperatures were tested: 40, 55 and 70 ºC, which were the same as in Section 6.2.4.3,

Figure 6.28 shows the typical process behavior. During the first two hours all the concentrations change considerably more or less achieving the equilibrium concentration values corresponding to the initial compositions and the fixed temperature. During this period the reaction predominates. After 2 hours the water concentration goes to a maximum and then starts decreasing due to the pervaporation process. In the mean time the acetal concentration starts increasing above its equilibrium concentration. It is clear that comparing the reaction rate and the pervaporation rate, the first one is much faster being pervaporation process the limiting step under the chosen conditions (catalyst loading and membrane area). However, it must be mentioned that the membrane area was quite small (24.2 cm^2) for the processed feed amount (1.6 liters).

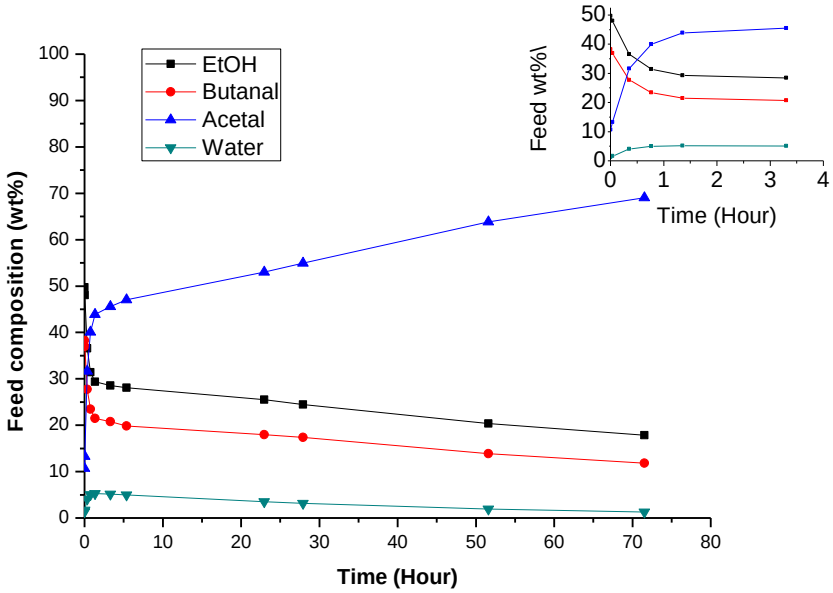

Figure 6.28 Typical process behavior. Conditions: ratio EtOH/butanal: 2:1 in moles, 40 ºC, catalyst loading 0.5 wt%. (Solid lines connecting experimental points are represented for a better trend understanding).

Figure 6.29 shows the evolution of the conversion at the three selected temperatures. As can be observed, an increase of the temperature implies a decrease in the equilibrium conversion that can be estimated from the initial compositions and the selected temperature (which corresponds with the achieved conversion during the first 2 hours of reaction and separation approximately). At higher temperatures the water removal rate is much faster. Thus, after around 15 hours, the achieved conversion at 70 ºC is higher than the achieved ones at 40 and 55 ºC. If a larger membrane area would have been used, these times could have been decreased significantly.

Figure 6.30 shows the water concentration profiles in the feed side and in the permeate side. Following the previous reasoning, it can be observed that water concentration in the feed side shows a maximum in the 2nd hour. This means that in the first 2 hours, the reaction rate was much more important than the water removal by pervaporation since the membrane was not able to remove all the generated water. From the 2nd hour on, the overall reaction rate decreases and becomes adjusted to the requirements provided by the pervaporation as water extraction de-equilibrates the mixture and the pervaporation becomes the main conversion governing process. This is caused by the decrease of the water content in the feed side and thus, conversion is increased.

In terms of the permeate, it can be observed that at lower temperatures the water concentration in the permeate is higher since the water concentration in the feed is also higher. On the other hand, the permselectivity between water and ethanol decreases increasing the temperature, so, the integral loss of ethanol is higher at high temperatures. However, this loss of ethanol does not seem to be very important at 70 ºC since the conversion is still the highest one after 50 hours.

The permeate composition during the first hours was water and mostly ethanol. At the end of the experiment e.g. at 55 ºC, the permeate concentration was the following one: 78.7 wt% water, 20.0 wt% ethanol, 1.3 wt% butanal and 0.4 wt% 1,1 diethoxy butane.

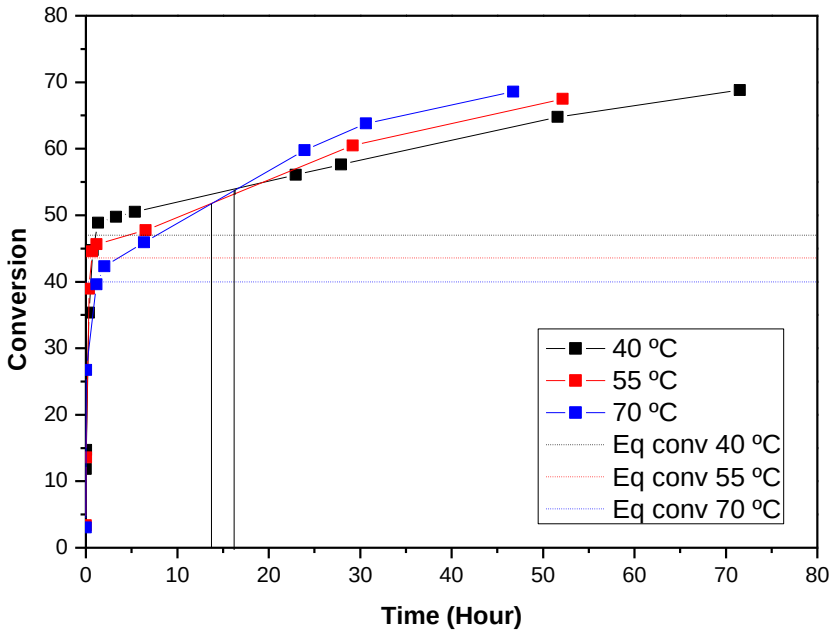

Figure 6.29 Effect of the temperature and time on conversion. Conditions: ratio EtOH/Butanal 2:1 in moles, catalyst loading 0.5 wt%.

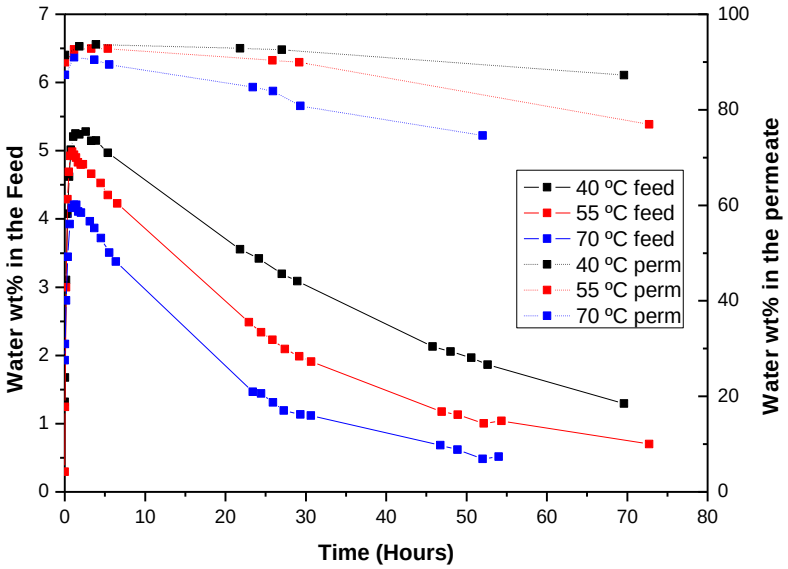

Figure 6.30 Effect of the temperature and time on water profiles in the feed and in the permeate. Conditions: ratio EtOH/Butanal 2:1 in moles, catalyst loading 0.5 wt%.

The water flux as function of time behaves as expected (Figure 6.31). In the beginning the feed water concentrations do not deviate very strongly at the different temperatures and thus the water flux measured at the same process reaction time is the highest for the highest temperature. As a function of time the water concentration in the feed decreases faster for the highest temperature. Thus it can be observed that the water flux decreases the quickest for the highest temperature. At a certain moment the water flux at 70 ºC at the same process runtime is even lower than at 40 or 55 ºC.

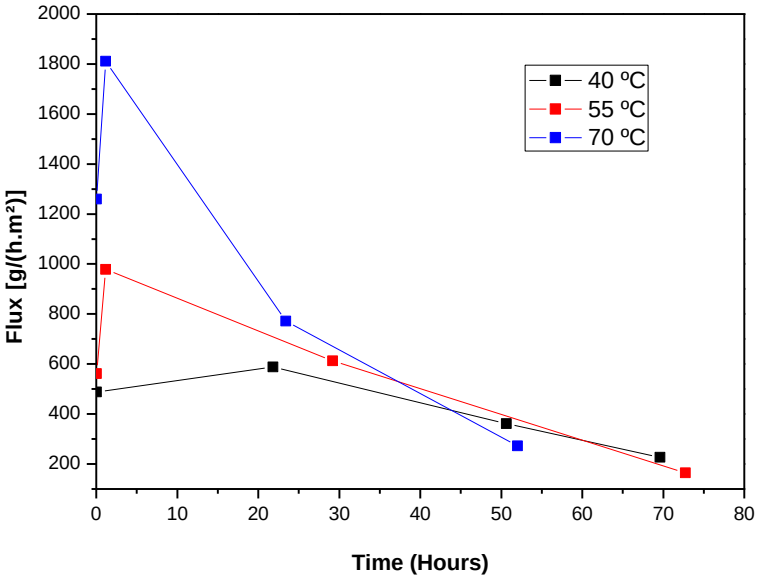

Figure 6.31 Effect of the temperature and time on water flux. Conditions: ratio EtOH/Butanal 2:1 in moles, catalyst loading 0.1 wt%.

6.2.4.4.2 Catalyst loading effect

The catalyst loading was varied from 0.1 % wt% to 1.0 % wt%. In Section 6.2.4.4.1 it was found that pervaporation is the limiting step. In order to enhance the pervaporation and to try to have a pervaporation process that is as fast as possible, all these experiments were carried out at 70 ºC. The objective of these experiments was to see how different catalyst loadings could affect to the pervaporation process. Figure 6.32 shows that, despite working with a very low catalyst loading (0.1 wt%), pervaporation is still the limiting process since the conversion profile along the time does not change significantly with the catalyst loading. Even though small differences can be observed for example, at the lowest catalyst loading where the equilibrium conversion (after about 2 hrs of reaction and pervaporation) is lower than at the catalyst loadings of 0.5 and 1 wt%.

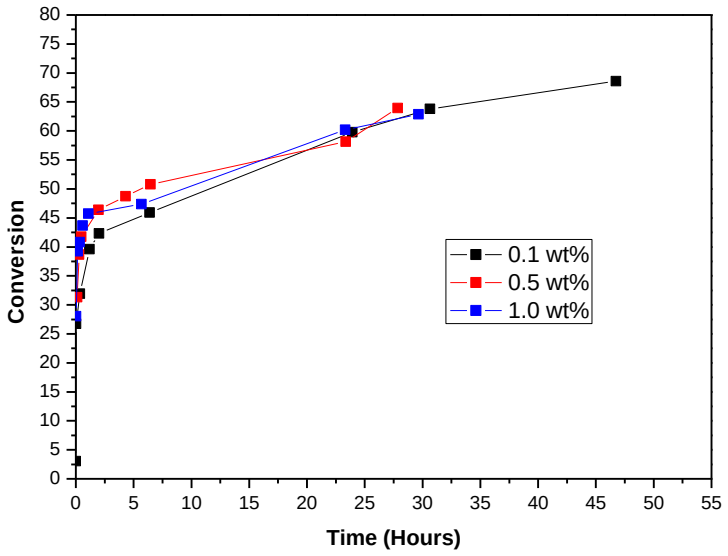

Figure 6.32 Effect of catalyst loading on the process. Conditions: ratio EtOH:Butanal 2:1 in moles; temperature: 70 ºC.

6.2.4.4.3 Feed composition effect

It is known that working with an excess of one of the reactants higher conversions are achieved. In this case, different ethanol excess ratios were used since this reactant is cheaper than butanal. However, from the pervaporation point of view, ethanol is the smallest organic molecule in the studied component matrix, i.e., it is the compound that has a higher tendency to go through the membrane. For this reason, the tested excess ratios (EtOH/Butanal) were not extremely high.

The stoichiometric feed ratio (2:1 in moles) and 2.5:1 and 3:1 ratios were used. Figure 6.33 shows the conversion profiles for the mentioned feed ratios. Also in this case, all the experiments were performed at 70 ºC and the used catalyst loading was 0.1 wt% since in Section 6.2.4.4.2 it was found that even using 0.1 wt% of catalyst loading, pervaporation was the limiting process. In this figure it can be seen that the higher the feed ratio the higher the conversion, as expected.

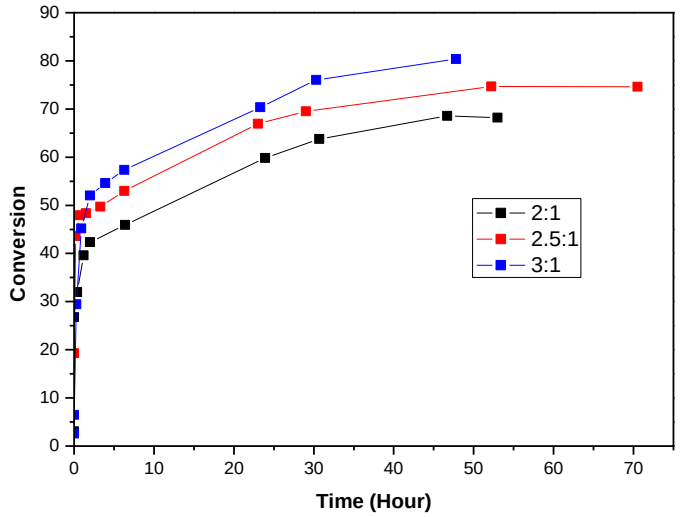

Figure 6.33 Effect of the ethanol/butanal feed mole ratio on the process conversion. Conditions: Temperature 70 ºC, Catalyst loading: 0.1 % wt%.

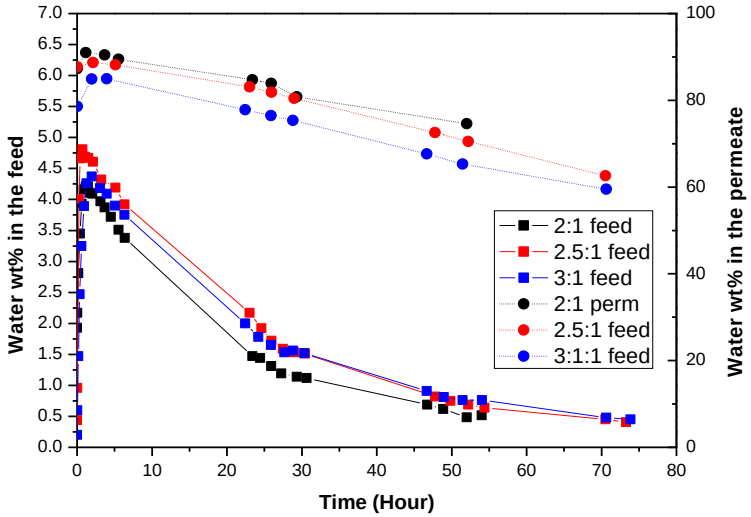

Figure 6.34 Effect of the ethanol/butanal feed mole ratio. Water concentration profiles, both, in the feed side and in the permeate side. Conditions: Temperature 70 ºC, Catalyst loading: 0.1 % wt%.

In Figure 6.34 it can be observed that when increasing the ethanol/butanal ratio, the water concentration in the permeate side decreases. This is because more and more ethanol is permeating. Especially at the highest feed ratio this permeate concentration is

below 80% during all the experiment so it is not logical to test even higher ethanol excess feed ratios.

6.2.4.5 Long term membrane performance

All the experiments presented in Sections 6.2.4.3 and 6.2.4.4 were performed with the same membrane tube (BTESM) throughout 4 months showing a good behavior in all the cases. Moreover, it must be taken into account that the membrane suffered strong process conditions, receiving catalyst impacts.

Figure 6.35 shows a general overview of the membrane performance in the different experiments performed with the mentioned membrane.

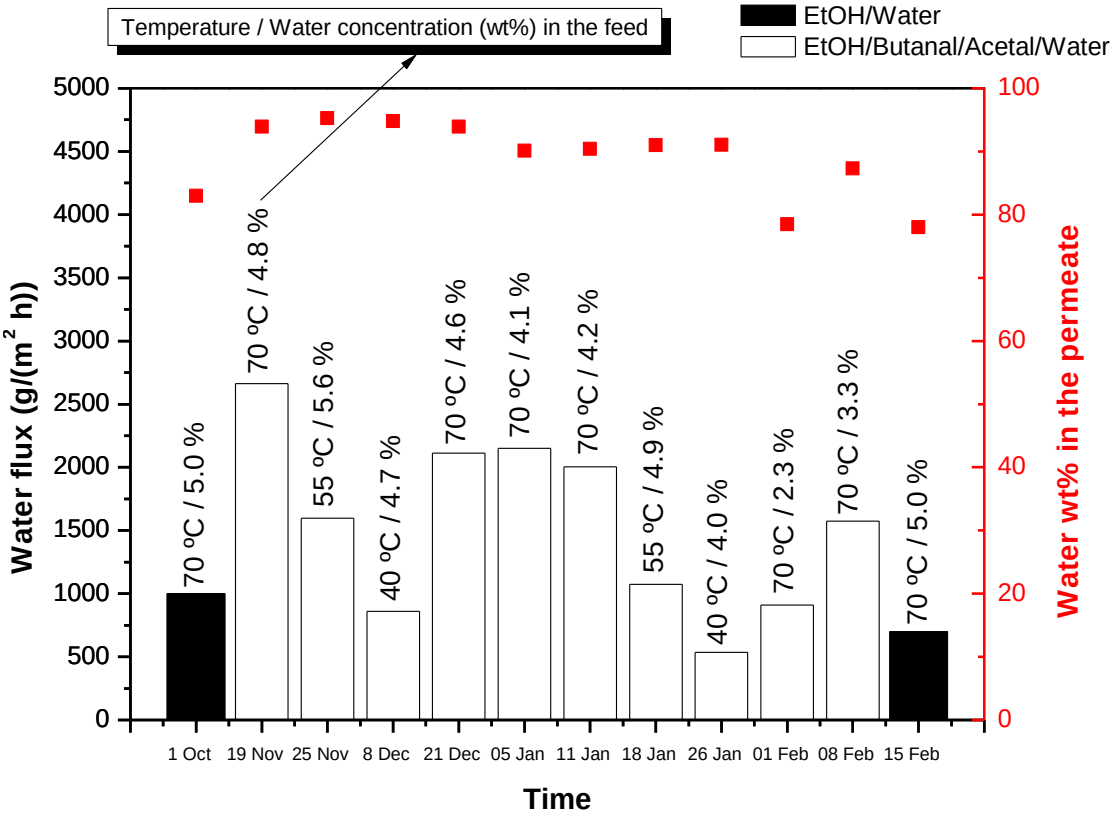

Figure 6.35 Water flux and water concentration (wt%) in the permeate in the different experiments carried out with M32 BTESM 08 BFS0912 membrane in 4 months.

The first and the last columns in Figure 6.35 represent an ethanol/water standard test performed under the same conditions (95:5 wt% EtOH/water at 70 ºC) just before and after performing all the experiments. It can be observed that the flux has slightly decreased as well as the water concentration in the permeate side. However, these

differences are not really large taking into account the amount of experiments completed in between. These differences could also have occurred when just binary water-ethanol pervaporation tests would have run for 4 months.

6.3 Conclusions

Some clear conclusions can be obtained from the experimental part. The most important evidence is that HybSi® membranes are selective for ethanol/butanal/1,1 diethoxy butane/water mixtures and that they can shift the equilibrium of the acetalization reaction significantly. It must be taken into account that butanal, as most of the aldehydes, is quite an aggressive organic compound. The membrane is practically impermeable to 1,1 diethoxy butane and the butanal permeance could also be considered negligible. Due to the membrane selectivity, water could be removed efficiently from the reaction mixture and equilibrium conversions were overcome.

The used membrane area in the experiments was really low for the feed amount that was treated and in this process pervaporation was the limiting step. Even working with really small amounts of catalyst, the achieved conversions were limited by the pervaporation rate.

In terms of the temperature, it is clear that working at higher temperatures the water flux through the membrane increases. From the reaction point of view, being an exothermic reaction, it is known that the higher the temperature is, the lower equilibrium conversion is. However, operating at the highest temperature for the combined pervaporation – reaction system better results were obtained.

By using different ethanol/butanal feed ratios, it was observed that working with an excess of one of the reactants (ethanol) the final conversion is higher. However, working with 3:1 ethanol:butanal ratio, the ethanol driving force was quite important and therefore, ethanol flux and loose through the membrane was considerable.

Regarding the membrane mechanical resistance, it was found that HybSi membranes can handle Amberlyst 47 particle impacts. It was checked that, in spite of the impacts, the membrane behavior was completely stable.

Chapter VII

Membrane reactors. Modeling part

7 Membrane reactors. Modeling part.

In Chapter VI it was experimentally checked that the continuous water removal using dehydration membranes shifts the reaction to the forward direction overcoming thermodynamic limitations.

In the present chapter a semi-batch process modelization is presented in order to validate it with experimental results presented in Chapter VI. After validating the model a sensitivity analysis will be shown. MATLAB software package was chosen to implement the equations and run the model.

On the other hand, an initial continuous process design of the acetalization reaction including dehydration by pervaporation will be developed in this Chapter. In this case ASPEN CUSTOM MODELER (ACM) was the chosen software package. I this case ACM was chosen since its suitability to model different unit operations and modules and link them to each other.

7.1 Semi-batch model

The final objective of the present study is the development of a continuous process for acetal production. As all the experiments were performed in a semi-batch pervaporation installation there was no way to validate the continuous operation of a membrane module with experimental data. For this reason, a semi-batch model was developed in order to check the experimentally obtained permeance values and validate, in an indirect way, the continuous pervaporation model that will be described in Section 7.2. A simple scheme of the modeled semi-batch membrane reactor is shown in Figure 7.1.

Moreover, the developed model was used to study in more detail the performance of the process in semi-batch mode, to perform a parametric sensitivity study and to calculate and search the optimum process conditions.

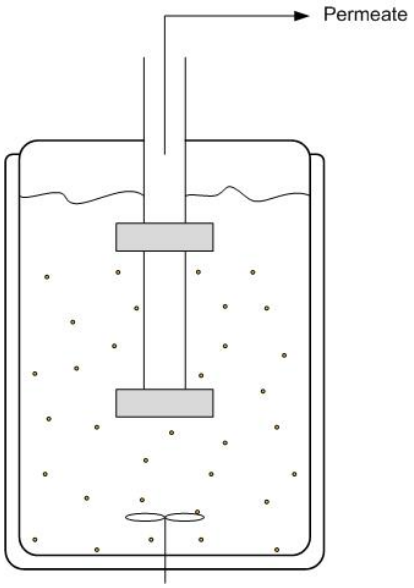

Figure 7.1 Scheme of the modeled semi-batch membrane reactor

The general model assumptions used in the development of the equations are the following ones:

- A pseudo-homogeneous kinetic model was assumed.
- Perfect mixing was considered, i.e., there are no concentration and temperature gradients in the reactor.
- An isothermal process was considered.
- Concentration polarization and temperature polarization on the membrane was assumed not to be present.
- The membrane is completely inert and it does not influence the reaction kinetics.
- Permeance values depend only on temperature. The influence of the concentration of each compound on permeance values was considered negligible.
- Constant mixture density was considered.
- Volume change related to the pervaporation was taken into account.

Some authors (70;71) considered that the volume change could be considered negligible and some others took into account this variation (69). In the experimental part of the present study it was observed that the volume could change around 15%, due to both the reaction and the pervaporation process so it was taken into account.

7.1.1 Degrees Of Freedom (DOF) analysis. Equations

As the first step of the modeling, a study of degrees of freedom was performed. This study is essential in order to know if the mathematical model can be solved or not.

Table 7.1 Variables and equations for the semi-batch membrane reactor.

Variables		**Equations**	
Feed composition	4	Material balance	4
Flux through the membrane	4	Transport through the membrane	4
Permeate composition	4	Flux quotients	4
TOTAL	12	TOTAL	12

7.1.1.1 Mass balance

The model will be described using molar balances of each component. The generic component balance for each component is the following one:

[In by flow] – [Out by flow] – [Out through the membrane] + [Generation/consumption]=[Accumulation]

$$0 \quad - \quad 0 \quad - \quad J_i A_m \quad + \quad r_i V_r \quad = \quad \frac{dN_i}{dt}$$

Rearranging this equation, the design equation is obtained:

$$\frac{d(V_r C_i)}{dt} = r_i V_r - J_i \, A_m \tag{7.1}$$

Where:

J_i is the flux of component *i* through the membrane $\left(\frac{mol}{m^2 \, s}\right)$ (see eq. (7.8)

A_m is the membrane area (m^2)

V_r is the reaction volume (m^3)

r_i is the reaction rate ($mol/m^3 s$)

The reaction volume changes as function of time due to the separation process through the membrane.

$$V_r \frac{d(C_i)}{dt} + C_i \frac{dV_r}{dt} = r_i V_r - J_i \, A_m \tag{7.2}$$

Rearranging equation (7.2):

$$\boxed{\frac{d(C_i)}{dt} = r_i - \frac{J_i\ A_m}{V_r} - \frac{C_i}{V_r}\frac{dV_r}{dt}} \tag{7.3}$$

7.1.1.2 Volume change

The volume variation can be obtained from a global mass balance of the system.

$$\frac{dm}{dt} = -F_P \tag{7.4}$$

Where

m is the total mass in the reactor (kg)

F_P is the mass which is going out through the membrane (kg/s)

Equation (7.4) can be expressed in terms of reaction volume:

$$\frac{d(V_r \rho_r)}{dt} = -F_P \tag{7.5}$$

$$\frac{dV_r}{dt} = \left(-F_P - V_r \frac{d\rho_r}{dt}\right)\frac{1}{\rho_r} \tag{7.6}$$

Where:

$$\boxed{F_P = \left(\sum_i J_i\right) A_m \frac{\overline{MW_P}}{10^3}} \tag{7.7}$$

F_P is the permeating mass flow rate (kg/s)

ρ_r is the average density in the reactor

V_r is the volume of the reaction mixture

J_i is the flux of component *i* through the membrane $\left(\frac{mol}{m^2\ s}\right)$

MW_P is the average molecular weight of the permeating fluid (kg/mol)

It can be assumed that the variation of the density in the reaction mixture is negligible since the density of ethanol, butanal and 1,1 diethoxy butane at 25 ºC are 0.79, 0.803 and 0.82 respectively. The density of the water is 1 but as it is being continuously removed, it does not affect considerably the density in the reaction mixture. Furthermore the water concentration is low as compared to the other components.

7.1.1.3 Transport through the membrane

The equation that describes the flux through the membrane for each component (7.8) is based on Fick's law. The development of the equation is explained in Section 6.1.

$$J_i = Q_i\ (\gamma_i x_i P_i^{sat} - y_i P_P) \tag{7.8}$$

Where:

Q_i	is the permeance	$\left(\frac{mol}{m^2\ s\ bar}\right)$
γ_i	is the activity coefficient	
P_i^{sat}	is the saturation pressure (bar)	
P_P	is the permeate pressure (bar)	
x_i	is the liquid molar fraction in the feed side	
y_i	is the vapor molar fraction in the permeate side	

The vapor molar fraction in the permeate side can be calculated from the fluxes and the feed molar fraction can be obtained from the concentrations.

$$y_j = \frac{J_j}{\sum_i J_i} \tag{7.9}$$

$$x_j = \frac{C_j}{\sum_i C_i} \tag{7.10}$$

The permeance values needed were obtained in the ethanol/butanal/1,1 diethoxy butane/water dehydration experiments (without reaction) and average permeance values were obtained at each temperature. These average permeance values were fitted to an Arrhenius' type correlation. (see Section 6.2.4.3)

The activity coefficients for each compound were calculated using Non-Radom-Two-Liquid (NRTL) model for the modeling calculations as well as in the experimental part

(see Section 6.1.2.2). All the parameters required for the saturation pressure calculation are shown in Section 5.1.3.4.

7.1.1.4 Reaction rate

The reaction between ethanol and butanal is carried out in two different steps as explained in Chapter III but the kinetics can be described using the global reaction. The reaction rate of each component can be expressed in the following way:

$$r_A = -2wk'C_A^2C_B + 2wk_4^{'}C_CC_D \tag{7.11}$$

$$r_B = -wk'C_A^2C_B + wk_4^{'}C_CC_D \tag{7.12}$$

$$r_C = wk'C_A^2C_B - wk_4^{'}C_CC_D \tag{7.13}$$

$$r_D = wk'C_A^2C_B - wk_4^{'}C_CC_D \tag{7.14}$$

Where: w is the catalyst loading (kg/m^3)

$$k^{'} \rightarrow \frac{(m^3)^3}{mol^2\ s\ \ kgcat} \qquad k_4^{'} \rightarrow \frac{(m^3)^2}{mol\ s\ \ kgcat}$$

$$C_i \rightarrow \frac{mol}{m^3}$$

$$r \rightarrow \frac{mol}{m^3\ s}$$

The catalyst loading varies since the reaction volume changes. Therefore, it can be expressed as the quotient between catalyst mass (m_{cat}) over the reaction volume (V_r).

$$r_A = -2\frac{m_{cat}}{V_r}k'C_A^2C_B + 2\frac{m_{cat}}{V_r}k_4^{'}C_CC_D \tag{7.15}$$

$$r_B = -\frac{m_{cat}}{V_r}k'C_A^2C_B + \frac{m_{cat}}{V_r}k_4^{'}C_CC_D \tag{7.16}$$

$$r_C = \frac{m_{cat}}{V_r}k'C_A^2C_B - \frac{m_{cat}}{V_r}k_4^{'}C_CC_D \tag{7.17}$$

$$r_D = \frac{m_{cat}}{V_r}k'C_A^2C_B - \frac{m_{cat}}{V_r}k_4^{'}C_CC_D \tag{7.18}$$

The kinetic constants follow the Arrhenius' correlation as it is proved in Chapter III. In Table 5.4 the activation energy and the pre-exponential factor obtained in the kinetic study are shown. These values were implemented in the model.

Table 7.2 Arrhenius' correlation's parameters for the global reaction.

	Forward reaction	**Reverse reaction**
E_a (kJ/mol)	35.5	59.8
A	1.1 $\left(\frac{(m^3)^3}{kmol^2\ s\ \ kgcat}\right)$	1.1E+5 $\left(\frac{(m^3)^2}{kmol\ s\ \ kgcat}\right)$

7.1.1.5 Input data

Any mathematical model requires some input data in order to be solved. For this model, the required input data are the next ones:

- Temperature of the process.
- Permeate pressure.
- Membrane dimensions (length & outer diameter).
- Catalyst amount in grams.
- Initial conditions (initial composition in grams) and integration limits (time in seconds).
- Molecular weight (g/mol) and density (g/mL) of the components (in liquid phase).
- Kinetic and permeance data.
- Different parameters to calculate thermodynamic parameters like saturation pressure and activity coefficients.

7.1.1.6 Summary of equations

Table 7.3 shows a summary of all the equations that describe the semi-batch model.

Table 7.3 Summary of the model equations

- Mass balance

$$\frac{d(C_A)}{dt} = r_A - \frac{J_A\ A_m}{V_r} - \frac{C_A}{V_r}\frac{dV}{dt} \qquad r_A = -2\frac{m_{cat}}{V_r}k'C_A^2C_B + 2\frac{m_{cat}}{V_r}k_4^{'}C_CC_D$$

$$\frac{d(C_B)}{dt} = r_B - \frac{J_B\ A_m}{V_r} - \frac{C_B}{V_r}\frac{dV}{dt} \qquad r_B = -\frac{m_{cat}}{V_r}k'C_A^2C_B + \frac{m_{cat}}{V_r}k_4^{'}C_CC_D$$

$$\frac{d(C_C)}{dt} = r_C - \frac{J_C\ A_m}{V_r} - \frac{C_C}{V_r}\frac{dV}{dt} \qquad r_C = \frac{m_{cat}}{V_r}k'C_A^2C_B - \frac{m_{cat}}{V_r}k_4^{'}C_CC_D$$

$$\frac{d(C_D)}{dt} = r_D - \frac{J_D\ A_m}{V_r} - \frac{C_D}{V_r}\frac{dV}{dt} \qquad r_D = \frac{m_{cat}}{V_r}k'C_A^2C_B - \frac{m_{cat}}{V_r}k_4^{'}C_CC_D$$

$$\frac{dV_r}{dt} = \left(-F_P - V_r\frac{d\rho_r}{dt}\right)\frac{1}{\rho_r} \qquad F_P = \left(\sum_i J_i\right)A_m\frac{\overline{MW_P}}{10^3}$$

- Flux through the membrane

$$J_A = Q_A\ (\gamma_A x_A P_A^{sat} - y_A P_P) \qquad x_A = \frac{C_A}{\sum_i C_i} \qquad y_A = \frac{J_A}{\sum_i J_i}$$

$$J_B = Q_B\ (\gamma_B x_B P_B^{sat} - y_B P_P) \qquad x_B = \frac{C_B}{\sum_i C_i} \qquad y_B = \frac{J_B}{\sum_i J_i}$$

$$J_C = Q_C\ (\gamma_C x_C P_C^{sat} - y_C P_P) \qquad x_C = \frac{C_C}{\sum_i C_i} \qquad y_C = \frac{J_C}{\sum_i J_i}$$

$$J_D = Q_D\ (\gamma_D x_D P_D^{sat} - y_D P_P) \qquad x_D = \frac{C_D}{\sum_i C_i} \qquad y_D = \frac{J_D}{\sum_i J_i}$$

7.1.1.7 Model implementation

MATLAB software package was chosen to implement the developed equations and run the model. This mathematical package contains plenty of mathematical algorithms already programmed which make the modeling work much easier. Some other more complex programming tools exist for chemical process modeling (e.g. ASPEN CUSTOM MODELER) but in this case MATLAB was used since it is easy to use and it offers the necessary characteristics to fulfill the aim of this model.

The model consists of different functions (to solve differential equations and non linear algebraic equations) and ".M" files (to calculate different properties like the activity coefficients and saturation pressures). "EXE.M" is the main .M file where all the input data must be introduced and executing it, it calls to the different functions and files of the model in order to solve it.

If the membrane area is zero (setting the membrane length equal to zero) the model works as a conventional batch reactor. On the other hand, setting the catalyst amount equal to zero (grams) the model works as a semi-batch pervaporation system.

7.1.2 Model validation

The semi-batch model is a semi-empirical model where experimentally obtained kinetic and permeance data are used as input. As explained in Section 7.1.1, kinetic data were obtained from the kinetic study performed in Bilbao using a batch stirred tank reactor (BSTR); permeance data were obtained from ethanol/butanal/1,1 diethoxy butane/water pervaporation dehydration experiments (without any reaction). These empirical data were implemented in the model and the reaction + pervaporation processes, carried out in the same unit, where simulated.

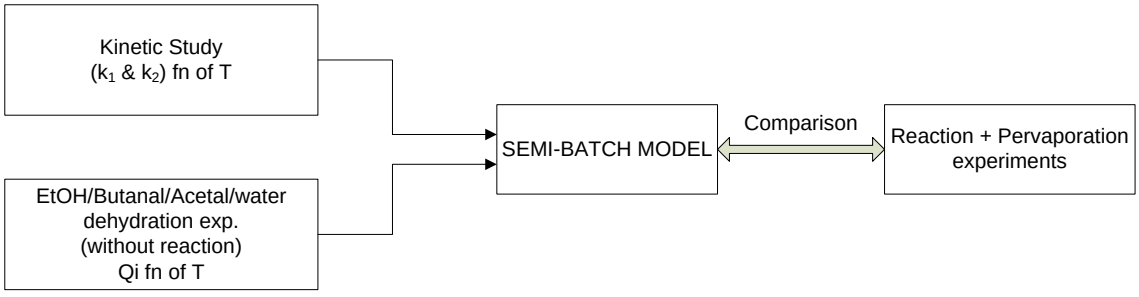

Figure 7.2 Flow chart of the validation process

The following examples show the feed concentration profile during time. They were performed at different conditions and all of them show a really good agreement between experimental and simulated data. Not all data available are presented though.

In all simulations the initial reaction mixture volume was 1.6 L, which is similar to the initial volume used in the pervaporation + reaction experiments.

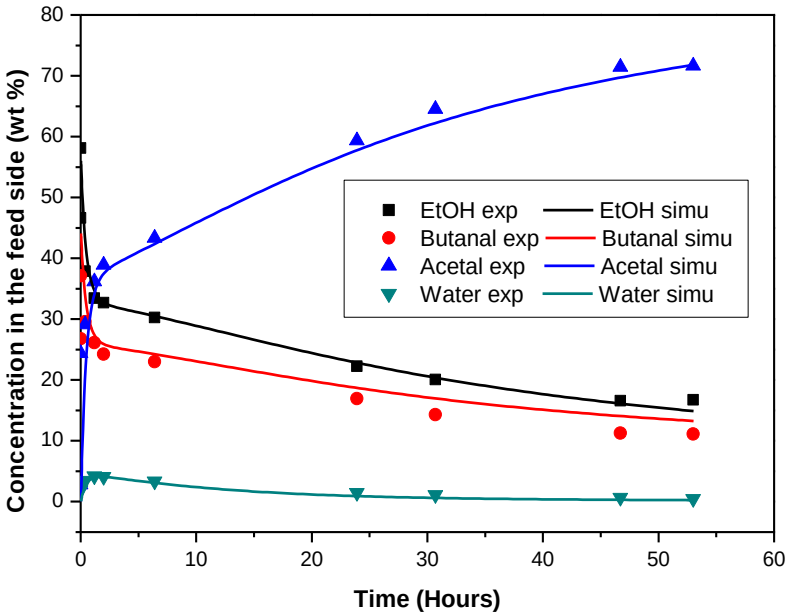

Figure 7.3 Comparison between experimental and simulated data. Conditions: EtOH/Butanal 2:1 ratio, 0.1 wt% catalyst loading, 70 ºC, membrane area: 24.2 cm^2.

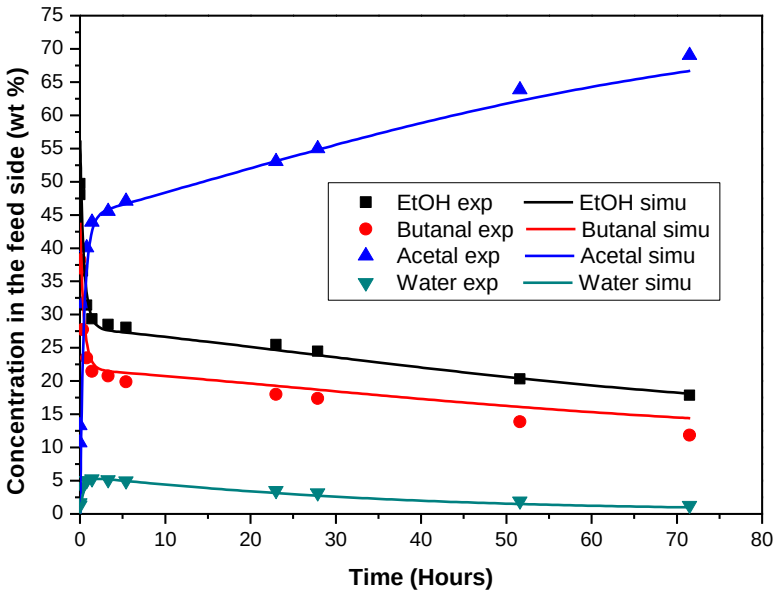

Figure 7.4 Comparison between experimental and simulated data. Conditions: EtOH/Butanal 2:1 ratio, 0.5 wt% catalyst loading, 40 ºC, membrane area: 24.2 cm^2.

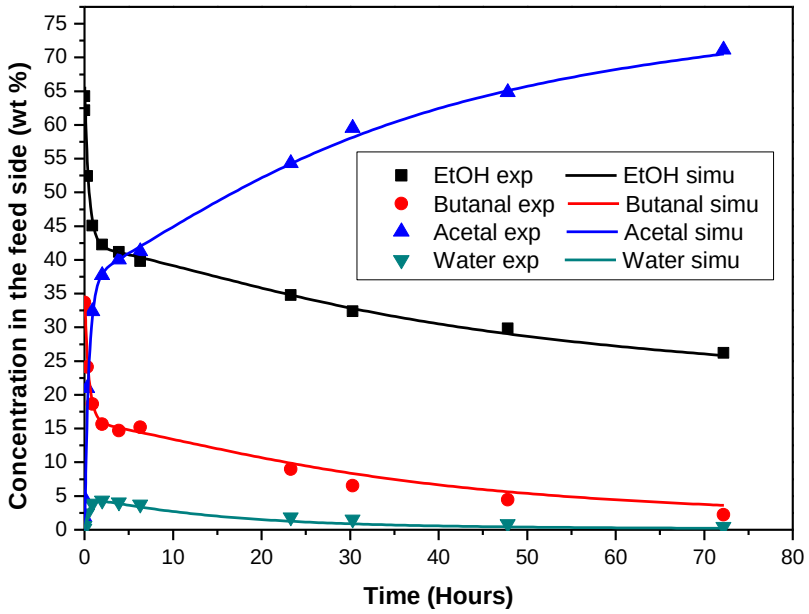

Figure 7.5 Comparison between experimental and simulated data. Conditions: EtOH/Butanal 3:1 ratio, 0.1 wt% catalyst loading, 70 ºC.

As it can be seen in Figure 7.3, Figure 7.4 and Figure 7.5 experimental data and simulated data are in a good agreement. It seems that the amount of butanal in the reaction mixture is a bit overestimated in the model calculation results, especially at long reaction times.

The density of the reaction mixture was considered constant. After performing different simulations the real reaction mixture density was recalculated and it was checked that its variation was not significant. The standard deviation and the percentage of the standard deviation with respect to the average value of the density were calculated and in all the cases it was below 1.0%.

Figure 7.6 shows the estimated variation of the reaction mixture density.

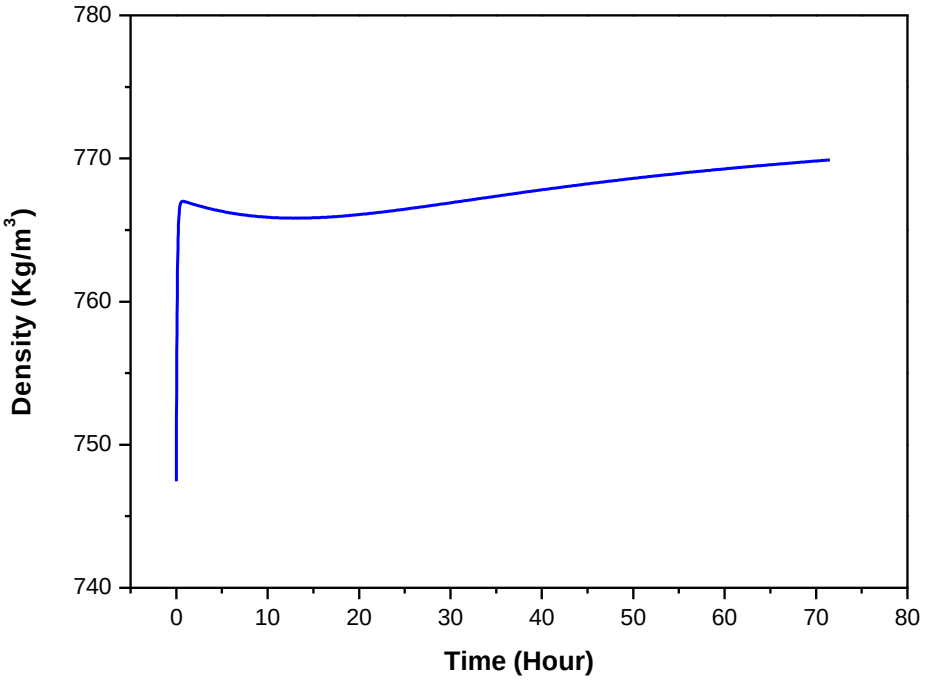

Figure 7.6 Variation of the density in the reaction mixture.

Furthermore, a constant permeance value was assumed for each temperature meaning that the permeance is not a function of the concentration. It is checked that in the water concentration range of the experiments, the average permeance values predict quite accurately the reaction + pervaporation process. However, looking in more detail to water concentration on the feed side, in Figure 7.7 it can be observed that when water concentration in the feed side is low the model predicts more permeation than what actually happens and at higher water concentrations, by contrast, the model predicts less permeation.

One of the reasons of this behavior could be the use of an average permeance value. However, in Figure 6.26 it was indicated that at 70 ºC the permeance decreases with a decrease in water concentration and for 40 ºC the permeance increases with a decrease in water concentration. As a consequence, Figure 7.7 should show opposite trends for 70 ºC and 40 ºC but is does not so, it seems that some other effects or assumptions are playing a role. Nevertheless, the average permeance values for each temperature are good enough in order to describe the overall process as it is checked in Figure 7.3, Figure 7.4 and Figure 7.5.

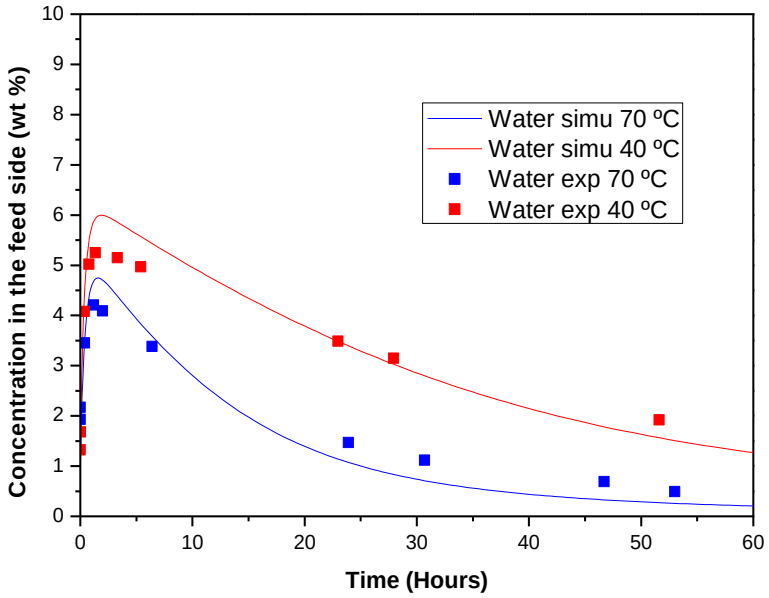

Figure 7.7 Comparison between experimental and simulated data for water concentration on the feed side. Conditions: EtOH/Butanal 2:1 ratio, 0.5 wt% catalyst loading, 70 ºC / 40 ºC, membrane area: 24.2 cm^2.

7.1.3 Sensitivity analysis

Since there is a good agreement between the simulated results and the experimental data a sensitivity analysis was performed using the model. In this section several process variables were tested in order to study the effect of each parameter and establish an appropriate process conditions. Effect of the temperature, catalyst loading, feed composition and the membrane area are the parameters that were varied.

In all simulations the experimental reaction mixture volume was 1.6 L, which is similar to the volume used in the pervaporation + reaction experiments.

7.1.3.1 Effect of the membrane area

All the experiments were performed with the same membrane area (24.2 cm^2) which was quite small compared to the reaction mixture volume (1.6 L). In the following simulations the membrane area was varied; taking into account the reactor dimensions. There is no problem to place longer membranes and even more membranes in the reaction vessel.

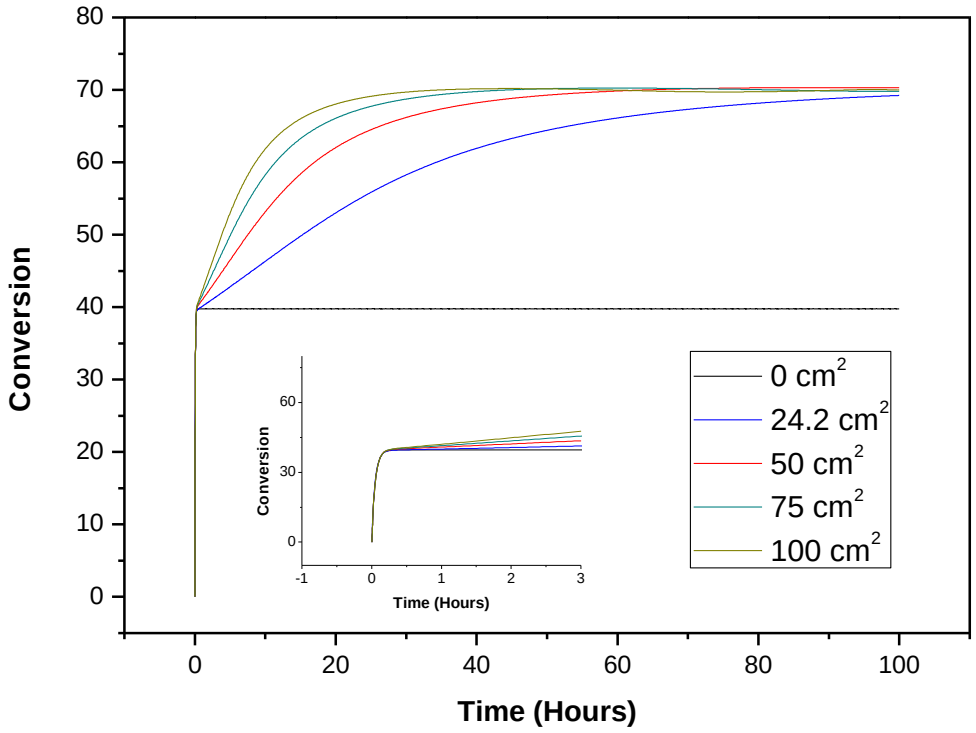

Figure 7.8 Effect of the membrane area on the conversion. Conditions: EtOH/butanal ratio in mol: 2:1, 1.0 wt% catalyst loading, temperature 70 ºC.

Figure 7.8 shows that the amount of the time that the process needs to achieve the maximum conversion (70 %) is proportional to the membrane area. With 24.2 cm^2 of membrane area more than 100 hours are necessary to achieve 70 % of conversion while with 100 cm^2 25 hours are enough. It is worth pointing out that there is 30 % of conversion difference between a normal reaction (0 cm^2 of membrane area, or the equilibrium conversion) and reaction + pervaporation process. Also important is to notice that the time to reach equilibrium is very fast as compared to the influence of the water removal rate. An optimum should be found between costs of the process (more membrane area costs extra) and the time needed to reach a certain maximum conversion of 70% for a batch operated process. On industrial scale probably a continuous process would be used.

Notice that, as expected, the membrane area plays in pervaporation the same role as a catalyst in a reaction, i.e., it does not modify the final conversion, what it modifies is the velocity to reach the final conversion (if membrane area > 0); i.e. using 25 cm^2 or using 100 cm^2 membrane area the final conversion is the same (70 %), the only thing that it changes is the time that it requires to reach the final conversion.

In all the cases ethanol and butanal are available in the reaction mixture and the water concentration in the feed is negligible. One of the reasons why the achieved conversions are not around 100% can be related to the kinetics. After 40-50 hours the acetal concentration in the feed side is really high while water concentration is really low; taking into account the reverse reaction the acetal excess with respect to the water is really large so the reverse reaction rate may be faster than the pervaporation dehydration rate. Thus, the water removed through the membrane is almost negligible and therefore 70% is the highest achievable conversion.

From this point on, all the simulations will be performed with 100 cm^2 of membrane area, using a feed volume of 1.6 liters.

7.1.3.2 Effect of the temperature

As well as in the experimental part different temperatures were simulated. The objective of this study is to see how the temperature change affects the reaction and the pervaporation process. The acetalization reaction between ethanol and butanal is an exothermic reaction so at low temperatures higher equilibrium conversions can be achieved. However, from the pervaporation point of view it was found (and expected) in the experimental part that higher temperatures enhance the water permeation through the membrane.

The advantage of working with a simulation model is that more than 3 different temperatures can be calculated easily and on the other hand longer process durations can be studied in order to find the maximum possible process conversion.

Several simulations were made at 70, 60, 50, 40, 30 and 20 ºC. In all the cases 5.0 wt% of catalyst loading was used in order to have the pervaporation as the limiting step of the process. The initial ethanol/butanal feed ratio was the stoichiometric one (2:1) and the used membrane area was 100 cm^2.

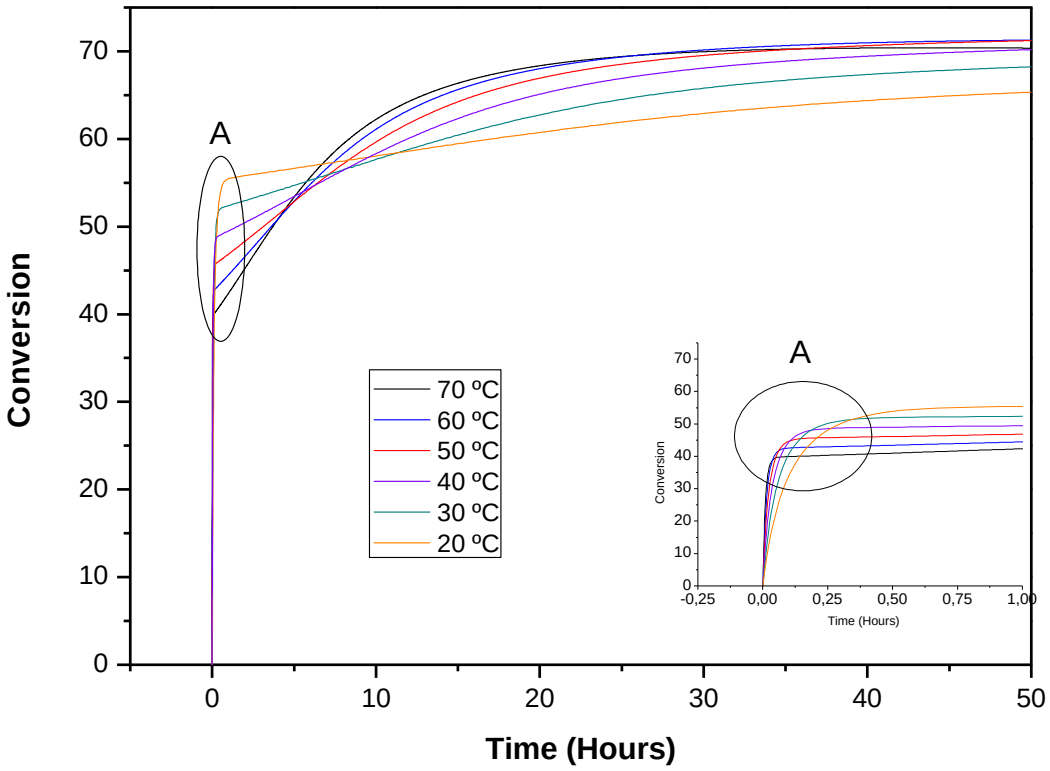

Figure 7.9 Effect of the temperature in the process. Conditions: EtOH/butanal ratio in mol: 2:1, 5.0 wt% catalyst loading and membrane area: 100 cm^2.

In Figure 7.9 "*A*" point represents the equilibrium conversion at each temperature that can be achieved in few hours. In the experimental part (Section 6.2.4.4.1) identical results were obtained using temperatures of 70, 55 and 40^oC. It can be observed that the lower the temperature, the higher equilibrium conversion is. Looking at the detailed insert in the figure it can be observed that after some minutes the conversion is the highest for the highest temperature. This is because the kinetics is faster. Then after about 1 hour the conversion at the lower temperature is higher than at higher temperature because thermodynamics stronger limit the reaction at higher temperature. Then after some 5-10 hours the conversion at the highest temperature passes the conversion at lower temperatures again and this is because the water removal rate at higher temperatures is faster than at lower temperatures. This is also nicely supported by the results presented in Figure 7.10.

Figure 7.10 shows the water concentration profile as function of time for different temperatures. It is clear that at low temperatures the water removal is not very efficient. That is the reason why the conversion does increase less fast that at higher temperatures.

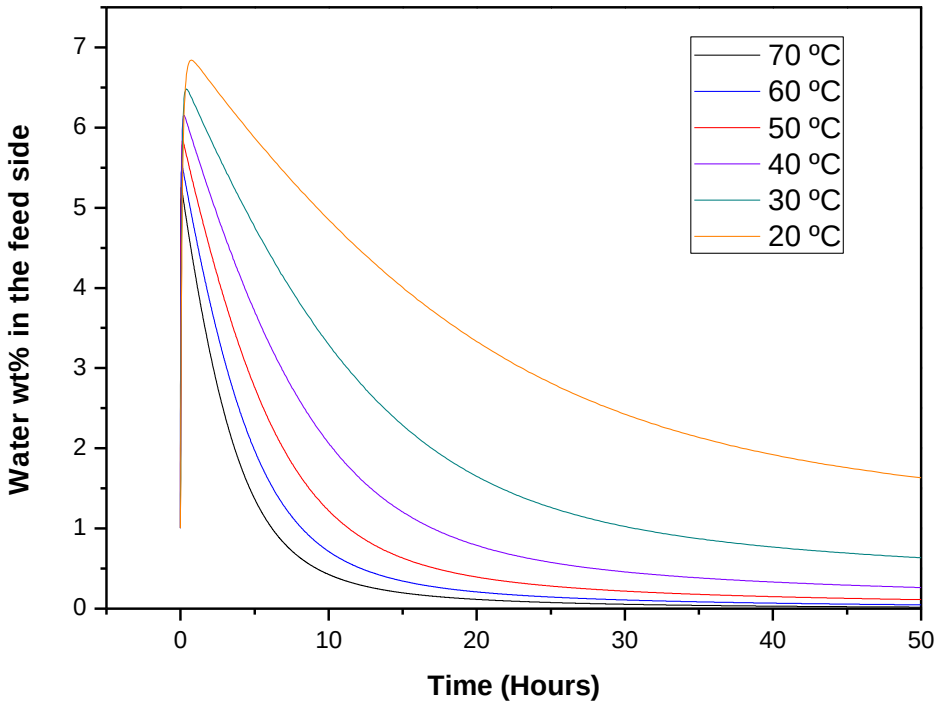

Figure 7.10 Effect of the temperature in the water concentration in the feed side. EtOH/butanal ratio in mol: 2:1, 1.0 wt% catalyst loading and membrane area: 24.2 cm^2.

Figure 7.11 shows the difference between equilibrium conversions and the predicted conversions after 50 hours. It is clear that at low temperatures the pervaporation process is less significant than at higher temperatures. The difference between the equilibrium conversion and the conversion reached using the combined reaction and separation process increases strongly with temperature. From the conversion point of view, temperatures higher than 50^oC are not needed. Economic calculations (taking into account e.g. membrane area, and process time) could lead to different conclusions though.

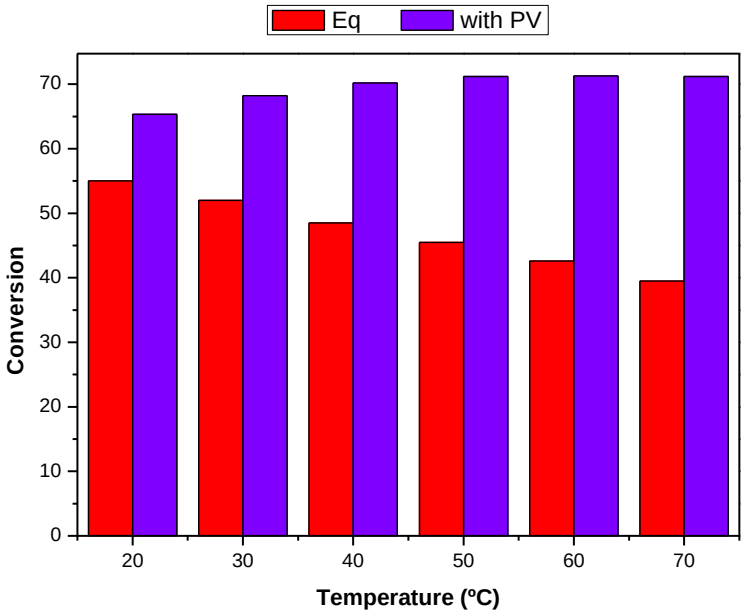

Figure 7.11 Comparison between the equilibrium conversion and the predicted ones after 50 hours. Conditions: Ethanol/butanal feed ratio: 2:1 in moles, 5.0 wt% catalyst loading and membrane area: 100 cm^2.

7.1.3.3 Effect of the catalyst loading

In the experimental part and in the previous sections, it was acknowledged that pervaporation was the limiting step, i.e., the achieved conversions are limited by the permeation rate and not by the reaction rate. In this section different simulations performed with different catalyst loadings will be presented. The aim of this study is to find the minimum catalyst loading in order to ensure that pervaporation is always the limiting step. This effect was checked at different temperatures since the reaction rate is a function of the temperature.

All these simulations were performed with 100 cm^2 as membrane area and 1.6 liters of initial reaction mixture.

Figure 7.12 shows that even when using 0.1 wt% of catalyst, the reaction is the limiting step and not the pervaporation. At 0.1 wt% of catalyst the time to reach the equilibrium conversion is much longer than at the higher catalyst loadings. Thus it is suggested not to reduce the catalyst loading below 0.1 wt% under the conditions used. In case of using 0.5wt%, 1.0 wt% and 5 wt% the conversion values are identical which means that in all the cases pervaporation is the limiting step and there is an overload of catalyst.

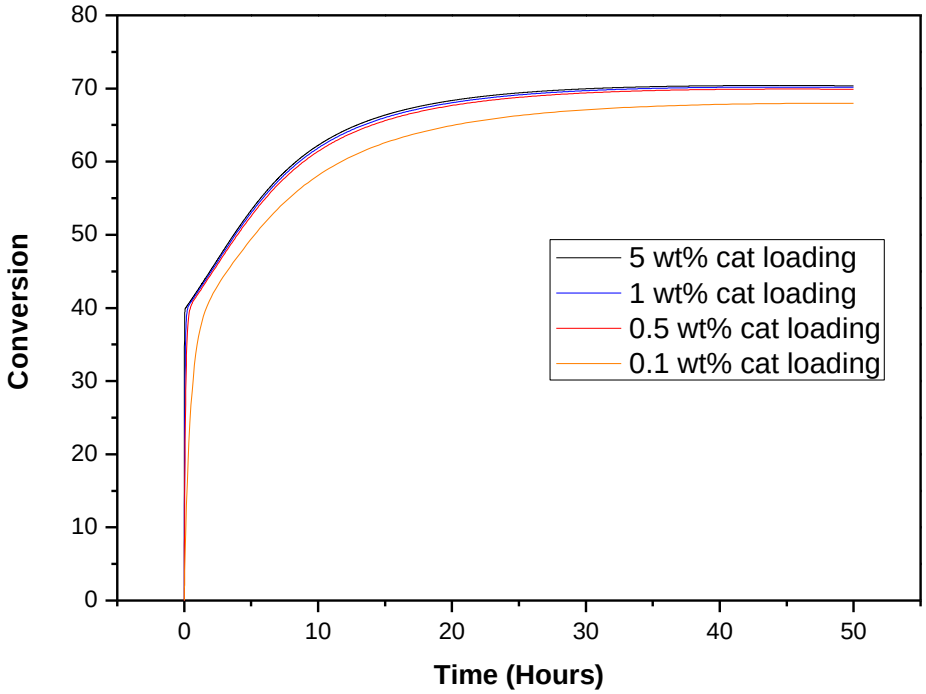

Figure 7.12 Effect of the catalyst loading at 70 ºC. Conditions: EtOH/Butanal mol ratio: 2:1, 100 cm^2 of membrane area.

In the experimental part (Section 6.2.4.4.2) identical results were obtained with 0.1 wt%, 0.5 wt% and 1.0 wt% of catalyst. It must be remembered that in that case the membrane area was 24.2 cm^2 and not 100 cm^2, thus the pervaporation was a slower process in the experiments.

Figure 7.13 shows the same performance as Figure 7.12 but in this case performed at 20 ºC. Kinetic constants strongly depend on the temperature and they decrease with a temperature decrease. That is the reason why in this case the difference between 0.1 wt% and 0.5 wt% is more important. It is demonstrated that for a feed volume/membrane area ratio of 1.6L/100 cm^2 working with 0.5 wt% of catalyst is enough between 20 and 70 ºC.

In order to reduce the amount of catalyst and the amount of membrane area (as the flux increases with temperature) a higher operation temperature is preferred.

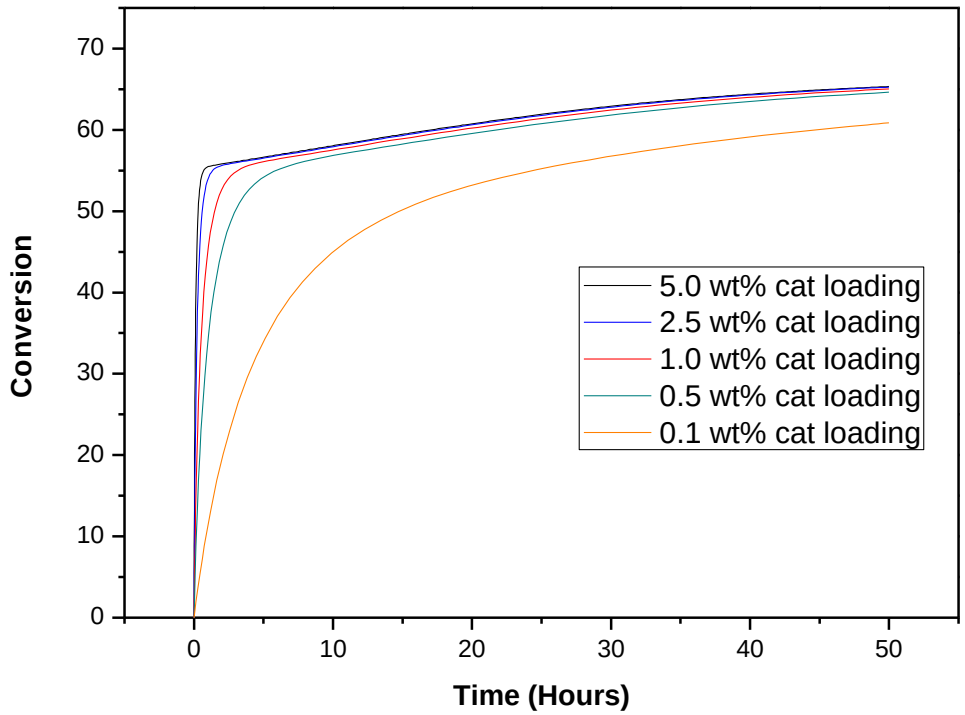

Figure 7.13 Effect of the catalyst loading at 20 ºC. Conditions: EtOH/Butanal mol ratio: 2:1, 100 cm^2 of membrane area.

In conventional reaction systems it is known that the catalyst amount does not change the final conversion, what it changes is the velocity in which the final conversion is achieved. In the present case the catalyst amount affects to the final conversion. In case of membrane reactors this fact is possible. With low catalyst loadings low amount of water per second is formed so less water permeates and more ethanol passes through the membrane. Thus, more ethanol is lost and lower conversions can be achieved. In Table 7.4 the total water and ethanol amounts that pass through the membrane at 20 and 70 ºC are shown.

Table 7.4 Total water and ethanol amounts (grams) that pass through the membrane at 20 and 70 ºC under different catalyst loadings

Cat. loading	**70 ºC**		**20 ºC**	
	g. EtOH	**g. Water**	**g. EtOH**	**g. Water**
0.1 %	82.5	134.7	21.0	120.0
0.5 %	78.0	141.6	19.9	131.5
1.0 %	77.4	142.7	19.7	133.4
5.0 %	76.9	143.7	19.6	135.3

In both cases, at 20 and 70 ºC, can be observed that with 0.1% of catalyst loading the amount of water that permeates is less than what permeates at higher catalyst loadings.

7.1.3.4 Effect of the feed composition

It is known that an excess of one of the reactants shifts the reaction to the forward direction achieving higher conversions. In the present case, from the industrial point of view, the use of ethanol in excess is more logical than using butanal in excess since ethanol is cheaper than butanal.

However, from the pervaporation point of view, ethanol is the smallest organic molecule in the reaction mixture and thus, it is the compound which has a higher tendency to pass through the membrane. For this reason it must be studied if the increase of ethanol driving force entails an important loss of this compound through the membrane.

Different ethanol/butanal feed ratios were used in the simulations in order to see the final conversion and on the other hand, see if an important amount of ethanol would be lost. According to the obtained results in the previous sections, all the simulations were performed at 70 ºC, 0.5 wt% of catalyst loading and 100 cm^2 of membrane area. As in every case, the reaction volume was 1.6 liters.

Figure 7.14 shows that with 2.5:1 and 3:1 ethanol/butanal feed ratios (in mol) significant conversion increases can be achieved. However, between 3:1 and 3.5:1 the difference is not that strong anymore. In Figure 7.15 the influence of the ethanol:butanal feed ratio is presented for both the equilibrium conversion and the conversion of the combined process. Both conversions increase with feed ratio and a maximum conversion of about 85% can be reached for a feed ratio of 3.5:1. At these higher feed ratios the loss of ethanol through the membrane will be high, as presented in the experimental Section 6.2.4.4.3 and in Figure 7.16.

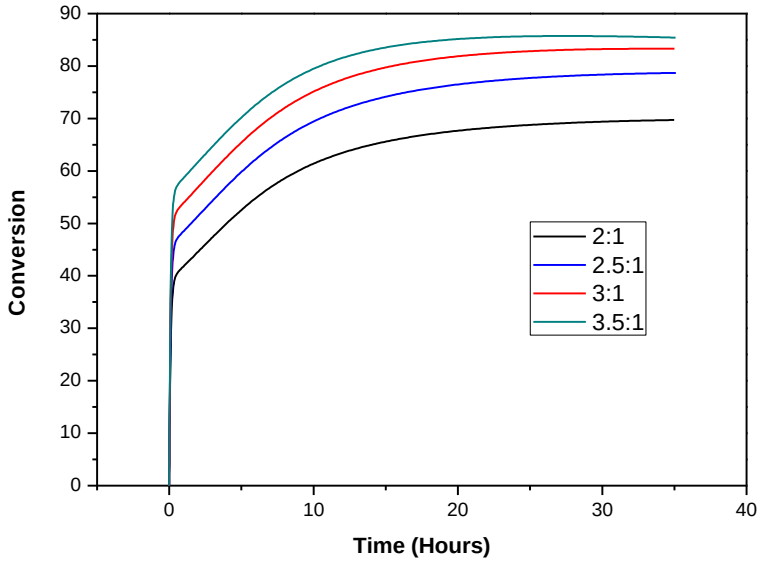

Figure 7.14 Achieved conversion with different feed ratios. Conditions: temperature: 70 ºC, 0.5 wt% catalyst loading and membrane area: 100 cm^2.

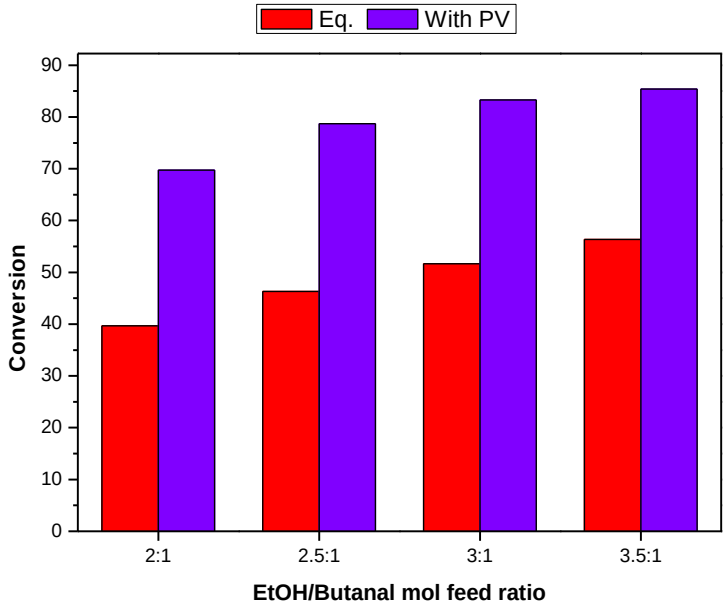

Figure 7.15 Comparison between equilibrium conversions and conversion achieved applying pervaporation. Conditions: temperature: 70 ºC, 0.5 wt% catalyst loading and membrane area: 100 cm^2.

In Figure 7.16 it can be observed that in the very beginning water and ethanol concentrations in the permeate show a strange shape: the water fraction in the permeate first strongly increases and then gradually decreases. For ethanol this is vice versa. This effect has a simple explanation, in the very beginning the water concentration in the feed side is very low and for that reason more ethanol permeates. After some minutes, water is formed due to the reaction and its concentration in the permeate side increases

considerably. Furthermore, it can be observed that the ethanol concentration in the permeate side is higher when its initial concentration in the feed composition was increased. However, it must be taken into account that when ethanol concentration in the permeate ends being high, the total flux remains quite low. Therefore the ethanol loose is not so high.

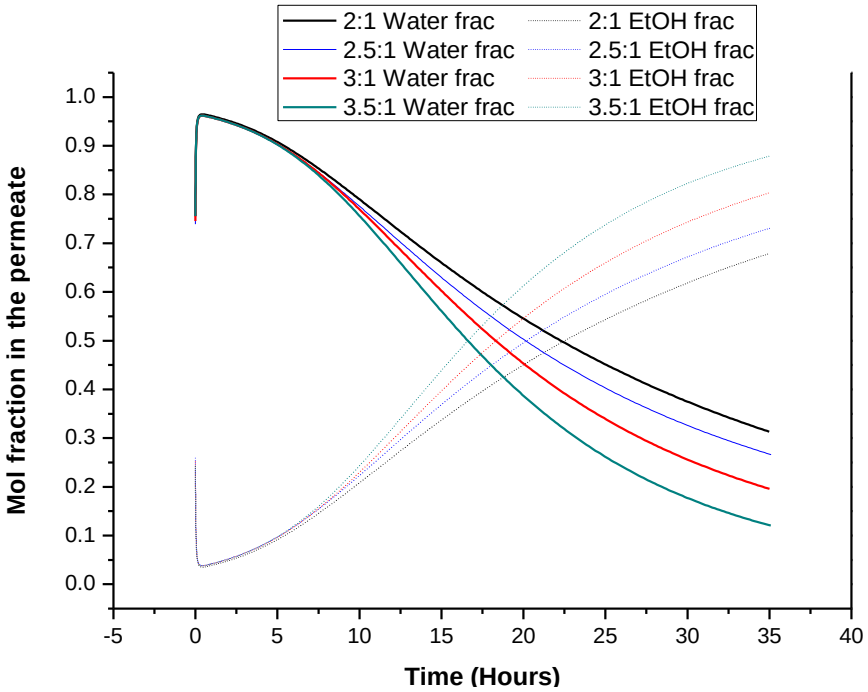

Figure 7.16 Water and ethanol molar fraction profiles along the time at different ethanol/butanal feed ratios. Conditions: temperature: 70 ºC, 0.5 wt% catalyst loading and membrane area: 100 cm^2.

Figure 7.17 shows total flux values. Surprisingly this total flux does not vary significantly with different feed ratios. In terms of total amount of ethanol and water that permeates through the membrane in 35 hours, Figure 7.18 shows how the water amount permeating decreases while the ethanol amount slightly increases. The total flux and the amount permeating being the same can be explained by the fact that ethanol is partly hindering the transport of water. At a higher feed ratio more water is formed and could permeate the membrane. Furthermore the feed contains more ethanol that can permeate as well. Ethanol, however, has a smaller permeance than water and thus ethanol is hindering the water transport, especially at higher ethanol:butanal feed ratios. In Figure 7.15 it can be seen that the difference in equilibrium conversion and the conversion in the combined reaction and separation process for different feed ratios is more or less the same. This means that the extra water formed at the higher feed ratios is not removed.

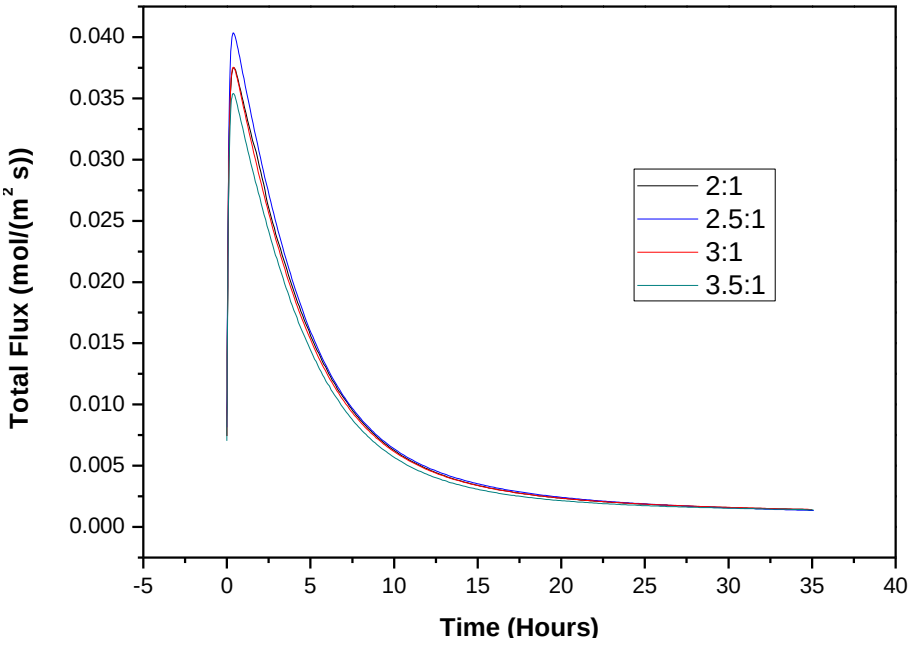

Figure 7.17 Total flux profiles along the time with different ethanol/butanal feed ratios. Conditions: temperature: 70 ºC, 0.5 wt% catalyst loading and membrane area: 100 cm^2.

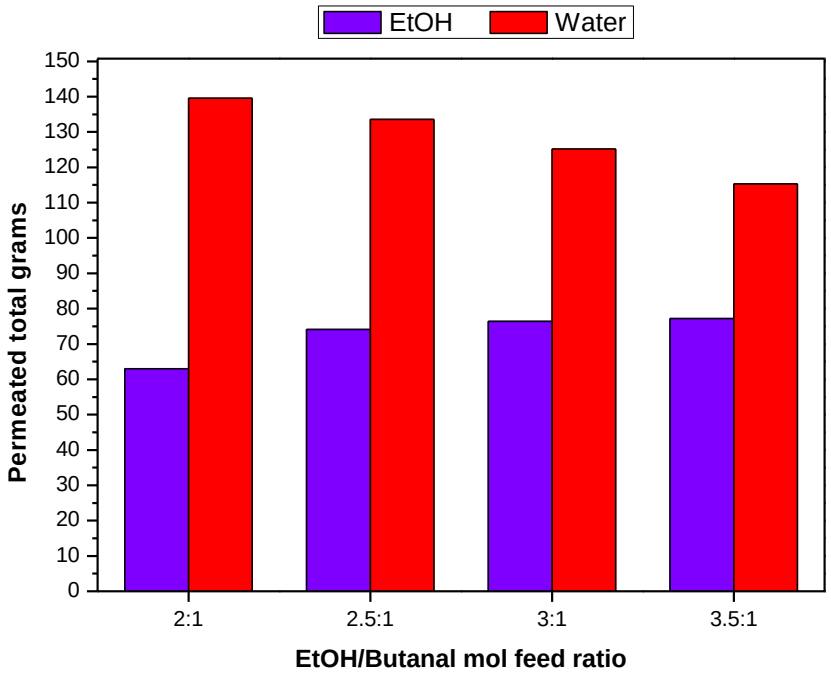

Figure 7.18 Permeated total grams of ethanol and water at different ethanol/butanal feed ratios after 35 hrs of process time. Conditions: temperature: 70 ºC, 0.5 wt% catalyst loading and membrane area: 100 cm^2.

As a general conclusion regarding the ethanol/butanal feed ratio, it can be said that an ethanol/butanal ratio between 2.5:1 and 3:1 would be a good option since high process conversion can be achieved without losing too much ethanol.

7.1.4 Conclusions

Experimental data and predicted data from batch model simulation were compared resulting in a very good agreement, proving that the used assumptions (constant mixture density, temperature and concentration polarization effects negligible...) were adequate.

The modeled batch process was used to do some sensitivity analysis giving the following main conclusions:

- The membrane area/reaction volume ratio is a key parameter since the time required to reach a certain conversion value depends on its relation. In terms of the temperature it was checked that at low temperatures the pervaporation process is not really significant and if high conversions are required it must be operated at higher temperatures.
- The amount of catalyst is an important parameter from the reaction point of view in order to compare the observed reaction rate and the pervaporation rate. It was concluded that between 20 and 70ºC working with, at least, 0.5 wt% of catalyst the pervaporation process is the limiting step. Higher temperatures would require less catalyst.
- Ethanol/butanal ratios between 2.5:1 and 3:1 seem to be the best options since high process conversion can be achieved without losing too much ethanol.

7.2 Application to a continuous process. Preliminary design

7.2.1 Introduction

An initial continuous process design of the acetalization reaction including dehydration by pervaporation will be developed in this section. The main objective of this section is to develop a continuous process checking that high conversions can be achieved by removing water from the reaction mixture using dehydration membranes. For this purpose ASPEN CUSTOM MODELLER (ACM) was the chosen software package. ACM is an equation orientated software tool and it is suitable to model different unit operations and modules and link them to each other. Moreover, all the physical, chemical and thermodynamic properties can be calculated via a direct communication with the ASPEN PLUS flow sheeting program.

In most of the publications on the combination of reaction and (by-)product removal using pervaporation membranes, lab scale batch studies and their later modelization (32;33;69-73) are presented. However some authors studied different continuous processes. Zhu et al (27) performed continuous pervaporation experiments in a tubular pervaporation membrane reactor as well as a modeling job for the study of esterification reactions using H_2SO_4 as homogenous catalyst. De la Iglesia et al. (74) also worked with esterification reactions performing their experiments in a continuous tubular reactor. In this case Amberlyst 15 was used as catalyst and it was placed inside the membrane. Lim et all (29) studied different process configurations (see Figure 7.19) and they concluded that tubular membrane reactors lead to a better performance than stirred tank membrane reactors. In terms of recycled systems, process conditions have an important effect since not always recycled systems enhance the final conversion.

Nemec et al (75) were the only ones who analyzed multifunctional tubular reactors (reaction and separation in the same unit) placing catalyst particles in the annular region between the membrane and the module shell and their results were not really satisfactory.

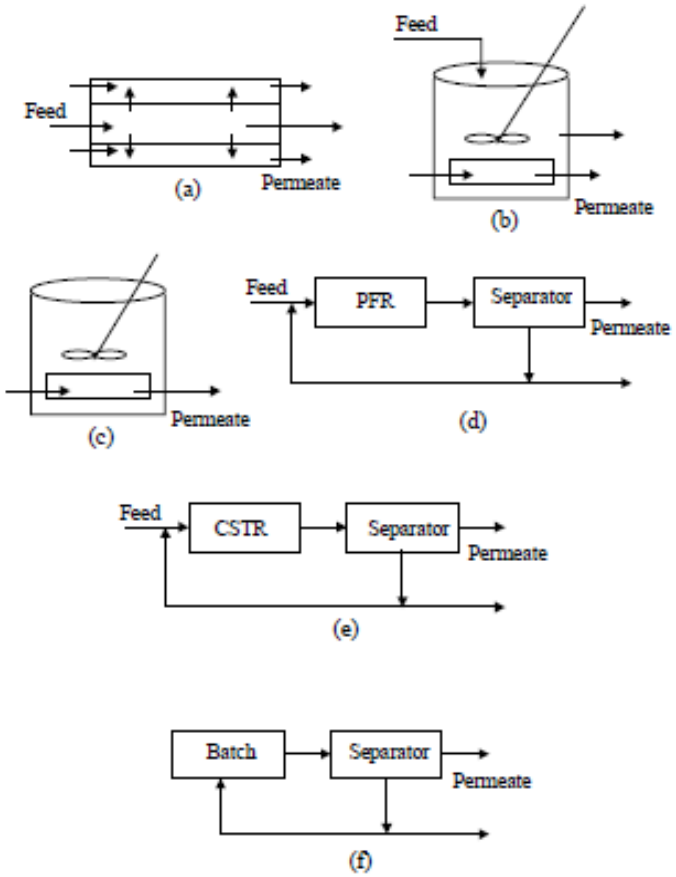

Figure 7.19 Schematic diagram of various membrane reactor configurations: (a) plug-flow pervaporation membrane reactor (PFPMR); (b) continuous stirred pervaporation membrane reactor (CSPMR); (c) batch pervaporation membrane reactor (BPMR); (d) recycle plug-flow pervaporation membrane reactor (RPFPMR); (e) recycle continuous stirred pervaporation membrane reactor (RCSPMR); and (f) recycle batch pervaporation membrane reactor (RBPMR).

Taking into account all these precedents, in the present study two different alternatives were mainly studied:

1. Multifunctional membrane reactor. Reaction and separation take place in the same unit. The development of this model and the results of the calculations using this model are presented in Section 7.2.2.
2. Plug flow reactor + pervaporation module. The development of this model and the results of the calculations using this model are presented in Section 7.2.3.

Moreover, some variations including recycle loops of the mentioned models were also developed. These alternatives have been chosen as the most suitable options according to Lim et al. (29)

In order to perform simulations with the different models a fresh feed flow rate must be specified. In all the cases 7 L/h was the chosen feed rate since all the reactive distillation simulations were performed with this feed flow rate. By using the same feed amount, the comparison between both processes is much easier.

7.2.2 Multifunctional membrane reactor development and calculations

As a first option a multitubular plug flow membrane reactor (MPFMR) model was developed. In principle, one unit where reaction and separation happens is the best option, shifting the reaction in the forward direction and getting a concentrated outlet stream in the desired product. However, the presence of the two processes implies some constraints to each other. Some of the difficulties appear finding proper process conditions as explained in the experimental part as well as in the batch model part (see Sections 6.2 and 7.1). Some other constraints appear in the design of the MPFMR; the presence of catalyst particles along the membrane tubes must be taken into account in order to specify the distance between them. All these problems and some others will be discussed in this section. A scheme of the model consisting of a packed bed and a membrane is shown in Figure 7.20. The following assumptions were made in developing the model equations:

- The reactor behaves as an ideal plug flow reactor (PFR).
- All transport resistance was concentrated in the selective top layer of the membrane.
- Concentration-polarization and temperature polarization effects were considered negligible.
- The selective top layer of the membrane was on the outside (shell side) of the membrane tube.
- The tube side (permeate side) was considered a perfect stirred mixture.
- A pseudo-homogeneous kinetic model was assumed.
- The membrane is completely inert and it did not influence the reaction kinetics.
- Permeance values depend only on the temperature. The influence of the concentration of each compound on permeance values was considered negligible.

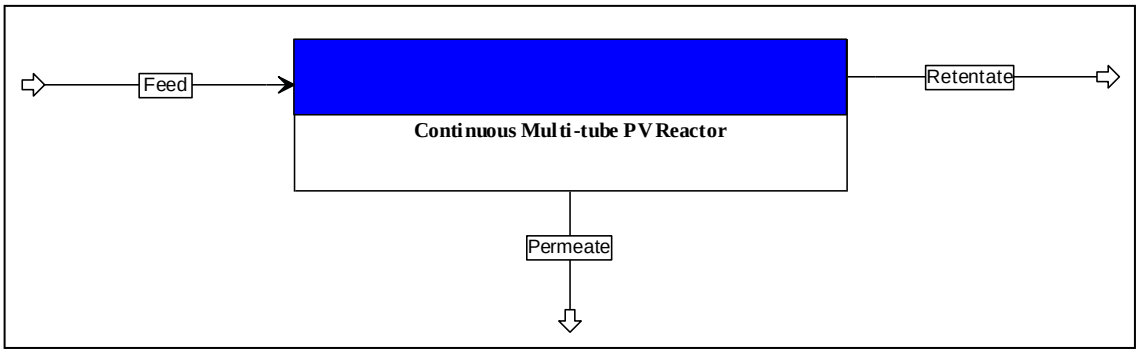

Figure 7.20 Scheme of the MPFMR model

Both, isothermal and adiabatic operated membrane reactors were considered.

7.2.2.1 Degrees Of Freedom (DOF) analysis

As the first step of the modeling, a study of degrees of freedom (DOF) was performed. This study is essential in order to know if the mathematical model can be solved or not.

The model is based on differential equations and therefore the length of the module was discretized. The DOF study was performed for a differential unit.

Table 7.5 Variables and equations for the MPFMR model in a differential.

Variables		**Equations**	
Molar flow in the shell side	4	Material balance	4
Flux through the membrane	4	Transport through the membrane	4
Permeate composition	4	Flux quotients	4
Temperature	1	Energy balance	1
Pressure	1	Momentum balance	1
TOTAL	14	TOTAL	14

7.2.2.2 Equations

Some variables are not expressed in the same units in this section and in the semi-batch model section. The reason of the change is because of ASPEN CUSTOM MODELER specifications; ACM default units were used.

7.2.2.2.1 Mass balance along the shell side

The generic mol balances on the chemical spices is slightly different from a conventional PFR reactor as it is showed below.

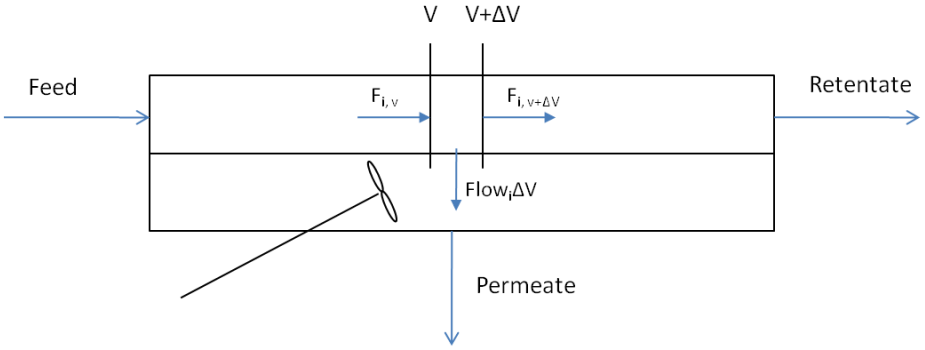

Figure 7.21 Basic scheme of the MPFMR module

[In by flow] – [Out by flow] – [Out through the membrane] + [Generation/consumption] = [Accumulation]

$$F_{i,V} - F_{i,V+\Delta V} - Flow_i\Delta V + r_i\Delta V = 0$$

Where: F_i molar flow rate for component i (kmol/h)

$Flow_i$ molar flow rate for component i that passes through the membrane (kmol/(h·m^3))

r_i reaction rate for component i (kmol/(h·m^3)

Dividing by ΔV and taking the limit as ΔV→ 0 gives

$$\frac{dF_i}{dV} = r_i - Flow_i \tag{7.19}$$

The molar flow which is going through the membrane in every differential, in order to have it as mol/(s·m^2) can be written as:

$$Flow_i = \frac{dJ_i}{dV} = \frac{f_i\ dA_m}{dV} \tag{7.20}$$

Where: A_m is the membrane area (m^2).

$$f_i = Q_i\ (\gamma_i x_i P_i^{sat} - y_i P_P) \tag{7.21}$$

Where:

Q_i is the permeance in $\frac{kmol}{h\ m^2\ bar}$

f_i is the flux in $\frac{kmol}{h\ m^2}$

J_i is the molar flow rate of component i across the membrane in $\frac{kmol}{h}$

$Flow_i$ is the molar flow rate of component i across the membrane in a differential in $\frac{kmol}{h\ m^3}$

γ_i is the activity coefficient

P_i^{sat} is the saturation pressure in bar

P_P is the permeate pressure in bar

x_i is the liquid molar fraction in the feed side

y_i is the vapor molar fraction in the permeate side

All the mixture/pure component properties (γ_i, P_i^{sat} ...) were calculated using the communication option between ASPEN PLUS and ACM. The NRTL activity coefficient method was the selected method for these calculations in ASPEN PLUS.

Both, dA_m and dV can be written as function of the reactor length:

$$dA_m = dl\ p_m \tag{7.22}$$

$$dV = dl\ A_t \tag{7.23}$$

Where:

A_t is the cross sectional area of the shell side (m^2). It is the cross sectional area without taking into account the membrane pipes. (Figure 7.25)

p_m is the perimeter of membrane tubes ($p_m = N\ \pi\ d_0$; in m);

N is the number of membrane tubes;

d_0 is the outer diameter of a membrane tube (m);

By combining equations (7.20), (7.22) and (7.23) with (7.19) the following expression is achieved:

$$\frac{dF_i}{A_t\, dl} = r_i - \frac{f_i\, p_m\, dl}{A_t\, dl} \tag{7.24}$$

Reorganizing equation (7.24):

$$\frac{dF_i}{dl} = A_t\, r_i - f_i\, p_m \tag{7.25}$$

It may be convenient to differentiate the equations over a normalized length parameter z, which values are between 0 and 1.

$$dl = L\, dz \tag{7.26}$$

Where, L is the total length of the membrane (reactor).

$$\boxed{\frac{dF_i}{dz} = L\ (A_t\, r_i - f_i\, p_m)} \tag{7.27}$$

The vapor molar fractions on the permeate side were calculated from the permeate flow rates.

$$y_i = \frac{\int_0^{A_m} f_i\, dA_m}{\sum_i \int_0^{A_m} f_i\, dA_m} \tag{7.28}$$

$$y_i = \frac{\int_0^{1} f_i\, A_m\, dz}{\sum_i \int_0^{1} f_i\, A_m\, dz} \tag{7.29}$$

7.2.2.2.2 Reaction rate

The reaction between ethanol and butanal is carried out in two different steps as explained in Chapter III but the kinetics can be described using the global reaction. The pseudo order for ethanol is 2, and the pseudo-order for butanal, 1,1 diethoxy butane and water is one.

$$r_1 = wk^{'} C_A^2 C_B \tag{7.30}$$

$$r_4 = wk_4^{'} C_C C_D \tag{7.31}$$

Where:

w is the catalyst loading of the shell side (kg/m^3)

$$k^{'} \rightarrow \frac{(m^3)^3}{kmol^2\ h\ \ kgcat}$$

$$k_4^{'} \rightarrow \frac{(m^3)^2}{kmol\ h\ \ kgcat}$$

$$C_i \rightarrow \frac{kmol}{m^3}$$

$$r \rightarrow \frac{kmol}{m^3\ h}$$

The reaction rate must be expressed in terms of molar flow since the mass balance is expressed in molar flows. The relation between molar flow rate and molar concentrations are shown in equation (7.32).

$$F_i = C_i \upsilon \tag{7.32}$$

Where:

F_i is the molar flow rate in kmol/h

C_i is the molar concentration is kmol/m^3

υ is the volumetric flow rate in m^3/h

So, substituting equation (7.32) in equations (7.31) and (7.30):

$$r_1 = wk^{'} F_A^2 F_B \frac{1}{\upsilon^3} \tag{7.33}$$

$$r_4 = wk_4^{'} F_C F_D \frac{1}{\upsilon^2} \tag{7.34}$$

Therefore, the reaction rate of each compound can be expressed as:

$$r_A = -2r_1 + 2r_4 \tag{7.35}$$

$$r_B = -r_1 + r_4 \tag{7.36}$$

$$r_C = r_1 - r_4 \tag{7.37}$$

$$r_D = r_1 - r_4 \tag{7.38}$$

The volumetric flow variation (m^3/h) can be obtained by dividing the total molar flow in every differential by the molar density (kmol/m3):

$$\upsilon = \frac{F}{\rho_m} \tag{7.39}$$

Where:

υ	is the volumetric flow in m^3/h
ρ_m	is the molar density (kmol/m^3)
F	is the total molar flow rate (kmol/h)

7.2.2.2.3 Energy balance

The energy balance for an isothermal and adiabatic case is developed in this section. In both expressions the enthalpy of reaction is required. A temperature dependant expression was developed in Section 5.1.3.3 using formation enthalpies of each compound.

The final expression for the enthalpy of reaction is given in the next equation. Remark that as it is a function of temperature, its value changes along the reactor.

$$\Delta H_r(T_i) = -31098 + (-73.069) * (T_i - 298.15) \tag{7.40}$$

- **Isothermal case**

In principle, it is not necessary to take into account an energy balance in an isothermal process since the temperature is known and constant. However, it is necessary to consider it in order to know the amount of heat that must be supplied or removed to/from the system. This heat is e.g. produced by the reaction or consumed by the evaporation of the components (mainly water) that are permeating through the membrane.

The generated amount of heat in the reaction can be compared to the latent heat needed in the phase change:

$$Q = -\Delta H_r(T)\, F_{B0} X - \int_0^1 J\, \bar{\lambda}\, A_m\, dz \tag{7.41}$$

Where:

$$\Delta H_r(T) = -31098 + (-73.069) * (T - 298.15) \ \ [kJ/kmol] \tag{7.42}$$

$$J = \sum_i f_i \ \ [kmol/(m^2\, h)] \tag{7.43}$$

F_{B0} is the initial butanal flow rate in (kmol / h) chosen as the limiting reactant

X is the total conversion

A_m is the membrane area in m^2

$\bar{\lambda}$ is the latent heat of the permeating fluid $[kJ/kmol]$

- **<u>Adiabatic case</u>**

In case of an adiabatic module the energy balance is the following one:

$$\sum F_i C_{p,i} T \ \big|_V + (-\Delta H_r)\, F_{B0} dX - \sum f_i\, dAm\, |\lambda_i(T)| = \sum F_i C_{p,i} T \ \big|_{V+dV} \tag{7.44}$$

Differentiating over V:

$$\sum (F_i C_{p,i}) \frac{dT}{dV} = (-\Delta H_r(T))\, F_{B0} \frac{dX}{dV} - \sum f_i \frac{dAm}{dV} |\lambda_i(T)| \tag{7.45}$$

dX/dz can be expressed in terms of concentration:

$$-r_B = F_{B0} \frac{dX}{dV} \tag{7.46}$$

$$\sum (F_i C_{p,i}) \frac{dT}{dz} = \left[(-\Delta H_r(T))\, (-r_B) - \sum f_i \frac{p_m}{A_t} |\lambda_i(T)| \right] L\, A_t \tag{7.47}$$

Substituting (7.22), (7.23) and (7.26):

$$\frac{dT}{dz} = \frac{\left[A_t\, (-\Delta H_r(T))\, (-r_B) - N\, \pi\, d_0\, (J\, |\bar{\lambda}_i(T)|) \right] L}{\sum (F_i C_{p,i})} \tag{7.48}$$

7.2.2.2.4 Momentum balance

The pressure drop does not affect the process but it may be convenient to calculate the pressure in the output (retentate stream) in order to know if it must be pressurized for further downstream processing. Moreover, it helps to ensure that all the feed-retentate side is in liquid phase.

The pressure drop in a packed bed reactor is given by the Ergun equation (7.49) (76).

$$\frac{dP_F}{dl} = \left[\frac{150\,\mu(1-\varepsilon)^2\, v_s}{\phi\,\varepsilon^3\, d_p^2} + \frac{1.75(1-\varepsilon)\, v_s^2\, \rho}{\phi\,\varepsilon^3\, d_p} \right] * 10^{-5} \tag{7.49}$$

As well as in the mass balance, by applying equation (7.26), the pressure is differentiated over a normalized length variable.

$$\frac{dP_F}{dz} = L \left[\frac{150\,\mu(1-\varepsilon)^2\, v_s}{\phi\,\varepsilon^3\, d_p^2} + \frac{1.75(1-\varepsilon)\, v_s^2\, \rho}{\phi\,\varepsilon^3\, d_p} \right] * 10^{-5} \tag{7.50}$$

Where:

P_F	is the pressure in the feed side (bar)
L	is the total length of the membrane tube (m)
μ	is the dynamic viscosity of the liquid in the feed-retentate side (Pa·s)
ε	is the void fraction
v_s	is the superficial velocity (m/s)
Φ	indicates the sphericity of particles (Φ=1)
d_P	is the catalyst particle diameter (m)
ρ	is the density of the liquid on the feed-retentate side (kg/m^3)

The void fraction or packed bed porosity is influenced by the effect of confining walls on the packing structure. Given an infinitely large container, the porosity of a randomly packed bed of spheres is approximately 0.4, if the particles have friction. Near the walls, the predicted void fraction is close to 1.0 due to the contact point requirement between the wall and a sphere (77). Theuerkauf et al. developed a model to predict the void fraction in a packed bed taking into account particle properties, friction coefficients, etc,. However, it was checked that Dixon`s correlation for spheres (78) (eq. (7.51) was a good correlation for d/D (particle diameter/reactor diameter) ratios smaller than 0.5. Therefore, Dixon's correlation was used for void fraction calculation.

$$\varepsilon = 0.4 + 0.05\,\frac{d}{D} + 0.412\,\left(\frac{d}{D}\right)^2 \qquad \frac{d}{D} < 0.5 \qquad (7.51)$$

In the present case the reactor diameter was substituted by the hydraulic diameter.

$$D_H = \frac{4\,Cross\ sectional\ area}{Wet\ Perimeter} = \frac{4\,A_t}{\pi\,(D - N\,d_0)} \qquad (7.52)$$

Where:

A_t	Cross sectional area (see Figure 7.25) in m^2
D	Module inner diameter in m
N	Number of membrane pipes
d_0	Outer diameter of membrane pipes in m

Dixon's correlation was derived for the bulk void fraction in a fixed bed by both geometrical arguments and empirical treatment of data.

7.2.2.2.5 Input data

Any mathematical model requires some input data in order to be solved. For this model, the required input data are:

- Molar feed flows (kmol/h)
- Feed pressure (bar)
- Feed temperature (ºC)
- Permeate pressure (bar)
- Kinetic and permeance data
- Catalyst type (choose among Amberlyst 15, 35, 70 & 47)* and catalyst amount (g/L)
- Geometrical design parameters (shell diameter, membrane diameter, distance between membrane tubes and module length) (m)

* In the kinetic study (Chapter III) it was found that the reaction performance with Amberlyst 15, 35, 70 & 47 is exactly the same under the tested temperature range (see Section 3.2.4).

7.2.2.2.6 Summary of equations

Table 7.6 Summary of the implemented equations

Equations	Unknown Variables
• Mass balance on the shell side $\frac{dF_i}{dz} = L\,(A_t\, r_i - f_i\, p_m)$ • Flux through the membrane $f_i = Q_i\,(\gamma_i x_i P_i^{sat} - y_i P_P)$ $\quad y_A = \frac{\int_0^1 f_A\, A_m\, dz}{\sum_i \int_0^1 f_i\, A_m\, dz}$	F_i
• Kinetics $r_A = -2r_1 + 2r_4$ $\quad r_C = r_1 - r_4$ $r_B = -r_1 + r_4$ $\quad r_D = r_1 - r_4$ $r_1 = wk'\, F_A^2 F_B \frac{1}{\upsilon^3}$ $\quad r_4 = wk_4'\, F_C F_D \frac{1}{\upsilon^2}$	y_i
	Q / T
• Energy balance $Q = -\Delta H_r(T)\, F_{B0} X - \int_0^1 J\,\bar{\lambda}\, A_m\, dz$ (Isothermal) $\frac{dT}{dz} = \frac{\left[A_t\,(-\Delta H_r(T))\,(-r_B) - N\,\pi\, d_0\,(J\,\lvert\bar{\lambda}_i(T)\rvert)\right]L}{\sum\left(F_i C_{p,i}\right)}$ (Adiabatic)	P_F
• Momentum balance $\frac{dP_F}{dz} = L\left[\frac{150\,\mu(1-\varepsilon)^2 v_s}{\phi\,\varepsilon^3 d_p^2} + \frac{1.75(1-\varepsilon) v_s^2\,\rho}{\phi\,\varepsilon^3 d_p}\right] * 10^{-5}$	

7.2.2.3 Model implementation

ASPEN CUSTOM MODELLER (ACM) was the chosen software package. ACM is an equation orientated software tool and it is suitable to model different unit operations and modules and link them. Moreover, all the physical, chemical and thermodynamic properties can be calculated via a direct communication with the ASPEN PLUS flow sheeting program.

7.2.2.4 Hydrodynamics

As it is indicated in the beginning of this section, concentration polarization and temperature polarization effects were not taken into account.

Concentration polarization is caused by the selectivity of the membrane. The rejected compounds of the feed mixture accumulate at the membrane surface, whereas the preferentially permeating compounds are depleted from the bulk toward the membrane. Temperature polarization is a consequence of the phase transition in the membrane. The necessary vaporization enthalpy is taken from the energy of the feed side decreasing the mixture temperature next to the membrane surface.

It is known that in laminar flow regime these effects are quite important and thus, pervaporation efficiency decreases considerably. Sommer et al. (79) studied the concentration and temperature polarization effect on different membranes. They observed that, for an annular duct type of module, there is steep efficiency increase at Re = 2300 (see Figure 7.22)

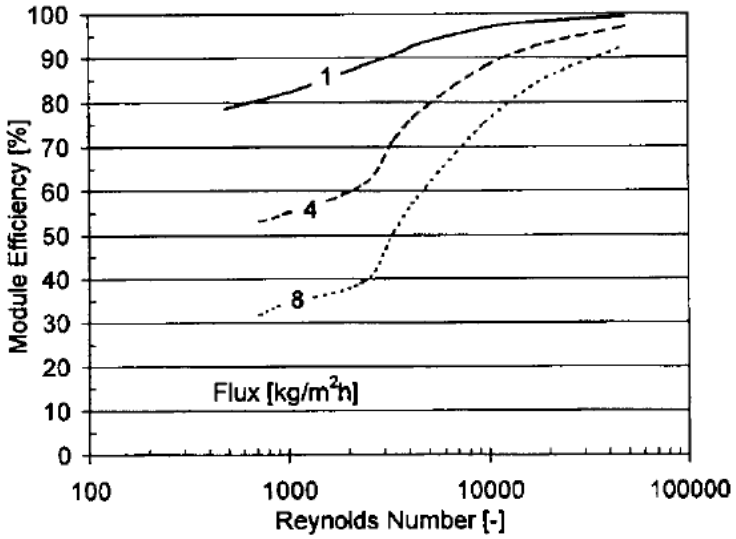

Figure 7.22 Calculated efficiency of an annular duct type technical module as a function of the Re number for different permeate fluxes. (Solid line: 1 kg m^{-2} h^{-1}; dashed line: 4 kg m^{-2} h^{-1}; dotted line: 8 kg m^{-2} h^{-1}.(79)

According to the measured fluxes in the experimental part of this report, the solid line would better describe the behavior in the present study.

Re = 2300 represents the transition zone from laminar regime to turbulent regime as it can be seen in Moody's chart for flow through pipes (see Figure 7.23) (60).

$$Re = \frac{D\ v\ \rho}{\mu} \tag{7.53}$$

Where: D hydraulic diameter (m)

v fluid velocity (m/s)

ρ density of the fluid (kg/m^3)

μ dynamic viscosity (Pa·s)

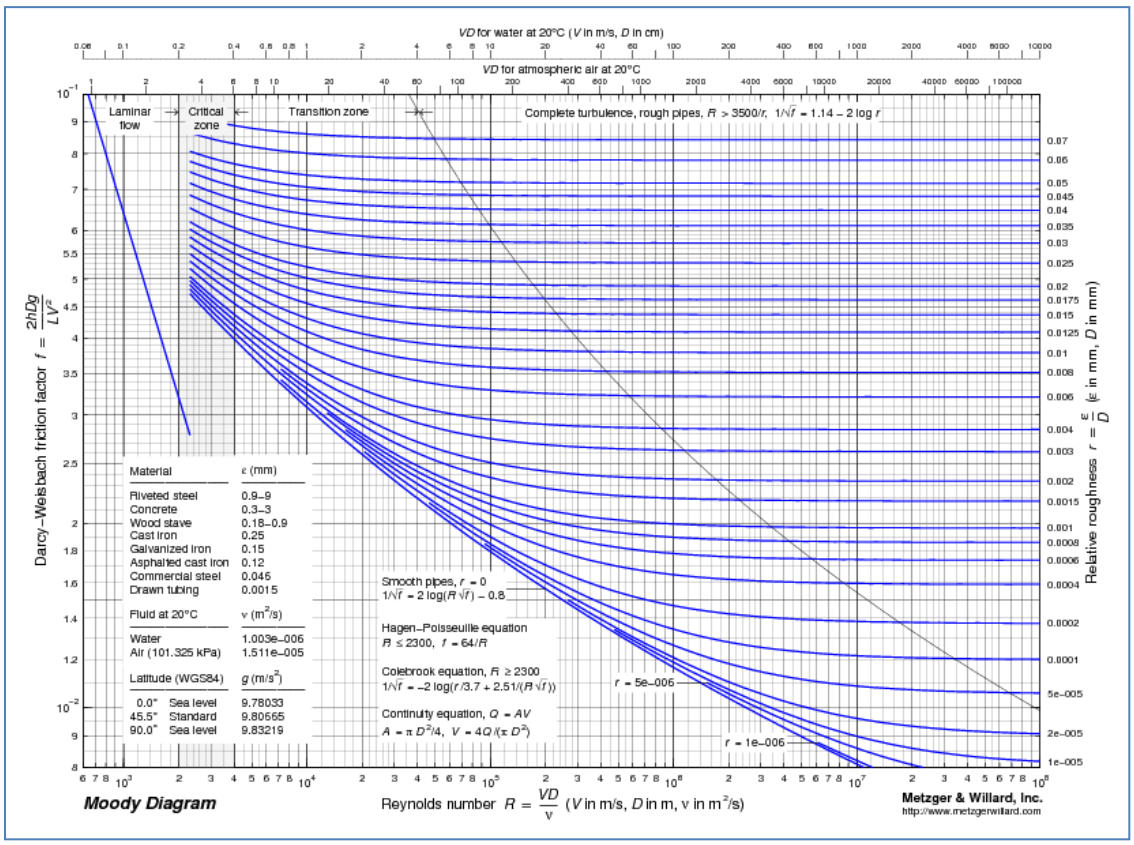

Figure 7.23 Moody's chart for flow through pipes.

In the present case, the shell side of the module is filled with catalyst particles, i.e., is a catalytic fixed bed. Therefore, the calculation of Reynolds number changes and also the limits of the laminar and turbulent regime zones. In case of packed beds the Reynolds number is calculated using the catalyst particle diameter (see equation (7.54) (76)

$$Re = \frac{d_p\ v\ \rho}{(1-\epsilon)\mu} \tag{7.54}$$

Where:

d_p	Catalyst particle diameter (m)
v	Superficial velocity of the fluid without taking into account the particles (m/s)
ρ	Fluid density (kg/m^3)
ε	Void fraction
μ	Dynamic viscosity of the fluid (Pa·s)

Figure 7.24 shows friction factors for packed beds. It can be observed that transition flow region between laminar and turbulent flow regimes (the equivalent to Re = 2300 in pipes) starts at Re = 10. For these reasons, all the simulations were performed at Re > 10.

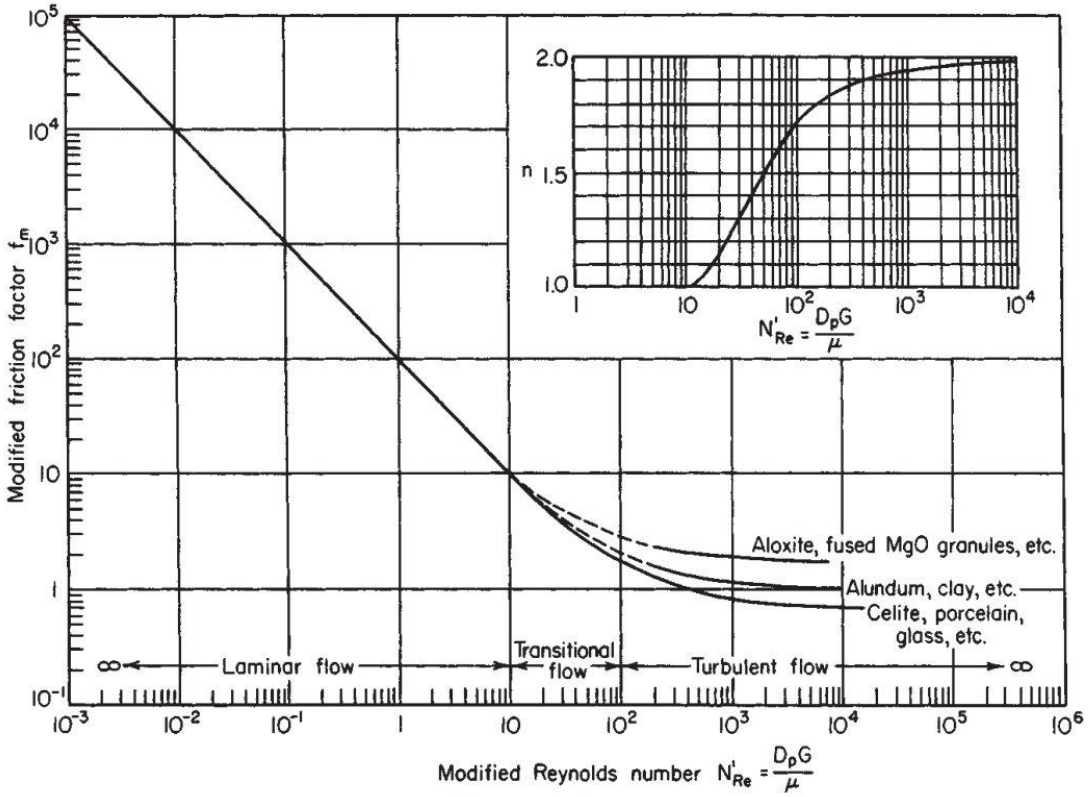

Figure 7.24 Friction factors for packed beds (60).

7.2.2.5 Multitubular module design

In order to ensure that the simulations were not in the laminar regime, an initial module design was required in order to know the cross section through which the fluid passes (to calculate the fluid velocity) and the maximum membrane area that can be placed per cubic meter of catalyst bed.

The module design is based on the shell-and-tube heat exchangers. Membrane pipes can be placed following different layouts but the equilateral triangular layout is the one which offers the highest membrane area (see Figure 7.25).

In terms of the distance between the membrane tubes in heat exchanger design, the typical pitch distance is 1.25 $d_{membrane}$. However, in this study the presence of catalyst is a major issue. In order to avoid wall effects the distances between pipes and between pipes and shell wall must be at least 8-10 times the particle diameter (80;81) (tube to tube and tube to wall distance $\geq$ 8-10 d_p).

The wall effects can be explained in two different ways. On the one hand, the void fraction or packed bed porosity is influenced by the confining walls on the packing structure. Given an infinitely large container, the porosity of a randomly packed bed of spheres should tend to be approximately 0.4, if the particles have friction. Near the walls, the predicted void fraction is close to 1.0 due to the contact point requirement between the wall and a sphere (77). If the distance among pipes is not big enough the low particle packing around the pipes would represent a large volume with respect to the shell volume. In this case, the predicted void fraction would be much more than the predicted one and thus, the real catalyst amount would be much lower. However this effect could be corrected using Dixon's correlation (eq. (7.51). On the other hand, the wall effect also influences the hydrodynamics. The existence of large low void fraction areas would imply the generation of large preferential flow areas and in this case the plug flow assumption would not be fully true.

Because of these limitations the distance between the tubes was established to be $8d_p$. Figure 7.25 shows all the geometrical characteristics of the pervaporation reactor. In general the $8d_p$ relation used means that the membrane area to volume ratio becomes small and that the pervaporation is definitely the limiting step as already discussed in the experimental Section 6.2.4. For the Amberlyst A47 the particle size is 1 mm (see Table 7.8). This would mean that the distance between the tubes is 8 mm. For a tube with a diameter of 14 mm (see Table 7.9) this distance is already too large but for a tube with a diameter of 3 mm this leads to an unrealistic module concept and membrane surface area to volume ratio.

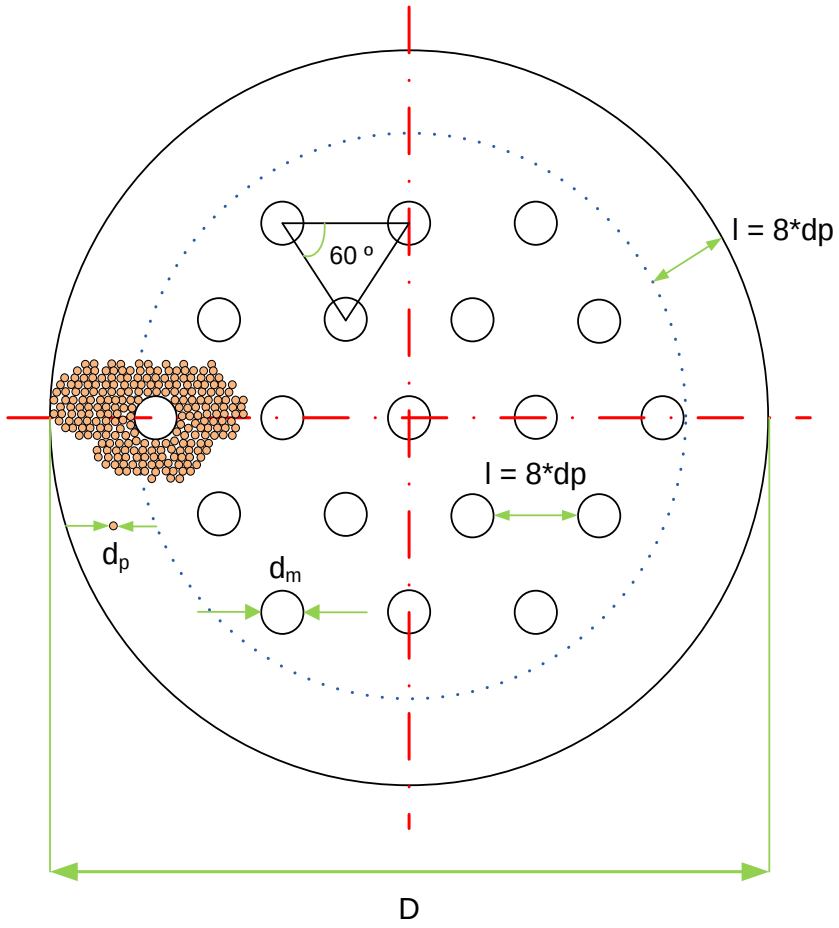

Figure 7.25 Geometric characteristics of the MPFMR.

Once the geometry of the MPFMR was defined, the next step was the calculation of the number of membrane pipes that can be placed in a certain module diameter. For this purpose a mathematical algorithm based on the shell diameter, membrane diameter and pipe to pipe distances was developed in ASPEN CUSTOM MODELER. The calculation steps of the algorithm are the following ones:

1. Definition of shell diameter, membrane diameter and catalyst particle diameter.
2. Calculation of the distance between the membrane rows.
3. Calculation of the maximum membrane rows
4. Calculation of the maximum number of membrane pipes in each row.
5. Checking if the perpendicular distance among the shell wall and the first and last pipes of each row fulfill the distance constraint and if necessary recalculate the number of pipes of each row.

The algorithm used for the calculations is shown in Figure 7.26.

```
// Determination of the particle size:

IF Cat_type=="Amberlyst-15" THEN
   dp:0.725*10^-3;
ELSEIF Cat_type=="Amberlyst-35" THEN
   dp:0.825*10^-3;
ELSEIF Cat_type=="Amberlyst-47" THEN
   dp:1*10^-3;
ELSEIF Cat_type=="Amberlyst-70" THEN
   dp:0.5*10^-3;
ENDIF

// Distance among tubes (between the outer diameters: p-(d0/2)-(d0/2)):
   l:8*dp;
// Distance between two membrane tubes (pitch distance):
   p:l+d0;
// Relation between "pitch distance" and membrane tube diameter:
   k:p/d0;
// Distance among membrane tube rows:
   height:p*SQRT(3)/2;
   NrOfFloors: truncate((0.5*D-l-d0/2)/height);

For i in [0:NrOfFloors] Do
 If truncate(i/2)==i/2 Then
   Len(i):SQRT((0.5*D)^2-(i*height)^2);
   NrOfPipesPerFloor_prov(i):1+2*truncate((Len(i)-0.5*d0-l)/p);
   dist_cen(i):sqrt(((truncate(NrOfPipesPerFloor_prov(i)/2))*p)^2+(i*height)^2);
   if (D/2-dist_cen(i))<(l+d0/2) Then
     NrOfPipesPerFloor(i):NrOfPipesPerFloor_prov(i)-2;
   Else
     NrOfPipesPerFloor(i):NrOfPipesPerFloor_prov(i);
   Endif
 Else
   Len(i):SQRT((0.5*D)^2-(i*height)^2);
   NrOfPipesPerFloor_prov(i):2*truncate((Len(i)-0.5*l)/p);
   dist_cen(i):sqrt(((NrOfPipesPerFloor_prov(i)/2-1)*p+p/2)^2+(i*height)^2);
   if (D/2-dist_cen(i))<(l+d0/2) Then
     NrOfPipesPerFloor(i):NrOfPipesPerFloor_prov(i)-2;
   Else
     NrOfPipesPerFloor(i):NrOfPipesPerFloor_prov(i);
   Endif
 EndIF
EndFor

TotalNumberOfPipes : 2*sigma(NrOfPipesPerFloor)-NrOfPipesPerFloor(0);
MembraneArea = TotalNumberOfPipes *3.14*d0*TubeLength;

End
```

Figure 7.26 Code to calculate the number of membrane pipes in a membrane module.

There are some other ways to calculate the number of pipes that can be placed in a certain module diameter. In Perry's Chemical Engineers' Handbook (60) tabulated data for shell-and-tube heat exchangers are given. By fitting these data the following correlation is obtained:

$$N_t = 0.68034 \left(\frac{D}{k\, d_0}\right)^{2.05508} \tag{7.55}$$

Where: N_t number of pipes

D shell diameter (m)

d_0 membrane tube outer diameter (m)

k pitch coefficient ($p = k \cdot d_0$) (tabulated data was for k: 1.25-1.33)

Some other references (82) propose the following calculation procedure:

1. Draw the equilateral triangle connecting three adjacent tube centres. Any side of the triangle is the tube pitch (recall 1.25 Do is minimum).
2. The triangle area is 0.5 hb where b is the base and h is the height.
3. This area contains 0.5 tubes.
4. Calculate the area occupied by all the tubes.
5. Calculate the shell diameter to contain this area.
6. Add one tube diameter all the way around (two tube diameters added to the diameter calculated above).
7. The result is the minimum shell diameter.

Following these steps the next correlation is obtained:

$$N_t = \frac{\pi}{4\ \sqrt{3}/2}\left(\frac{D - 2d_0}{k\ d_0}\right)^2 \tag{7.56}$$

However, these two correlations (7.55 and (7.56) entail quite important errors when small shell diameters are involved; i.e., they are based on geometrical approaches and by working with big module diameters the error is not so big since the amount of pipes is high. Table 7.7 shows the comparison between values calculated with these two correlations and the calculated ones with the algorithm implemented in Aspen Custom Modeler.

Table 7.7 Comparison between the calculated number of membrane pipes with the algorithm and correlations (7.55) & (7.56)

Shell diameter D (mm)		29	29	14	14
Tube outer diameter d_0 (mm)		3	4	3	4
Number of membrane pipes	Correlation (7.55)	3	3	0	0
	Correlation (7.56)	0	0	0	0
	Algorithm	1	1	1	1

Because of the large errors for the two equations, the number of pipes that can be placed in a module was calculated using the developed algorithm since these values are real values and the predicted ones with the correlations are based on geometrical approximations.

A preliminary design study was performed in order to choose the best geometrical configuration. In the kinetic study (Chapter III) four different Amberlyst catalysts (A15wet, A35wet, A70 & A47) were tested and all of them showed an identical performance. As the particle diameter of each one is different, all the possibilities were taken into account in the further modeling calculations.

Table 7.8 Particle diameter of each catalyst type (52)

	A15Wet	**A35Wet**	**A70**	**A47**
d_p (mm)	0.725	0.825	0.5	1.0

Commercially available membrane tube outer diameters were used for this study (3, 4, 6, 7, 10 and 14 mm). Table 7.9 shows all the tested configurations.

All the simulations were performed under the same conditions:

- Stoichiometric feed ratio (EtOH/Butanal 2:1 in moles)
- Feed volumetric flow rate of 7 L/h
- Catalyst loading: 500 g/L
- Permeate pressure: 5 mbar
- Adiabatic reactor
- Reactor length: 1 m

In these preliminary calculations, after doing some rough calculations, a module diameter of 29 mm was taken as a base for all 6 different membrane diameters. Then, based upon these results the configuration was optimized either by reducing the module diameter as far as possible but keeping the same number of membrane pipes in the reactor or by increasing the module diameter in order to introduce more membrane pipes.

Table 7.9 Different geometrical configurations for the MPFMR. Conditions: Length: 1m, stoichiometric feed ratio (ethanol:butanal = 2:1), feed flow rate: 7 L/h, Feed T: 70 ºC, adiabatic module, catalyst loading 500 g/L and a permeate pressure of 5 mbar.

Configuration No.→		1	2	3	4	5	6	7	8	9	10	11	12	13	14	15	16	17	18
	D (m)	0.029	0.019	0.041	0.029	0.02	0.045	0.029	0.022	0.05	0.029	0.023	0.053	0.029	0.027	0.063	0.029	0.03	0.074
	d0 (m)	0.003	0.003	0.003	0.004	0.004	0.004	0.006	0.006	0.006	0.007	0.007	0.007	0.01	0.01	0.01	0.014	0.014	0.014
	Nt	1	1	7	1	1	7	1	1	7	1	1	7	1	1	7	0	1	7
A47	**Am (m^2)**	0.0094	0.0094	0.0659	0.0126	0.0126	0.0879	0.0188	0.0188	0.1319	0.0220	0.0220	0.1539	0.0314	0.0314	0.2198	-	0.0440	0.3077
	m2_m3	14.42	34.09	51.92	19.39	41.67	58.55	29.81	53.57	74.73	35.35	58.33	79.48	53.98	63.59	85.65	-	79.55	95.52
	Conversion	0.38	0.38	0.48	0.39	0.39	0.50	0.40	0.40	0.55	0.40	0.40	0.57	0.42	0.42	0.62	-	0.44	0.66
	Re	12-12.5	31	5	12-12.5	25	5	12.5	20	3-5	9-10	20	2.5-4	14-12.5	16.5-15.5	2-3	-	12-15	1-2.5
	D (m)	0.029	0.015	0.033	0.029	0.016	0.036	0.029	0.018	0.042	0.029	0.019	0.045	0.029	0.022	0.054	0.029	0.026	0.066
	d0 (m)	0.003	0.003	0.003	0.004	0.004	0.004	0.006	0.006	0.006	0.007	0.007	0.007	0.01	0.01	0.01	0.014	0.014	0.014
	Nt	1	1	7	1	1	7	1	1	7	1	1	7	1	1	7	1	1	7
A15	**Am (m^2)**	0.0094	0.0094	0.0659	0.0126	0.0126	0.0879	0.0188	0.0188	0.1319	0.0220	0.0220	0.1539	0.0314	0.0314	0.2198	0.0440	0.0440	0.3077
	m2_m3	14.42	55.56	81.87	19.39	66.67	94.59	29.81	83.33	111.11	35.35	89.74	116.53	53.98	104.17	126.35	86.82	116.67	131.37
	Conversion	0.38	0.38	0.48	0.39	0.39	0.50	0.40	0.40	0.55	0.40	0.40	0.57	0.42	0.42	0.62	0.44	0.44	0.66
	Re	9	33.5-34.5	6-7	9	30-31	4.5-6	9	24-26	3.5-5	9.5-10	22-24	3-4	9-10	17.5-19.5	2-3.5	11.5-10	15.5-13.5	1-2.5
	D (m)	0.029	0.017	0.036	0.029	0.018	0.039	0.029	0.02	0.045	0.029	0.021	0.048	0.029	0.024	0.057	0.029	0.028	0.069
	d0 (m)	0.003	0.003	0.003	0.004	0.004	0.004	0.006	0.006	0.006	0.007	0.007	0.007	0.01	0.01	0.01	0.014	0.014	0.014
	Nt	1	1	7	1	1	7	1	1	7	1	1	7	1	1	7	1	1	7
A35	**Am (m^2)**	0.0094	0.0094	0.0659	0.0126	0.0126	0.0879	0.0188	0.0188	0.1319	0.0220	0.0220	0.1539	0.0314	0.0314	0.2198	0.0440	0.0440	0.3077
	m2_m3	14.42	42.86	68.13	19.39	51.95	79.49	29.81	65.93	94.75	35.35	71.43	99.95	53.98	84.03	109.85	86.82	95.24	115.67
	Conversion	0.38	0.38	0.48	0.39	0.39	0.50	0.40	0.40	0.55	0.40	0.40	0.57	0.42	0.42	0.62	0.44	0.44	0.66
	Re	10	30	6-7	10	26.5-28	4.5-6	10	22-23.5	3-5	10--11	20-22	3-4	11.5-10	16-18	3-4	13-11	12.5-14.5	1.5-2.5
	D (m)	0.029	0.025	0.036	0.029	0.028	0.04	0.029	0.014	0.034	0.029	0.015	0.037	0.029	0.019	0.047	0.029	0.022	0.058
	d0 (m)	0.003	0.003	0.003	0.004	0.004	0.004	0.006	0.006	0.006	0.007	0.007	0.007	0.01	0.01	0.01	0.014	0.014	0.014
	Nt	7	7	13	7	7	13	1	1	7	1	1	7	1	1	7	1	1	7
A70	**Am (m^2)**	0.0659	0.0659	0.1225	0.0879	0.0879	0.1633	0.0188	0.0188	0.1319	0.0220	0.0220	0.1539	0.0314	0.0314	0.2198	0.0440	0.0440	0.3077
	m2_m3	107.97	149.47	132.32	153.64	166.67	149.43	29.81	150.00	185.84	35.35	159.09	191.03	53.98	153.26	185.55	86.82	194.44	196.79
	Conversion	0.48	0.48	0.54	0.50	0.50	0.58	0.40	0.40	0.55	0.40	0.40	0.57	0.42	0.42	0.62	0.44	0.44	0.66
	Re	5.5-6.5	7.5-9	3-4.5	5-7	6-7.5	2.5-3.5	6	30-32	4-5.5	6	30-27	3.5-5	6-7	17.5-20	2-3.5	7-8	15-18	1.5-2.5

It can be observed that the best results were obtained having 14 mm diameter membrane tubes (the ones in red color). With 7 membrane pipes (*configuration 18*) 66% conversion was predicted. However, it must be taken into account that the Reynolds number under these conditions is really low and in a real process concentration polarization and temperature polarization effects would be quite important. Therefore, 66% of conversion is not a really realistic prediction. The best result having acceptable Re numbers are obtained with "*configuration 17*", 44% of conversion. In this case the best Re number was obtained by using A70 as catalyst (the smallest catalyst). Furthermore what can be observed is that at higher membrane surface area to reactor volume ratios the conversion is increasing.

Two different strategies were followed in order to improve these initial results:

1. Starting from configuration 17 A70 a sensitivity analysis was performed in order to improve the results.
2. Starting from configuration 18 A70 a recycle loop was implemented in order to increase the turbulence in the reactor keeping the same feed flow rate.

7.2.2.6 Sensitivity analysis (without recycling loop)

A sensitivity analysis based on *Configuration 17 A70* was performed in order to study the effect of different variables on the process. Different variables like the reactor length, temperature and catalyst loading were used in the ACM continuous process modeling calculations. Moreover, the difference between an isothermal and an adiabatic MPFMR was tested.

7.2.2.6.1 Effect of the reactor length

The increase of the reactor length implies the increase of the membrane area, thus more water could be removed and the final conversion should increase. Furthermore the residence time in the membrane reactor increases, which will also give an increase in conversion. The increase of the length implies some inconveniences since the pressure drop on the feed-retentate side can increase considerably.

Figure 7.27 shows the effect of the reactor length on the conversion and pressure drop. All these simulations were performed in an adiabatic mode with a stoichiometric feed ratio (2:1 of Ethanol:butanal in moles), feed temperature of 70 ºC, 5 mbar on the permeate side and with 500 g/L of catalyst loading. The inlet pressure was taken at 3 bar in all calculations. The flow over the different lengths of the packed bed reactor will lead to different pressure drops on the feed side. It should be remarked that the pressure

does not have an influence on the conversion. Furthermore the pressure is expected to have hardly any influence on the pervaporation process.

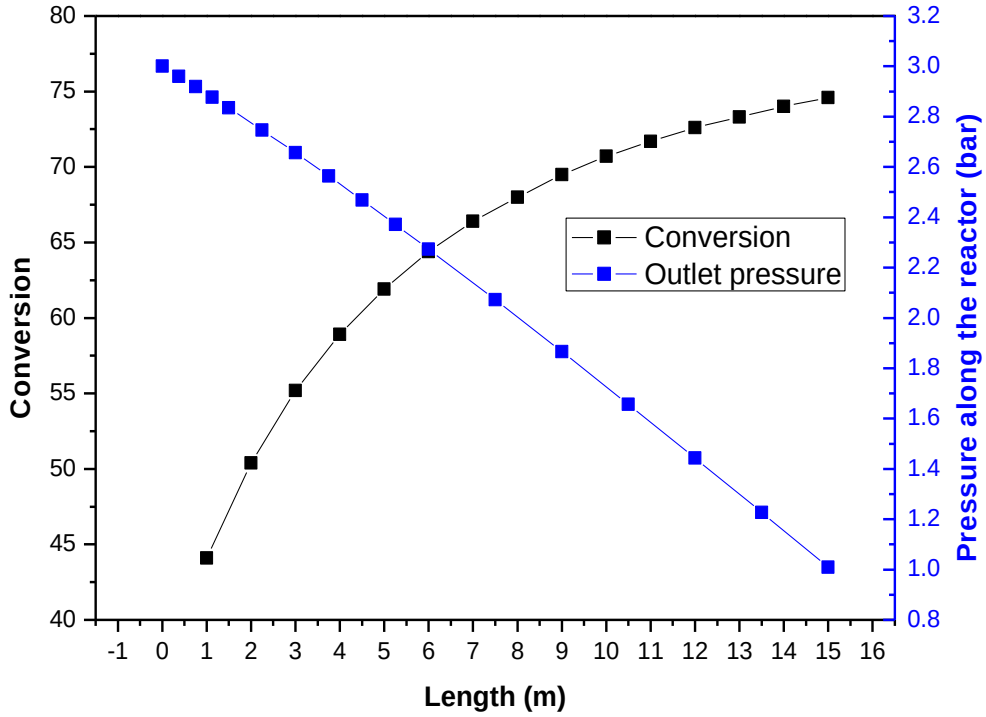

Figure 7.27 Conversion & pressure vs. reactor length. Conditions: 500 g/L of A70, feed temperature: 70 ºC, stoichiometric feed ratio, adiabatic reactor.

It can be observed that the pressure drop is very important. In a real situation different modules of e.g. 1 meter length should be placed in series with intermediate repressurization in order to avoid such a high pressure drop. Thus, possible vaporization in the feed-retentate side when operating close to the boiling point of the mixture would be prevented. Another option would be to pressurize enough the feed stream. At a feed pressure of 3 bar and a 15 meters long reactor a conversion of 74.6% can be achieved releasing the retentate a pressure of 1 bar. The advantage of pressurizing the feed up to 3 bar is that the liquid mixture keeps on being liquid and no vaporization occurs (see Section 7.2.3.3.1).

Notice that using 7 meters of reactor length the achieved final conversion is 66 %, which is the same conversion that could be achieved with 1 meter length of *configuration 18 A70* which includes 7 membrane pipes of the same diameter. But now this conversion is achieved within an acceptable Re regime. In both cases the amount of membrane area is the same, geometrical configuration is the only change (and thus, Re regime).

Figure 7.28 shows that in the first centimeters of the reactor the equilibrium composition is already achieved. After some 25 cm water permeation is getting more important. This leads to the fact that the water concentration is going through a maximum. At further increased lengths the acetal concentration and thus process conversion grows up and above the equilibrium estimated for the fresh feed composition. However, water depletion is quite slow due to the relatively small membrane area.

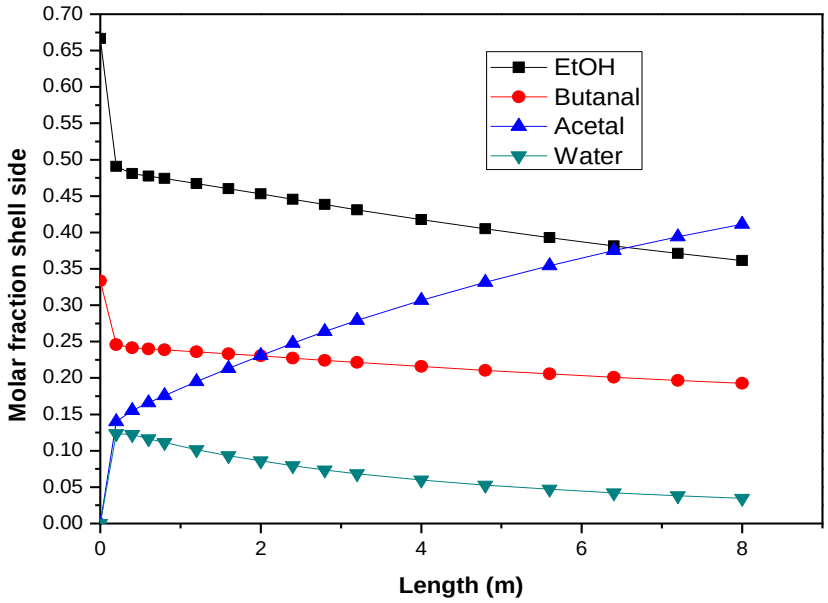

Figure 7.28 Molar fraction profile. Conditions: Reactor length: 8 m, feed temperature: 70 ºC, 500 g/L of A70, 5 mbar in the permeate and stoichiometric feed ratio.

Figure 7.29 shows one of the great advantages of using a membrane reactor for the studied acetalization reaction. In conventional pervaporation processes the temperature drop along the module is quite important, thus losing flux and separation efficiency. In the present case, the reaction between ethanol and butanal is exothermic so there is a large temperature increase in the beginning of the reactor. Then, when the further process conversion is limited by the pervaporation rate the temperature decreases. The temperature change along the reactor is important but overall, the average temperature is roughly 70°C.

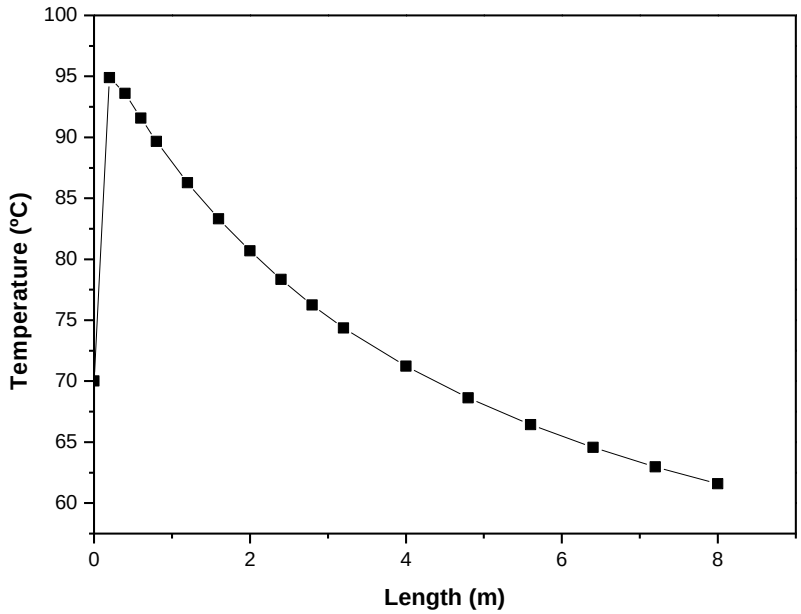

Figure 7.29 Temperature profile along the reactor. Conditions: Reactor length: 8 m, feed temperature: 70 ºC, 500 g/L of A70, 5 mbar in the permeate and stoichiometric feed ratio.

For a reactor length of 8 meter the feed, retentate and permetate conditions as calculated in ACM are presented in Table 7.10.

Table 7.10 Feed, retentate and permetate conditions. Conditions: Reactor length: 8 m, feed temperature: 70 ºC, 500 g/L of A70, 5 mbar in the permeate and stoichiometric feed ratio.

Conditions	**Feed**	**Retentate**	**Permeate**
Molar flow (kmol/h)	0.1	0.055	0.022
P (bar)	1	0.0030	0.005
T (ºC)	70	61.57	-3.5
EtOH molar frac	0.66	0.361	0.062
Butanal molar frac	0.33	0.193	9.36E-04
Acetal molar frac	0	0.411	0
Water molar frac	0	0.035	0.937

7.2.2.6.2 Effect of the temperature

The influence of temperature was calculated in order to search the most suitable one for the process. All the simulations were performed in an adiabatic mode with a stoichiometric feed ratio (2:1 of Ethanol:butanal in moles), 5 mbar in the permeate side and with 500 g/L of catalyst loading. The length of the reactor was 5 meters in all the cases in order to fulfill pressure drop requirements. Figure 7.30 and Figure 7.31 show the performance of the MPFMR at different feed temperatures.

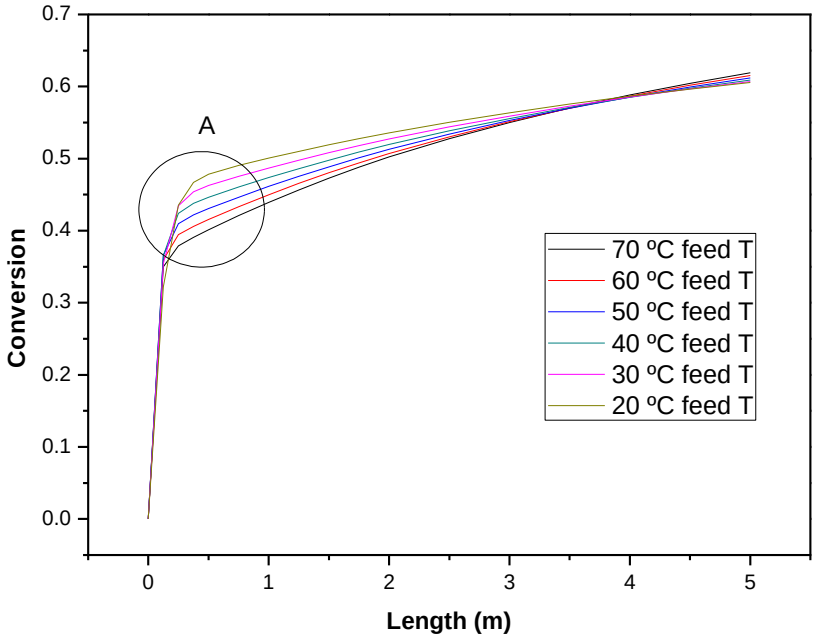

Figure 7.30 Effect of the temperature on the conversion along the reactor. Conditions: adiabatic mode with a stoichiometric feed ratio, 5 mbar in the permeate side and with 500 g/L of catalyst loading (A70).

The "*A*" point in Figure 7.30 represents the equilibrium conversion of each temperature for the case without pervaporation. Due to the low membrane area, up to a reactor length of 4 meters, the achieved conversion at lower temperatures was higher than at higher temperatures. The acetalization reaction between ethanol and butanal is an exothermic reaction so at low temperatures higher equilibrium conversions can be achieved. However, from the pervaporation point of view, as it was found in the experimental and in the semi-batch modeling part, high temperatures enhance the water permeation through the membrane thus the pervaporation rate is much faster. This effect of the higher permeation becomes dominant at larger membrane lengths and above a length of 4 meters the conversion was becoming the highest at the highest temperature. Not surprisingly the shape of this curve was exactly the same as the shape of the curve

calculated in the batch mode for the influence of temperature on the conversion: compare Figure 7.30 with Figure 7.9 in the batch calculations.

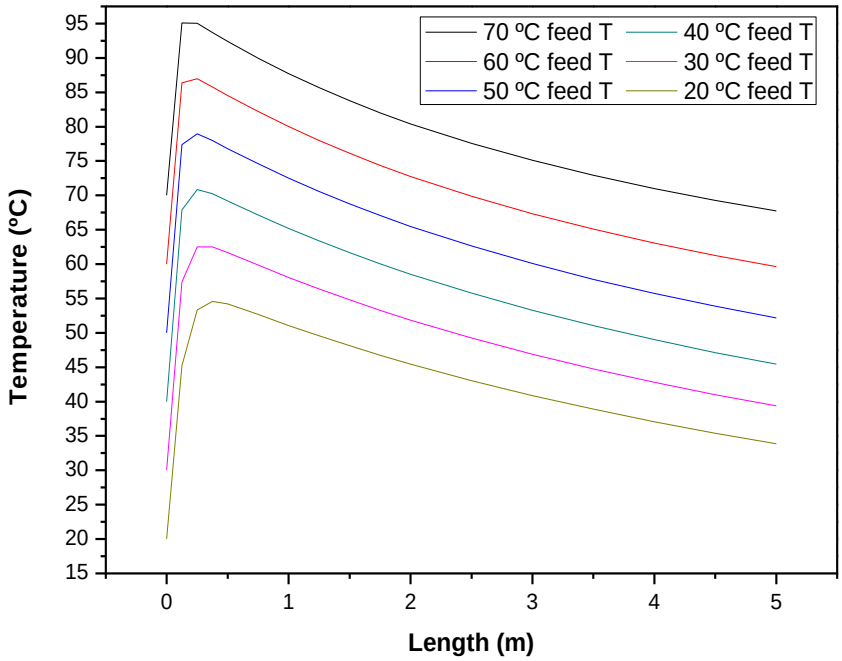

Figure 7.31 Temperature profile along the reactor at different feed temperatures. Conditions: adiabatic mode with a stoichiometric feed ratio, 5 mbar in the permeate side and with 500 g/L of catalyst loading (A70).

All the temperature profiles along the membrane/reactor as presented in Figure 7.31 follow the same trend. First a temperature increase due to the exothermic reaction and then a decrease due to fact that the heat needed for the pervaporation process was more than the one produced by the reaction. The temperature increase in the first approximately 30 cm of the reactor at low feed temperature was larger than at higher feed temperature. This is because the conversion at low temperature was larger.

7.2.2.6.3 Effect of the catalyst loading

In the experimental and semi-batch modeling part, it was found that pervaporation was the limiting step, i.e., the achieved conversions are limited by the permeation rate and not by reaction rate. In this section different calculations performed with different catalyst loadings will be shown.

As a first step, the maximum bed density was calculated (550 g/L) by measuring the weight and the volume (with a graduated cylinder) of a certain amount of catalyst. (see Table 7.11)

Table 7.11 Packed bed density of Amberlyst 47 ion exchange resin.

Vol (mL)	Weight (g)	g/L	Ave. g/L
10	5.64	564.00	
20	10.69	534.50	
30	16.48	549.33	550.8
40	22.15	553.75	
45	24.87	552.67	

All the simulations were performed in an adiabatic mode with a stoichiometric feed ratio (2:1 of Ethanol:butanal in moles), 5 mbar in the permeate side and with 5 meters of reactor length.

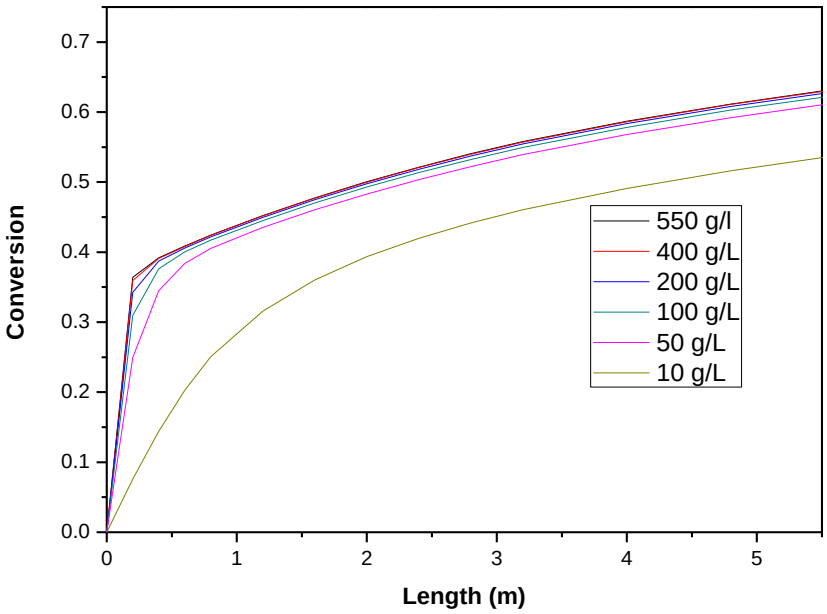

Figure 7.32 Effect of the catalyst loading on the conversion along the reactor. Conditions: feed temperature 70 ºC in adiabatic mode with a stoichiometric feed ratio, 5 mbar in the permeate side and 5.5 meters of reactor length.

Figure 7.32 shows that by using 10 g/L of catalyst the reaction was the limiting step and not the pervaporation. In case of using more catalyst the conversion values were almost identical which means that in all the cases pervaporation was the limiting step and there was an overload of catalyst. A catalyst amount of 50 g/L seems to be enough under the conditions used. Again and not surprisingly the shape of this curve was exactly the same as the shape of the curve calculated in the batch mode for the influence of catalyst amount on the conversion: compare Figure 7.32 with Figure 7.12 in the batch calculations.

The same calculations were performed at lower temperatures (20 ºC feed temperature) since the reaction rate is strongly dependent of the temperature. Figure 7.33 shows the performance of the MPFMR with different catalyst loadings. Operating below 150 g/L, the model crashes because it calculates a negative driving force for water in the beginning of the reactor. With low catalyst loadings the water formation in the beginning of the reactor was very low. On the other hand, a well mixed permeate side was assumed in the model so a high water concentration in the permeate side was assumed all along the reactor. Due to these two reasons a negative driving force can be obtained (at least mathematically) in the beginning of the reactor.

Comparison of Figure 7.32 with Figure 7.33 it can be seen that at a lower process temperature the amount of catalyst loaded is more critical.

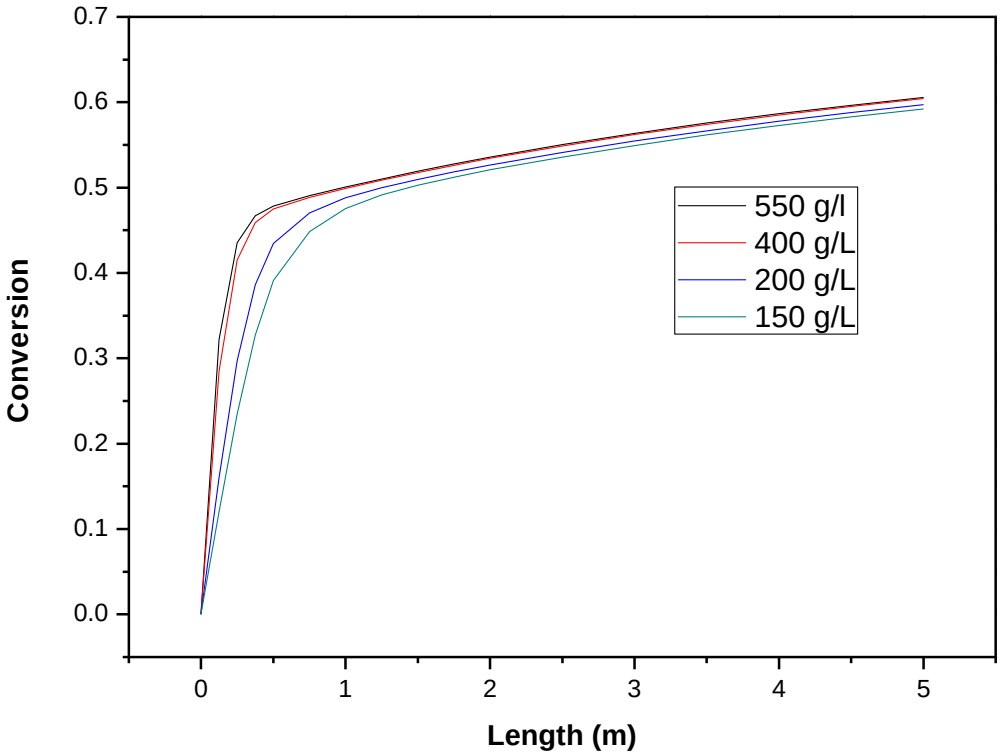

Figure 7.33 Effect of the catalyst loading on the conversion along the reactor. Conditions: feed temperature 20 ºC in adiabatic mode with a stoichiometric feed ratio, 5 mbar in the permeate side and 8 meters of reactor length.

7.2.2.6.4 Effect of the feed composition

As already explained in previous sections, it is known that an excess of one of the reactants shifts the reaction to the forward direction achieving higher conversions. In the present case, from the industrial point of view, the use of ethanol in excess is more logical than using butanal in excess since ethanol is far cheaper than butanal.

However, from the pervaporation point of view, ethanol is the smallest organic molecule in the reaction mixture and thus, it is the compound which has a higher tendency to pass through the membrane. For this reason it must be studied if the increase of ethanol driving force entails an important loss of this compound through the membrane.

Different ethanol/butanal feed ratios were used in the simulations in order to see the final conversion and on the other hand, to check if an important amount of ethanol would be lost. According to the obtained results in the previous sections, all the simulations were performed at 70 ºC as feed temperature (adiabatic reactor), 50 g/L of catalyst loading (in the previous section it was found that 50 g/L of catalyst is enough) and 8 meters of reactor length. As in every case, the volumetric feed flow rate was 7 L/h.

Figure 7.34 shows that by increasing the excess of ethanol significant conversion increases can be achieved. Working with 4:1 ethanol/butanal molar feed ratio, interesting conversions (around 70 %) can be achieved with 2 meters of reactor. When increasing the reactor length the conversion still increases rather strongly. This implies that the amount of water that was removed was not yet maximized. A reactor length of 20 meter will give a conversion of about 95%. If this is still realistic from a cost and revenue point of view is a different question.

In Figure 7.35 it can be observed that the ethanol loss through the membrane was not so significant at higher ethanol feed ratios, even though the driving force increased strongly. The main reason for this was that the water concentration in the feed was rather high and the membrane still permeated a lot of water (see Figure 7.36). As compared to the batch simulations done at different feed ratios here the water concentration in the permeate was still high. This indicates that the membrane area could still be increased to increase the conversion without having a too large loss of ethanol.

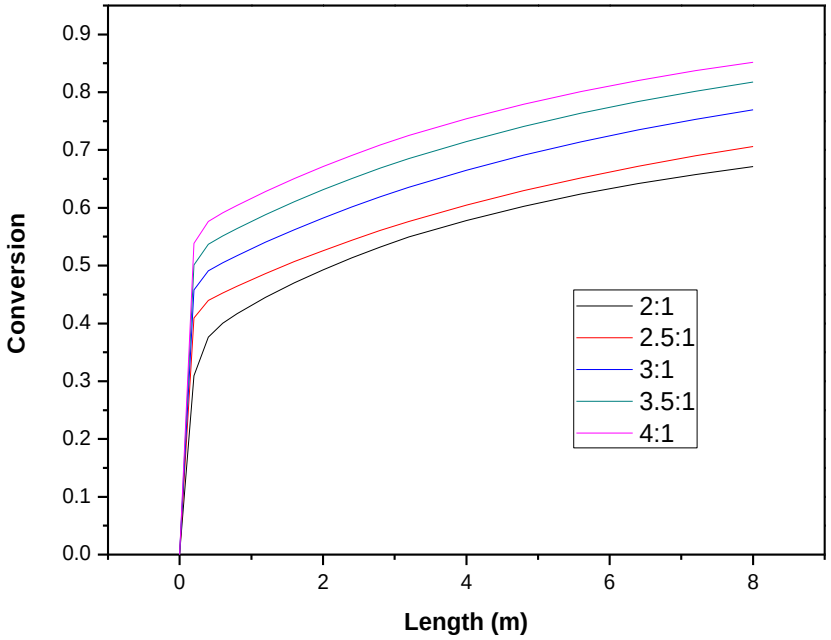

Figure 7.34 Achieved conversion vs. reactor length at different feed ratios. Conditions: Feed temperature: 70ºC, 8 meters of reactor length, 50 g/L of catalyst loading and 5 mbar in the permeate.

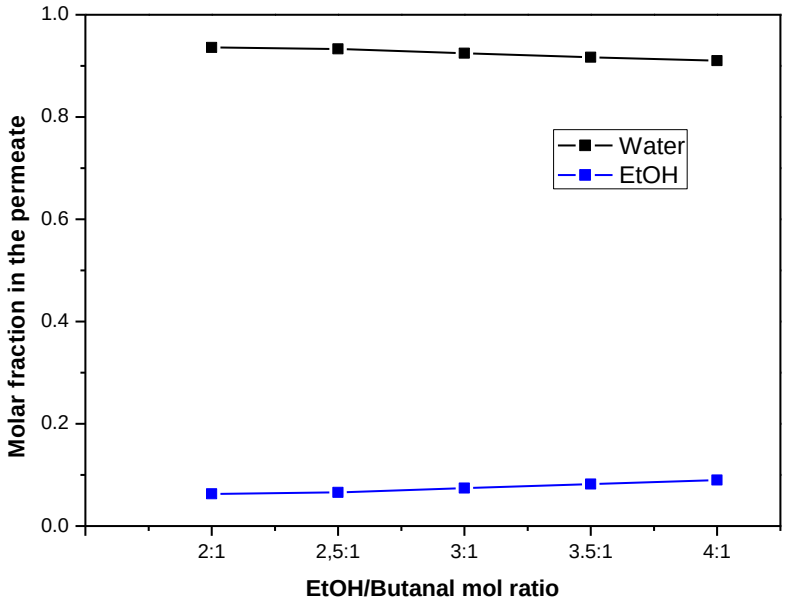

Figure 7.35 Ethanol and water molar fraction in the permeate at different ethanol/butanal feed ratios. Conditions: Feed temperature: 70ºC, 8 meters of reactor length, 50 g/L of catalyst loading and 5 mbar in the permeate.

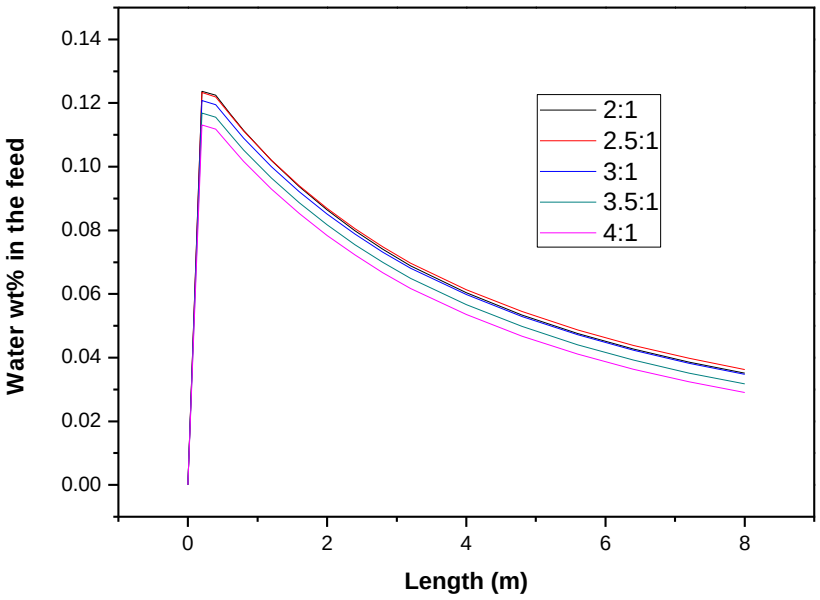

Figure 7.36 Water molar fraction in the feed at different ethanol/butanal feed ratios. Conditions: Feed temperature: 70ºC, 8 meters of reactor length, 50 g/L of catalyst loading and 5 mbar in the permeate.

7.2.2.6.5 Adiabatic vs Isothermal MPFMR

In this section the performance of an adiabatic MPFMR and an isothermal one will be compared. Figure 7.37 shows the performance of the reactor under the following conditions:

- Feed temperature: 70 ºC
- Feed flow rate: 7 L/h
- Stoichiometric feed ratio (2:1 in mol of ethanol/butanal)
- 50 g/L of catalyst loading
- 5 mbar in the permeate
- Reactor length: 5m

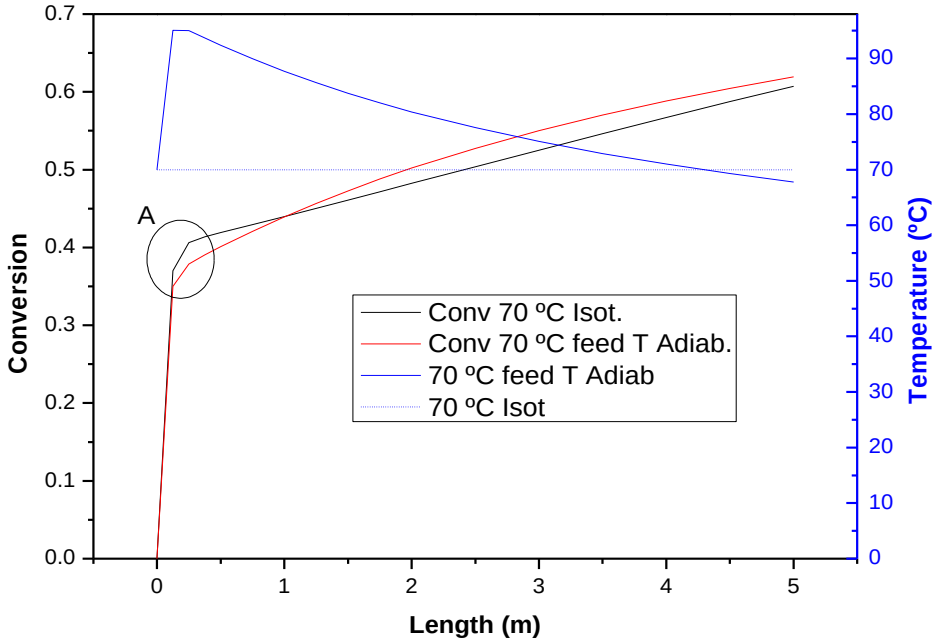

Figure 7.37 Conversion for an adiabatic vs. an isothermal reactor as function of the reactor length. Conditions: Feed T: 70 ºC, stoichiometric feed ratio, reactor length: 5 m, 50 g/L of catalyst loading and 5 mbar in the permeate side.

It can be observed that in the adiabatic case the equilibrium conversion for the initial conditions ("*A*" point) was lower than in the isothermal case due to the reaction exothermicity but then the conversion increase was higher due to a more efficient pervaporation process. These observations can be easily explained by the temperature profile along the reactor. In the adiabatic case, in the very first reactor sections the temperature increased considerably due to the reaction and therefore, the corresponding equilibrium conversion was lower. Then the temperature started decreasing due to the pervaporation but most of the time it remained above 70 ºC, which was higher than in the isothermal case and that is the reason why the pervaporation rate (and thus conversion) was higher in the adiabatic case. At longer reactor lengths the temperature in the adiabatic reactor would become (much) lower than in the isothermal case and then the conversion in the isothermal case could be above the adiabatic one again.

There is not any significant difference between an isothermal and an adiabatic case. However, at an industrial scale, an isothermal process is much more expensive and very difficult to implement. The overall energy produced and consumed is maybe close to zero but first a strong reactor cooling is needed and then a slow heat input is needed. To couple these two heat exchanger systems is maybe possible but difficult.

7.2.2.6.6 Effect of the permeance

In the previous sections it was estimated that it is possible to achieve conversions around 75% with a stoichiometric feed ratio. However, 15 meters of reactor were necessary to treat 7 L/h of feed flow rate which is not really feasible. An option was to increase the membrane surface area to volume ratio but this would mean that wall slip effects become significant, as explained in Section 7.2.2.5. Here the effect of membrane different permeance values will be studied; i.e., how much should the permeance increase in next membrane generations in order to have compact reactor dimensions in order to keep the same conversion (for the case under study).

Figure 7.38 shows the necessary reactor length to achieve 75% of conversion. All the simulations were performed using the following conditions:

- Feed pressure: 3 bar
- Feed temperature: 70 ºC (adiabatic mode)
- Stoichiometric feed ratio
- 5 mbar in the permeate
- 50 g/L of catalyst loading
- The permeance values of all the components were increased in the same range keeping the same permselectivities.

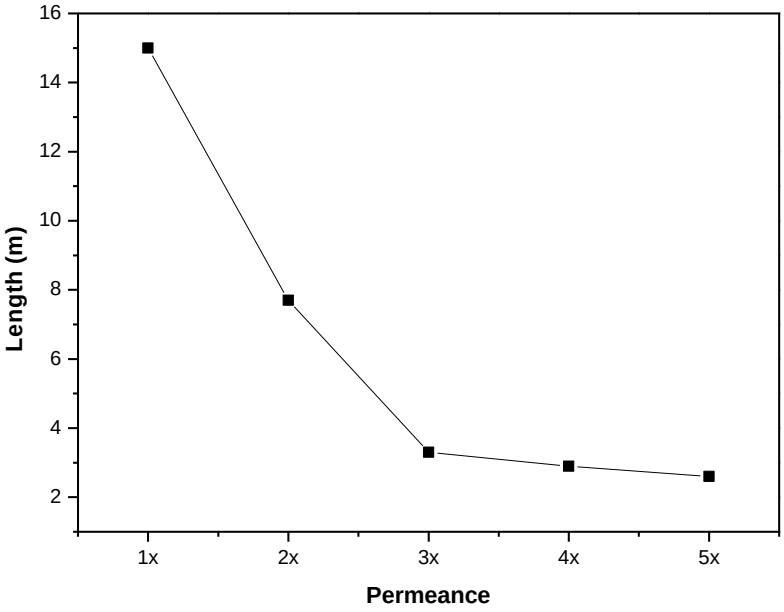

Figure 7.38 Effect of the permeance values based on simulation results. Conditions: Feed pressure: 3 bar, feed temperature: 70 ºC, stoichiometric feed ratio, 5 mbar in the permeate, 50 g/L of catalyst loading.

It can be observed that by increasing the permeance values 3 times the necessary reactor length is 3.3 meters and no significant improvement was achieved with a further increase of the permeance values. In all these simulations the permselectivities were assumed to be constant in all the cases.

This same effect could be achieved by increasing the surface area to volume ration by a factor of 3.3. However, for the options 17 (Table 7.9) not much improvement was possible anymore if the criteria of the tube distance = 8* the catalyst particle size is not modified.

7.2.2.7 Effect of a recycle loop

In Sections 7.2.2.5 and 7.2.2.6 different reactor configurations were tested. "*Configuration 17 A70"* was tested so far, as the best configuration within an acceptable Re regime. These simulations were done without using recycle to optimize the process and conversion. "*Configuration 18 A70"* offers a somewhat higher membrane area to volume ratio (Table 7.9) and thus higher conversions but the Reynolds number indicates a laminar regime. At such low Re numbers, concentration- and temperature polarizations effects could become very important. They were not taken into account in the model equations and calculations and thus the real conversion must be lower than the predicted one.

In this section a new process configuration is tested only for "*Configuration 18 A70"* and the Multifunctional membrane reactor. Part of the retentate can be recycled to the feed increasing the total flow rate in the reactor and thus, increasing the Re number. The objective is to check if it is possible to keep or increase the conversion by increasing the Re number in this way.

A simple stream splitter was placed in Aspen Custom Modeler after the membrane reactor. The temperature, pressure and composition of "Recycle", "Finalretentate" and "Retentate" streams are maintained exactly the same. The mixer placed before the reactor works as a mixer but also as a pump and a heat exchanger in order to ensure that feed temperature and pressure keep on being 70 ºC and 1 bar respectively. Figure 7.39 shows the scheme of the process. All the simulations were performed in the following conditions:

- Module diameter: 58 mm (using the A70 catalyst, see Table 7.9)
- Membrane outer diameter: 14 mm
- Number of membrane pipes: 7
- Length of the reactor: 1m

- Feed temperature to the reactor: 70 ºC (adiabatic case)
- Feed pressure to the reactor: 1 bar
- Stoichiometric feed ratio (Ethanol/butanal ratio 2:1 in mols)
- Permeate pressure: 5 mbar
- Catalyst loading: 50 g/L

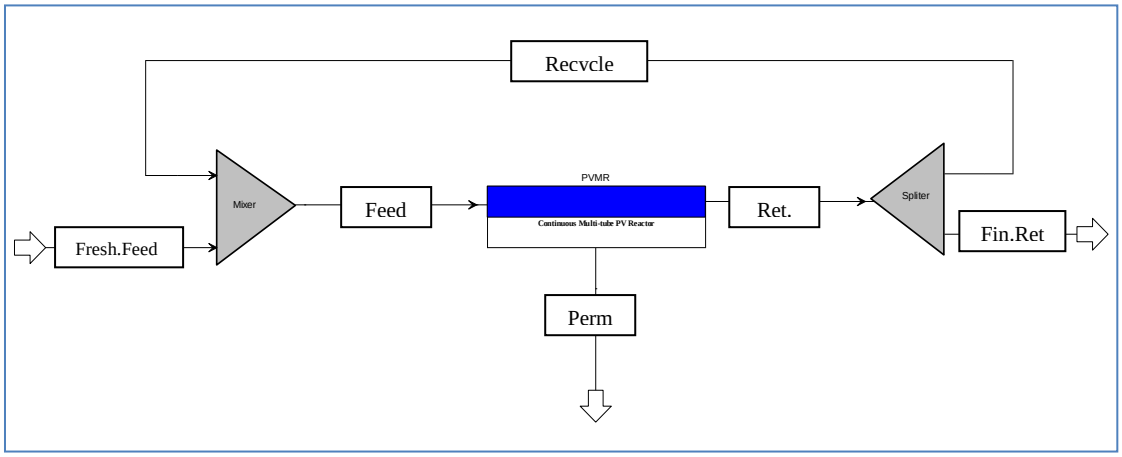

Figure 7.39 Scheme of the new process configuration including a recycling loop.

Table 7.12 shows the effect of the recycle ratio (R) on the process. The recycle ratio was defined as the quotient between the recycle stream molar flow rate and the molar flow rate of the retentate stream. It can be observed that by increasing the recycle ratio the conversion decreases considerably. Moreover, the water molar fraction in the retentate increases with the recycle ratio due to the lower residence time. On the other hand, only with the highest recycle ratio (0.9) acceptable Re numbers could be achieved.

Table 7.12 Effect of the recycle ratio on the process conversion, water concentration in the retentate and Re number.

R	Conversion	Re	Water molar frac. Retentate
0	66.4	1.4 - 2.5	0.0389
0.1	63.3	1.6 - 2.7	0.0403
0.2	59.7	1.9 - 2.9	0.0420
0.3	55.5	2.2 - 3.2	0.0439
0.4	50.8	2.6 - 3.5	0.0460
0.5	45.3	3.1 - 4.1	0.0483
0.6	39.0	4.0 - 4.9	0.0509
0.7	31.6	5.4 - 6-2	0.0537
0.8	22.9	8.1 -9	0.0569
0.9	12.0	16.4-17.2	0.0603

Further simulations were performed with R = 0.9 and increasing the length of the reactor in order to decrease the water concentration in the retentate and thus increase the conversion. However, insignificant improvement was observed in the conversion values (see Figure 7.40). It seems that the presence of the (extra) acetal in the feed affects the reaction in a negative way by decreasing the ethanol and butanal concentrations and increasing the effect of the reverse reaction.

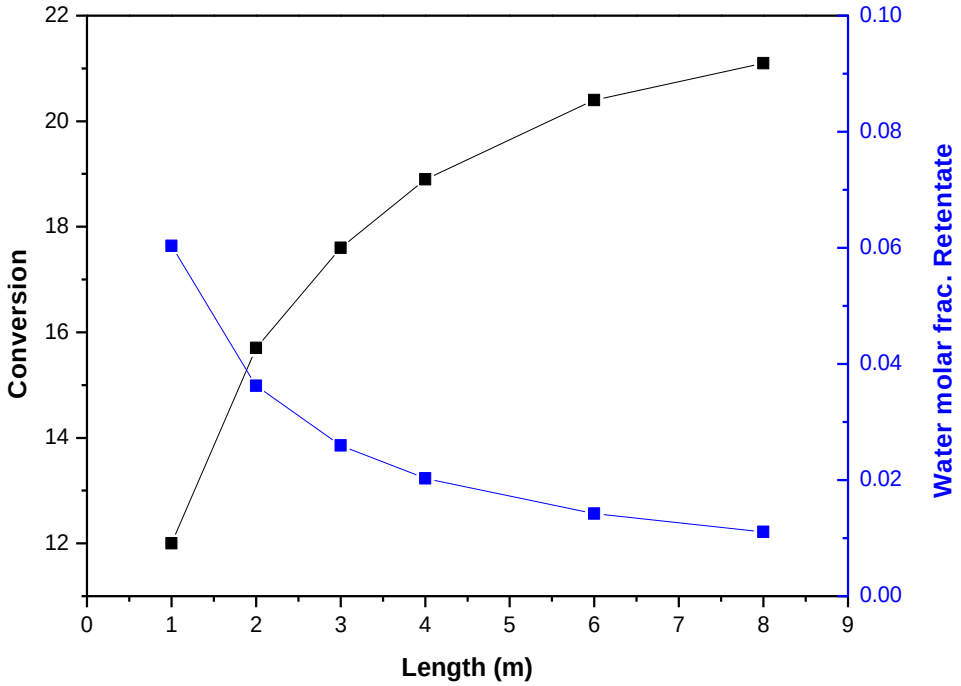

Figure 7.40 Effect of the reactor length on the conversion and the water concentration in the retentate.

7.2.2.8 Conclusions for a multitube plug flow membrane reactor configuration

A multitube plug flow membrane reactor (MPFMR) was modeled. By using this continuous reactor and separator the conversion of the acetalization reaction can be increased to above the equilibrium conversion.

Comparison of the modeling results of this continuous process with the batch process in Section 7.1.3 shows that the results are comparable. As the batch model was validated with experiments this is a clear indication that the continuous model is also validated.

First of all an optimum reactor geometry was calculated. In general the larger the outer diameter of the membrane tube the more optimal the reactor geometry. The reason for this was that the membrane surface area to volume ratio was increasing under the constraints used. Two different configurations were chosen "*Configuration 17 A70"* and

"Configuration 18 A70" as the most suitable ones. The first of the configurations (having an optimized feed flow characteristic) showed low conversion values but after a sensitivity analysis it was checked that 75 % of conversion could be reached. However, 15 meters long reactor would be necessary in order to achieve this conversion.

Secondly, *"Configuration 18 A70*" (having an optimized membrane surface area) showed interesting conversion values but at very low Re numbers. This could lead to not acceptable polarization effects that were not considered in the simulation model. In order to increase the turbulence part of the retentate was recycled to the feed. It was checked that increasing the Re number the conversion decreases considerably.

Operating the system in an adiabatic mode is preferred over an isothermal mode. The reason is that in the adiabatic mode the temperature increase because of the exothermic reaction helps increasing the membrane flux. Thus the water removal rate is higher and the shift over equilibrium is increased further.

It can be said that in order to avoid wall effects due to the presence of catalyst particles, the distance among membrane pipes is too high. As a consequence, the available membrane area in the reactor is not high enough to achieve high conversions with reasonable reactor dimensions in a continuous process mode. However, it was checked that if a new membrane generation offers 3 times higher fluxes than the actual ones, the developed membrane reactor would have acceptable dimensions to treat 7 L/h of feed flow.

For this reason, other process designs where the reaction and pervaporation take place in different units were studied. This is reported in the next section.

7.2.3 Plug flow reactor (PFR) + Pervaporation (PV) module development and calculations

In the model development and calculations presented in this section reaction and pervaporation processes were uncoupled in order avoid design constraints due to the presence of catalyst particles among membrane tubes. The main design constraint as presented in the previous section seems to be the catalyst amount and membrane area to be too strongly coupled to each other. With the configuration presented here this is hopefully overcome. In this case, similar assumptions were made to develop the model equations. The only difference is that the pressure drop was considered negligible in the pervaporation module. This assumption is based upon the fact that now the pervaporation process was not taking place in a packed bed. The used assumptions are:

- The reactor behaves as an ideal plug flow reactor (PFR).
- The main transport resistance was in the selective top layer of the membrane.
- Concentration polarization and temperature polarization effects were considered negligible.
- The selective top layer of the membrane was on the outside (shell side) of the membrane tube.
- The tube side (permeate side) is considered a perfect stirred mixture.
- A pseudo-homogeneous kinetic model was assumed.
- The membrane is completely inert and it did not influence the reaction kinetics.
- Permeance values depend only on the temperature. The influence of the concentration of each compound on permeance values was considered negligible.

Different process configurations were tested. In all the cases the base case was a plug flow reactor followed by a pervaporation module as shown in Figure 7.41. The cases that were calculated and which results are presented in detail in Section 7.2.3.5 are:

- PFR + PV modules in series
- PFR + PV including a recycle loop
- PFR + PV + Distillation column recycling the top stream of the distillation

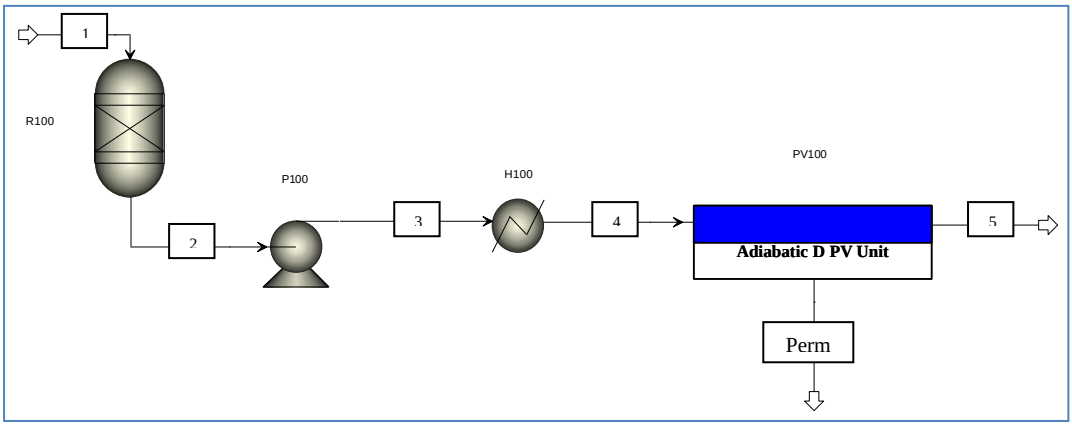

Figure 7.41 Scheme of the base configuration: a PFR reactor followed by a PV module. A heat exchanger and a pump were also included.

Adiabatic reactors and pervaporation modules were considered. From the reaction point of view it is known that at low temperatures higher conversions can be achieved but the reaction rate would be lower and longer/larger reactors would be necessary. By operating in adiabatic mode the reactants can be fed at room temperature (low temperature) but in the output of the reactor the temperature would be much higher (exothermic reaction) which is beneficial for the pervaporation process that is placed afterwards.

7.2.3.1 Equations

All the equations that describe the plug flow reactor and the pervaporation module were developed exactly in the same way than in Section 7.2.2.2. In fact, in the end, the developed equations are simplifications of the previous ones. Table 7.13 shows the equations for the reactor while Table 7.14 shows the corresponding ones for the pervaporation module.

Table 7.13 Developed equations for the plug flow reactor (PFR)

Equations	**Unknown variables**
• **<u>PLUG FLOW REACTOR (PFR)</u>**	
• <u>Mass balance on the shell side</u>	
$\frac{dF_A}{dz} = L\,A_t\,r_A$	
$\frac{dF_B}{dz} = L\,A_t\,r_B$	F_A
$\frac{dF_C}{dz} = L\,A_t\,r_C$	$F_{B,}$
$\frac{dF_D}{dz} = L\,A_t\,r_D$	$F_{C,}$
• <u>Kinetics</u>	
$r_A = -2r_1 + 2r_4$ $\quad r_1 = wk'\,F_A^2 F_B \frac{1}{\upsilon^3}$	F_D
$r_B = -r_1 + r_4$	
$r_C = r_1 - r_4$ $\quad r_4 = wk_4'\,F_C F_D \frac{1}{\upsilon^2}$	
$r_D = r_1 - r_4$	
• <u>Energy balance</u>	
$\frac{dT}{dz} = \frac{\left[(-\Delta H_r(T))\,(-r_B)\right] L\,A_t}{\sum(F_i C_{p,i})}$	T
• <u>Momentum balance</u>	
$\frac{dP_F}{dz} = L\left[\frac{150\,\mu(1-\varepsilon)^2 v_s}{\phi\,\varepsilon^3 d_p^2} + \frac{1.75(1-\varepsilon) v_s^2\,\rho}{\phi\,\varepsilon^3 d_p}\right] * 10^{-5}$	P

Where:

F_i	molar flow rate (kmol/h) for component *i*
L	reactor length (m)
A_t	cross sectional area (m^2)
r	reaction rate (kmol/h)
T	temperature (ºC)
ΔH_r	enthalpy of reaction (kJ/kmol)
C_P	specific heat (kJ/(kmol·K))
P_F	pressure on the feed side (bar)
μ	dynamic viscosity of the liquid on the feed-retentate side (Pa·s)

ε	void fraction
v_s	superficial velocity (m/s)
Φ	indicates the sphericity of particles (Φ=1)
d_P	catalyst particle diameter (m)
ρ	density of the liquid on the feed-retentate side (kg/m^3)

Table 7.14 Developed equations of the pervaporation module (PV).

Equations		**Unknown variables**
• **PERVAPORATION MULTI-TUBE MODULE (PV)**		
• Mass balance on the shell side		
$\frac{dF_A}{dz} = -f_A \; p_m \; L$		F_A
$\frac{dF_B}{dz} = -f_B \; p_m \; L$		$F_{B,}$
	$f_i = Q_i \; (\gamma_i x_i P_i^{sat} - y_i P_P)$	
$\frac{dF_C}{dz} = -f_C \; p_m \; L$		$F_{C,}$
$\frac{dF_D}{dz} = -f_D \; p_m \; L$		F_D
• Permeate side		
$y_A = \frac{\int_0^{A_m} f_A \, dA_m}{\sum_i \int_0^{A_m} f_i \, dA_m}$	$y_B = \frac{\int_0^{A_m} f_B \, dA_m}{\sum_i \int_0^{A_m} f_i \, dA_m}$	y_A
		y_B
$y_{Ci} = \frac{\int_0^{A_m} f_C \, dA_m}{\sum_i \int_0^{A_m} f_i \, dA_m}$	$y_D = \frac{\int_0^{A_m} f_D \, dA_m}{\sum_i \int_0^{A_m} f_i \, dA_m}$	y_C
		y_D
• Energy balance		
$\frac{dT}{dz} = \frac{N \pi d_0 L \left[-J \left\lvert \overline{\lambda_i} \right\rvert \right]}{\sum (F_i C_{p,i})}$	$J = \sum_i f_i$	T

Where:

F_i	molar flow rate (kmol/h) for component *i*
f_i	the flux (kmol/(m^2·h))
p_m	outer perimeter of membrane tubes (m)
L	length of the PV module (m)
Q_i	permeance (kmol/(m^2·h·bar))
γ_i	activity coefficient
P_i^{sat}	saturation pressure (bar)
P_P	permeate pressure (bar)
x_i	liquid molar fraction on the feed side
y_i	vapor molar fraction on the permeate side
A_m	membrane area (m^2)
N	number of membrane tubes
d_0	membrane outer diameter (m)
λ_i	latent heat of the permeating fluid (kJ/kmol)
C_P	specific heat (kJ/(kmol·K))
J	total flux (kmol/(m^2·h))

7.2.3.2 Multi-tube pervaporation module design

As well as in the MPFMR case, in order to ensure that all the simulations were not in the laminar regime, an initial module design was required to know the cross section through which the fluid passes (to calculate the fluid velocity) and the maximum membrane area that can be placed per cubic meter of module.

The module design was based on the shell-and-tube heat exchangers. Membrane pipes can be placed following different layouts and also in this case the equilateral triangular layout was chosen. This kind of configuration is the one which offers the highest membrane area to volume ratio. In the present case the absence of catalyst particles between membrane pipes allows to have smaller membrane to membrane pipe distances and thus more membrane area is available per cubic meter of pervaporation module. The typical pitch distance between pipes in heat exchangers is 1.25-1.33 times the pipe diameter (60;83) (see Figure 7.42). In this kind of configurations, membrane tubes create turbulence and the limiting Re numbers for laminar and turbulent flow regimes are slightly different comparing to Re limits for flow through pipes. For shell-and-tube heat exchangers the Re limits are the following ones (60;83):

Re < 20	Laminar flow
20 < Re < 100	Transition zone
Re > 100	Fully turbulent flow

In these cases, the outer diameter of the membrane pipes must be used for Re number calculation (see equation (7.57) (83):

$$Re = \frac{d_0\, v\, \rho}{\mu} \tag{7.57}$$

Where:
- d_0 membrane pipe outer diameter (m)
- v fluid velocity (m/s)
- ρ density of the fluid (kg/m^3)
- μ dynamic viscosity (Pa·s)

In all the simulations the Re number was between 20 and 100. Moreover, in this kind of module configurations more turbulent regimes can be achieved by inserting different baffles along the module.

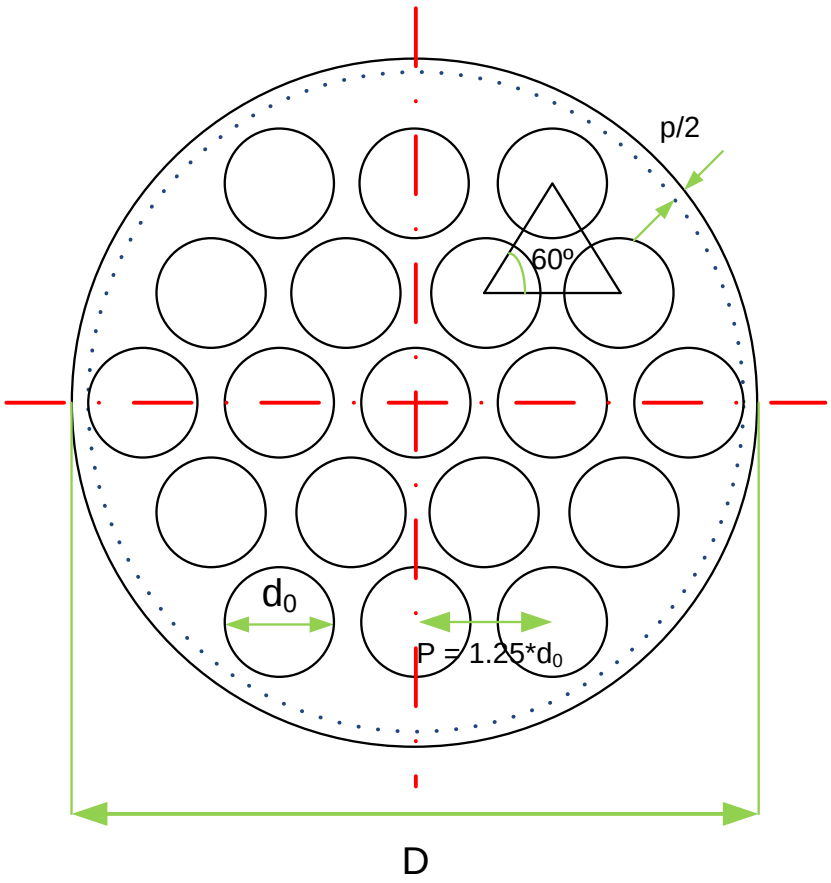

Figure 7.42 Geometric characteristics of the PV module.

Once the geometry of the MPFMR was defined, the next step was the calculation of the number of membrane pipes that can be placed in a certain module diameter. Also in this case three different calculation methods were available:

- Mathematical algorithm based on the shell diameter, membrane diameter and pipe to pipe distances which was developed in ASPEN CUSTOM MODELER.
- 2 different correlations (7.55) & (7.56) based on geometrical approximations

The mathematical algorithm was chosen as the best method. As it is explained in section 7.2.2.5 the two correlations entail quite important errors when small shell diameters are involved. The only difference between this algorithm and the developed one in case of the MPFMR deals with the pipe to pipe distance definition. In this case it is function of the pitch coefficient and membrane diameter instead of the catalyst particle diameter. The code used for the calculations is shown in Figure 7.43.

```
// Relation between "pitch distance" and membrane tube diameter:

   p:pitch coef*Membrane diameter;

// Distance among membrane tube rows:

   height:p*SQRT(3)/2;
   NrOfFloors: truncate((0.5*Shell diameter-(p/2-Membrane diameter/2)-Membrane diameter/2)/height);

For i in [0:NrOfFloors] Do
 If truncate(i/2)=i/2 Then
   Len(i):SQRT((0.5*Shell diameter)^2-(i*height)^2);
   NrOfPipesPerFloor prov(i):1+2*truncate((Len(i)-0.5*Membrane diameter-(p/2-Membrane diameter/2))/p);
   dist_cen(i):sqrt(((truncate(NrOfPipesPerFloor_prov(i)/2))*p)^2+(i*height)^2);
   if (Shell diameter/2-dist cen(i))<(p/2) Then
     NrOfPipesPerFloor(i):NrOfPipesPerFloor prov(i)-2;
   Else
     NrOfPipesPerFloor(i):NrOfPipesPerFloor prov(i);
   Endif
 Else
   Len(i):SQRT((0.5*Shell_diameter)^2-(i*height)^2);
   NrOfPipesPerFloor prov(i):2*truncate(Len(i)/p);
   dist_cen(i):sqrt(((NrOfPipesPerFloor prov(i)/2-1)*p+p/2)^2+(i*height)^2);
   if (Shell diameter/2-dist cen(i))<(p/2) Then
     NrOfPipesPerFloor(i):NrOfPipesPerFloor prov(i)-2;
   Else
     NrOfPipesPerFloor(i):NrOfPipesPerFloor prov(i);
   Endif
 EndIF
EndFor

TotalNumberOfPipes : 2*sigma(NrOfPipesPerFloor)-NrOfPipesPerFloor(0);
MembraneArea = TotalNumberOfPipes *3.14*Membrane_diameter*TubeLength;

End
```

Figure 7.43 Code to calculate the number of membrane pipes in the PV module.

A preliminary design study was performed in order to choose the best geometrical configuration. Commercially available membrane tube outer diameters were used for this study (3, 4, 6, 7, 10 and 14 mm). Table 7.15 shows all the tested configurations.

Table 7.15 Different geometrical configurations for the PV module. Conditions: Length: 1m, feed flow rate: 7 L/h, Feed T: 70 ºC, adiabatic module, permeate pressure of 5 mbar and 5wt% of water in the feed.

	1	2	3	4	5	6	7	8	9
D (m)	0.029	0.027	0.03	0.029	0.025	0.032	0.029	0.023	0.034
d0 (m)	0.003	0.003	0.003	0.004	0.004	0.004	0.006	0.006	0.006
N_t	37	37	43	19	19	31	7	7	13
Am (m^2)	0.35	0.35	0.41	0.24	0.24	0.39	0.13	0.13	0.24
m2_m3	874.0	1121.2	1005.8	566.1	947.0	939.4	285.2	606.5	453.5
Re	17.6-30.8	22.6-39.5	17-30.5	23.8-38.8	39.9-64.9	22.2-39.5	37-53.1	78.8-113	27.8-45.5
η (%)	71.0	71.0	73.4	63.5	63.5	72.8	48.8	48.8	64.0

	10	11	12	13	14	15	16	17	18
D (m)	0.029	0.027	0.04	0.029	0.013	0.038	0.029	0.018	0.053
d0 (m)	0.007	0.007	0.007	0.01	0.01	0.01	0.014	0.014	0.014
N_t	7	7	13	1	1	7	1	1	7
Am (m^2)	0.15	0.15	0.29	0.03	0.03	0.22	0.04	0.04	0.31
m2_m3	393.57	507.77	377.99	53.98	579.71	376.34	86.82	437.50	272.79
Re	49.4-73.3	63.8-94.5	22.44-37.9	62.3-70.3	669-755	43.7-70	96.2-113	485-570	29.7-50.8
η (%)	52.8	52.8	67.3	17.9	17.9	61.6	23.5	23.5	68.8

"η" indicates the water separation efficiency (%):

$$\eta = \frac{F_{w,0} - F_{w,1}}{F_{w,0}} \tag{7.58}$$

Where:

$F_{w,0}$ water molar flow rate on the feed side (kmol/h)

$F_{w,1}$ water molar flow rate on the retentate side (kmol/h)

In these preliminary calculations a module diameter of 29 mm was taken as a basis for all 6 different membrane diameters. Then, based upon these results the configuration was optimized either by reducing the module diameter as far as possible but keeping the same number of membrane pipes in the reactor or by increasing the module diameter in order to introduce more membrane pipes.

"*Configuration 3*" was chosen as the best one since it offers the best water separation efficiency. This separation efficiency was the highest one as the membrane area to volume ratio was also the highest one. Re numbers were just in the limit between laminar flow and transition zone but it did not represent any problem since a more turbulent flow can be obtained inserting some baffles.

7.2.3.3 Sensitivity analysis of the reactor

A sensitivity analysis of the plug flow reactor (not including the pervaporation section) was performed in order to check that the model behavior was completely logical. As it is indicated in Section 7.2.3 an adiabatic reactor was considered since a temperature increase is obtained having higher temperatures in the feed side of the pervaporation module.

As a standard reactor configuration a length of 0.5 metro and a diameter of 15 mm were chosen. With this geometry and 7 L/h as a feed flow rate the turbulence was high enough in order to assume a plug flow and wall effects can be neglected.

The effect of the temperature and feed composition were studied.

7.2.3.3.1 Effect of the temperature

Four different feed temperatures were used in the modeling calculations: 25, 40, 55 and 70 ºC. As it is explained the acetalization reaction between ethanol and butanal is an exothermic reaction and operating in adiabatic mode the temperature increases along the reactor. Figure 7.44 shows the effect of feed temperature on the conversion as function of the normalized length of the reactor section.

As it was expected, the higher the feed temperature, the lower the conversion but the faster the equilibrium conversion is reached. The final conversions cannot be directly compared to the conversions obtained in the kinetic study since the temperature is not constant in the present case. Even though, predicted non isothermal conversions and the ones experimentally measured (isothermal) are quite similar (see Figure 3.5).

All the simulations performed in this section were in an appropriate flow regime according to the calculated Re numbers for packed beds (see Figure 7.45). It must be remembered that the limit between the laminar regime and the transition zone in packed beds is at Re = 10 (see Figure 7.24)

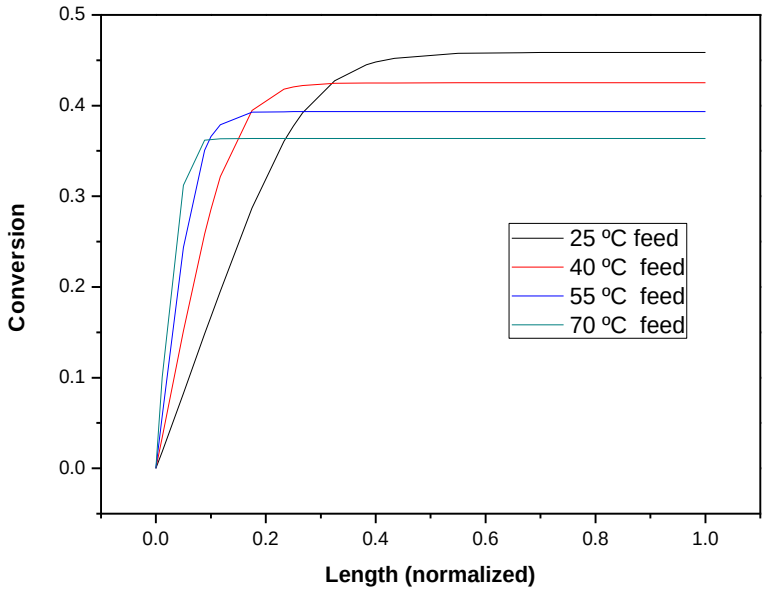

Figure 7.44 Effect of the feed temperature on the conversion vs normalised reactor length. Conditions: stoichiometric feed ratio, feed pressure: 1 bar.

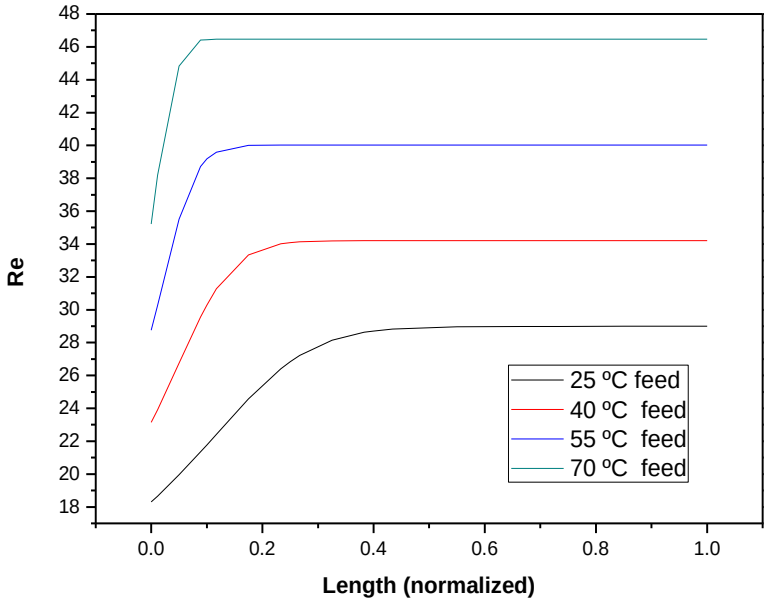

Figure 7.45 Re number along the reactor. Conditions: stoichiometric feed ratio, feed pressure: 1 bar.

As indicated previously, the temperature changes along the adiabatic reactor because of the negative enthalpy of reaction. The achieved temperature profiles are shown in Figure 7.46.

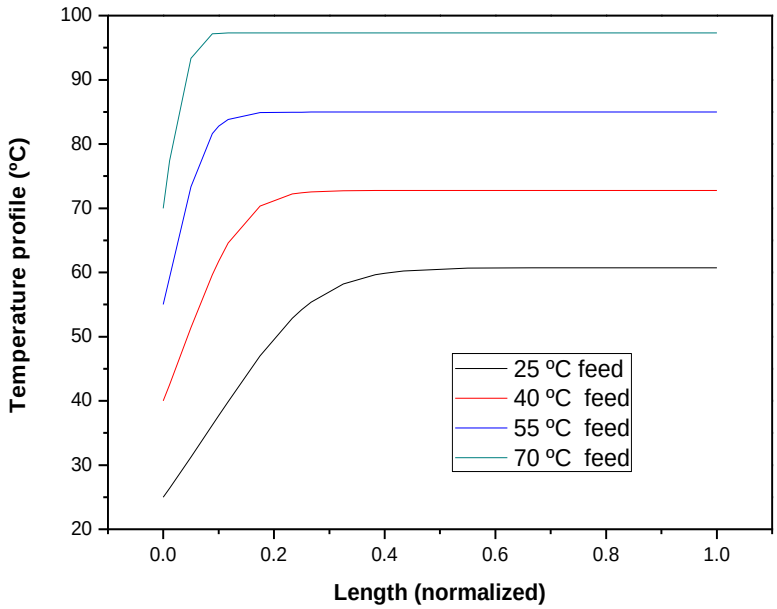

Figure 7.46 Temperature profile along the reactor. Conditions: stoichiometric feed ratio, feed pressure: 1 bar.

The temperature increases up to 97 ºC when the feed side temperature is 70 ºC. At higher feed temperatures the temperature reaches higher values with length than at lower temperatures as the kinetics are faster. However, the temperature increase is less as the limiting conversion at higher temperatures is lower. The vapor fraction profile was calculated along the reactor in order to ensure that the whole stream remains in liquid phase. It must be remembered that the reaction takes place in the liquid phase. Table 7.16 shows the vapor fractions at the different conditions.

It can be observed that by operating at atmospheric pressure vaporization occurs above certain temperatures. Figure 7.47 shows that the pressure drop in the reactor is not really important (only 25 ºC and 40 ºC feed temperature cases were considered since only liquid phase is assumed in the pressure drop calculation). As this pressure drop is very small (at least for these two temperatures) it was not considered important for a possible phase change of liquid into vapor.

Table 7.16 Vapor fraction profile along the reactor at different feed temperatures.

Length (normalized)	**Vapor fraction (ºC)**			
	25 ºC feed	**40 ºC feed**	**55 ºC feed**	**70 ºC feed**
0.000	0	0	0	0
0.011	0	0	0	0.971
0.050	0	0	0	1
0.089	0	0	0.798	1
0.100	0	0	0.825	1
0.117	0	0	0.842	1
0.175	0	0	0.856	1
0.233	0	0	0.857	1
0.250	0	0	0.857	1
0.267	0	0	0.857	1
0.325	0	0	0.858	1
0.383	0	0	0.859	1
0.400	0	0	0.859	1
0.434	0	0	0.860	1
0.550	0	0	0.862	1
0.666	0	0	0.863	1
0.700	0	0	0.864	1
0.734	0	0	0.864	1
0.850	0	0	0.866	1
0.966	0	0	0.868	1
1.000	0	0	0.868	1

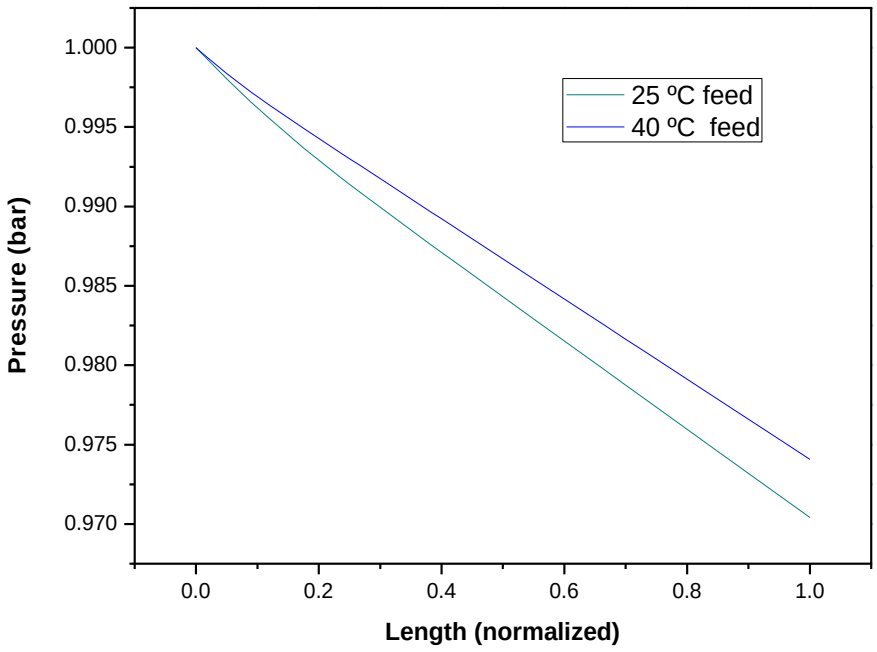

Figure 7.47 Pressure profile along the reactor. Conditions: stoichiometric feed ratio, feed pressure: 1 bar.

As indicated above, in all the simulations the reactor length was 0.5 m. It can be observed in Figure 7.44, Figure 7.45 and Figure 7.46 that the length can be reduced considerably depending on the process conditions to still reach the equilibrium in the reactor.

7.2.3.3.2 Effect of the feed composition

Three different ethanol/butanal molar feed ratios where tested: 2:1 (stoichiometric ratio), 3:1 and 4:1. As expected, by increasing the ethanol/butanal feed ratio higher equilibrium conversions can be achieved (see Figure 7.48). According to Le Chatelier principle an excess of one of the reactants implies higher equilibrium conversions at the same temperature. Also in this case, the achieved conversions cannot be directly compared to the conversion values obtained in the kinetic study because the temperature is not constant in this case. However, the predicted conversion values are comparable to the achieved ones experimentally.

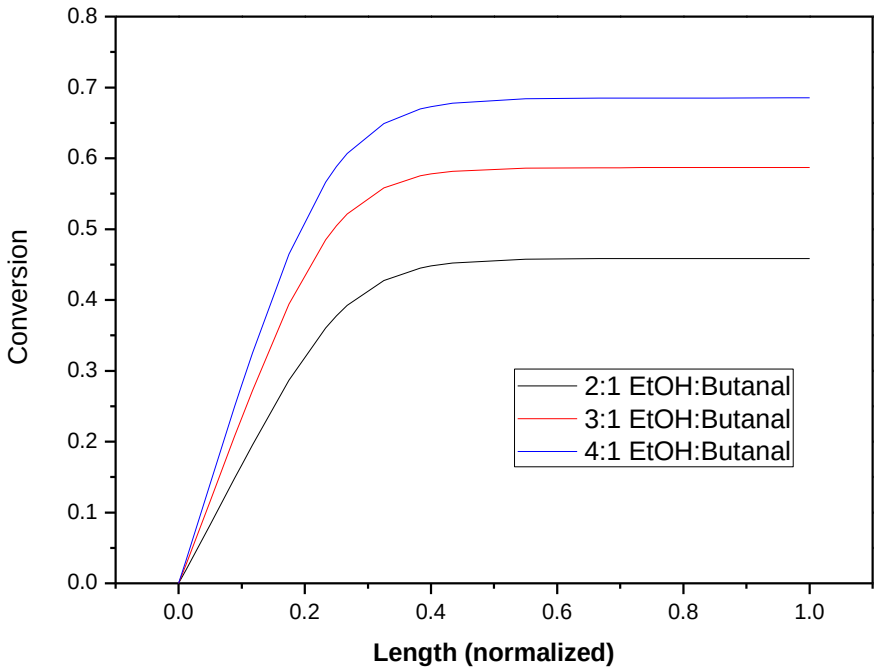

Figure 7.48 Effect of the EtOH/Butanal molar feed ratio on the conversion along the reactor. Feed temperature 25 ºC, reactor length: 0.5 m and reactor diameter 15 mm.

From this feed ratio sensitivity study it is clear that the reactor behavior is completely logical and as expected.

7.2.3.4 Pervaporation (PV) module

The pervaporation module was modeled at different feed temperatures. Also in this case an adiabatic module was chosen. At industrial scale adiabatic operated pervaporation processes are more common than isothermal processes. However, most of the times the pervaporation processes consist of series of pervaporation modules and heat exchangers in between. In these heat exchangers the retentate of the previous module is reheated to the feed temperature of the next module in order to maintain a high flux. In case of pervaporation isothermal modules show better efficiencies than adiabatic ones but the energy consumption is considerable. The choice of isothermal modules, intermediate heat exchangers or complete adiabatic operation depends on the costs. When the temperature drop is large, the membrane area needed strongly increases and thus the costs increase making isothermal operation the preferred option.

"*Configuration 3*" was the chosen geometrical configuration (see Section 7.2.3.2) in the calculations presented below. One meter of pervaporation module length was used in all the simulations. The PV feed composition was the output composition of the reactor as predicted by the plug flow reactor model (fed at 25 ºC) (see Table 7.17).

Table 7.17 Feed conditions for the pervaporation module.

Vol. Flow (L/h)	6.6
Pressure (bar)	0.97041
Molar frac. EtOH	0.432837
Molar frac. Butanal	0.210527
Molar frac. Acetal	0.178318
Molar frac. Water	0.178318

Figure 7.49 shows water concentration profiles along the module at different feed temperatures. As expected, the water concentration in the shell side decreases much faster at high feed temperatures, being a much more efficient process.

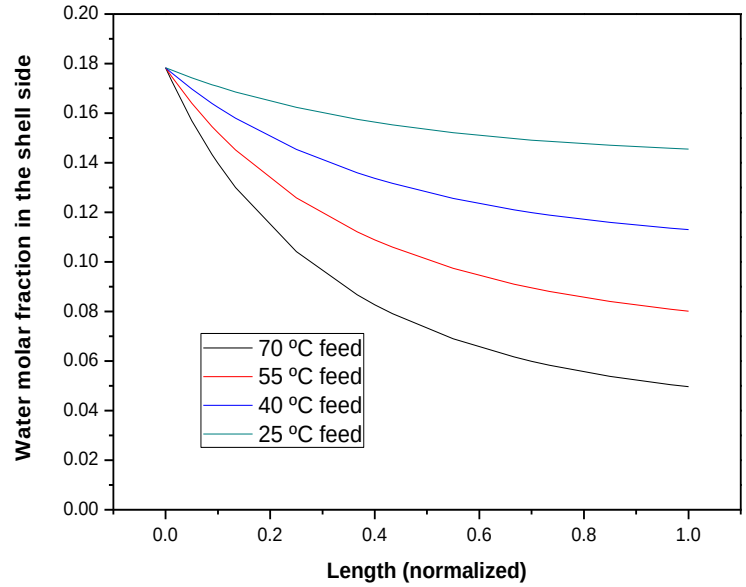

Figure 7.49 Water concentration profile along the PV module at different feed temperatures.

Figure 7.50 shows the temperature profile along the pervaporation module at different feed temperatures. It can be seen that the temperature drop was quite important at the highest temperatures. This effect is logical since at higher temperatures more water is evaporated and separated through the membrane and the heat for evaporation is taken from the feed. This graph indicates that from a membrane cost point of view it could be wise to have an isothermal operation of the pervaporation process. As a rule of thumb the membrane area needed doubles with a temperature decrease of 20°C.

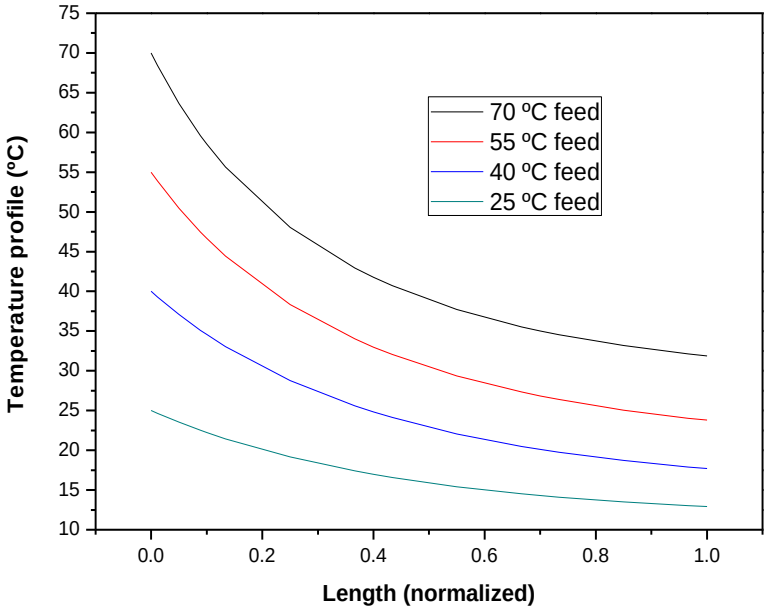

Figure 7.50 Temperature profile along the PV module at different feed temperatures.

Figure 7.51 shows the stage cut and the water molar fraction in the permeate at different feed temperatures. The stage cut is defined as the permeate molar flow rate / feed molar flow rate. Therefore, a higher stage cut value implies more separation through the membrane. It can be observed how the stage cut is in good agreement with the previous charts as it increases with the temperature. Besides, it was checked that the water concentration in the permeate did not change significantly in the studied temperature range. (The defined membrane area was 0.40506 m^2). The water content in the permeate was high. This water concentration first increased with temperature as the driving force for water transport increased faster than for the other components due to the reaction producing it. At higher temperatures this concentration then decreased as the feed stream was depleted in water and the permeation of the other components became more important.

Figure 7.52 shows the Re profile along the module. Due to the water separation (and thus the decrease of feed flow) it decreased considerably and it was below 20 in an important part of the membrane tube. In order to avoid concentration and temperature polarization effects some baffles should be included in the module in order to increase the turbulence rate.

In general the pervaporation modeling results were as expected and were in line with experimental results.

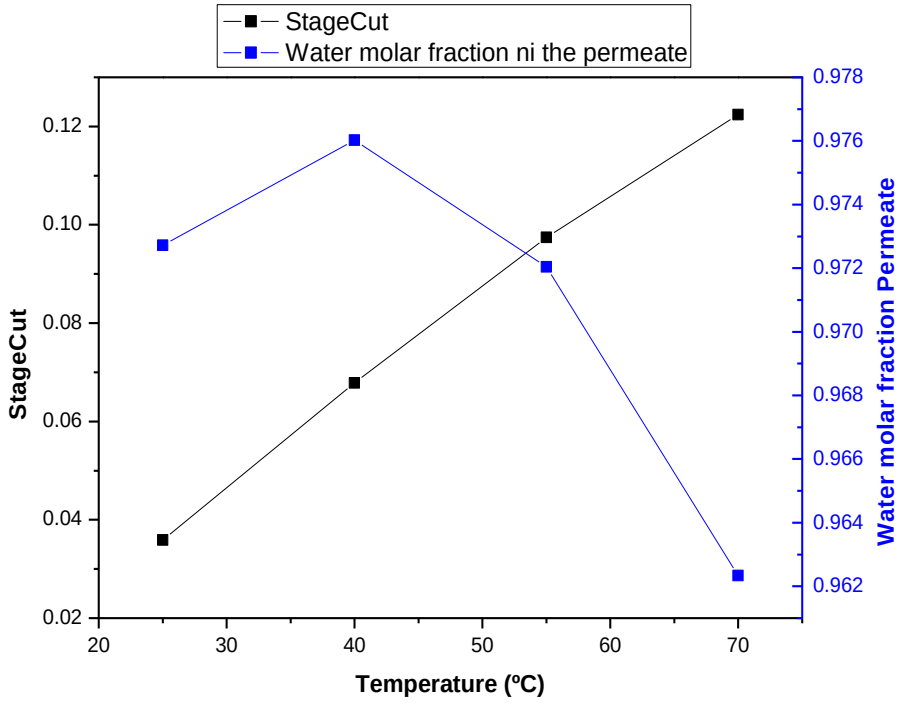

Figure 7.51 Stage cut and water concentration in the permeate at different feed temperatures.

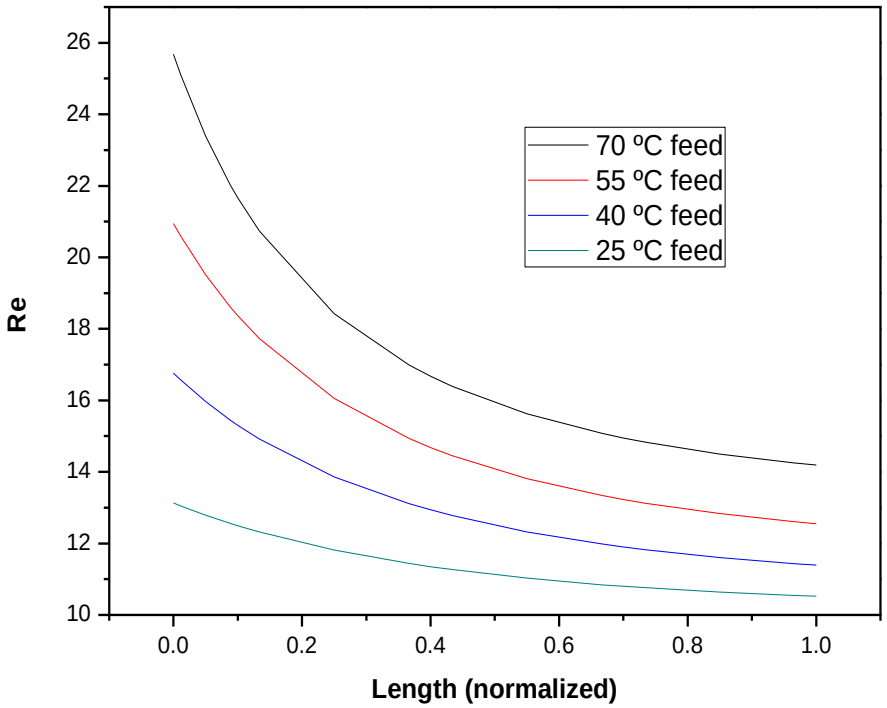

Figure 7.52 Re profile along the PV module at different feed temperatures.

7.2.3.5 Different process configurations based on PFR + PV units

In Section 7.2.2 it was found that an extremely long (15m) multi-tube plug flow membrane reactor (MPFMR) would be necessary in order to achieve high conversions. That was for a combined reactor-separator in one unit operation. In this section different alternatives were studied and in all the cases reaction and pervaporation processes were placed in different units. Three different process designs were calculated:

- PFR + PV modules in series
- PFR + PV including a recycle loop
- PFR + PV + Distillation column recycling the head of the distillation

7.2.3.5.1 PFR + PV modules placed in series.

Different adiabatic plug flow reactors and pervaporation modules were placed in series as shown in Figure 7.53. The main advantage of this configuration is that small reactors can be used with the maximum catalyst loading (550 g/L of Amberlyst 47) and on the other hand, more membrane area can be placed in pervaporation units putting membrane tubes much closer to each other as it is mentioned in Section 7.2.3.2.

The optimum number of reactors and PV units were estimated. As indicated above, adiabatic reactors and pervaporation units were chosen. Moreover, according to the sensitivity analysis performed in Sections 7.2.3.3 and 7.2.3.4 the input temperature to each pervaporation module should be as high as possible. For this purpose a heat exchanger, which warms up the mixture up to its bubble point temperature (around 77-80ºC) in each case, was placed after each PFR. The required energy to warm up the liquid mixture up to its bubble point was considered negligible. Table 7.18 shows reactor outlet temperatures.

The feed of the first reactor was chosen at 25 ºC. The temperatures of next feed streams to the reactor were the retentate temperatures of the previous PV modules. It must be taken into account that the temperature drop in PV modules is quite important. On the other hand, this lower temperature in the reactor inlet leads to a higher conversion. A liquid pump was placed after each plug flow reactor in order to compensate pressure drops. For the calculations these pressure drops in the pervaporation modules were considered negligible.

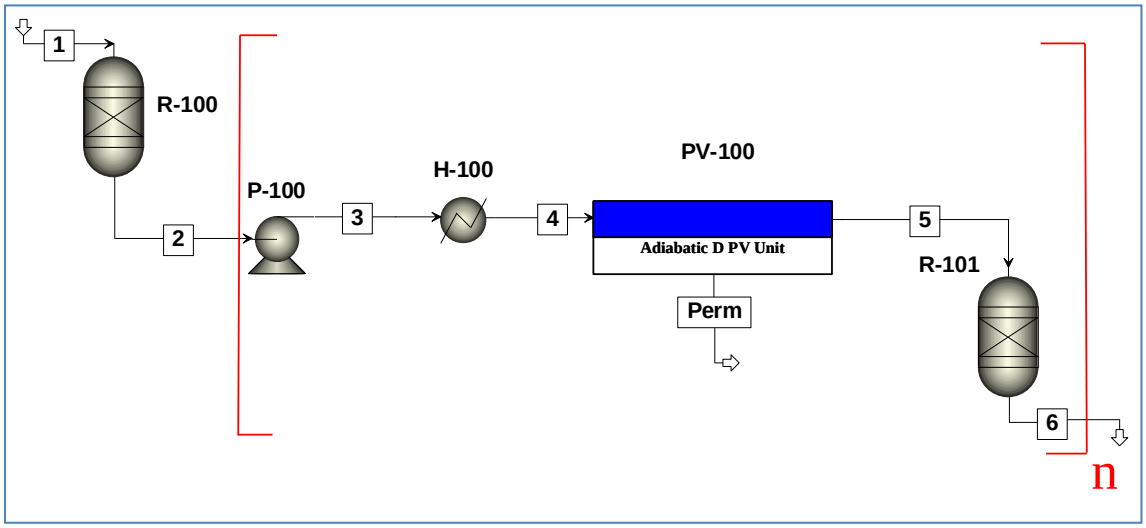

Figure 7.53 PFR and PV modules placed in series.

In case of pervaporation units "*Configuration 3*" was used in all the cases. In terms of the length the maximum one was used in all the calculated cases; i.e., the maximum length until the water driving force is negative or zero. If the module length is too long water partial pressure in the permeate side can be higher than water vapor pressure in the shell side due to its low concentration. One example of water concentration profile in the shell side is shown in Figure 7.54. In reality a pervaporation process would not be operated up to a driving force becoming almost zero as this leads to unrealistic high areas while there is hardly any further process improvement, see e.g. Figure 7.49. For the calculations performed here it does give the highest conversion though.

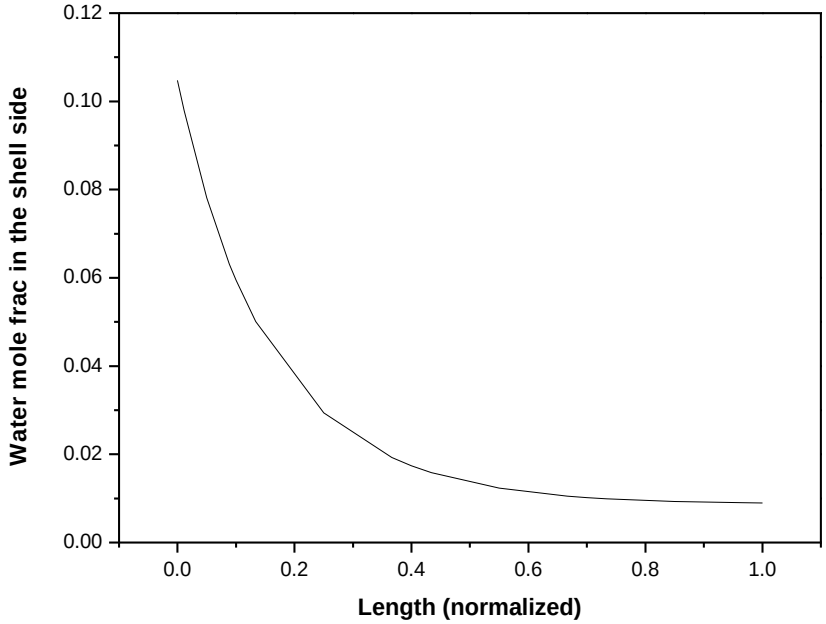

Figure 7.54 Water concentration profile in the shell side along the reactor.

The standard PFR diameter used in this simulation was 15 mm. The length was adjusted in each case in order to ensure that the mixture reaches the equilibrium. All these data are shown in Table 7.18.

Table 7.18 Process parameters in each unit.

	R100	**PV100**	**R101**	**PV101**	**R102**	**PV102**	**R103**	**PV103**	**R104**
Diameter (m)	0.015	0.03	0.015	0.03	0.015	0.03	0.015	0.03	0.01
Length (m)	0.3	2.24	0.5	1.19	0.25	0.86	0.15	0.5	0.1
Global conversion	45.8		60.3		66.3		69.3		71.2
η (efficiency)		85.8		92.4		93.6		91.2	
Re range	13-21	14-28	13-16	18-26	17-18	21-25	19-20	22-25	19-20
Inlet Temp (ºC)	25	76.6	33.1	78.6	54	81.4	69.7	83.1	76.8
Outlet Temp. (ºC)	60.7	33.1	46.5	54	59.9	69.7	72.8	76.8	78.8
Outlet molar frac									
X ethanol	0.433	0.505	0.397	0.430	0.376	0.377	0.347	0.342	0.322
X butanal	0.211	0.252	0.197	0.222	0.195	0.208	0.193	0.201	0.191
X acetal	0.178	0.213	0.301	0.339	0.385	0.411	0.438	0.455	0.473
X water	0.178	0.030	0.105	0.009	0.044	0.003	0.022	0.002	0.014

"η" indicates the water separation efficiency (%):

$$\eta = \frac{F_{w,0} - F_{w,1}}{F_{w,0}} \tag{7.59}$$

Where: $F_{w,0}$ water molar flow rate on the feed side (kmol/h)
$F_{w,1}$ water molar flow rate on the retentate side (kmol/h)

Most of Re numbers were in the suitable range, however, PV100 should need some baffles to increase a bit the turbulence.

It can be observed that with 5 PFR reactors and four PV modules the achieved maximum conversion was 71.2% which is comparable to the experimental conversions achieved in semi-batch mode. However, hardly significant conversion increase was obtained adding the last reactor. The conversion tendency can be observed more clearly in Figure 7.55.

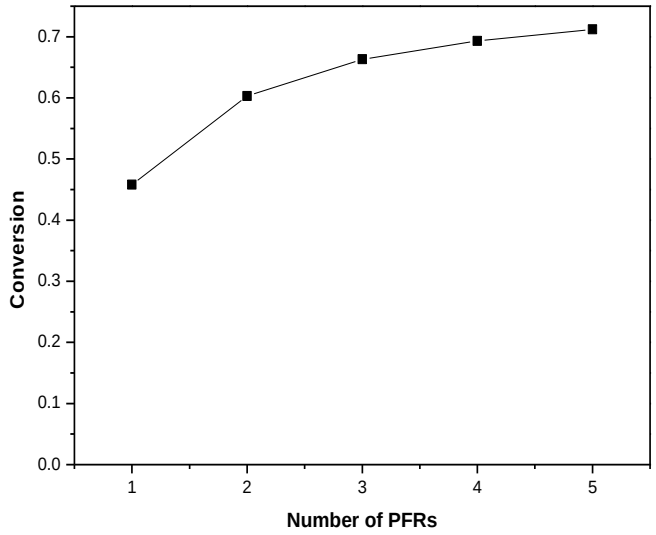

Figure 7.55 Evolution of the conversion with different amounts of PFRs.

Based on Figure 7.54, shorter pervaporation module lengths can be used as the last part of the module does not seem to work really efficiently. Table 7.19 shows that having the 50% of the membrane area almost the same conversion can be achieved.

Table 7.19 Effect of using 50% of membrane area.

Number of PV modules	**Length until ΔP < 0**	**Optimized length**
1	2.2	1.1
2	1.2	0.6
3	0.9	0.5
4	0.5	0.25
Total length	4.8	2.45
Membrane area (m^2)	1.95	1.0
Conversion	71.2	70.6

Based upon these results some observations can be made:

- The first PV100 module was much longer (=larger) than the other modules. The reason is that a lot of water had to be separated and hardly any driving force was let as the temperature drop was larger. It could be a wise choice to dehydrate to e.g. 0.05 mol fr. water instead of 0.03 mol fr.
- The inlet temperature of reactors R103 and R104 was rather high and a small cooler could improve the conversion of this reactor. This cooler could maybe be a heat exchanger between the outlet of section PV100 and R103.
- The ethanol:butanol feed ratio in the first reactor was about 2:1, the stoichiometric ratio. In the other reactors this ratio was gradually decreasing as ethanol permeates through the membrane. Adding some extra ethanol e.g. before reactor R103 would help shifting the equilibrium further.

To sum up it can be said that in this case a much smaller process configuration is required than in the combined reactor and separator but more membrane area is required in this case. 1.2 m of reactor (15mm of diameter) and 2.45 meters of PV modules (43 membrane tubes of 2.45 m or 1.0 m^2 of membrane area) are now required vs. some 15 meter of necessary combined reactor length (0.66 m^2 of membrane area). A further advantage of this reactor and pervaporation section in series as compared to the combined reactor is that the pressure drop is much lower now.

7.2.3.5.2 PFR + PV modules with a recycle loop

In the simulation above the membrane area needed was 1.0 m^2. Using these 43 membrane tubes with a length of 2.45 m to treat 7 L/h seems to be a bit excessive. Because of that a recycle loop was implemented. Thus, only one PFR and one PV module were required. Figure 7.56 shows the basic process configuration.

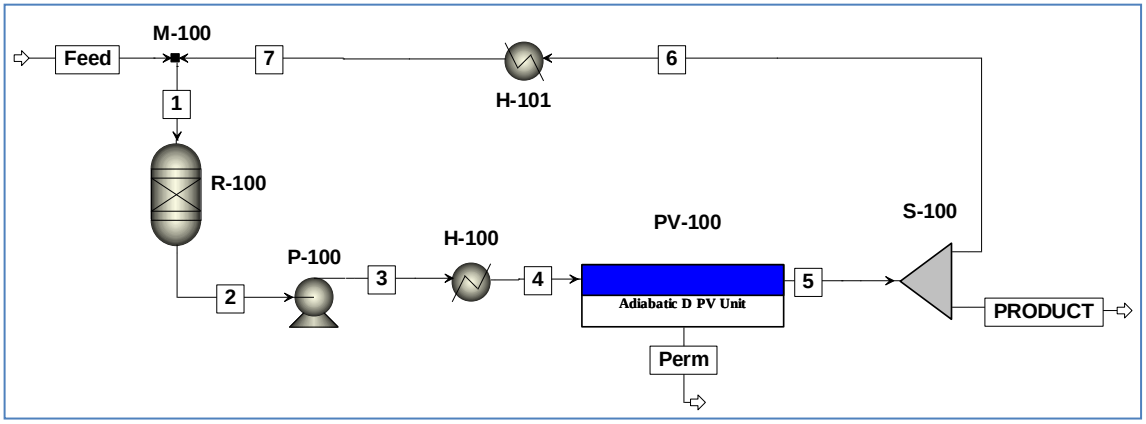

Figure 7.56 Basic scheme of the process configuration including a recycling loop.

The basic configuration was exactly the same as in Section 7.2.3.5.1 including a heat exchanger and a liquid pump between the PFR and PV module. Also in the present case, H100 heat exchanger warms up the liquid mixture up to the bubble point temperature in order to optimize the use of the membranes. The required energy to warm up the liquid mixture up to its bubble point was considered negligible as well as the cooling required energy in H101. Table 7.20 shows all the temperatures.

As in the previous case (PFR + PV in series), "*Configuration 3*" was used in the PV module and the length was optimized until a negative driving force was obtained. For each recycle ratio calculated both the reactor length and the PV module length were adjusted. It must be taken into account that by increasing the recycle ratio the flow rate in the reactor increases. Thus, the residence time decreases and longer reactors but also longer membrane modules are required in order to end with the same water separation efficiency and conversion. In terms of the plug flow reactor, also the diameter was optimized with each recycle ratio in order not to have an extremely long reactor.

For recycling part of the retentate a common stream splitter was placed after the pervaporation module. The outlet stream properties of the splitter and the inlet stream properties were exactly the same. The recycle ratio (R) was defined as the quotient between the recycle stream molar flow rate and the molar flow rate of the retentate stream.

A new heat exchanger (H101) was placed just before the mixer. The aim of this heat exchanger was cooling down the liquid mixture to room temperature since at lower temperatures higher conversions are achieved in the reactor.

All the simulations were performed under the following conditions:

- Feed temperature to the process: 25 ºC
- Feed pressure to the reactor: 1 bar
- Stoichiometric feed ratio (Ethanol/butanal ratio 2:1 in mols)
- Catalyst loading: 550 g/L (adiabatic reactor)
- H100 heat exchanger: warms up the liquid up to its bubble point temperature
- Pump: outlet pressure is 1 bar
- PV module configuration: 30 mm of shell diameter and 47 membrane tubes of 3 mm, "*Configuration 3*"
- Permeate pressure: 5 mbar
- H101 heat exchanger: cools down the liquid mixture to 25 ºC

Table 7.20 shows all the process parameters at different recycle ratios. Interesting conversions were achieved but only at very high recycle ratios (0.8 & 0.9). Moreover, an 8.4 meters long PV module (3.4 m^2 of membrane area) was required with R=0.9 which is not really suitable. In Figure 7.57 the evolution of the conversion can be observed more clearly. It must be taken into account that the flow increases exponentially with the recycling ratio (see Figure 7.58) so the dimensions of the modules change also significantly. The maximum conversion obtained of 68.3% at the length of 8.4 meters was still lower than the 71.2% conversion in the case without recycling and a length of the PV section of 4.3 meters.

Table 7.20 Process parameters in each unit at different recycling ratios.

	R = 0		R = 0.1		R = 0.2		R = 0.3		R = 0.4		R = 0.5		R = 0.6		R = 0.7		R = 0.8		R = 0.9	
	R100	**PV100**	**R100**	**PV100**	**R100**	**PV100**	**R100**	**PV100**	**R100**	**PV100**	**R100**	**PV100**	**R100**	**PV100**	**R100**	**PV100**	**R100**	**PV100**	**R100**	**PV100**
Diameter (m)	0.015	0.03	0.015	0.03	0.015	0.03	0.015	0.03	0.015	0.03	0.02	0.03	0.02	0.03	0.025	0.03	0.03	0.03	0.045	0.03
Length (m)	0.3	2.3	0.3	2.5	0.4	2.7	0.4	2.9	0.55	3.3	0.5	3.5	0.8	4	0.8	4.5	1.2	5.7	1.5	8.4
Reactor conversion (%)	45.8		44.8		43.6		42.2		40.5		38.6		36.0		32.5		27.3		17.9	
Proc. conv (%)	45.8		47.4		49.1		51.0		53,1		55.6		58.4		61.6		65.1		68.3	
η (efficiency)		84.4		85.0		85.7		86.2		86.7		89.6		90.1		91.7		92.2		92.6
Inlet L/h	7.0		7.5		8.3		9.4		10.7		12.7		15.6		20.3		29.4		55.0	
Re range	13-21	14-27	14-22	16-30	16-24	18-33	18-26	21-37	21-29	25-42	14-19	31-51	17-22	40-61	14-17	51-71	14-17	90-117	11-12	189-222
Inlet T (ºC)	25.0	74.6	25.0	74.3	25.0	73.9	25.0	73.3	25.0	72.3	25.0	75.1	25.0	74.2	25.0	75.8	25.0	75.5	25.0	77.0
Outlet T (ºC)	60.7	31.6	58.7	32.8	56.5	34.2	54.1	35.9	51.5	37.4	48.7	43.1	45.4	45.9	41.8	51.9	37.4	57.1	32.0	65.5
Outlet molar frac																				
X ethanol	0.433	0.504	0.430	0.498	0.426	0.490	0.421	0.481	0.416	0.470	0.407	0.455	0.396	0.435	0.378	0.407	0.348	0.364	0.284	0.284
X butanal	0.211	0.251	0.209	0.248	0.208	0.245	0.207	0.242	0.205	0.238	0.203	0.234	0.201	0.229	0.199	0.224	0.199	0.219	0.210	0.224
X acetal	0.178	0.212	0.189	0.224	0.201	0.237	0.215	0.252	0.232	0.270	0.255	0.294	0.283	0.322	0.321	0.360	0.373	0.410	0.458	0.489
X water	0.178	0.033	0.172	0.031	0.165	0.028	0.157	0.025	0.147	0.023	0.135	0.016	0.120	0.014	0.102	0.010	0.080	0.007	0.049	0.004

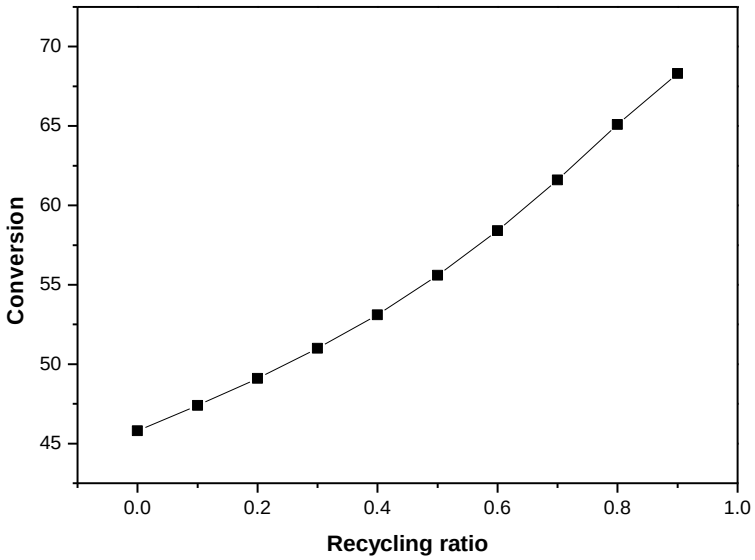

Figure 7.57 Evolution of the conversion with the recycling ratio.

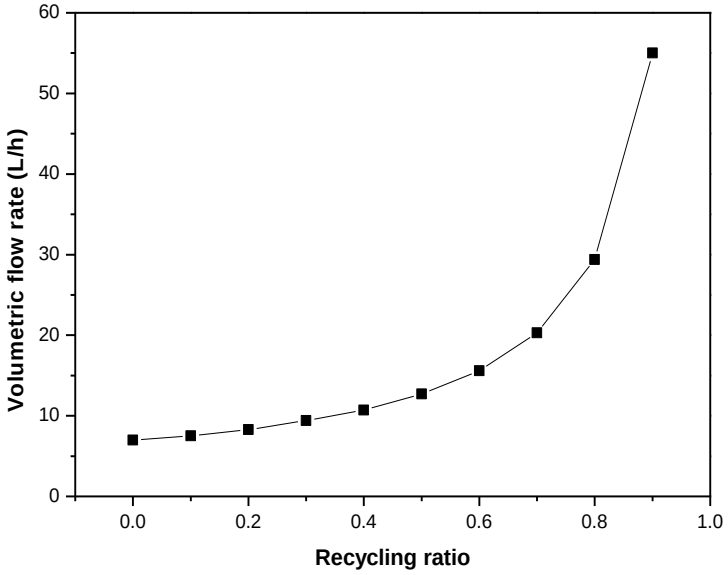

Figure 7.58 Volumetric flow rate at different recycling ratios.

However, at the highest recycle ratios Re numbers were really high in the PV module so another geometrical configuration may be used. In this case the shell diameter was increased in order to lower the Re number and accommodate more membrane tubes inside the module. With the following configuration (see Table 7.21) adequate Re numbers were obtained and the separation efficiency is also good enough. In this case the PV module length was 1.2 meters and 283 membrane tubes of 3 mm can be placed inside it (3.2 m^2 of membrane area). The conversion was 68.6 % which is comparable to the 68.3% in the previous case in which longer membranes and a smaller module (3.4 m^2 of membrane area) diameter were used.

Table 7.21 Optimum configuration for R=0.9

	R = 9	
	R-100	**PV-100**
Diameter (m)	0.045	0.07
Length (m)	1.5	1.2
Reactor conversion (%)	18.1	
Proc. conv (%)	68.6	
η (efficiency)		92.6
Inlet L/h	55.0	
Re range	11-12	41-49
Inlet T (ºC)	25.0	77.0
Outlet T (ºC)	32.0	65.7
Reactor outlet molar frac		
X ethanol	0.286	0.286
X butanal	0.207	0.207
X acetal	0.458	0.458
X water	0.049	0.049

Figure 7.59 shows the water molar fraction profile along the pervaporation module obtained with the geometry showed in Table 7.21.

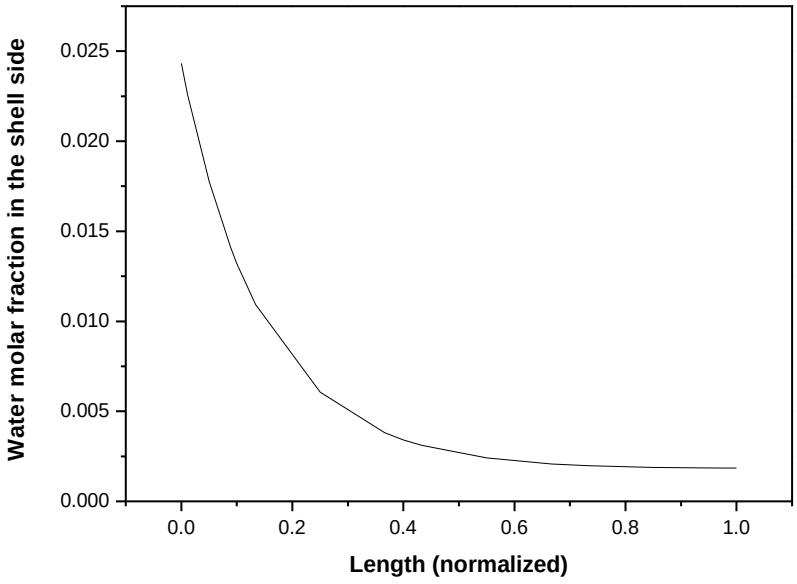

Figure 7.59 Water molar fraction profile along the reactor. Input data: Table 7.21

Based on Figure 7.59, shorter pervaporation module lengths can be used as the last part of the module does not seem to work really efficiently. Figure 7.39 shows that having

the 50% of the membrane area even more conversion can be achieved since less ethanol permeates through the membrane.

Table 7.22 Achieved conversions with different pervaporation module lengths.

PV module length (m)	1.2	0.6
Membrane area (m^2)	3.2	1.6
Conversion	68.6 %	71.0 %
Permeated Ethanol amount (g/h)	379.2	212.0

7.2.3.5.3 PFR + PV + Distillation column with a recycling loop

Two different process configurations were calculated so far: reactors and pervaporation units in series and one reactor and one pervaporation unit recycling part of the retentate. Both configurations showed that a large membrane area is necessary in order to fulfil all the hydrodynamic constraints and achieve high conversions.

A last process configuration was modeled. The only change with respect to the previous process configuration was the substitution of the splitter by a distillation column. In principle, the inclusion of a distillation column increases the process costs due to the power supply that it requires and the more expensive unit than just a splitter. The idea was to recycle ethanol and butanal (the reactants) from the top of the column and have an acetal rich stream at the bottom. On one hand, this should enhance the reaction and on the other hand, the flow in the reactor and in the PV modules would not be as high as in the previous configuration making the unit dimensions much smaller. In general, this could lead to lower costs per amount of acetal produced as the conversion is expected to increase. Figure 7.60 shows the basic process configuration.

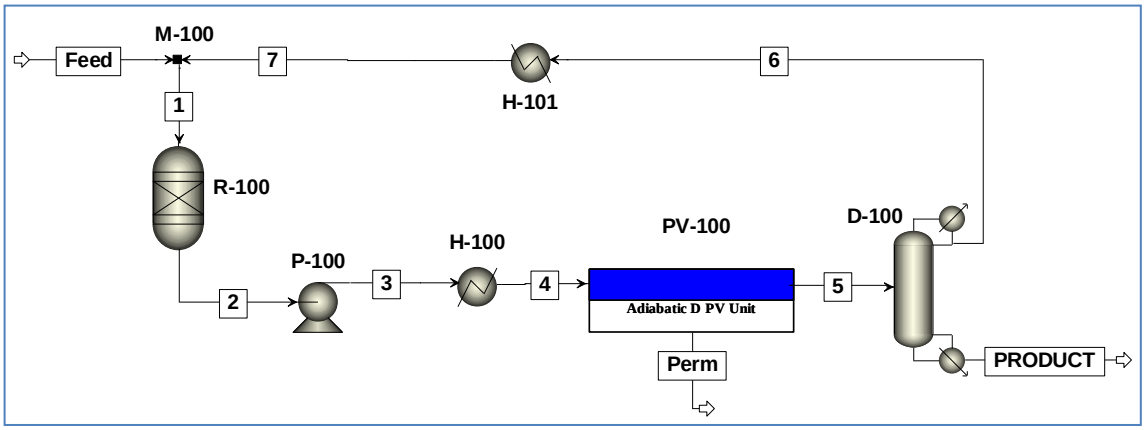

Figure 7.60 Basic scheme of the process configuration including a distillation column and a recycling loop.

The plug flow reactor and the pervaporation unit could not be successfully exported to ASPEN PLUS from ASPEN CUSTOM MODELER. It seems that the solving algorithms are not exactly the same and ASPEN PLUS is not able to solve the models programmed in ACM. Therefore, the distillation column was solved in ASPEN PLUS and a component splitter was programmed in ACM. Iteratively, the distillation column results were incorporated to the component splitter of ACM.

A pervaporation module, similar to the ones used in the previous cases (PFR + PV in series and with a recycling loop), "*Configuration 3*" (see 7.2.3.2) was used and the length of the pervaporation section was optimized until having a negative driving force. The reactor length and diameter were also adjusted in order to reach the corresponding equilibrium values and fulfill all the hydrodynamic conditions.

As in the previous configuration, a heat exchanger and a liquid pump were placed between the reactor and the pervaporation module. H-100 heat exchanger warms up the liquid mixture up to the bubble point temperature in order to optimize the use of the membranes. H-101 heat exchanger was placed before the mixer (M-100) in order to cool down the liquid mixture to 25°C since at lower temperatures higher conversions are achieved in the reactor. Moreover, according to the sensitivity analysis performed with the reactor (see Section 7.2.3.3.1) it was checked that the feed temperature to the reactor should be quite low in order to avoid vaporization effects.

All the simulations were performed using the following conditions:

- Feed temperature to the process: 25 ºC
- Feed pressure to the reactor: 1 bar
- Stoichiometric feed ratio (Ethanol/butanal ratio 2:1 in mols)
- Catalyst loading:550 g/L (adiabatic reactor)
- H100 heat exchanger: warms up the liquid up to its bubble point temperature
- Pump: outlet pressure is 1 bar
- PV module configuration: 30 mm of shell diameter and 47 membrane tubes of 3 mm diameter.
- Permeate pressure: 5 mbar
- H101 heat exchanger: cools down the liquid mixture to 25 ºC
- Distillation column operated with a total condenser

Table 7.23 shows all the process parameters and variables. 99.8% of conversion was achieved in all the cases. The pervaporation unit separates most of the water and the distillation column separates almost all the acetal to the bottoms. As a consequence, mainly non-reacted ethanol and butanal were recycled increasing the final conversion. Moreover, as the recycled flow was not really high, the Re number was around 40-70 in the pervaporation unit and around 11-17 in the reactor. Furthermore the units were not as big as in the previous cases.

High process conversions were achieved because of the combined water separation in the PV unit and acetal separation in the distillation column. In the previous configurations, conversions above the equilibrium but below the conversions obtained here were achieved because only water was separated.

Separation of the four component mixture using distillation is difficult. The water separation by pervaporation makes the distillation process much easier and only 4 equilibrium stages (+ condenser and reboiler) are necessary (see Table 7.24) to get 99.5% (in moles) of acetal in the bottom stream of this column.

Table 7.23 Process parameters in the reactor and in the PV module for two different PV unit lengths.

	R-100	**PV-100**	**R-100**	**PV-100**
Diameter (m)	0.025	0.03	0.025	0.03
Length (m)	0.25	2	0.25	4
Membrane area (m^2)		0.81		1.62
Reactor conversion (%)	43.5		39	
Proc. conv (%)	99.8		99.8	
η (efficiency)		79.4		87.3
Inlet L/h	15.9		15.9	
Re range	11-17	40-70	11-17	40-70
Inlet T (ºC)	25.0	80	25.0	79.5
Outlet T (ºC)	57.8	35.5	58.2	33.2
Reactor outlet molar frac				
X ethanol	0.167	0.200	0.172	0.208
X butanal	0.208	0.249	0.258	0.312
X acetal	0.424	0.501	0.382	0.451
X water	0.201	0.050	0.189	0.029

Table 7.24 Distillation column design parameters for a PV unit of 2 meters and of 4 meters length.

PV Length (m)	2	4
Condenser duty (kW)	-7.46	-6.07
Reboiler duty (kW)	7.95	6.58
Stages	4 + cond + reb	4 + cond + reb
Feed stage	3	3
Recycling ratio	4.3	3.6
Head/feed molar ratio	0.81	0.8
Bottom/Feed molar ratio	0.19	0.2
Outlet T (ºC) Head	75.4	75
Outlet T (ºC) Bottoms	140.5	141.1
Outlet molar frac Head		
X ethanol	0.010	0.010
X butanal	0.308	0.388
X acetal	0.621	0.566
X water	0.061	0.036
Outlet molar frac Bottoms		
X ethanol	0.995	0.995
X butanal	0.002	0.010
X acetal	0.001	0.001
X water	0.002	0.000

It can be observed that the design of the distillation column does not change using either 2 meters long or a 4 meters long PV module. For the longer pervaporation section the advantage is that less energy is required in the reboiler and less energy must be extracted from the condenser.

The main conclusion of this part is that by combining pervaporation and distillation conversions of almost 100% can be achieved. Moreover, the length of the pervaporation module would be 2 meters and the distillation column would have 4 equilibrium stages plus the condenser and the reboiler. In terms of energy savings, the process can be optimized by using the bottoms stream of the distillation column (140.5ºC) to warm up the liquid stream in H-100 heat exchanger from 58 to 80 ºC (see Figure 7.61).

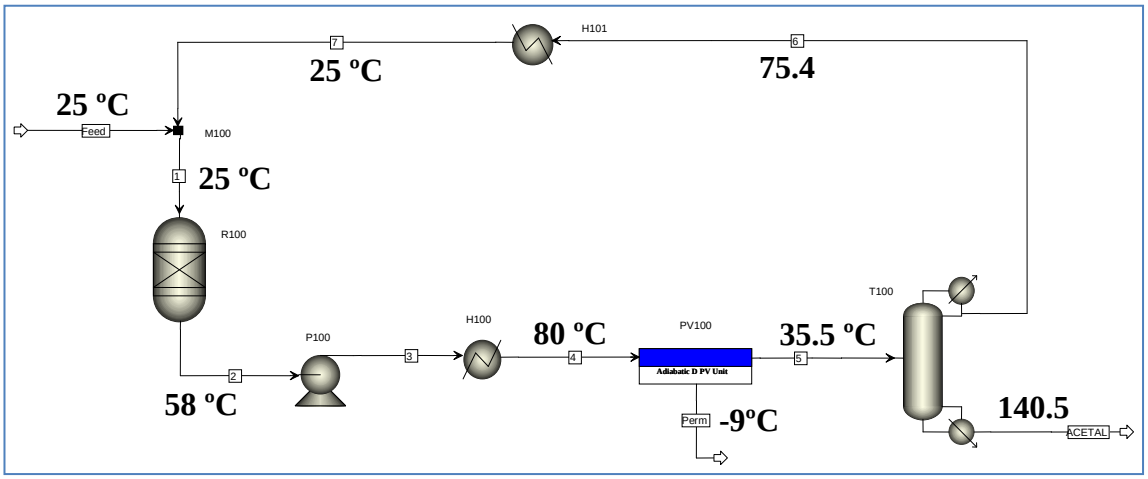

Figure 7.61 Basic scheme of the process with stream temperatures for the given conditions in Table 7.23.

7.2.3.6 Conclusions

Via a sensitivity analysis of the reactor and the pervaporation module separately, using adiabatic systems, it was concluded that the reactor feed should be at low temperatures while the pervaporation feed should be as warm as possible (always in liquid phase).

Three different process configurations were tested being the base case a plug flow reactor followed by a pervaporation module to separate the water from the mixture. A liquid pump and a heat exchanger were placed in between:

1. PFR + PV modules in series
2. PFR + PV including a recycling loop
3. PFR + PV + Distillation column recycling the head of the distillation column

The first two configurations showed that conversions around 70 % can be achievable. These values are in good agreement with the observed experimental conversions, the predicted conversion values by the semi-batch model as well as the predicted ones by the MPFMR model. However, these configurations require a large membrane area (1.0 m^2 of membrane area "in series" configuration and 1.6 m^2 of membrane area with a simple recycle loop) to treat 7 L/h of volumetric feed flow. From the unit size point of view the recycling option is preferred above the series configuration. The third configuration includes a distillation column and from the energetic point of view, a priori, it is not the most suitable one. However, this configuration allows conversions around 100% and the required membrane area is much smaller (0.81 m^2) than in the previous cases.

In the first two cases the conversion increase is due to the water separation while in the last case is due to the water and acetal separation from the liquid mixture and the recycle of the non-reacted ethanol and butanal. Thus, using a small pervaporation unit and a small distillation column, almost 100% of conversion can be achieved.

Chapter VIII

Preliminary process engineering calculations and cost estimations

8 Preliminary process engineering calculations and cost estimations

In this chapter conceptual process engineering work and cost estimations will be presented. Based on the experimental results and the modeling work, different processes at industrial scale were developed on ASPEN PLUS:

- Process based on a conventional tubular reactor.
- Using reactive distillation.
- Using dehydration membrane modules.

Once all the processes were developed the main equipments were dimensioned and capital and manufacturing costs were estimated. Thus, comparing technical and economic aspects the best alternative was stated.

8.1 Process design

In order to determine the best alternative for 1,1 diethoxy butane production different alternatives were studied and compared:

- Conventional reaction-separation process.
- Catalytic reactive distillation (RD) system.
- Conventional process incorporating dehydration membranes.

According to the experimental results different acetal production alternatives at industrial scale were developed in ASPEN PLUS. In all the cases the production target was established at 50000 t acetal/year. This production rate is based on an average size of a comparable ETBE production plant. "Petróleos del Norte" (PETRONOR which is part of REPSOL YPF group), the biggest Spanish refinery placed in Muskiz (next to Bilbao), produces 62000 t/year of ETBE while "CEPSA Gibraltar" produces 34000 t/year. The predetermined purity was 99.5 % (molar) of acetal in every single case.

The studied cases were the following ones:

- Base case: Tubular reactor followed by a distillation train.

- Reactive distillation: in *Chapter IV and V* it was observed that at high reflux ratios high conversions could be achieved while at low reflux ratios low conversions were obtained but the acetal concentration in the reboiler was very

high facilitating its later purification. For this reason both alternatives were studied in the present case.

- At high reflux ratios: higher conversions, the acetal goes out from the reboiler at low concentration and a distillation train is required in order to get the purified product.
- At low reflux ratios: the conversion is really low but the acetal concentration in the reboiler is quite high, being easier its later purification. Two alternatives were studied:
  - Adding a 2nd purification distillation column in order to separate the water before recirculation the reactants.
  - Recycling directly the distillate of the reactive distillation column.

- Tubular reactor followed by a PV module and a distillation column. This process was developed for a lab scale production in Section 7.2.3.5.3.

8.1.1 Base case: tubular reactor followed by a distillation train

In this section a theoretical base case was developed. A conventional tubular reactor was placed as a reaction system and after it a distillation train was added. The found optimum process, in addition to the reactor, consists of two different distillation columns (see Figure 8.1). The objective of the first distillation column (D-100) is to obtain the purified acetal from the reboiler. In order to avoid side reactions due to the high temperatures in the reboiler, (see Section 4.2) this column operates at 0.5 bara. As a consequence, lower temperatures are used in the reboiler.

The aim of the second distillation column (D-101) is to remove water from the system. If water remains in the system without removing it the efficiency of the process drops considerably. The feed to this second column basically consists of ethanol, butanal and water; 1,1 diethoxy butane amounts can be considered negligible. The problem stems from the difficulty of separating water from this ternary mixture.

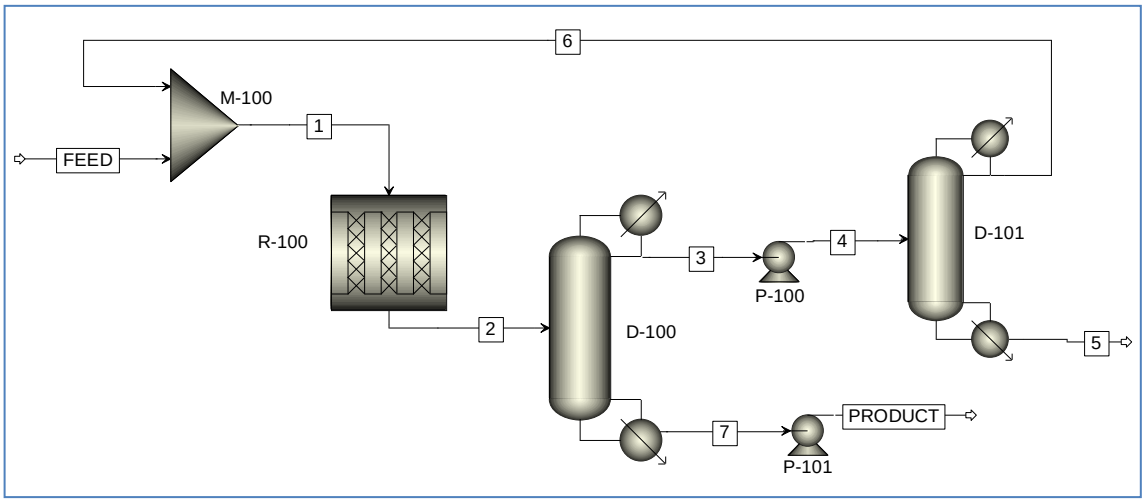

Figure 8.1 Base case Block Flow Diagram (BFD).

Table 8.1 represents the required equilibrium stages in order to separate a certain amount of water in the second distillation column (D-101).

Table 8.1 Water removal percentage vs. the required equilibrium stages in a distillation column.

% of water removal	Equilibrium stages
50 %	11
55 %	14
60 %	17
65 %	23
70 %	32
75 %	52
80 %	116
84 %	843

In addition to these results, the residue curves of the ternary map of ethanol, butanal and water mixtures indicates the difficulty of their separation (Figure 8.2).

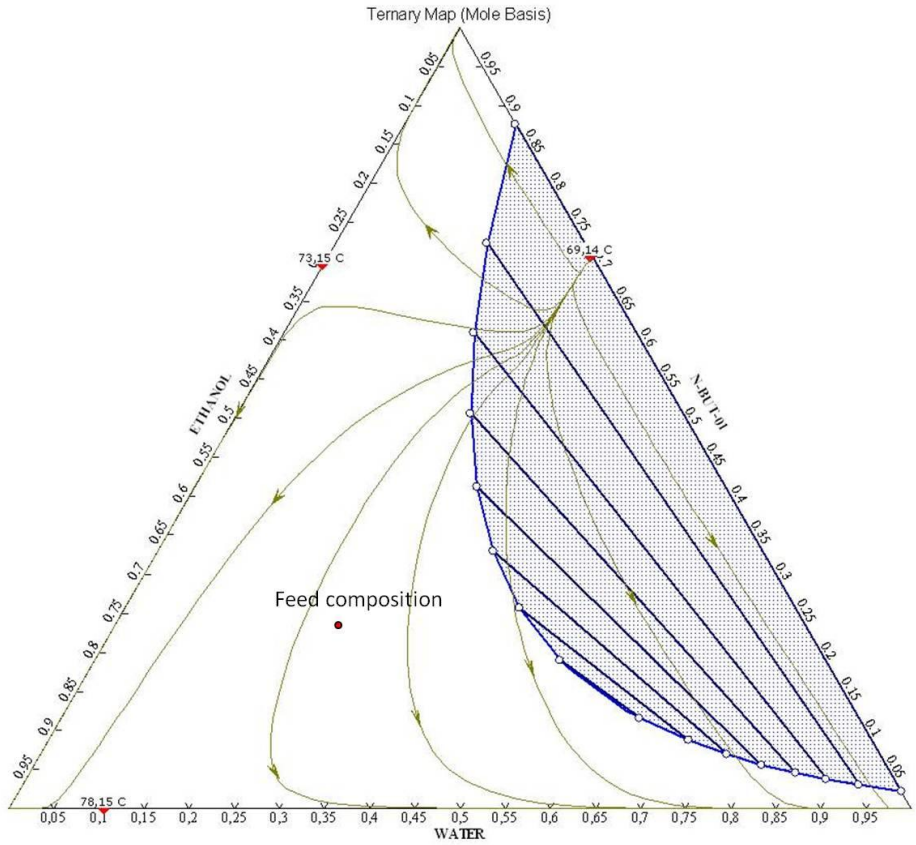

Figure 8.2 Liquid-liquid equilibrium diagram and residue maps for ethanol, butanal and water mixture.

After observing all these evidences, the adopted criterion was to remove the 55 % of water from the system using this second distillation column. In this way the distillation column requires a reasonable number of equilibrium stages.

In order to get the optimum column configurations, first of all, distillation DSTWU model was used. This model is used as a shortcut distillation design method. Once the first column configuration approximation was obtained RADFRAC model was used in order to obtain the most accurate configuration as possible using different sensitivity and optimization tools.

In terms of the reaction system, a conventional adiabatic fix bed tubular reactor (PFR) was placed. In order to calculate the reactor dimensions the model made in ASPEN CUSTOM MODELLER was used as ASPEN PLUS does not provide reasonable dimensions.

All the process parameters are showed in Table 8.2:

Table 8.2 Process and block parameters for the base case.

PROCESS		
Product yield (kg acetal/kg reactants)		0.66
Overall process conversion		0.94
PFR conversion		0.34
R-100		
Diameter	0.5	m
Length	0.3	m
D-100		
Equilibrium stages	10	
Feed stage	7	
Reflux ratio	2	
Reboiler duty	10.1	MW
Condenser duty	-10.2	MW
Bottom to feed ratio	0.11	(molar ratio)
Pressure	0.5	bara
D-101		
Equilibrium stages	14	
Feed stage	7	
Reflux ratio	2	
Reboiler duty	7.3	MW
Condenser duty	-7.1	MW
Bottom to feed ratio	0.27	(molar ratio)
Pressure	1	bara

8.1.2 Reactive distillation at high reflux ratios

In the present case an acetal production process using a reactive distillation system operating at high reflux ratios was developed. As well as in the base case, in addition to the reactive system (reactive distillation column) two additional distillation columns are required (see Figure 8.3). As it was demonstrated in Chapter IV & V, the maximum achievable conversion at the studied operating conditions is 50% so one distillation column is required in order to get purified acetal. This column operates at 0.5 bara. The second distillation column (D-101) removes water from the system following the explained criterion in Section 8.1.1. All the process parameters are showed in Table 8.3.

In all the cases the optimum column configuration found for reactive distillation in Chapter V was applied in ASPEN PLUS obtaining comparable results simulating only the reactive distillation column.

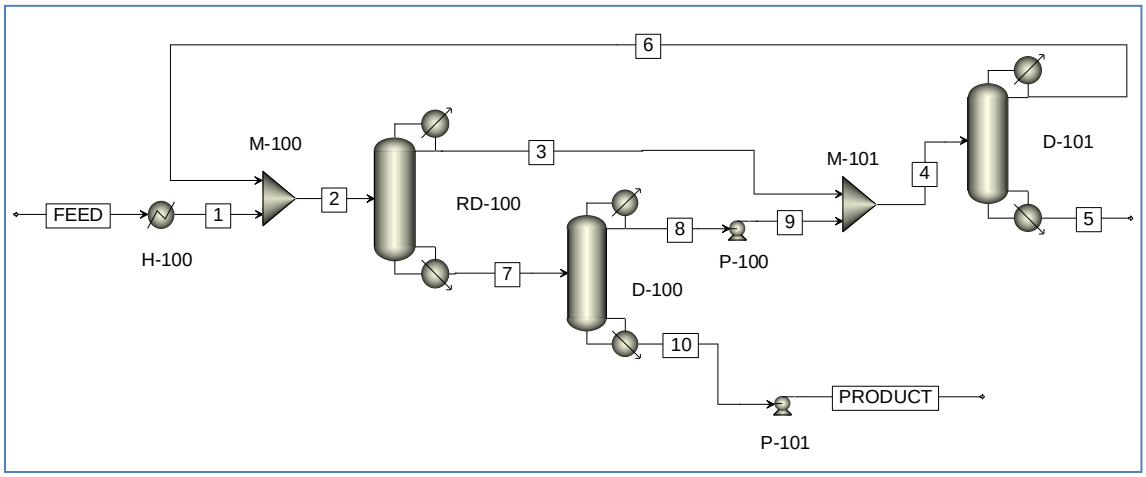

Figure 8.3 Acetal production Block Flow Diagram (BFD) using a reactive distillation column operating at high reflux ratios.

As well as in the previous case, the first distillation column (D-100) operates at 0.5 bara and its aim is the separation of 1,1 diethoxy butane from the mixture. The second distillation column removes water from the system following the explained criterion in Section 8.1.1. All the process parameters are showed in Table 8.3.

Table 8.3 Process and block parameters for the reactive distillation at high reflux ratio case.

PROCESS		
Product yield (kg acetal/kg reactants)		0.74
Overall process conversion		0.83
RD conversion		0.45
RD-100		
Stages	8	
Feed stage	2	
Reflux ratio	5	
Reboiler duty	8.7	MW
Condenser duty	-9.0	MW
Bottom to feed ratio	0.45	(molar ratio)
Pressure	1	bara
D-100		
Stages	8	
Feed stage	4	
Reflux ratio	2	
Reboiler duty	4.2	MW
Condenser duty	-4.1	MW
Bottom to feed ratio	0.246	(molar ratio)
Pressure	0.5	bara

D-101		
Stages	15	
Feed stage	7	
Reflux ratio	2	
Reboiler duty	6.7	MW
Condenser duty	-6.7	MW
Bottom to feed ratio	0.2038	(molar ratio)
Pressure	1	bara

8.1.3 Reactive distillation at low reflux ratios

In case of the reactive distillation process working at low reflux ratios, 2 different alternatives were studied. The first one follows the same process configuration as in the previous case, i.e., a reactive distillation column followed by two conventional distillation columns. In the second studied case only one distillation column was added after the reactive distillation column. Working at low reflux ratios low conversions are obtained and thus, the recirculated water amount is not really high.

8.1.3.1 RD at low reflux ratios + 2 conventional distillation columns

As it can be observed, the Block Flow Diagram presented in Figure 8.4 is the same as the presented one in Figure 8.3.

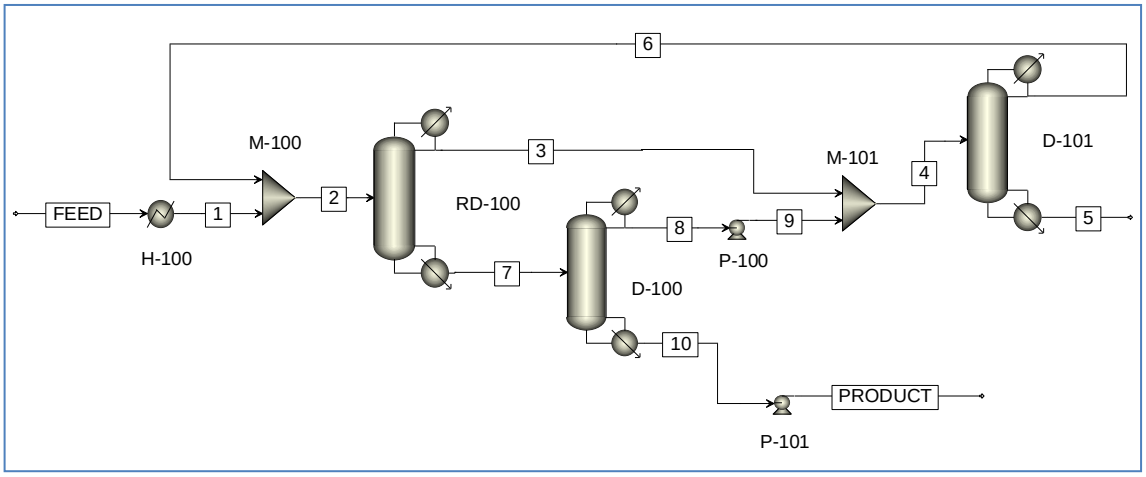

Figure 8.4 Acetal production Block Flow Diagram (BFD) using a reactive distillation column operating at low reflux ratios.

As well as in the previous cases, the first conventional distillation column after the reactive distillation column operates at 0.5 bara in order to obtain 99.5% (molar) of acetal from the reboiler avoiding side reactions. The second distillation column removes water from the system, but in this case the separation process is much more difficult

needing much more separation equilibrium stages. All the process parameters are showed in Table 8.4:

Table 8.4 Process and block parameters for the reactive distillation process at low reflux ratio case.

PROCESS		
Product yield (kg acetal/kg reactants)		0.45
Overall process conversion		0.92
RD conversion		0.23
RD-100		
Stages	8	
Feed stage	2	
Reflux ratio	1	
Reboiler duty	9.4	MW
Condenser duty	-9.7	MW
Bottom to feed ratio	0.114	(molar ratio)
Pressure	1	bara
D-100		
Stages	6	
Feed stage	5	
Reflux ratio	2	
Reboiler duty	1.0	MW
Condenser duty	-1.0	MW
Bottom to feed ratio	0.593	(molar ratio)
Pressure	0.5	bara
D-101		
Stages	34	
Feed stage	13	
Reflux ratio	5	
Reboiler duty	19.7	MW
Condenser duty	-19.7	MW
Bottom to feed ratio	0.3405	(molar ratio)
Pressure	1	bara

8.1.3.2 RD at low reflux ratios + 1 conventional distillation column

In the present case only one conventional distillation column was added after the reactive distillation column (Figure 8.5). The conversion value in the reactive distillation column is really low and thus, small amounts of water are being formed. In this way, the distillate flow of the RD column was directly recirculated to the feed of the system. All the process parameters are showed in Table 8.5.

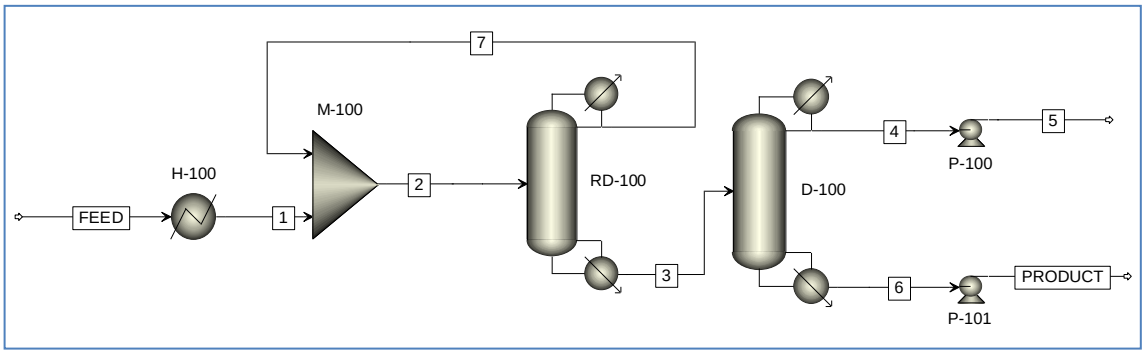

Figure 8.5 Acetal production Block Flow Diagram (BFD) using a reactive distillation column operating at low reflux ratios.

Table 8.5 Process and block parameters for the reactive distillation process at low reflux ratio case.

PROCESS		
Product yield (kg acetal/kg reactants)		0.68
Overall process conversion		0.86
RD conversion		0.16
RD-100		
Stages	8	
Feed stage	2	
Reflux ratio	1	
Reboiler duty	16.9	MW
Condenser duty	-17.2	MW
Bottom to feed ratio	0.114	(molar ratio)
Pressure	1	bara
D-100		
Stages	6	
Feed stage	5	
Reflux ratio	2	
Reboiler duty	2.6	MW
Condenser duty	-2.6	MW
Bottom to feed ratio	0.652	(molar ratio)
Pressure	0.5	bara

8.1.4 Base case including a dehydration membrane module

The last case study is the developed one in Section 7.2.3.5.3. In this process a dehydration membrane module was placed after the adiabatic fix bed tubular reactor and a conventional distillation column after the membrane module. (Figure 8.6)

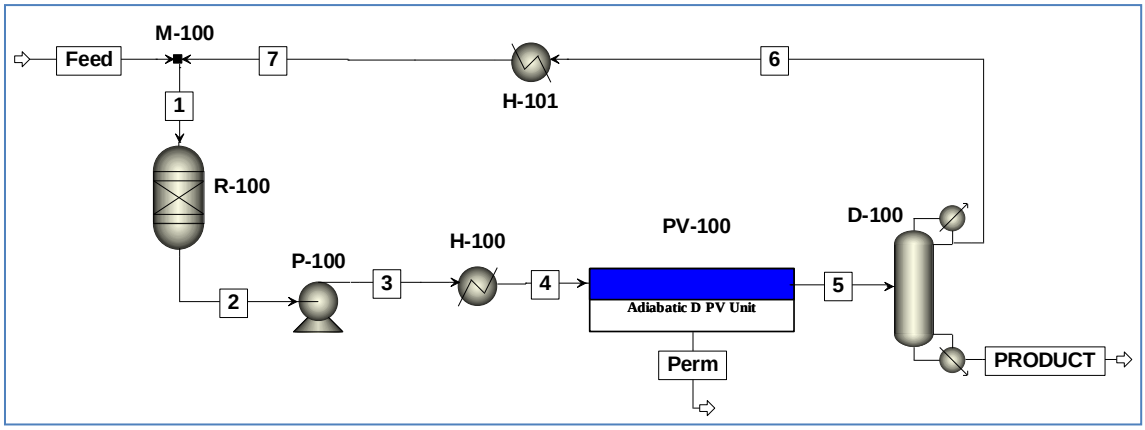

Figure 8.6 Acetal production Block Flow Diagram (BFD) using a dehydration membrane module.

In Section 7.2.3.5.3 this process was developed using experimental permeation data at lab scale in order to treat 7 L/h of raw materials. In the present case it was scaled up in order to produce 50000 tons of acetal per year. The increase of the shell diameter, introducing more membrane tubes and keeping the same flow regime (same Re numbers) was the followed criterion in order to calculate the required membrane area. Probably, at industrial scale, this type of module configuration is not the most suitable one (maybe multi-channel membranes can be used) but in order to compare different alternatives and their costs it is considered as an adequate approximation. As it is explained in Section 8.3.1, in order to make the first cost estimations for membrane modules, the total membrane area is the required parameter.

As well as in the previous cases, the distillation column operates at 0.5 bara in order to avoid possible side reactions in the reboiler due to the achieved high temperatures at higher pressures.

All the process parameters are showed in Table 8.6.

Table 8.6 Process and block parameters for the PFR + PV+Distillation process.

PROCESS		
Product yield (kg acetal/kg reactants)		0.88
Overall process conversion		0.995
PFR conversion		0.44
R-100		
Diameter	0.5	m
Length	0.7	m
PV-100		
PV Diameter	1	m
PV Length	1.6	m
N tubes	64037	
Diameter mem. tubes	0.003	m
Mem. area	965	m2
Permeate pressure	5	mbara
D-100		
Stages	6	
Feed stage	3	
Reflux ratio	3.45679275	
Reboiler duty	8.0	MW
Condenser duty	-7.6	MW
Bottom to feed ratio	0.803	(molar ratio)
Pressure	0.5	bara

8.1.5 Comparison among different alternatives

Table 8.7 shows the summary of the most important process characteristics. It can be observed that the process in which a PV module was implemented is the one which offers the best product yield, the highest conversion and the least power consumption. Further comparison will be performed through a cost study (capital costs, manufacturing costs…) in order to select the best option.

Table 8.7 Comparison of the most important process characteristics.

	Process				
	Base case	**RD ↑R**	**RD ↓R (2 dist)**	**RD ↓R (1 dist)**	**With PV**
Product yield	0.66	0.74	0.45	0.68	0.88
Process conversion	0.94	0.83	0.92	0.86	0.995
PFR or RD conversion	0.34	0.45	0.23	0.16	0.44
Energy consum. (MW)	17.4	19.6	30.2	19.5	8.0
Cooling energy (MW)	-17.3	-19.8	-30.3	-19.8	-7.6

8.2 Unit sizing

In order to calculate the capital costs of each process the major equipments must be sized. As it is explained in Section 8.1.1 and 8.1.4, the size of the fixed bed tubular reactors were estimated using ASPEN CUSTOM MODELLER and in case of the pervaporation module, in order to have a first capital cost estimation, the membrane area value is the only required parameter. Therefore the size of the different distillation columns must be calculated (diameter & height). Different calculation procedures were used as reactive distillation columns are packed columns and the conventional ones were chosen as sieve tray columns as the most advisable column type for initial installations (84).

8.2.1 Tray columns

8.2.1.1 Column diameter

In order to calculate the tower diameter the procedure explained by McCabe et al. (85) was followed. In principle a tray spacing of 24 inches (60.96 cm) was chosen as the typical tray spacing for column diameters bigger than 1.5 m. For column diameters bigger than 6 meters a tray spacing of 30 inches (76.2 cm) should be chosen (60). The diameter calculation steps are the following ones:

1. Assume a tray spacing of 24 inches
2. Calculate "Kv" (empirical coefficient) value using Figure 8.7 in order to calculate "u_c"
   - Abscissa axis: $\frac{L}{V}\left(\frac{\rho_V}{\rho_L}\right)^{0.5}$

     Where: $\frac{L}{V} = \frac{R}{R+1}$ liquid-vapor mass flow ratio in the head of the column

     ρ_L liquid density (kg/m^3)

     ρ_V vapor density (kg/m^3)

   - Ordinates axis: $K_V = u_c \left(\frac{\rho_V}{\rho_L - \rho_V}\right)^{0.5}\left(\frac{\sigma}{20}\right)^{0.2}$

     Where: u_c maximum allowed vapor velocity (ft/s)

     K_v empirical coefficient

     σ superficial tension of the distillate (dyne/cm) (calculated with ASPEN PLUS)

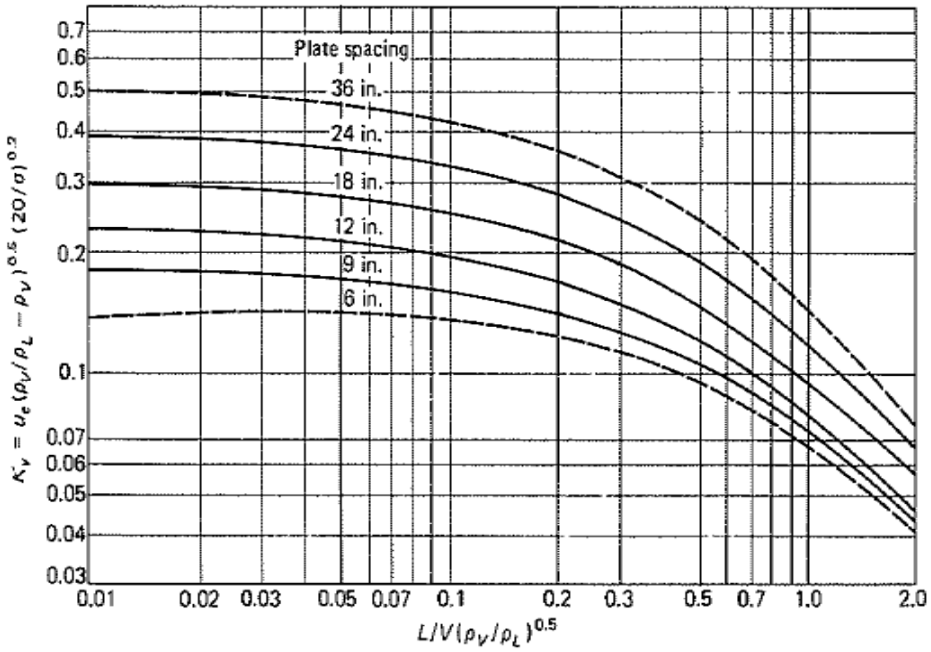

Figure 8.7 K_v values in flooding conditions for sieve tray columns (85).

3. Calculation of the vapor mass flow (V)

   V = D (R+1)

   Where: V vapor mass flow in the head of the column (kg/s)
   D distillate mass flow rate (kg/s)
   R reflux ratio

4. Bubbling area of tray = $\frac{V}{u_c}$ (m^2)
   Total area = Bubbling area / 0.70
   Total area = $\pi \frac{D^2}{4}$ where D column diameter

8.2.1.2 Column height

In order to calculate the column height an heuristic rule was used (86).

Total height = (Real stages-1) · tray spacing + 1.2 m at the top for vapor disengagement
+ 1.8 m at bottom for liquid level and reboiler return

In order to calculate the real stages a place efficiency of 50% was used.

8.2.2 Packed columns

8.2.2.1 Column diameter

In case of packed columns a different procedure explained by Seider et al. (84) was followed in order to calculate the column diameter:

1. Evaluation of the "density function" (for density ratios from 0.65 to 1.4):

$$f\{\rho_L\} = -0.8787 + 2.6776 \left(\frac{\rho_{H_2O_{(L)}}}{\rho_L}\right) - 0.6313 \left(\frac{\rho_{H_2O_{(L)}}}{\rho_L}\right)^2$$

Where: $\rho_{H_2O_{(L)}}$ water liquid density (kg/m^3)
ρ_L liquid density (kg/m^3)

2. Evaluation of the "viscosity function" (for random packings of 1 inch or greater nominal diameter. For liquid viscosities from 0.3 cP to 20 cP)

$$f\{\mu_L\} = 0.96\, \mu_L^{0.19}$$

Where: μ_L dynamic viscosity of the liquid phase

3. Calculation of the flow ratio parameter: F_{LG}

$$F_{LG} = \frac{L}{V}\left(\frac{\rho_V}{\rho_L}\right)^{0.5}$$

Where: $\frac{L}{V} = \frac{R}{R+1}$ liquid-vapor mass flow ratio in the head of the column
ρ_L liquid density (kg/m^3)
ρ_V vapor density (kg/m^3)

4. Calculation of the flooding velocity factor (Y) using Leva's generalized correlation (for 0.01 < Y < 10):

$$Y = EXP[-3.7121 - 1.0371\,(\ln F_{LG}) - 0.1501\,(\ln F_{LG})^2 - 0.007544\,(\ln F_{LG})^3\,]$$

5. Calculation of the flooding velocity (U_f)

$$Y = \frac{U_f^2 \, F_P}{g} \left(\frac{\rho_V}{\rho_{H_2O_{(L)}}} \right) f\{\rho_L\} \, f\{\mu_L\}$$

Where: g 32.2 ft/s^2 (9.8 m/s^2)
F_P Packing factor (ft^2/ft^3).

In the studied cases metallic Pall rings of 2 inches (F_P = 27) were used. This size is the recommended one for higher gas rates than 56.6 m^3/min (86). Moreover, with this Pall ring size the tower diameter/packing diameter ratio is higher than 15 in all the studied cases (which is also within the suggested range).

6. Calculation of the vapor mass flow (V)

V = D (R+1)

7. Column diameter:

$$D = \left[\frac{4V}{(fU_f)\,\pi\rho_V} \right]^{0.5}$$

Where: f fraction of the cross sectional area (typical values of 0.7)
D diameter of the column (ft)

8.2.2.2 Column height

In this case, a similar heuristic rule was followed to calculate the column height. However, two different calculation ways were followed for the reactive section and for the non-reactive sections.

- Reactive section

In Chapter V it was found that 3 reaction stages were the optimum ones for the best column performance using KATAPAK SP-11 structured packings. The number of reaction stages is independent of the treated feed amount. In the present simulations at industrial scale, the characteristics of KATAPAK SP-11 modules were used because all the separation and reaction experimental data was obtained with this kind of catalytic

structured packing. There are more suitable KATAPAK modules to be used at industrial scale but in the present study the characteristics of SP-11 were extrapolated. In this way, 3 equilibrium stages correspond to 1.8 meters (58).

- Stripping and rectification sections

In order to calculate the height of the stripping and the rectification sections another heuristic law was used. The Height Equivalent to Theoretical Stage (HETS) for vapor-liquid contacting is 0.76-0.9 meters for 2 inches Pall rings (86).

Finally, in order to calculate the final column height the following heuristic low was used (86):

Total height = Reactive section height + Stripping and rectification stages · 0.9 + 1.2 m at the top for vapor disengagement + 1.8 m at bottom for liquid level and reboiler return

In Table 8.8 all the calculated dimensions are showed. It can be observed that all of them fulfill the heuristic rule in which Height / Diameter ratio should be less than 30. Moreover, the highest column has 53.3 meter, the maximum advisable height because of wind load and foundation considerations. (86).

Table 8.8 Column dimensions in each process configuration.

Height / Diameter (m)	**Process**				
	Base case	**RD ↑R**	**RD ↓R (2 dist)**	**RD ↓R (1 dist)**	**With PV**
RD-100	-	1.6 / 8.4	2.0 / 8.4	1.6 / 8.4	-
D-100	3.5 / 14.0	1.8 / 11.5	0.8 / 7.6	1.3 / 7.6	3.6 / 9.1
D-101	3.8 / 18.9	3.6 / 20.1	6.5 / 53.3	-	-

8.3 Cost study

In this section, the economic evaluation of all five alternatives presented in Section 8.1 will be presented. The evaluation of capital costs and operating costs associated with the construction and operation of the presented alternatives will be discussed.

In order to perform all these calculations CAPCOST v.2, software provided by Turton et al. (86) was used.

8.3.1 Capital costs

The "capital costs" are associated to the necessary money that is required to build a new chemical plant. There are five generally accepted classifications of capital cost estimates:

1. Order of magnitude estimate.
2. Study estimate.
3. Preliminary estimate.
4. Definitive estimate.
5. Detailed estimate.

In the present thesis, "Study" type estimations will be presented. These estimations utilize the list of the major equipment found in the processes. Each piece of equipment is roughly sized and the approximate cost is determined. The accuracy of this estimation type goes from +30% to -20%.

Capital costs estimated by CAPCOST are related to 1996 year. This price information must be updated as the economic conditions change every year and therefore inflation must be included in the calculations. *Chemical Engineering Plant Cost Index (CEPCI)* index was used to update the price information. The used value was the given one at the end of 2009 year: CEPCI: 511.8.

In a parallel process, the capital cost for a chemical plant must take into consideration many costs other than the purchased cost of the equipment. In this way, apart from the equipment costs, costs related to the required material for installation, labor to place equipments and some other indirect project expenses like insurances, taxes, construction overheads, etc. must be taken into account. All these factors are included in the "*Bare module cost*" and they are also estimated by CAPCOST software based upon multiplication cost factors. Finally, the capital cost will be given as *"grass roots"* value

which refers to a completely new facility starting the construction on an underdeveloped land, a grass field. All the correlations in order to calculate the *"Bare module cost"* and *"grass roots"* values are presented in Turton et al. (86).

All capital prices were calculated in the same way except the price of the membrane module. This kind of equipment is not really conventional and therefore it is not included in CAPCOST equipment list. Its cost was estimated taking Mitsui Zeolite A membrane system cost as a basis (87) (Mitsui Zeolite A membrane cost and HybSi® membrane cost are comparable) and combining these data with module prices based upon the Dutch Association of Cost Engineers. In principle, in order to get "study estimation" type capital cost value, the total membrane area value is enough; at this level the internal geometry is not so critical. The *"Bare module cost"* and the price increase from 2004 to 2009 were also estimated using a correction factor (88).

The construction material used for all the equipments was stainless steel. According to some chemical resistance charts, the stainless steel is not the best material to handle butanal but in the absence of any other chemical resistance data all the calculations were performed with the mentioned material. In order to compare the capital costs of all the alternatives this aspect is not a critical issue since the cost increment related to a more resistant material would affect to the cost of all alternatives in a very similar way.

Following this procedure the capital cost of each studied alternative are showed in Table 8.9, Table 8.10, Table 8.11, Table 8.12 and Table 8.13. It can be observed that the reactive distillation alternative at low reflux ratios and one distillation column is the cheapest one according to the capital costs. However, manufacturing costs or operating costs must be studied before drawing any conclusion.

Table 8.9 Capital cost of the base case.

Equipment	Height/Length (meters)	Diameter (meters)	Pressure (barg)	Purchased Equipment Cost (M€)	Bare Module Cost (M€)	Grass Root Cost (M€)
D-100	14	4	0	0.21	0.91	
D-101	19	4	2	0.34	1.83	5.00
R-100	0	1	2	0.002	0.02	

Table 8.10 Capital cost of the RD case at high reflux ratios.

Equipment	Height/Length (meters)	Diameter (meters)	Pressure (barg)	Purchased Equipment Cost (M€)	Bare Module Cost (M€)	Grass Root Cost (M€)
RD-100	8.4	1.6	2	0.04	0.15	
D-100	11.5	1.8	0	0.05	0.24	3.87
D-101	20.1	3.6	2	0.33	1.76	

Table 8.11 Capital cost of the RD case at low reflux ratios (2 distillation columns).

Equipment	Height/Length (meters)	Diameter (meters)	Pressure (barg)	Purchased Equipment Cost (M€)	Bare Module Cost (M€)	Grass Root Cost (M€)
RD-100	8.4	1.6	2	0.04	0.15	
D-100	8.0	1.0	0	0.01	0.07	49.10
D-101	53.0	7.0	2	9.05	26.83	

Table 8.12 Capital cost of the RD case at low reflux ratios (1 distillation column).

Equipment	Height/Length (meters)	Diameter (meters)	Pressure (barg)	Purchased Equipment Cost (M€)	Bare Module Cost (M€)	Grass Root Cost (M€)
RD-100	8.4	1.6	2	0.04	0.15	0.62
D-100	7.6	1.3	0	0.02	0.11	

Table 8.13 Capital cost of the PFR + PV + Distillation case.

Equipment	Height/Length (meters)	Diameter (meters)	Pressure (barg)	Purchased Equipment Cost (M€)	Bare Module Cost (M€)	Grass Root Cost (M€)
R-100	1	1	2	0.002	0.02	
PV-100	1.6	1	0	1.23	3.07	5.60
D-100	9	4	0	0.13	0.63	

8.3.2 Manufacturing costs

Manufacturing or operating costs (COM) are the associated ones with the day-to-day operation of a chemical plant. There are lots of factors that contribute to the cost of manufacturing. Some of them are considered as “direct manufacturing costs”; these costs represent operating expenses that vary with production rate. Raw material, waste treatment, utilities like electric power or cooling water, operating labor or maintenance

costs are in this group. Some others form the "Fixed Manufacturing Costs" group; this group includes property taxes, insurance and this kind of costs. Finally there is the "General expenses" group. In this group management, sales, financing and research functions are included.

The aim of the present cost study is to compare and determine the best alternative for 1,1 diethoxy butane production. Most of the described manufacturing costs are common for all the alternatives. That is the reason why the utility costs (cooling water, refrigerant fluid and heating steam) and raw material costs were the only studied manufacturing costs in this section. It must be remembered that the product yield was different in each case (Section 8.1.5).

Cooling water was necessary for the condensers of every single distillation column. Low pressure steam (50 psig) was necessary in order to use it in the reboilers. On the other hand a refrigerant fluid was necessary in order to condensate the permeate stream of the membrane module.

The used utility costs values were updated to June 2010 and they were supplied by PETRONOR. On the other hand, the ethanol price was kindly provided by RYTTSA, the product trading of REPSOL YPF. In terms of butanal, it seems that there is not any supplier at industrial scale or at least its price was not found at this scale. Therefore lab scale ethanol-butanal price ratio was applied in order to calculate the butanal price. Depends on the commercial brand this ratio varies from 1 to 1.8; in the present case 1.5 was the used ratio. The used values are tabulated in Table 8.14.

Table 8.14 Used utility and raw material prices.

Cooling water[1]	0.64 €/t
Low pressure steam (50 psig – 147.5 ºC)[1]	29.95 €/t
Electric power[1]	0.037759 €/kW·h
Ethanol 99%[2]	0.50 €/L
Butanal 99%	0.75 €/L

[1] Supplied by PETRONOR

[2] Supplied by RYTTSA

For the condensation of the permeate, a cooling system was used (requiring electrical energy) using a cooling cycle with a coefficient of performance (COP) of 4 (87). The cooling cost was calculated following the next equation (60):

$$C_{perm} = \frac{Q_{perm} C_{elec}}{COP \ 3600} \tag{60}$$

Where: Q_{perm} heat withdrawn for permeate condensation (kJ/h)
C_{elec} electric power
COP coefficient of performance of the cooling fluid

On the other hand, the cooling and heating costs were estimated using CAPCOST software once utility costs were updated. Table 8.15, Table 8.16, Table 8.17,

Table 8.18 and Table 8.19 show all the calculated operating costs for each alternative.

Table 8.15 Manufacturing costs of the base case.

		Cooling cost (M€/y)	Heating cost (M€/y)	Energy cost (M€/y)	Manufacturing costs (M€/y)
Energy	**D-100**	1.88	4.30	10.57	63.94
	D-101	1.29	3.10		
		Feed mass flow (kg/h)	**Raw Material cost (M€/y)**		
Raw Materials	**Ethanol**	5690.00	29.99	53.37	
	Butanal	3006.20	23.40		

Table 8.16 Manufacturing costs of the RD case at high reflux ratios.

		Cooling cost (M€/y)	Heating cost (M€/y)	Energy cost (M€/y)	Manufacturing costs (M€/y)
Energy	**RD**	1.66	3.70	12.01	61.07
	DIST	0.76	1.77		
	D-101	1.22	2.90		
		Feed mass flow (kg/h)	**Raw Material cost (M€/y)**		
Raw Materials	**Ethanol**	4322.20	22.77	49.06	
	Butanal	3379.20	26.30		

Table 8.17 Manufacturing costs of the RD case at low reflux ratios (2 distillation columns).

		Cooling cost (M€/y)	Heating cost (M€/y)	Energy cost (M€/y)	Manufacturing costs (M€/y)
Energy	**RD**	1.78	4.00	18.37	92.83
	DIST	0.17	0.42		
	D-101	3.60	8.40		
		Feed mass flow (kg/h)	**Raw Material cost (M€/y)**		
Raw Materials	**Ethanol**	9620.50	50.67	74.46	
	Butanal	3056.20	23.78		

Table 8.18 Manufacturing costs of the RD case at low reflux ratios (1 distillation column).

		Cooling cost (M€/y)	Heating cost (M€/y)	Energy cost (M€/y)	Manufacturing costs (M€/y)
Energy	**RD**	3.20	7.20	11.98	64.50
	DIST	0.47	1.11		
		Feed mass flow (kg/h)	**Raw Material cost (M€/y)**		
Raw Materials	**Ethanol**	5150.90	27.13	52.52	
	Butanal	3262.00	25.39		

Table 8.19 Manufacturing costs of the PFR + PV + Distillation case.

		Cooling cost (M€/y)	Heating cost (M€/y)	Energy cost (M€/y)	Manufacturing costs (M€/y)
Energy	**DIST**	1.39	3.40	4.82	39.15
	PV	0.34	-		
		Feed mass flow (kg/h)	**Raw Material cost (M€/y)**		
Raw Materials	**Ethanol**	3704.03	19.51	34.33	
	Butanal	2855.60	14.82		

8.4 Comparison of the studied alternatives

In the present thesis chapter five different acetal production alternatives were studied. In the first step all the alternatives were developed and optimized using ASPEN PLUS and ASPEN CUSTOM MODELLER for a production target of 50000 t/year of 1,1 diethoxy butane. In this step all the major and necessary equipments were determined as well as the energy requirements for each one. From a technical point of view, the alternative in which a dehydration membrane module was implemented was the most promising one regarding to its higher product yield and lower energy consumption.

However, nowadays the required membrane technology is not as developed as other conventional technologies like distillation. As a consequence, investment cost of this kind of separation modules is quite high. For this reason a cost study had to be performed and in order to perform this economic study all the main equipments had to be dimensioned. Once all the column diameter and heights were calculated capital and manufacturing costs were calculated using CAPCOST v2.0 software.

All the process technical and economical aspects are summarized in Table 8.20:

Table 8.20 Comparison of the most important process characteristics and economic costs.

	Process				
	Base case	**RD ↑R**	**RD ↓R (2 dist)**	**RD ↓R (1 dist)**	**With PV**
Product yield	0.66	0.74	0.45	0.68	0.88
Process conversion	0.94	0.83	0.92	0.86	0.995
PFR or RD conversion	0.34	0.45	0.23	0.16	0.44
Energy consum. (MW)	17.4	19.6	30.2	19.5	8.0
Cooling energy (MW)	-17.3	-19.8	-30.3	-19.8	-7.6
Capital costs (M€)	5.0	3.9	49.1	0.6	5.6
Manufacturing costs (M€/y)	63.9	61.1	92.8	64.5	39.1

According to capital costs, the pervaporation dehydration module case is the most expensive one. However, it can be observed that the manufacturing costs are the most important ones as these costs are one order of magnitude bigger than the capital costs and therefore, it is clear that the PFR+PV+Distillation case is the cheapest one.

As it could be observed in Section 8.3.2, within manufacturing costs the raw material costs are the most important ones. As the butanal price it is not known precisely a sensitivity analysis was performed in order to see how it influences on the different alternatives. Thus, four different cases were evaluated according to the price ratio between butanal and ethanol: Butanal/ethanol price ratios of 1, 1.5, 2 and 2.5. In Table 8.21 and Figure 8.8 it can be observed that in all the cases PFR + PV + Distillation case is the cheapest one. However, the price difference between the reactive distillation case at high reflux ratios and the base case reduces increasing the butanal/ethanol price ratio.

Table 8.21 Manufacturing costs for different butanal/ethanol price ratios.

	Manufacturing costs (M€/year)				
€But/€EtOH	**Base case**	**RD ↑R**	**RD ↓R (2 dist)**	**RD ↓R (1 dist)**	**With PV**
0.50	56.14	52.31	84.90	56.03	39.15
0.75	63.94	61.07	92.83	64.50	46.56
1.00	71.73	69.84	100.75	72.96	53.97
1.25	79.53	78.61	108.68	81.42	61.37

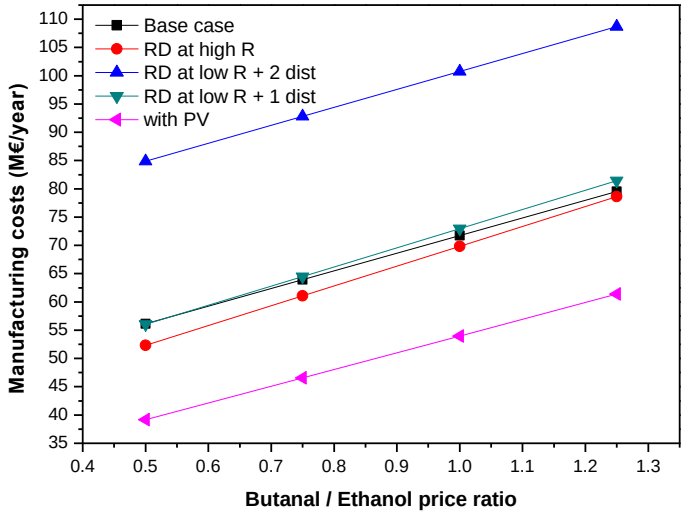

Figure 8.8 Manufacturing costs for different butanal/ethanol price ratios.

In terms of possible energy price fluctuations, they do not seem to be a critical item in order to choose a particular alternative because the energy costs represent 20% or less of the total manufacturing costs (Table 8.22). Furthermore, in case of an increment of energy price this would beneficiate to PFR+PV+Distillation case since this alternative is the one which requires less energy (see Section 8.3.2).

Table 8.22 The energy cost percentage with respect to manufacturing cost.

	Base case	**RD ↑R**	**RD ↓R (2 dist)**	**RD ↓R (1 dist)**	**With PV**
Energy cost/Manufacturing cost	16.5%	20.0%	20.0%	18.6%	12.3%

To sum up, it can be said that the studied last case, PFR + PV + Distillation case, is the best one from the process engineering point of view and also from the economic point of view. As a second alternative, it seems that the reactive distillation case at high reflux ratios offers better results than the other cases but the difference with respect to the base case reduces with the increase of the butanal price. Finally, it must be mentioned that reactive distillation case at low reflux ratios followed by two distillation columns is completely uneconomic and the case in which 1 distillation column is placed downstream is really similar to the base case in terms of economic estimations.

Chapter IX

Conclusions

9 Conclusions

9.1 Executive summary

The two main objectives of the present doctoral thesis were fulfilled: two different innovative and advanced reaction systems were developed (reactive distillation and dehydration membrane reactors), both experimentally and by modeling studies. The reaction between ethanol and butanal to produce 1,1 diethoxy butane (a promising biodiesel additive) and water, a highly thermodynamically limited reversible reaction, was used for the application and validation of the developed innovative reaction systems.

- Development of innovative and advance reaction systems

A continuous update of the new relevant published information was carried out along the four years that this work has been performed. Design, set up and start up of the reactive distillation semi-pilot plant was carried out. In case of the membrane reactor, the existing lab scale plant and the operating way were adapted to the experiment requirements. Moreover, some initial tests were performed in order to determine if some membrane protection elements were required in order to protect it from catalyst impacts. Finally, the corresponding experimental studies (experimental proposal) were determined in order to optimize their utilization and get as much information as possible in order to compare both systems.

- Development of acetal (1,1 diethoxy butane) production processes

    - The thermodynamic study of the chemical and physical equilibria involved in the studied system was absolutely necessary for a better understanding of the separation processes as well as determine adequately the experimental conditions (avoid non-miscible mixtures etc.). On the other hand, this study was required in order to estimate different physical and chemical properties and use them in the modeling works.

    - The kinetic study of 1,1 diethoxy butane production performed in a conventional batch reactor has allowed to determine the kinetics of the reaction

in order to apply them in the modeling studies of the reactive distillation and membrane reactor systems. On the other hand, the maximum conversions achievable using conventional reaction systems was estimated (around 40% at acceptable kinetic range).

- The experimental and modeling work performed with reactive distillation and dehydration membrane reactors has lead to find the best configuration in each case. Thus, it was checked that using reactive distillation the process conversion could be slightly increased from 40% (the achieved ones in a conventional reactor) to 50% at certain conditions. On the other hand, using appropriate process conditions, it was checked that using a dehydration membrane reactor the conversion could be increased from 40% to 70%.

  In this way one of the main objectives of the present doctoral thesis was fulfilled: two different advanced and non-conventional reaction systems were developed checking that their use leads to achieve higher conversions than in conventional reactors.

- By means of an initial process engineering calculations both developed systems were compared to each other and to a base case based on a conventional tubular reactor. The *material and energy balances* showed that the process in which dehydration pervaporation modules were included is the best one, both from the product yield point of view and also from the energetic point of view (the lowest energy/product ratio).

  In terms of the *final process economy*, as it was stated in the "Objectives" chapter, it is not possible to state that 1,1 diethoxy butane is a possible economic biodiesel additive (€/J) nowadays. Butanal is not still a commodity for this kind of industries and therefore its price is rather high for this purposes. In the near future it is envisaged that bio-butanol market will increase in an important way and therefore, obtaining its derivates (like butanal) will be far cheaper. On the other hand, with the accuracy level of calculation of the manufacturing costs (the common manufacturing costs for all the alternatives – property taxes, insurances, sale & financing costs etc,. where not calculated), it is not possible to give a reliable value of the €/J for 1,1 diethoxy butane in order to see if it is comparable to the €/J ratio of biodiesel.

Below some more detailed conclusions are explained for each chapter.

9.2 Kinetic study

- As a result of the kinetic study, it is proved that the acetalization reaction between ethanol and butanal is carried out in two different steps: the first one, where the hemiacetal is formed, is quasi instantaneous in absence of catalyst and also at room temperature while the second step, where the acetal is formed, is the controlling one and requires an acid catalyst. Also this second step can be carried out at room temperature with an acceptable reaction rate.

- Amberlyst ion exchange resins provide a good reaction performance avoiding side reactions. The tested resins (Amberlyst 15Wet, 35Wet, 70 and 47) offer almost the same performance for the studied reaction.

- No external mass transfer was observed at low stirring speeds (500 rpm) and it was checked that the order of reaction with respect to ethanol is two and one with respect to butanal.

- Significant thermodynamic limitations of the reaction achieving quite low equilibrium conversion at kinetically acceptable temperatures were also observed.

9.3 Reactive distillation

9.3.1 Experimental part

A semi-pilot plant was used in order to study the effect of different parameters like the pressure drop, catalyst amount, feeding temperature, location of the catalytic section and different feeding configurations. As catalytic bed, KATAPAK SP-11 modules with Amberlyst 47 ion exchange resin were used. The drawn conclusions are the following ones:

- The reaction does not take place in absence of catalyst.

- Higher pressure drops in the column imply higher conversions due to a better liquid-catalyst contact. As a drawback, this configuration implies more power supply in the reboiler which makes the process more expensive from the energetic point of view.

- Increasing the catalyst loading (more KATAPAK modules) higher conversions were achieved, especially operating at low reflux ratios. At high reflux ratios the catalyst amount is not so critical as the molecules have more opportunities to react.

- Conversions higher than the corresponding ones to equilibrium in conventional systems (without simultaneous separation), operating at the same conditions, were only observed for quite high reflux ratios. This can be explained by the limited achievable separation of water from non-reacted ethanol and butanal. Reactive distillation systems would overcome more efficiently thermodynamic limitations operating with reactants that can be separated from water more easily by distillation.

- The variation of the stripping section height showed that more separation stages implies higher conversions at low reflux rates but, depending on the configuration of the catalytic section, lower conversions could be achieved at high reflux ratios. In principle, more stripping height implies higher concentration of the volatile compounds (the reactants) and lower acetal concentrations through the reactive section. According to this explanation, the achieved conversion should have been higher with higher stripping section for all the reflux ratios but this is not true for the highest ones. This fact can be explained in the following way: as a consequence of having a higher stripping height, the top part of the catalytic section works better and therefore, more acetal is formed there. Due to its low relative volatility, the acetal goes down towards the reboiler as soon as it is formed. Thus, acetal concentrations in the lowest part of the catalytic section could be important enough in order to favor the reverse reaction and as a result reach lower conversions.

- Regarding the different feed configurations, the main conclusion is that feeding the reactants mixture from the top side of the reactive section, the achieved conversion increases significantly. Thus it is concluded that the volatility difference between butanal and ethanol is not important enough in order to take advantage of it.

- After performing all the experiments it was concluded that the optimum column configuration for the used semi-pilot plant is the following one:
    - 5 Katapak SP-11 modules
    - One unique feed point, at the top side of the catalytic section
    - Feed composition: 4:1 EtOH:Butanal
    - Feed flow: 3.5 L/h
    - Feed temperature: as close as possible to the saturation conditions of the mixture

- High pressure drops

9.3.2 Modeling part

- It was demonstrated that a reactive distillation mathematical steady-state model can simulate quite accurately the experimental results. A unique *tuning factor* was used in order to adjust the model with the results and it can be considered constant for similar fluid dynamics behavior. This *tuning factor* includes several factors like, plate efficiency, and catalyst wet factor. On the other hand, it is known that 3 Katapak modules are equivalent to 0.6 theoretical stages and in the present case they were assumed to be one stage (due to the impossibility of introducing 0.6 stages in the model); this effect is also considered in the *tuning factor*.

- It was checked that there is not any resistance to the external mass transfer and thus, the reaction is controlled by its kinetics.

- The optimum number of stages was found and it was concluded that the increase of reaction stages does not imply higher conversions. Depending on the operating conditions it may happen that in the lower side of the catalytic section the reverse reaction ends being more important than the forward reaction, which implies a conversion decrease.
- It was also concluded that the conversion cannot be increased rising the number of stripping stages. Besides that, operating at high reflux ratios, an increase in the number of stripping stages implies a conversion decrease. This effect was also observed experimentally.

- In terms of rectification stages, the great volatility difference between acetal and the reactants implied that one rectification stage seems to be enough.

- Regarding the different effects checked varying different parameters, in all the cases could be verified that the experimentally observed trends agree with the model predicted trends. Thus, it was proved that feeding a stoichiometric mixture from the top of the catalytic section, higher conversions than feeding through 2 different feed heights are achieved. Moreover, it was observed that modifying the bottoms flow rate, different conversions are achieved and an optimal rate can be found.

- Another interesting conclusion is that depending on the catalyst loading or the number of reaction stages, an increase in the feed temperature can imply a decrease in

the conversion. In this effect, the most important parameter is the residence time. With low residence times (low catalyst amount) an increase of the feed temperature increases the conversion because equilibrium limitations may not have important influence. At higher residence times (higher catalyst amount) the effect of the reverse reaction becomes significant decreasing the conversion.

9.4 Dehydration membranes

It was proven that the conversion of the acetalization reaction can be improved to above the equilibrium by adding a pervaporation dehydration unit operation both experimentally and through modeling. In a continuous process where a reactor, a pervaporation section to separate the water formed, and a small distillation section to separate the acetal and recycle the non reacted ethanol and butanal are used a conversion of almost 100% can be reached. The equilibrium conversion under similar reactor conditions without separation was only about 40%.

The batch model results compare very well with the batch experiments showing that the model that has been developed is valid. Comparison of the modeling results of the continuous process with the batch process shows that the results are comparable as well and thus the continuous model is also validated.
Adiabatic operation of the continuous process with the reactor and separator in series is preferred over isothermal operation as this favors the process heat integration and the temperatures in the reaction and pervaporation section. More concrete conclusions of each part are described below

9.4.1 Experimental part

- The most important evidence is that HybSi® membranes are selective for ethanol/butanal/1,1 diethoxy butane/water mixtures and that they can shift the equilibrium of the acetalization reaction significantly. It must be taken into account that butanal, as most of the aldehydes, is quite an aggressive organic compound. The membrane is practically impermeable to 1,1 diethoxy butane and the butanal permeance could also be considered negligible. Due to the membrane selectivity, water could be removed efficiently from the reaction mixture and equilibrium conversions were overcome.

- The membrane area used in the experiments was really low for the feed amount that was treated and as a result, pervaporation was the limiting step in the performed experiments. Even working with really small amounts of catalyst, the achieved conversions were limited by the pervaporation rate.

- In terms of the temperature, it is clear that working at higher temperatures the water flux through the membrane increases. From the reaction point of view, being an exothermic reaction, it is known that the higher the temperature is, the lower equilibrium conversion is. However, in order to get considerable conversions, operating at the highest temperature for the combined pervaporation – reaction system better results are obtained.

- By using different ethanol/butanal feed ratios, it was observed that working with an excess of one of the reactants (ethanol) the final conversion is higher. However, working with 3:1 ethanol:butanal ratio, the ethanol driving force was quite important and therefore, ethanol flux and loss of ethanol through the membrane were considerable.

- Regarding the membrane mechanical resistance, it was found that HybSi membranes can handle Amberlyst 47 particle impacts. It was checked that, in spite of the impacts, the membrane behavior was completely stable.

9.4.2 Modeling part

9.4.2.1 Semi-batch model

- First of all experimental data and predicted data by batch model simulation were compared resulting in a very good agreement between them. Therefore, the batch process model was used to do some sensitivity analyses.

- The membrane area/reaction volume ratio is a very important parameter since the time required to reach a certain conversion value depends on their ratio. At higher membrane area/reaction volume ratios faster water separation is obtained, reaching faster the final conversion. In terms of the temperature it was checked that at low temperatures the pervaporation process is not really significant and if high conversions are required it must be operated at higher temperatures.

- The importance of the catalyst loading was also studied. The amount of catalyst is an important parameter from the reaction point of view in order to compare the

observed reaction rate and the pervaporation rate. It was concluded that between 20 and 70ºC working with, at least, 0.5 wt% of catalyst the dehydration process is the limiting step in order to get high conversions. Higher temperatures require less catalyst.

- The last parameter studied was the feed composition. Ethanol/butanal ratios between 2.5:1 and 3:1 seem to be the best options since high process conversion can be achieved without losing too much ethanol.

9.4.2.2 Continuous model

- A multitube plug flow membrane reactor (MPFMR) was modeled. By using this continuous reactor and separator system the conversion of the acetalization reaction can be increased to above the equilibrium conversion.

- Comparison of the modeling results of this continuous process with the batch process shows that the results are comparable. As the batch model is validated with experiments the continuous model is also validated indirectly.

- First of all an optimum reactor geometry was calculated. In general the larger the outer diameter of the membrane tube the more optimal the reactor geometry. The reason for this is that the membrane surface area to volume ratio is increasing under the constraints used. Two different configurations were chosen "*Configuration 17 A70"* and *"Configuration 18 A70*" as the most suitable ones. The first of these configurations (having an optimized feed flow characteristic or Re values) showed low conversion values but after a sensitivity analysis it was checked that 75 % of conversion could be reached. However, a 15 meters long reactor would be necessary in order to achieve this conversion.

- Secondly, *"Configuration 18 A70*" (having an optimized membrane surface area) showed interesting conversion values but at very low Re numbers. This could lead to undesired polarization effects that have not been estimated. In order to increase the turbulence part of the retentate was recycled to the feed. It was checked that increasing the Re number the conversion decreases considerably.

- The operation of the system in an adiabatic mode is preferred over an isothermal mode. The reason is that in the adiabatic mode the temperature increase because of the exothermic reaction helps increasing the membrane flux. Thus the water removal rate is higher and the shift of the equilibrium is further increased.

- It can be said that in order to avoid wall effects due to the presence of catalyst particles, the distance among membrane pipes is too big. As a consequence, the available membrane area in the reactor is not big enough to achieve high conversions with reasonable reactor dimensions in a continuous process mode. However, it was checked that if a new membrane generation offers 3 times higher fluxes than the actual ones, the developed membrane reactor would have acceptable dimensions to treat 7 L/h of feed flow. For this reason, other process designs where the reaction and pervaporation take place in different units were studied.

- Via a sensitivity analysis of the reactor and the pervaporation module separately, using adiabatic operation, it was concluded that the reactor feed should be at low temperatures while the pervaporation feed should be as warm as possible (always in liquid phase).

- Three different process configurations where tested being the base case a plug flow reactor followed by a pervaporation module to separate the water from the mixture. A liquid pump and a heat exchanger were placed in between:

1. PFR + PV modules in series
2. PFR + PV including a recycling loop
3. PFR + PV + Distillation column recycling the head of the distillation column

The first two configurations showed that conversions around 70 % were achievable. These values are in good agreement with the observed experimental conversions, the predicted conversion values by the semi-batch model as well as the predicted ones by the MPFMR model. However, these configurations require a large membrane area (1.0 m^2 of membrane area "in series" configuration and 1.60 m^2 of membrane area with a simple recycling loop) to treat 7 L/h of volumetric feed flow. From the unit size point of view the recycling option is preferred above the series configuration. The third configuration includes a distillation column and from the energetic point of view, a priori, it is not the most suitable one. However, this configuration offers conversions around 100% and the required membrane area is much smaller (0.81 m^2) than in the previous cases.

In the first two cases the conversion increase is due to the water separation while in the last case is due to the water and acetal separation from the liquid mixture and to the recycle of the non-reacted ethanol and butanal. Thus, using a small pervaporation unit and a small distillation column, almost 100% of conversion can be achieved.

9.5 Process design & economic study: general conclusions

- Five different acetal production alternatives were studied. In the first step all the alternatives were developed and optimized using ASPEN PLUS and ASPEN CUSTOM MODELLER for a production target of 50000 t/year of 1,1 diethoxy butane. In this step all the major and necessary equipments were determined as well as the energy requirements for each one. From a technical point of view, the alternative in which a dehydration membrane module was implemented was the most promising one because of its higher product yield and lower energy consumption.

- An economic study was also performed in order to check if the dehydration membranes alternative was economically viable. Capital and manufacturing costs were estimated and it was observed that the pervaporation dehydration module case is the most expensive one in terms of capital costs. However, the manufacturing costs are the most important ones in all the cases as these costs are one order of magnitude bigger than the capital costs and therefore, the PFR+PV+Distillation case looks as the cheapest one.

- As the butanal price is not available as a raw material at industrial scale, a sensitivity analysis was performed with its price. It was concluded that the butanal price is not a critical parameter in order to choose one of the studied alternatives.

- Possible energy price fluctuations were also taken into account. They do not seem to be a critical item in order to choose a particular alternative because the energy costs represent 20% or less of total manufacturing costs. Furthermore, in case of an increment of energy price this would beneficiate to PFR+PV+Distillation case since this alternative is the one which requires less energy

➢ **FINAL CONCLUSION**

It can be said that the studied last case, PFR + PV + Distillation case, is the best one from the process engineering point of view and also from the economic point of view.

As a second alternative, it seems that the reactive distillation case operating at high reflux ratios offers better results than the other cases but the difference with respect to the base case reduces with the increase of the butanal price.

Finally, it must be mentioned that reactive distillation case at low reflux ratios followed by two distillation columns is completely uneconomic and the other case in which 1 distillation column is placed downstream is really similar to the base case in terms of economic estimations.

Chapter X

Bibliography

10 Bibliography

(1) IEA. IEA. Key World Energy Statistics. 2009. 2009.

(2) BP. Statistical Review of World Energy. June 2007.

(3) IEA. World Energy Outlook 2007.

(4) Environmental Protection Agency (EPA). Climate Change Indicator in the United States. 2009.

(5) CIEMAT, Ministerio de ciencia y educación. Life Cycle Environmental Aspects of Biofuel Goals in spain. Energy and global warming. 2007 Mar 19.

(6) Abengoa Bioenergy. Abengoa 2008Available from: URL: http://www.abengoabioenergy.com/trading/index.cfm?page=23&lang=2&loc=3

(7) McCormick RL, Graboski MS, Alleman TL, Herring AM, Tyson KS. Impact of Biodiesel Source Material and Chemical Structure on Emissions of Criteria Pollutants from a Heavy-Duty Engine. Environmental Science and Technology 2001;35(9):1742-7.

(8) Moser BR, Erhan SZ. Branched chain derivatives of alkyl oleates: Tribological, rheological, oxidation, and low temperature properties. Fuel 2008 Aug;87(10-11):2253-7.

(9) Keskin A, Gürü M, AltIparmak D. Influence of tall oil biodiesel with Mg and Mo based fuel additives on diesel engine performance and emission. Bioresour. Technol. 2008 Sep;99(14):6434-8.

(10) Burtscher H, Matter U, Skillas G. The effect of fuel additives on diesel engine particulate emissions. J. Aerosol Sci. 1999 Sep;30 (Supplement 1):S851-S852.

(11) Kim H, Choi B. Effect of ethanol-diesel blend fuels on emission and particle size distribution in a common-rail direct injection diesel engine with warm-up catalytic converter. Renewable Energy 2008 Oct;33(10):2222-8.

(12) Li Dg, Zhen H, Xingcai L, Wu-gao Z, Jian-guang Y. Physico-chemical properties of ethanol-diesel blend fuel and its effect on performance and emissions of diesel engines. Renewable Energy 2005 May;30(6):967-76.

(13) Frusteri F, Spadaro L, Beatrice C, Guido C. Oxygenated additives production for diesel engine emission improvement. Chem. Eng. J. 2007 Nov 1;134(1-3):239-45.

(14) Filley J. New lubricants from vegetable oil: cyclic acetals of methyl 9,10-dihydroxystearate. Bioresour. Technol. 2005 Mar;96(5):551-5.

(15) Mahajani S.M. Reactions of glyoxylic acid with aliphatic alcohols using cationic exchange resins as catalysts. React. Func. Polym. 2000 Mar 15;43(3):253-68.

(16) Chang B.H. A facile synthesis of acetals and aldehydes from allylic ethers catalyzed by cobalt compounds. Journal of Organometallic Chemistry 1995 Apr 19;492(1):31-4.

(17) Kumar R., Chakraborti A.K. Copper(II) tetrafluoroborate as a novel and highly efficient catalyst for acetal formation. Tetrahedron Letters 2005 Nov 28;46(48):8319-23.

(18) Capeletti M.R., Balzano L., de la Puente G., Laborde M., Sedran U. Synthesis of acetal (1,1-diethoxyethane) from ethanol and acetaldehyde over acidic catalysts. Appl. Catal. Catal., A 2000 May 15;198(1-2):L1-L4.

(19) Mahajani S.M., Kolah A.K., Sharma M.M. Extractive reactions with cationic exchange resins as catalysts (acetalization of aldehydes with alcohols). React. Func. Polym. 1995 Dec;28(1):29-38.

(20) Kaufhold M., El-Chahawi M., inventors; Huels Aktiengesellschaft, assignee. Process for preparing acetaldehyde diethyl acetal. Germany patent 5527969. 1996 Jun 18.

(21) Chopade SP, Sharma MM. Acetalization of ethylene glycol with formaldehyde using cation-exchange resins as catalysts: batch versus reactive distillation. React. Func. Polym. 1997 Sep;34(1):37-45.

(22) Chopade SP, Sharma M.M. Reaction of ethanol and formaldehyde: use of versatile cation-exchange resins as catalyst in batch reactors and reactive distillation columns. React. Func. Polym. 1997 Jan;32(1):53-65.

(23) Andrade J., Arntz D., Kraft M., Prescher G., inventors; Degusa Aktiengesellschaft, assignee. Method for preparation of acetals. Germany patent 4579979. 1986 Apr 1.

(24) Green T.W. Protective Groups in Organic Synthesis. New York: Willey; 1981.

(25) Sharma MM. Some novel aspects of cationic ion-exchange resins as catalysts. React. Func. Polym. 1995 Sep;26(1-3):3-23.

(26) Calvar N., González B., Dominguez A. Esterification of acetic acid with ethanol: Reaction kinetics and operation in a packed bed reactive distillation column. Chem. Eng. Process 2007;46:1317-23.

(27) Zhu Y, Minet RG, Tsotsis TT. A continuous pervaporation membrane reactor for the study of esterification reactions using a composite polymeric/ceramic membrane. Chem. Eng. Sci. 1996 Sep;51(17):4103-13.

(28) Feng X, Huang RYM. Studies of a membrane reactor: Esterification facilitated by pervaporation. Chem. Eng. Sci. 1996 Oct;51(20):4673-9.

(29) Lim Y, Park B, Hung F, Sahimi M, Tsotsis T. Design issues of pervaporation membrane reactors for esterification. Chem. Eng. Sci. 2002;57(22-23):4933-46.

(30) Domingues L, Recasens F, Larrayoz MA. Studies of a pervaporation reactor: Kinetics and equilibrium shift in benzyl alcohol acetylation. Chem. Eng. Sci. 1999 May;54(10):1461-5.

(31) Benedict DJ, Parulekar SJ, Tsai S. Pervaporation-assisted esterification of lactic and succinic acids with downstream ester recovery. J. Membr. Sci. 2006 Sep 15;281(1-2):435-45.

(32) Sanz MT, Gmehling J. Esterification of acetic acid with isopropanol coupled with pervaporation: Part I: Kinetics and pervaporation studies. Chem. Eng. J. 2006 Oct 1;123(1-2):1-8.

(33) Sanz MT, Gmehling J. Esterification of acetic acid with isopropanol coupled with pervaporation: Part II. Study of a pervaporation reactor. Chem. Eng. J. 2006 Oct 1;123(1-2):9-14.

(34) Dhale AD, Myrant LK, Chopade SP, Jackson JE, Miller DJ. Propylene glycol and ethylene glycol recovery from aqueous solution via reactive distillation. Chem. Eng. Sci. 2004 Jul;59(14):2881-90.

(35) Klöker M., Kenig E.Y., Górak A., Markusse A.P., Kwant G., Moritz P. Investigation of different column configurations for the ethyl acetate synthesis vio reactive distillation. Chem. Eng. Process 2004;43:791-801.

(36) Taylor R., Krishna R. Modelling reactive distillation. Chem. Eng. Sci. 2000 Apr 12;55:5183-229.

(37) Mulder M. Basic Principles of Membrane Technology. Dordrecht, The Netherlands: Kluwer Academic Publishers; 1996.

(38) Baker R.W. Membrane Technology and Applications. 2nd Edition ed. WILEY; 2000.

(39) Peters TA, van der Tuin J, Houssin C, Vorstman MAG, Benes NE, Vroon ZAEP, et al. Preparation of zeolite-coated pervaporation membranes for the integration of reaction and separation. Catal. Today 2005 Jun 30;104(2-4):288-95.

(40) Peters TA, Benes NE, Keurentjes JTF. Preparation of Amberlyst-coated pervaporation membranes and their application in the esterification of acetic acid and butanol. Appl. Catal. Catal., A 2007 Jan 27;317(1):113-9.

(41) Bagnell L, Cavell K, Hodges AM, Mau A, Seen AJ. The use of catalytically active pervaporation membranes in esterification reactions to simultaneously increase product yield, membrane permselectivity and flux. J. Membr. Sci. 1993 Dec 2;85(3):291-9.

(42) Castricum HL, Sah A, Kreiter R, Blank DHA, Vente JF, ten Elshof JE. Hybrid ceramic nanosieves: stabilizing nanopores with organic links. Chem Commun (Cambridge, U K) 2008;(9):1103-5.

(43) Bernal M, Coronas J, Menɛndez M, Santamaria J. Coupling of reaction and separation at the microscopic level: esterification processes in a H-ZSM-5 membrane reactor. Chem. Eng. Sci. 2002 May;57(9):1557-62.

(44) Sommer S, Melin T. Performance evaluation of microporous inorganic membranes in the dehydration of industrial solvents. Chem. Eng. Process 2005 Oct;44(10):1138-56.

(45) Kang M, Choi Y, Moon S. Water-swollen cation-exchange membranes prepared using poly(vinyl alcohol) (PVA)/poly(styrene sulfonic acid-co-maleic acid) (PSSA-MA). J. Membr. Sci. 2002 Sep 15;207(2):157-70.

(46) Lee Y, Nam S, Woo D. Pervaporation of ionically surface crosslinked chitosan composite membranes for water-alcohol mixtures. J. Membr. Sci. 1997 Sep 17;133(1):103-10.

(47) ECN 2010 Available from: URL: http://www.hybsi.com

(48) Castricum HL, Sah A, Kreiter R, Blank DHA, Vente JF, ten Elshof JE. Hydrothermally stable molecular separation membranes from organically linked silica. J Mater Chem 2008;18(18):2150-8.

(49) Castricum HL, Kreiter R, van Veen HM, Blank DHA, Vente JF, ten Elshof JE. High-performance hybrid pervaporation membranes with superior hydrothermal and acid stability. J. Membr. Sci. 2008 Oct 31;324(1-2):111-8.

(50) Kreiter R, Rietkerk Marielle DA, Castricum HL, van Veen HM, ten Elshof JE, Vente JF. Stable hybrid silica nanosieve membranes for the dehydration of lower alcohols. ChemSusChem 2009;2(2):158-60.

(51) Chapman PD, Oliveira T, Livingston AG, Li K. Membranes for the dehydration of solvents by pervaporation. J. Membr. Sci. 2008 Jun 20;318(1-2):5-37.

(52) Rohm & Haas. Product data sheet of Amberlyst resins. 2003.
Ref Type: Catalog

(53) Chopade S.P., Sharma M.M. Reaction of ethanol and formaldehyde: use of versatile cation-exchange resins as catalyst in batch reactors and reactive distillation columns. React. Func. Polym. 1997 Jan;32(1):53-65.

(54) Abad B. Identificación de la presencia de hemiacetal en una mezcla etanol:butanal (2:1 en moles). SGIKER. General Analysis Department of the University of the Basque Country.; 2008 Apr 21.

(55) Letcher TM, Redhi GG, Radloff SE, Domanska U. Liquid-Liquid Equilibria for Mixtures of Butanal + an Alkanol + Water at 298.15 K. J. Chem. Eng. Data 1996;41(4):707-12.

(56) NIST Chemistry. Available from URL: http://webbook.nist.gov/chemistry/

(57) J.M.Prausnitz, B.E.Polling, J.P.O'Connell. The properties of Gases and Liquids. 5th Edition ed. 2007.

(58) Götze L, Bailer O, Moritz P, von Scala C. Reactive distillation with KATAPAK«. Catal. Today 2001 Sep 15;69(1-4):201-8.

(59) J.M.Smith, H.C.van Ness, M.M.Abbott. Introduction to Chemical Engineering Thermodynamics. 6th Edition ed. McGraw Hill; 2001.

(60) Perry R.H., Green D.W. Perry's Chemical Engineers' Handbook. 8th Edition ed. McGraw Hill; 2007.

(61) Bowen TC, Li S, Noble RD, Falconer JL. Driving force for pervaporation through zeolite membranes. J. Membr. Sci. 2003 Nov 1;225(1-2):165-76.

(62) de Vos RM, Maier WF, Verweij H. Hydrophobic silica membranes for gas separation. J. Membr. Sci. 1999 Jun 1;158(1-2):277-88.

(63) Feng X, Huang RYM. Estimation of activation energy for permeation in pervaporation processes. J. Membr. Sci. 1996 Sep 4;118(1):127-31.

(64) ten Elshof JE, Abadal CR, Sekulic J, Chowdhury SR, Blank DHA. Transport mechanisms of water and organic solvents through microporous silica in the pervaporation of binary liquids. Microporous Mesoporous Mater. 2003 Nov 4;65(2-3):197-208.

(65) Bettens B, Dekeyzer S, Van der Bruggen B, Degreve J, Vandecasteele C. Transport of Pure Components in Pervaporation through a Microporous Silica Membrane. J Phys Chem B 2005;109(11):5216-22.

(66) Sommer S, Melin T. Influence of operation parameters on the separation of mixtures by pervaporation and vapor permeation with inorganic membranes. Part 1: Dehydration of solvents. Chem Eng Sci 2005;60(16):4509-23.

(67) Benedict DJ, Parulekar SJ, Tsai SP. Esterification of lactic acid and ethanol with/without pervaporation. Ind Eng Chem Res 2003;42(11):2282-91.

(68) Goncalves FDR, Borges LEP, Borges CP. Synthesis of ethyl acetate by coupling a heterogeneous catalytic system with a pervaporation unit. Sep Sci Technol 2004;39(7):1485-500.

(69) Izak P, Mateus NMM, Afonso CAM, Crespo JG. Enhanced esterification conversion in a room temperature ionic liquid by integrated water removal with pervaporation. Sep. Purif. Technol. 2005 Feb;41(2):141-5.

(70) Wasewar K, Patidar S, Agarwal VK. Esterification of lactic acid with ethanol in a pervaporation reactor: modeling and performance study. Desalination 2009;243(1-3):305-13.

(71) Wasewar KL. Modeling of pervaporation reactor for benzyl alcohol acetylation. Int J Chem React Eng 2007;5:No.

(72) Hazarika S, Dutta A, Dutta N. Pervaporation Aided Esterification of Carboxylic Acids with Ethanol Catalyzed by Porcine Pancreatic Lipase. Biocatal Biotransform 2003;21(3):101-13.

(73) Tanna NP, Mayadevi S. Analysis of a membrane reactor: influence of membrane characteristics and operating conditions. Int J Chem React Eng 2007;5:No.

(74) de la Iglesia O, Mallada R, Menθndez M, Coronas J. Continuous zeolite membrane reactor for esterification of ethanol and acetic acid. Chem. Eng. J. 2007 Jul 1;131(1-3):35-9.

(75) Nemec D, Van Gemert R. Performing Esterification Reactions by Combining Heterogeneous Catalysis and Pervaporation in a Batch Process. Ind Eng Chem Res 2005;44(25):9718-26.

(76) Geankoplis C.J. Transport processes and separation process principles. 3rd Edition ed. Compañia editorial continental, S.A de C.V., México; 1998.

(77) Theuerkauf J, Witt P, Schwesig D. Analysis of particle porosity distribution in fixed beds using the discrete element method. 2006 Jul 13;165(2):92-9.

(78) Dixon AG. Correlations for wall and particle shape effects on fixed bed bulk voidage. Can J Chem Eng 1988;66(5):705-8.

(79) Sommer S, Klinkhammer B, Schleger M, Melin T. Performance efficiency of tubular inorganic membrane modules for pervaporation. AIChE J 2005;51(1):162-77.

(80) Froment GF. Chemistry and Chemical Engineering of Catalytic Process. 1st edition ed. Maryland: Springer; 1980.

(81) Albright's Chemical Engineering Handbook. CRC Press. Taylor & Francis Group; 2008.

(82) Branan C.R. Rules of Thumb for Chemical Engineers. 3rd Edition ed. Elsevier; 2010.

(83) G.F.Hewitt. Heat Exchanger Design Handbook. 2002.

(84) Warren D.Seider, J.D.Seader, Daniel R.Lewin. Product & Process Design Principles. New York (USA): Wiley; 2004.

(85) W.L.McCabe, P.Harriott, J.C.Smith. Operaciones Unitarias en Ingeniería Química. McGraw Hill; 2007.

(86) Richard Turton, Richard C.Bailie, Wallace B.Whiting, Lyle F.Albright. Analysis, Sinthesis, and Design of Chemical Processes. Pearson Education Heg USA; 2009.

(87) Van Hoof V, Van den Abeele L, Buekenhoudt A, Dotremont C, Leysen R. Economic comparison between azeotropic distillation and different hybrid systems combining distillation with pervaporation for the dehydration of isopropanol. Sep Purif Technol 2004;37(1):33-49.

(88) ECN internal communication. 2010.
Ref Type: Personal Communication

Appendix

APPENDIX A Notation, list of abbreviations

A	Pre-exponential factor, $(m^3)^3/(mol^2 \cdot s \cdot kgcat)$ for forward reaction & $(m^3)^2/(mol \cdot s \cdot kgcat)$ for reverse reaction
a_c	Catalyst surface area, m^2/kg
A_m	Membrane area, m^2
A_t	Cross sectional area of the shellside (without taking into account the membrane pipes), m^2
c	Number or components
C_{elec}	Electric power
C_i	Molar concentration for component i, mol/m^3
C_{iL}	Concentration of component "i" in the liquid bulk, mol/L
COP	Coefficient of performance of the cooling fluid
Cp_i	Specific heat for component i, kJ/(kmol K)
D	Diameter of the column, ft
D_{AB}	Butanal diffusivity in the mixture
D_i	Diffusion coefficient, cm^2/s
d_o	Membrane tube diameter, m
d_P	Catalyst particle diameter, m
E_a	Activation energy, J/mol
f	Fraction of the cross sectional area
f_i	Flux through the membrane for component i, $kmol/(m^2\ h)$
f_i	Fugacity of component *i* as a pure component, bar
F_i	Molar flow rate in the shellside for component i, $kmol/(m^3\ h)$
F_p	Mass which goes through the membrane, kg/s
F_p	Packing factor, ft^2/ft^3
g	Gravitational aceleration, m/s^2
h	Enthalpy of the liquid phase, J/h
H	Enthalpy of the vapour phase, J/h
J_i	Flux through the membrane for component i, $mol/(m^2\ h)$
K	Equilibrium constant
k'_1	Kinetic constant for the forward reaction, $(m^3)^3/(mol^2 \cdot s \cdot kgcat)$
k'_2	Kinetic constant for the forward reaction, $(m^3)^2/(mol \cdot s \cdot kgcat)$
k_c	Mass transfer coefficient, m/s

Kv	Empirical coefficient to calculate column diameters
L	Liquid flow, mol/h
L	Reactor length
m_{cat}	Catalyst amount, kg
MW	Average molecular weight of the permeating fluid, kg/mol
N	Number of membrane tubes
N_s	Concentration of acid sites, H^+/g·cat
Pc	Critic pressure, bar
P_F	Pressure in the feed side, bar
p_m	Perimeter of total membrane tubes, m
P^{perm}	Total pressure in the permeate side, bar
$P_{sat,i}$	Saturation pressure for component i, bar
Q	Heat, J/h
Q_0	Pre-exponential factor for permeances, mol/(m^2 h bar)
Q_i	Permeance value for component i, mol/(m^2 h bar)
Q_{perm}	Heat withdrawn for permeate condensation, kJ/h
Qv	Volumetric flow rate, L/s
R	Universal gas constant, J/(mol·K)
R	Reflux ratio
r_i	Reaction rate for component i, mol/(m^3·s)
r_i	Reaction rate for component i, kmol/(m^3·s)
t	Time, s
T	Temperature, K
T_c	Critic temperature, K
T_N	Turnover number, min^{-1}
u_c	Maximum allowed vapor velocity, ft/s
V	Vapour flow, mol/h
V_r	Reaction volume, m^3
v_s	Superficial velocity, m/s
w	Catalyst loading, kgcat/m^3
x	Liquid molar fraction
x_i	Liquid molar fraction in the feed mixture
y	Vapour molar fraction
y_i	Vapor molar fraction in the permeate mixture
z	Normalized length (0…1)
$\hat{f}_i$	Fugacity of component *i* in a mixture, bar.

Greek Letters

ΔH_r	Enthalpy of reaction, kJ/mol
ΔH_f	Enthalpy of formation, kJ/mol
ΔHvap	Enthalpy of vaporization, kJ/mol
ΔG^0	Free energy of Gibbs, J/mol
γ_i	Activity coefficient for component i
ε	Void fraction
μ	Dynamic viscosity of the liquid in the feed-retentate side, Pa·s
ν_i	Stoichiometric coefficient for component i
ρ	Density of the liquid on the feed-retentate side, kg/m^3
ρ_r	Average density of the reaction mixture, kg/m^3
υ	reaction volume, L
Φ	Sphericity of particles (Φ=1)
$\hat{\phi}_i$	Fugacity coefficient of component i. (at low or moderate pressures ~ 1)
$\overline{\lambda}$	The latent heat of the permeating fluid, kJ/kmol

Subscripts of Chapter V

i	step in the distillation tower
j	compound

APPENDIX B Publications related to the present Doctoral Thesis

In the present Appendix all the published articles related to the present doctoral thesis are showed as well as the contributions to different international conferences.

B.1 Contribution to international conferences

Authors: Agirre I., Barrio V.L, Güemez B., Cambra J., Arias P.L.,
Title: Oxygenated diesel additives from bioalcohols: a kinetic study of 1,1 diethoxy butane production
Conference: 11th Mediterranean Chemical Engineering Congress
Publication: Multimedia publication of the conference

Place: Barcelona (Spain) **Date**: October 2008

Authors: Agirre I., Barrio V.L, Güemez B., Cambra J., Arias P.L.,
Title: The development of a reactive distillation process for the production of 1,1 diethoxy butane from bioalcohol: kinetic study and simulation model
Conference: Bioenergy II: Fuels And Chemicals From Renewable Resources
Publication: Conference abstract book

Place: Rio de Janeiro (Brazil) **Date**: March 2009

Authors: Agirre I, Güemez B., Veen H.M., Vente J.F., Arias P.L.,
Title: Improvement in the production of oxygenated diesel additives from bioalcohols using dehydration pervaporation membrane reactors.
Conference: International Scientific Conference on Pervaporation and Vapor Permeation
Publication: Conference abstract book

Place: Turun (Poland) **Date**: April 2010

Authors: Agirre I., Iriondo A., Requies J., Barrio V.L., Güemez B., Cambra J.F. López A. and Arias P.L.

Title: From bioalcohols (ethanol and n-butanol) to oxigenated diesel additives: 1,1 diethoxy butane

Conference: 3rd International Conference on Engineering for Waste and Biomass Valorization

Publication: Conference abstract book

Place: Beijing (China) **Date**: May 2010

Authors: Agirre I., Barrio V.L, Güemez B., Cambra J., Arias P.L.

Title: Development of a reactive distillation process for acetal production: experimental study and simulation model

Conference: XIX International Conference on Chemical Reactors. CHEMREACTOR-19

Publication: Multimedia publication of the conference

Place: Vienna (Austria) **Date**: Septiembre 2010

B.2 Published articles

Journal:	International Journal of Chemical Reactor Engineering				
Title:	Bioenergy II: The development of a reactive distillation process for the production of 1,1 diethoxy butane from bioalcohol: kinetic study and simulation model				
Authors:	Agirre I., Barrio V.L, Güemez B., Cambra J., Arias P.L.,				
Year:	2010	**Volume**:	8	**Article**:	A86

INTERNATIONAL JOURNAL OF CHEMICAL REACTOR ENGINEERING

Volume 8 2010 *Article* A86

Bioenergy II: The Development of a Reactive Distillation Process for the Production of 1,1 Diethoxy Butane from Bioalcohol: Kinetic Study and Simulation Model

Ion Agirre* V. Laura Barrio† Belen Güemez‡
Jose F. Cambra** Pedro L. Arias††

*Bilbao (UPV/EHU), ion.agirre@ehu.es
†Bilbao (UPV/EHU), laura.barrio@ehu.es
‡Bilbao (UPV/EHU), belen.guemez@ehu.es
**Bilbao (UPV/EHU), jose.cambra@ehu.es
††Bilbao (UPV/EHU), pedroluis.arias@ehu.es

ISSN 1542-6580

Bioenergy II: The Development of a Reactive Distillation Process for the Production of 1,1 Diethoxy Butane from Bioalcohol: Kinetic Study and Simulation Model*

Ion Agirre, V. Laura Barrio, Belen Güemez, Jose F. Cambra, and Pedro L. Arias

Abstract

1,1 Diethoxy butane was produced carrying out the reaction between ethanol and butanal in a batch stirred reactor using Amberlyst cation-exchange resins as catalyst. The kinetics of this reaction was studied working at different temperatures, feed compositions and catalyst type and loadings. Due to thermodynamic limitations, maximum conversions are quite low for kinetically acceptable temperatures. That is why the kinetic information gathered has been used to develop a model for reactive distillation, which has predicted promising results.

KEYWORDS: acetals, diethoxy butane, butanal, ethanol, kinetic study, Amberlyst, reactive distillation, acid catalyst

*The authors gratefully acknowledge the financial support of this work by the Spanish Ministry of Science and Technology (ENE2006-15116-C04-03/CON), the Basque Government (IE06-171) and the University of the Basque Country (UPV/EHU). Besides, the authors want to mention the collaboration of Rohm & Haas for kindly supplying different Amberlyst resins. The authors are affiliated with the School of Engineering, Bilbao (UPV/EHU.

Journal:	Bioresource Technology
Title:	Catalytic reactive distillation process development for 1,1 diethoxy butane production from renewable sources
Authors:	Agirre I., Barrio V.L, Güemez B., Cambra J., Arias P.L.,
Year: 2011	**Volume**: 102 **Pages**: 1289-1297

Bioresource Technology 102 (2011) 1289–1297

Contents lists available at ScienceDirect

Bioresource Technology

journal homepage: www.elsevier.com/locate/biortech

Catalytic reactive distillation process development for 1,1 diethoxy butane production from renewable sources

I. Agirre *, V.L. Barrio, B. Güemez, J.F. Cambra, P.L. Arias

Chemical and Environmental Engineering Department, Engineering School of Bilbao Alameda Urquijo s/n, 48013 Bilbao, Spain

ARTICLE INFO

Article history:
Received 31 May 2010
Received in revised form 19 August 2010
Accepted 22 August 2010
Available online 26 August 2010

Keywords:
1,1 Diethoxy butane
Reactive distillation
Steady-state model
Amberlyst
Katapak

ABSTRACT

Some acetals can be produced from renewable resources (bioalcohols) and seem to be good candidates for different applications such as oxygenated diesel additives. In the present case the production of 1,1 diethoxy butane from bioethanol and butanal is presented. Butanal can be obtained from biobutanol following a partial oxidation or a dehydrogenation process. In this paper innovative process development about the synthesis of the mentioned acetal including catalytic reactive distillation experimental and simulation results will be presented and discussed. Katapak SP modules containing Amberlyst 47 resin were used as structured catalytic packings. This reactive system allowed reaching higher conversions than the equilibrium ones at the same temperatures. All the experimental data gathered allowed to tune a simulation model for the reactive distillation operation which showed a fairly good behavior in order to perform initial 1,1 diethoxy butane production process design studies.

1. Introduction

In the last years, production of oxygenated compounds like ETBE as petrol additive from isobutylene and bioethanol has increased significantly. Nowadays, the use of different biofuels in conventional car engines has become one of the technological goals towards a sustainable development. Biodiesel is an alternative fuel obtained from vegetable oils or animal fats and it has several technical advantages over petro-diesel such as the reduction of exhaust emissions, improved lubricity and biodegradability, higher flash point and reduced toxicity. There are some other properties like cetane number, gross heat of combustion and viscosity that are very similar in biodiesels and in conventional diesels. But biodiesels are worse than conventional ones in terms of oxidation stability, nitrogen oxides emissions, energy content and cold weather operability (Moser and Erhan, 2008). A possible solution to these limitations is the use of additives. Metal based additives (manganese, iron, copper, barium…) were the most important ones so far (Burtscher et al., 1999). However, due to the harmful emissions that this kind of additives imply, the use of renewable ashless diesel combustion enhancer additives like acetals seem to be the most suitable ones (Capeletti et al., 2000). The acetals can be obtained from reactions between alcohols (bioalcohols) and aldehydes. The aldehydes can be obtained from their corresponding alcohols following a partial oxidation or a dehydrogenation process (Agirre et al., 2010b). Thus, the acetals can be produced from just renewable raw materials.

Acetals are produced via homogeneous catalytic processes using strong mineral acids as catalysts such as H_2SO_4, HF, HCl or p-toluensuphonic acid (Frusteri et al., 2007; Green, 1981; Kaufhold and El-Chahawi 1996). Kaufhold et al. proposed in a patent (1996) an industrial process for acetal production. In this process, apart from a homogeneous strong acid catalyst an entrainer (hexane, pentane) is used with a normal boiling point between 298.15 K and 348.15 K. This entrainer must be water insoluble (<3% soluble in water), thus the water is continuously removed from the reacting phase shifting the acetalization reversible reaction to the desired direction. However, these processes entail corrosion problems, are uneconomical and they are not environmentally friendly. The use of a heterogeneous catalytic process would overcome most of the previously indicated problems. As a consequence, several solid acid catalysts are being tested currently.

Capeletti et al. (2000) reported the performance of several solid acid catalysts, from commercial, natural and laboratory sources. They concluded that exchange resins show better performance than other catalysts allowing reaching equilibrium values much faster than with other alternatives.

Acetalization reactions show high thermodynamic limitations achieving really low equilibrium conversions (around 50% depending on the operating conditions) if they are carried out in a conventional batch reactor (Agirre et al., 2010; Capeletti et al., 2000; Chopade and Sharma, 1997a,b; Mahajani et al., 1995; Sharma, 1995). The reactive distillation (RD) technology seems to be one

* Corresponding author. Tel.: +34 946017297; fax: +34 946014179.
E-mail addresses: ion.agirre@ehu.es (I. Agirre), laura.barrio@ehu.es (V.L. Barrio), belen.guemez@ehu.es (B. Güemez), jose.cambra@ehu.es (J.F. Cambra), pedroluis.arias@ehu.es (P.L. Arias).

0960-8524/$ - see front matter © 2010 Elsevier Ltd. All rights reserved.
doi:10.1016/j.biortech.2010.08.064

Journal: Journal of Membrane Science

Title: Acetalization reaction of ethanol with butyraldehyde coupled with pervaporation. Semi-batch pervaporation studies and resistance of HybSi® membranes to catalyst impacts**.**

Authors: I. Agirre, M.B. Güemez, H.M. van Veen, A. Motelica, J.F. Vente, P.L. Arias

Year: 2011 (accepted) **Volume**: XX **Pages**: XX-XX

Acetalization reaction of ethanol with butyraldehyde coupled with pervaporation. Semi-batch pervaporation studies and resistance of HybSi® membranes to catalyst impacts.

I. Agirre[1,2*], M.B. Güemez[1], H.M. van Veen[2], A. Motelica[2], J.F. Vente[2], P.L. Arias[1]

[1] Chemical and Environmental Engineering Department, Engineering School of Bilbao (UPV-EHU). Alameda Urquijo s/n, 48013 Bilbao, Spain
Phone: +34-946017297; Fax: +34-946014179;
ion.agirre@ehu.es, belen.guemez@ehu.es, pedroluis.arias@ehu.es

[2] Energy research Centre of the Netherlands (ECN), Unit: Efficiency & Infrastructure, Group: Membrane Technology, P.O. Box 1, 1755 ZG Petten, the Netherlands
vanveen@ecn.nl, motelica@ecn.nl vente@ecn.nl

Abstract

Acetals are seen as important bio-based diesel additives. The production of these compounds from an alcohol and an aldehyde suffers from low conversions due to thermodynamic limitations. These limitations can be overcome through the continuous removal of the by-product water. One of the most promising innovative reaction systems is a membrane reactor equipped with a dehydration membrane. Water selective organic/inorganic HybSi® membranes were used for this purpose. As a representative example the production of 1,1 diethoxy butane from ethanol and butyraldehyde was studied. Permeance data were determined from pervaporation dehydration experiments using non-reacting quaternary mixtures at various temperatures. Membrane reactor experiments show that the conversion of the acetalization reaction can be increased from the thermodynamic value of 40% to 70% at 70ºC and a stoichiometric initial composition. The reactor experiments could be predicted using kinetic data of the reaction and a simple empiric membrane performance relation. The chemical stability of the membrane in the presence of aggressive organic solvents, like butyraldehyde, and its mechanical resistance against the solid catalyst particles of Amberlyst 47 were shown to be satisfactory.

Keywords: Acetal, Pervaporation, HybSi®, Amberlyst, Membrane reactor.